

Phenotype-Directed Discovery of Antibacterials

Abbie Louise Leggott

Submitted in accordance with the requirements for the degree of
Doctor of Philosophy

The University of Leeds

School of Chemistry

July 2021

The candidate confirms that the work submitted is her own and that appropriate credit has been given where reference has been made to the work of others.

This copy has been supplied on the understanding that it is copyright material and that no quotation from the thesis may be published without proper acknowledgement.

The right of Abbie Louise Leggott to be identified as Author of this work has been asserted by her in accordance with the Copyright, Designs and Patents Act 1988.

© 2021 The University of Leeds and Abbie Louise Leggott

i. Acknowledgements

I am very grateful to have been given the opportunity to undertake a PhD under the supervision of Adam and Stuart and I would like to thank them for their support throughout my PhD both personally and academically. I am also extremely thankful that I was given the opportunity to collaborate with Alex. I have always been treated as a member of their group, been taught many new, useful skills, and met some incredible people. Being a member of both the Nelson group and O'Neill group has been an amazing experience and I have met so many interesting people who I am sure will be friends for life!

To the Nelson group and the rest of G.56, I would like to say thank you! It has been amazing working with all of you and you have made my last few years in Leeds so enjoyable. I am still so incredibly proud of all of us for completing the Yorkshire Three Peaks Challenge together, it was an amazing trip. I will miss you all and I am sure you will all go on and do amazing things with your lives! Scott, you are my best friend and have been amazingly supportive over the last few years through some difficult times. You always have the wittiest comments and are truly the best synthetic chemist I have ever met! Chris and Luke, thanks for being the best fumehood buddies, you made me laugh so many times. And Jack, it has been great working together, there is no one else I would rather go to ADS meetings with.

To the O'Neill group, thank you for making me feel a part of the group and helping teach me microbiology techniques. You are all amazing and I am so thankful for all the spontaneous nights out we have had! Justin, you are the kindest and smartest person I know. I will miss our chat's but look forward to hanging out with you in the future! Merianne, I loved going to belly-dance with you and I will never forget the SupaProtein incident. Thank you both for taking me to the best conference of my life! And Abiud, gracias for all the tequila!

I am also extremely grateful to my friends Chelsea and Sophie; I have loved our coffee dates and it has been great to talk to another PhD student outside the lab when things are not going to plan. Finally, I would like to thank my fiancé Yngve, my family and all my friends who have supported me throughout my PhD. You have all been incredible over the last four years and have supported me at every step. I love you all!

ii. Abstract

With antibacterial resistance on the rise, there is an urgent need for new, effective, and safe antibiotics to be brought to clinic as quickly as possible. Although many antibiotics have been developed using conventional drug development approaches, these have their limitations, with drug attrition rates >95%. Activity-directed synthesis (ADS) is one technique developed to speed up early drug development and reduce the time invested in the development of inactive compounds. Catalytic reactions are harnessed, as they can form multiple different products from common substrates, and reactions are performed in a microscale format, with mixtures being screened, without purification, against the selected target.

This thesis initially shows how ADS, driven by a phenotypic assay, can be harnessed to expand the structure-activity relationships (SAR) of a class of antibacterials by designing, executing, and screening an array of 200 reactions based on Pd-catalysed carbonylation chemistry, without purification of individual products. LC-MS analysis of a random 10% of reaction wells confirmed significant conversion to bioactive products. Results show the discovery of new micromolar active antibacterial ligands based on a 4(3*H*)-quinazolinone core that possess antibacterial activity against multiple strains of *S. aureus*. Scale-up reactions were prioritised according to activity, and the structure of these products was elucidated. This approach therefore enabled rapid and efficient expansion of the SAR of antibacterials.

ADS was also utilised to aid in the discovery of novel antibacterial chemotypes. This was possible as arrays were designed with no known antibacterial fragments incorporated into them. Two arrays, with a total of 375 reactions based on Rh carbenoid chemistry were performed and mixtures were screened directly against *S. aureus*. After scale-up and purification, novel antibacterial compounds with micromolar activity were identified, confirming this approach could aid in antibacterial drug development. Active compounds were further assessed for both eukaryotic toxicity and activity against different bacterial strains to assess their use as an antibacterial. It was demonstrated that ADS also aided in the discovery of new chemosynthetic pathways to antibacterials. This project confirmed ADS has the potential to be of more general value in the discovery of new antibacterial classes.

iii. List of Abbreviations

ADS	Activity-Directed Synthesis
AlogP	Partition Coefficient
app	Apparent
<i>B. fragilis</i>	<i>Bacteroides fragilis</i>
BIOS	Biology Oriented Synthesis
br	Broad
C-C	Carbon-Carbon
CAS	Chemical Abstracts Service
CDI	Carbonyldiimidazole
<i>C. difficile</i>	<i>Clostridioides difficile</i>
CLSI	Clinical and Laboratory Standards Institute
COSY	Homonuclear Correlation Spectroscopy
<i>C. perfringens</i>	<i>Clostridium perfringens</i>
CXCR ₂	Cys-X-Cys Chemokine
d	Doublet
DMF	Dimethylformamide
DMSO	Dimethylsulfoxide
dtbbpy	4,4'-Di-tert-butyl-2,2'-bipyridine
<i>E. coli</i>	<i>Escherichia coli</i>
<i>E. faecalis</i>	<i>Enterococcus faecalis</i>
<i>E. faecium</i>	<i>Enterococcus faecium</i>
ES	Electrospray
ESKAPE	<i>Enterococcus faecium</i> , <i>Staphylococcus aureus</i> , <i>Klebsiella pneumoniae</i> , <i>Acinetobacter baumannii</i> , <i>Pseudomonas aeruginosa</i> , and <i>Enterobacter spp.</i>
FabH	β -Ketoacyl-Acyl Carrier Protein Synthase III
FabI	Enoyl-Acyl Carrier Protein Reductase
FBS	Fetal Bovine Serum
FDA	U.S. Food and Drug Administration
FRET	Förster Resonance Energy Transfer
ISB	Iso-Sensitest Broth
HA	Heavy Atoms

<i>H. influenzae</i>	<i>Haemophilus influenzae</i>
HPLC	High-Performance Liquid Chromatography
HMBC	¹ H- ¹³ C Heteronuclear Multiple Bond Correlation Spectroscopy
HR-MS	High Resolution Mass Spectrometry
HSQC	Heteronuclear Single Quantum Coherence
HTS	High-Throughput Screening
IC ₅₀	Half-Maximal Inhibitory Concentration
<i>K. pneumoniae</i>	<i>Klebsiella pneumoniae</i>
LBD	Ligand Binding Domain
LC-MS	Liquid Chromatography–Mass Spectrometry
LCMS-MS	Liquid Chromatography-Tandem Mass Spectrometry
LPS	Liposaccharides
MetRS	Methionyl tRNA Synthetase
MHA-II	Mueller-Hinton Agar II
MHB-II	Cation-Adjusted Mueller-Hinton Broth
MIC	Minimum Inhibitory Concentration
MoA	Mechanism/Mode of Action
m.p.	Melting Points
m	Multiplet
MptpB	Mycobacterium tuberculosis protein tyrosine phosphatase
MRSA	Methicillin-Resistant <i>Staphylococcus aureus</i>
NOESY	Nuclear Overhauser Effect Spectroscopy
NME	New Molecular Entity
NMR	Nuclear Magnetic Resonance
NP	Natural Product
OD	Optical Density
<i>p</i> -ABSA	4-Acetamidobenzenesulfonyl azide
<i>P. aeruginosa</i>	<i>Pseudomonas aeruginosa</i>
PBP ₁	Penicillin-Binding Protein 1
PBP _{2a}	Penicillin-Binding Protein 2a
PBPs	Penicillin-Binding Proteins
PDF	Peptide Deformylase
PheRS	Phenylalanyl-tRNA Synthetase
PPI	Protein-Protein Interaction

ppm	Parts per Million
PSSC	Protein Structure Similarity Clustering
PTFE	Polytetrafluoroethylene
q	Quartet
RB	Rotatable Bonds
Rh ₂ Cap ₄	Dirhodium Tetracaprolactamate
Rh ₂ Pfb ₄	Tetrakis(perfluorobutyrate)dirhodium
Rh ₂ Piv ₄	Dirhodium Tetrapivalate
RNaseP	Ribonuclease P
rRNA	Ribosomal Ribonucleic Acid
s	Singlet
SAR	Structure-Activity Relationship
<i>S. aureus</i>	<i>Staphylococcus aureus</i>
SCONP	Structural Classification of Natural Products
<i>S. epidermidis</i>	<i>Staphylococcus epidermidis</i>
<i>S. pneumoniae</i>	<i>Streptococcus pneumoniae</i>
t	Triplet
THF	Tetrahydrofuran
TU	Thiourea

iv. Table of Contents

i.	Acknowledgements	i
ii.	Abstract.....	ii
iii.	List of Abbreviations	iii
iv.	Table of Contents	vi
v.	List of Figures	viii
1	Chapter 1. Chemical Approaches to Enable the Discovery of Novel Antibacterial Scaffolds	1
1.1	The Drug Discovery Pipeline	1
1.2	Natural-Product Inspired Approaches to Drug Discovery	8
1.3	The Discovery of Antibiotics.....	18
1.4	Summary	36
1.5	Project Outline	36
2	Chapter 2. Activity-Directed Expansion of the SAR of Antibacterials	39
2.1	Rationale for the Selection of Pd ⁰ Catalysed Chemistry to Underpin ADS... ..	39
2.2	Configuration of Carbonylation Chemistry for Activity-Directed Synthesis	44
2.3	Establishment of Phenotypic Assay for Activity-Directed Antibacterial Discovery	52
2.4	Design and Synthesis of Substrates for Activity-Directed Synthesis.....	60
2.5	Carbonylation Reaction Arrays	69
2.6	Scale-up and Structural Elucidation of Antibacterial Ligands	77
2.7	Summary	83
3	Chapter 3. Activity-Directed Discovery of Novel Antibacterial Classes.....	85
3.1	Rationale for the Selection of Rh Catalysed Chemistry to Underpin Target-Agnostic ADS	85
3.2	Design and Synthesis of Substrates for Activity-Directed Synthesis.....	87
3.3	Rh Catalysed Reaction Arrays	93
3.4	Scale-up and Structural Elucidation of Antibacterial Ligands	100
3.5	Rh Catalysed Reaction Array with Scavenging.....	108
3.6	Scale-up and Structural Elucidation of Antibacterial Ligands	114
3.7	Biological Evaluation of Active Compounds	121
3.8	Chemistry Leading to Active Compounds.....	125
3.9	Summary and Conclusions.....	128
4	Future Work	130

4.1	Future work: Investigation of Mechanism of Action of Novel Antibacterials 130	
4.2	Future work: Extension of the Scope of ADS	131
5	Experimental	134
5.1	General Information and Instrumentations	134
5.2	Chemistry.....	135
5.3	Biology.....	173
6	List of References	177
	Appendix A Growth Inhibition Calculations	187
	Appendix B NMR Spectra	190
	B.1 Identification of Rotamers within Quinazolinone 38b	190
	B.2 Confirmation of the Structure of 111	192
	B.3 Evidence to Support the Hypothesised Structure of 130	194
	B.4 NOESY NMR Confirming Z Alkene in Compound 126	195
	Appendix C Dose Response Curves to Assess Eukaryotic Activity	197

v. List of Figures

Figure 1.1 Ligand optimisation in drug discovery	2
Figure 1.2 Hit-to-Lead optimisation of a triazolethiol CXCR ₂ receptor antagonist	3
Figure 1.3 Total number of new molecular entities (NMEs) brought to market within the last decade	5
Figure 1.4 Percentage of compounds within the CAS database containing a certain percentage of hetero frameworks.....	6
Figure 1.5 Reaction types commonly used in the medicinal chemistry toolkit obtained from pharmaceutical patents between 1976-2015.....	7
Figure 1.6 Taxol, 3 and Mevastatin, 4, two natural product-based drug	9
Figure 1.7 Analogy between small molecules and proteins as the inspiration for Biology-Oriented Synthesis (BIOS)	11
Figure 1.8 Compound collections based on the BIOS approach and ligands discovered from each library.....	12
Figure 1.9 An overview of activity-directed synthesis	14
Figure 1.10 α -Diazoamides scaffold exploited in activity-directed synthesis intramolecular study of the androgen receptor	15
Figure 1.11 Androgen agonists identified from an intermolecular activity-directed synthesis protocol.....	17
Figure 1.12 Schematic of the composition of the envelope within Gram-positive and Gram-negative bacteria	20
Figure 1.13 The Discovery of Linezolid	27
Figure 1.14 A selection of some structures of antibacterial quinazolinones, 38 and their corresponding minimum inhibitory concentrations (MIC) against <i>S. aureus</i> strain ATCC29213.....	29
Figure 1.15 Structure-Activity Relationships (SAR) of a selection of reported antibacterial quinazolinones.....	30
Figure 1.16 The eNTRy rules.....	34
Figure 2.1 Potential of Pd-catalysed chemistry to yield alternative scaffolds from structurally related substrates and, in some cases, a carbon monoxide source.....	40
Figure 2.2 Outline mechanisms for aminocarbonylation (red) ¹⁰³ , the Heck catalytic cycle (black) ¹⁰⁴ and the Buchwald-Hartwig Amination (blue) ¹⁰⁵	43
Figure 2.3 Photographs of the experimental set-up used to conduct heated microscale reactions.....	47
Figure 2.4 Configuration of <i>S. aureus</i> growth time in Iso-Sensitest Broth (ISB).....	52
Figure 2.5 Comparison of MIC data obtained in MHB-II (A) and ISB (B).....	55
Figure 2.6 Schematic of the screening procedure used to determine activity within reaction mixtures	58
Figure 2.7 Growth inhibition values of individual reaction components, a reaction that forms a positive control and a reaction that forms a negative control against ATCC29213	59
Figure 2.8 Design criteria to allow synthesis of quinazolinones ⁷⁸ in an ADS reaction array.....	60
Figure 2.9 Summarised flow chart of the Pipeline Pilot filtering protocol -	61

Figure 2.10 Set of 19 co-substrates chosen for the Pd-catalysed carbonylation array and their molecular properties – Panel A, B and C: Selected co-substrates where.....	63
Figure 2.11 Set of 10 anilide substrates chosen for the Pd-catalysed carbonylation array and their molecular properties.....	65
Figure 2.12 Potential of Pd-catalysed chemistry to yield alternative scaffolds from common substrates.....	66
Figure 2.13 Possible products, with masses that were observed, that could have formed within in the reactions listed in Table 2.5.....	72
Figure 2.14 Photograph of a reaction array plate of ATCC29213 after incubation for 10 h at 37 °C.....	73
Figure 2.15 Activity-directed antibacterial discovery (see table 2.2 for reaction conditions).....	75
Figure 2.16 Reinvestigation of reaction hits that had been active against one colony.....	76
Figure 2.17 The two rotamers of quinazolinone 38u and the diastereotopic protons identified in 38y.....	81
Figure 2.18 SAR expanded using ADS. ⁹⁷	84
Figure 3.1 Alternative Rh-catalysed carbenoid reactions that yield different chemotypes.....	86
Figure 3.2 Summarised flow chart of the Pipeline Pilot filtering protocol -.....	88
Figure 3.3 Set of 21 co-substrates chosen for the Rh-catalysed array and their molecular property distribution -.....	89
Figure 3.4 Set of 6 substrates chosen for the Rh-catalysed array and their molecular property distribution -.....	90
Figure 3.5 Growth inhibition values of individual reaction components in Rh reaction array without catalyst scavenging, Penicillin G, 24 (Pos) and a 1% DMSO Control against <i>S. aureus</i> ATCC29213.....	94
Figure 3.6 Possible products, with masses that were observed, that could have formed within the reactions listed in Table 3.1.....	97
Figure 3.7 Activity-directed antibacterial discovery using Rh Carbenoid Chemistry without catalyst scavenging.....	99
Figure 3.8 Key NMR peaks used in the identification of 111.....	102
Figure 3.9 Possible mechanism for the synthesis of 111 from S5 and C20.....	103
Figure 3.10 Comparison of the retention times of 109a and 109b with the crude reaction mixture between S2 and C5.....	106
Figure 3.11 Growth inhibition values of individual reaction components in Rh reaction array with catalyst scavenging, Penicillin G, 24 (Pos) and a 1% DMSO Control (Blank) against <i>S. aureus</i> ATCC29213.....	109
Figure 3.12 A selection of possible products, with masses that were observed, that could have formed within in the reactions listed in Table 3.4.....	112
Figure 3.13 Activity-directed antibacterial discovery using Rh Carbenoid Chemistry with catalyst scavenging.....	113
Figure 3.14 6-Point dose Response values (total product concentration: 200 – 6.25 µM) of active combinations against ATCC29213.....	116
Figure 3.15 Key NMR peaks used in the identification of 130.....	119
Figure 3.16 Activity-directed emergence of chemosynthetic pathways to antibacterials.....	127
Figure 3.17 Six compounds identified with antibacterial activity.....	129

Figure 4.1 The Potential for a Late-Stage Functionalisation approach to be harnessed within an ADS workflow..... 132

1 Chapter 1.

Chemical Approaches to Enable the Discovery of Novel Antibacterial Scaffolds

1.1 The Drug Discovery Pipeline

The discovery and development of new drug candidates is a complex process that involves the design, synthesis and testing of many functionally optimised compounds over many years.^{1,2} It is currently estimated that the cost to bring a single new molecular entity (NME) to market is at least US \$1.8 billion (including costs incurred from failed campaigns).³ This cost is largely due to the high drug attrition rates during phase II and phase III clinical trials, estimated at 66% and 30% respectively leading to overall attrition rates >95%.^{3,4} As attrition rates are high, multinational pharmaceutical companies have invested in the development of innovative, more efficient techniques of drug discovery that allow the exploration and selection of better drug candidates earlier into the drug discovery process.^{5,6}

1.1.1 Overview of Drug Discovery Pipeline

Most drug discovery programmes are initiated when a disease or condition has an unmet clinical need¹ and the development of a new drug would be both beneficial to most of the population affected and profitable to the company. In the initial research phase, a target is usually identified which, upon successful binding of a ligand, stimulates the desired response. Sites of activity capable of stimulating responses must be identified to ensure the correct ligand binding domain (LBD) is targeted and all molecules designed contain the relevant structural features for successful binding.

Once chosen, the hit discovery process¹ and lead discovery phases begin. High throughput screening (HTS) is commonly performed during the hit identification phase on large compound libraries to identify molecules in the companies collection that interact with the target and produce the desired response.^{1,7} Screening compounds are organised into compound collections and binding interactions with the target of

interest are identified using molecular modelling. In traditional drug discovery, all compounds that have good binding and could potentially be active are designed, synthesised, purified and tested against a biological assay of the target (Figure 1.1).

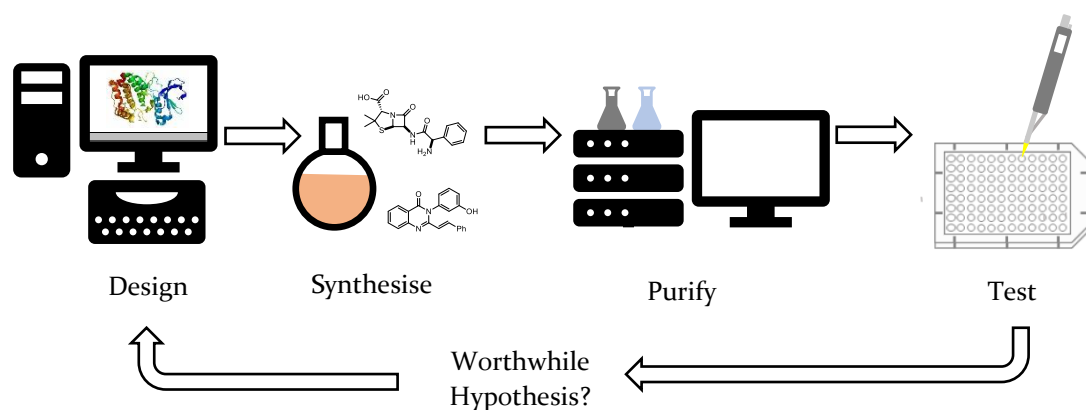


Figure 1.1 Ligand optimisation in drug discovery - In the initial stages of drug discovery, a disease or condition with an unmet clinical need is identified and an initial target is chosen. Large compound libraries are synthesised, purified and tested against the target before the hypothesis can be deemed worthwhile.¹⁷ In the later stages of drug discovery, lead compounds are optimised and chosen for clinical development.

The most successful compounds (hit compounds) are then optimised to increase their potency and improve deficiencies in their structure.¹ When performing lead optimisation, different functional groups on the hit compound are altered systematically to identify their effect on the overall potency. If the activity of the modified hit increases against the target, this modification is exploited in different combinations. A robust structure-activity relationship (SAR) is constructed within this phase with compounds initially being tested *in vitro* until a lead compound is identified.⁸

Lead optimisation is more effective when a larger number of structural modifications are performed as this allows the production of a more informed SAR. An example SAR⁹, during lead optimisation of a triazolethiol hit **1**, was reported. This hit was shown to target the Cys-X-Cys chemokine (CXCR₂) receptor (Figure 1.2). Analogues of **2** were synthesised, systematically altering the structure of R, R₁ and R₂ to

identify lead compound, **2a**, with submicromolar activity. Compounds **2b-2e** evaluated different analogues of the thiol in the R₂ position and showed that with a hydroxy (**2c**), amino (**2d**) or methylthiol (**2e**) analogue, the triazolethiol was inactive against CXCR₂. Formation of compounds **2f-2h** showed that activity was only present within analogues that contained a benzyl group (with/without substitution) in the R₁ position of the triazolethiol. Modification of R within compounds **2i-2q** and substitution on the benzyl ring in position R₁ aided in the identification of lead compound, **2b**.

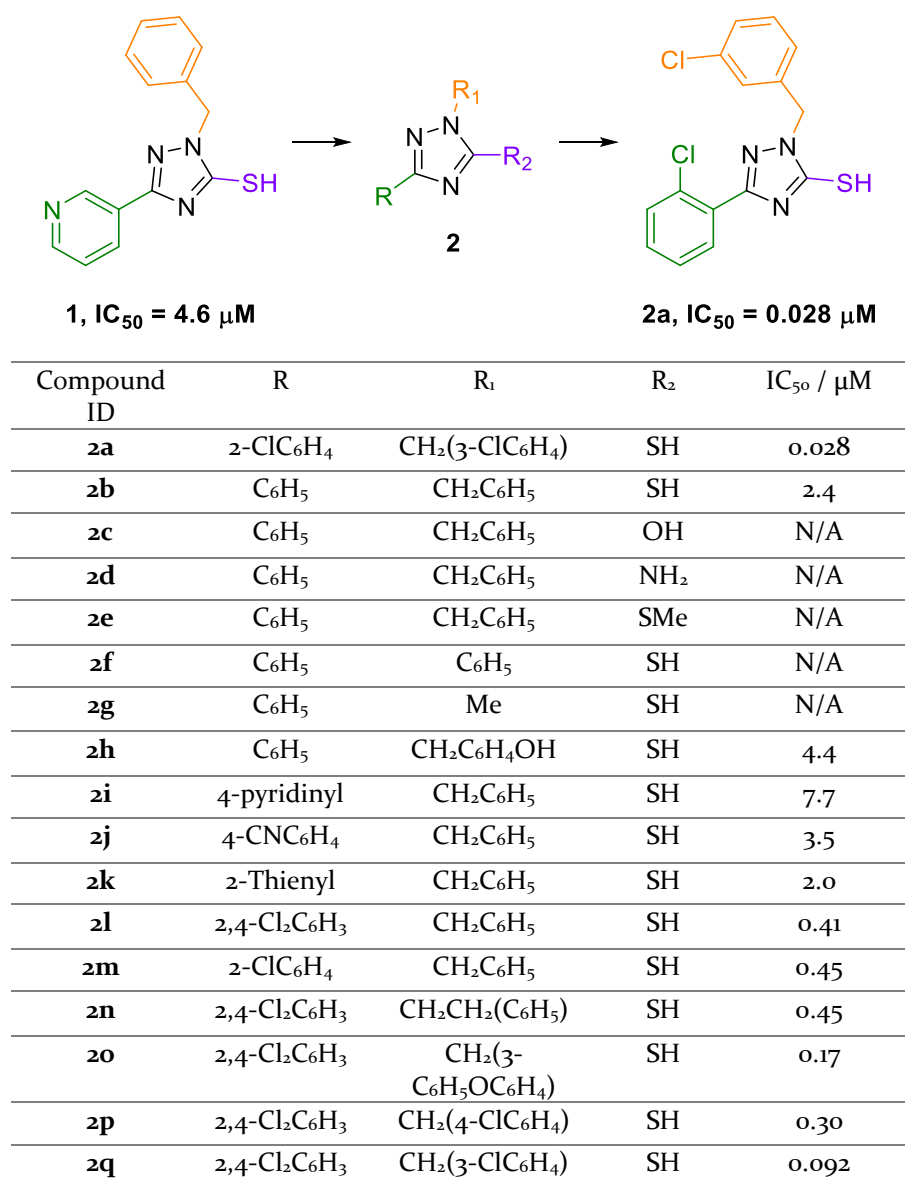


Figure 1.2 Hit-to-Lead optimisation of a triazolethiol CXCR₂ receptor antagonist
 - Panel A: The Hit-to-Lead optimisation of triazolethiol **1** to triazolethiol **2a** using high

throughput screening. Panel B: A selection of triazolethiol **2** compounds synthesised and their respective IC₅₀ values against the CXCR₂ receptor.⁹

For an NME to be approved for clinical use, physiological screening must be performed on the lead compound to determine its toxicology *in vivo*. Successful structures are selected for clinical development, where they must pass all three phases of clinical trials. Phase I clinical trials aim to assess the safety of the lead compounds over a 30-day period on healthy volunteers. Between 2015-2017, the probability of launching a candidate from entry into phase I was 7% due to high failure rates caused by either the safety or efficacy of the drug (79% of all failures), operational shortcomings (1% of all failures), strategic realignment (13% of all failures) or commercial reasons (7%).¹⁰ Phase II clinical trials assess the efficacy of the drug on hundreds of patients with the disease. The probability of launch from this phase was 15% between 2015-2017.¹⁰ If a drug enters phase III clinical trials, it is compared to known medication and tested on thousands of volunteer patients. As safety and efficacy have already been assessed, the probability of launch at this phase was 62% between 2015-2017.¹⁰

Within the last decade, the number of small molecules launched has remained fairly constant, with the increasing trend likely caused by the development of new strategies for hit identification and drug development (Figure 1.3).¹¹ Between 2015-2017, only 82 NMEs were approved, low compared to the number of clinical trials performed on a yearly basis but understandable due to the high attrition rates drugs face within the final stages of drug discovery.

Although all this time is invested into drug discovery, is not guaranteed that an NME will be discovered, therefore, medicinal chemists have utilised an arsenal of techniques i.e. robust reactions, common drug like motifs etc. to increase the probability of success. Although these methods have reduced the costs for many companies, they have caused an unprecedented “bottleneck”,³ reducing scaffold diversity and the amount of drug-like chemical space explored.

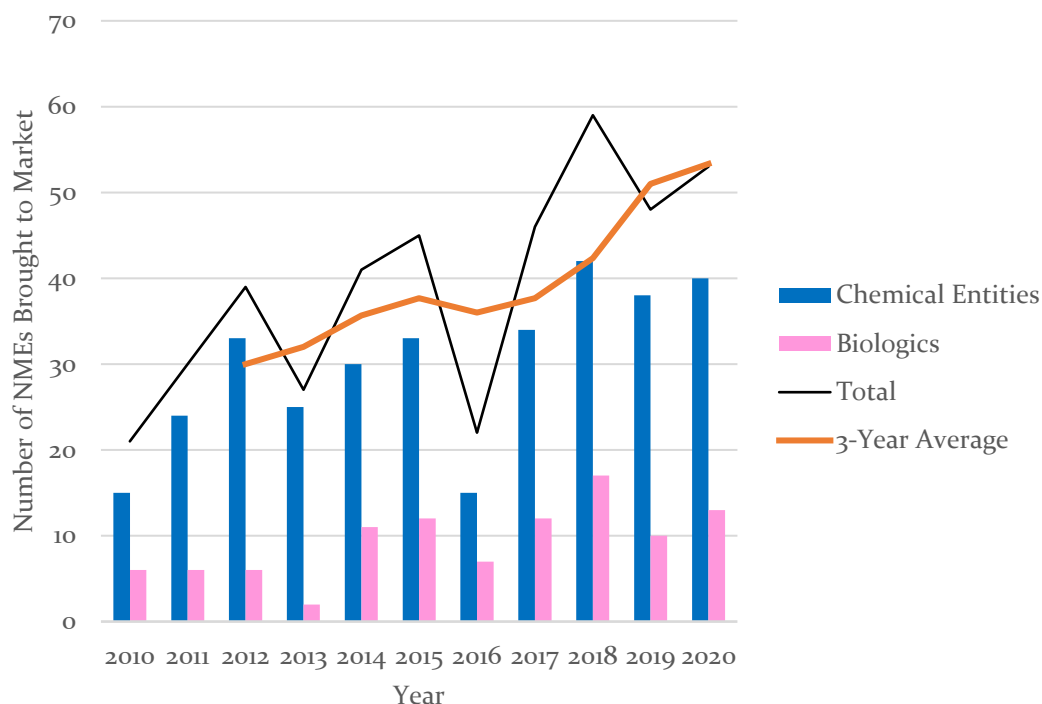


Figure 1.3 Total number of new molecular entities (NMEs) brought to market within the last decade - Small molecules (blue), biological drugs (pink) and the total number of NMEs (black line) have been indicated for each year. A three-year rolling average has been plotted (orange line) to show the number of NMEs discovered over the last decade has been increasing. Data was obtained from the U.S. Food and Drug Administration (FDA).¹¹⁻¹⁵

1.1.2 Historic Exploration of Chemical Space

Chemical space is vast and so it is practically impossible to thoroughly examine all areas, ultimately leaving chemists with the decision of which areas are best and contain the most promising drug candidates.¹⁶ A commonly used approach to this problem is to measure the chemical diversity of compounds to allow the exploration of new regions of chemical space.¹⁷ Structures chosen can then be characterised by using various molecular descriptors (i.e. physicochemical properties) to assess differences in their properties.¹⁷ Alternatively, analysis of frameworks can enable assessment of structural diversity among organic molecules.¹⁷ If all areas of space were explored evenly, a plot of the percentage of compounds versus the percentage of hetero

frameworks for all the CAS database would be linear, however, it was found that this plot was curved with a top-heavy distribution (Figure 1.4).¹⁷ The initial steep increase of the curve indicated that only a small percentage of frameworks were found in a large percentage of compounds (10% of hetero frameworks account for 80% of compounds) and the sharp turn in the data separated these from the uncommon frameworks (90% of hetero frameworks account for less than 20% of compounds).

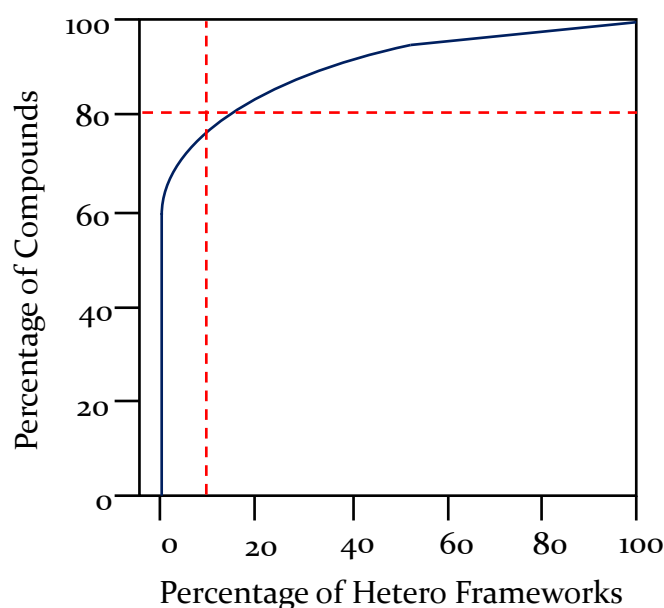


Figure 1.4 Percentage of compounds within the CAS database containing a certain percentage of hetero frameworks - A small percentage (c.a. 10%) of Hetero Frameworks account for 80% of compounds with the CAS database.¹⁷

This trend has arisen as reliable synthetic routes are the foundations of all drug discovery programmes, and without them, target-oriented methods of drug discovery would be less viable. Even though robust reactions still aid in the development of new drugs, the amount of transformations they can undergo is limited¹⁸⁻²¹ which consequently reduces product diversity.¹⁷ In addition, NMEs are flatter, more lipophilic and larger as a consequence of these reaction types, adversely affecting their physical properties.²² The most common reaction types were identified²¹ from 9 million granted US patents and US patent applications between 1976-2016. A total of 1.32 million unique

reactions were identified from this data set, and upon limiting results to pharmaceutical patents, 1.15 million unique chemical reactions were identified. The most common reactions found include heteroatom alkylations and arylations, acylations, deprotections and carbon-carbon (C-C) bond formation that account for over 70% of all reactions (Figure 1.5). The most common reactions are similar to those identified in 2011, obtained from medicinal chemistry publications between 2008-2009.¹⁸

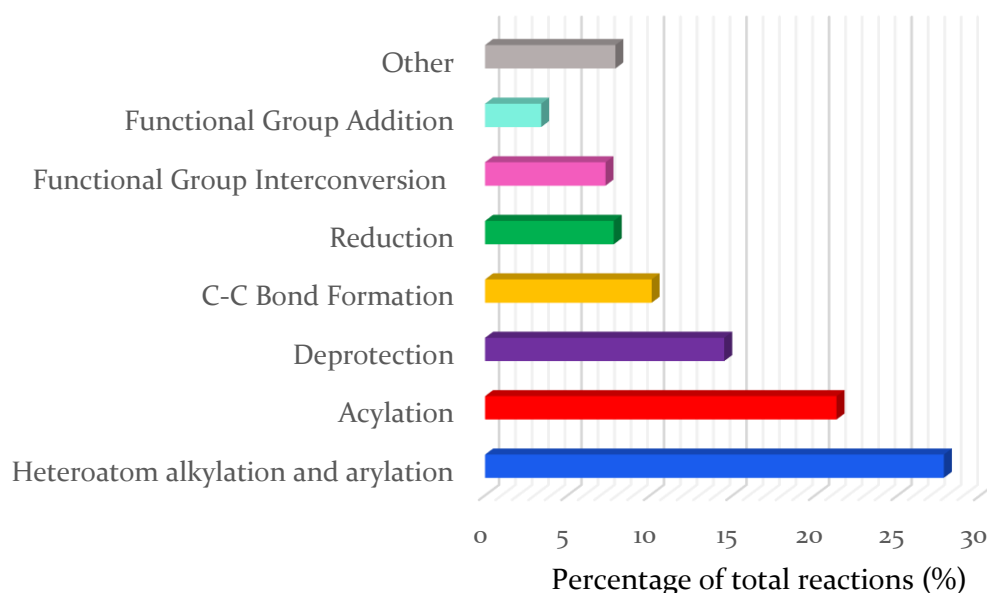


Figure 1.5 Reaction types commonly used in the medicinal chemistry toolkit obtained from pharmaceutical patents between 1976-2015 - Reaction types have been classified by their respective type.²¹

The data set shows the limitations of the medicinal chemists' toolkit as although many reactions can be performed, they are usually restricted to the functionalisation of one group. The formation of carbon-heteroatom bonds are the most common reaction type in the data set (49.1% of reactions including acylations, alkylations and arylations) whereas carbon-carbon bond formations and heterocycle formations only account for 10.1% and 1.6% respectively even though they allow the formation of much more diverse scaffolds.²¹ The data shows that medicinal chemists

still rely on a small number of reactions (even though some allow a large diversity of functionalities) and highlights the need for new methodologies or improvements in existing transformations to be used in order to broaden product diversity and allow the exploration of drug-like chemical space more evenly.¹⁸

1.2 Natural-Product Inspired Approaches to Drug Discovery

Natural products (NPs), also known as secondary metabolites, are small compounds that are synthesised in living organisms and have frequently been used as the inspiration behind many pharmaceuticals.²³⁻²⁵ NPs result from millions of years of evolution and are therefore encoded to exhibit the optimal interactions with biological macromolecules thus making them promising starting points for future drug candidates.²⁶⁻²⁸ Within the last 30 years, roughly 60% of all NMEs have in some way been inspired by natural products. Within one study conducted between 1981 and 2014, it was calculated that out of all the approved small molecule NMEs, 26% were NP inspired or derived, 27% were natural product mimics and 5% contained an NP pharmacophore.^{26,29} Some examples of the FDA approved natural product based drugs include the widely used breast cancer drug, paclitaxel, **3** (Taxol[®]), isolated from the bark of the Pacific Yew, *Taxus brevifolia*²⁷ and mevastatin, **4** produced by *Penicillium citrinum* which after its development, paved the way to a large group of synthetic statins (Figure 1.6).^{26,30} NPs have shown and will probably continue to show promise as future drug candidates and so some researchers²⁴ have invested into the design of algorithms that can predict the natural-product likeness of any compound and thus aid in the development of more NP pharmacophore containing molecules and NP mimics.^{24,25}

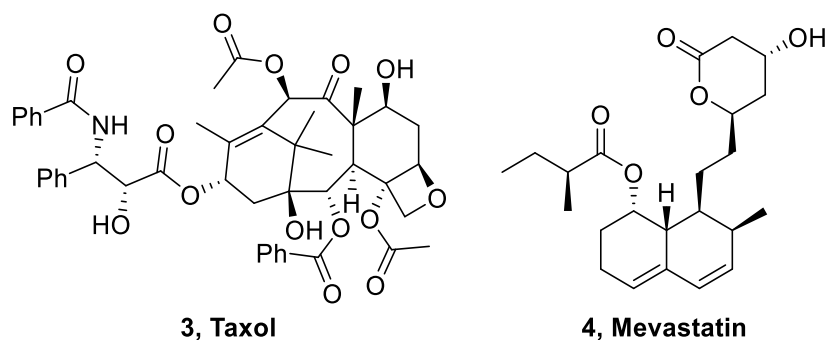


Figure 1.6 Taxol, 3 and Mevastatin, 4, two natural product-based drug - Mevastatin, 4 has also inspired the statin class more generally, aiding in the discovery of many cholesterol therapies.^{23,31}

Another valuable source of inspiration for drug discovery is the exploration and probing of biological systems using small molecules (molecular weight less than 800 g mol⁻¹).³² Chemical probes need to be of a high quality, selective, potent, have a clearly defined structure and mechanism of action (MoA) and be available for all proteins coded by the human genome.^{32,33} This presents a huge challenge for chemical biologists as they must find one compound class that interacts with a single protein function for each protein in the human genome.³² This challenge is made more difficult as it is impossible to investigate all possible small molecule combinations (10⁶⁰) since there is not enough matter in the universe to make one copy of every molecule!^{34,35} As there are so many compounds to explore, researchers are left with two important questions, how can one identify the areas of chemical space that are enriched with biologically relevant compounds and how can this space be navigated?³²

1.2.1 Biology-Oriented Synthesis

Biology-Oriented Synthesis (BIOS) is an approach that has been designed to find biologically relevant areas of chemical space and explore them with the aim of the method being to develop small molecules that bind solely to specific targets. BIOS combines structural analysis of the protein and the small molecule world with structural conservatism and diversity in nature to fulfil the goal of small molecule development.^{32,36} Natural product scaffolds³⁷⁻³⁹ are evolutionary selected chemical

structures that encode the properties that are required for specific protein binding and thus give a reliable interpretation of the chemical space explored by nature over the millions of years of its existence.⁴⁰ By exploiting these scaffolds to form compound collections, small molecule exploration can be focussed in areas of chemical space validated by evolution. BIOS is not restricted solely to NPs: if a non-natural product scaffold is biologically relevant, it can be used as a valid starting point.

BIOS can either be performed by using structural classification of natural products (SCONP), protein structure similarity clustering (PSSC) or by applying both methods synergistically (using biologically relevant compounds) to explore a vast area of chemical space and discover new, biologically relevant areas.³² SCONP derived libraries are structure based and use the scaffolds of the bioactive small molecules to guide the design and synthesis of new compounds whereas PSSC, although structure based, uses the collective protein structure to fuel the reasoning for the design of compound collections.³² This combination is possible as within proteins, shape is conserved within ligand binding sites due to the number of possible folds, leading to amino acid sequences determining the interaction patterns. Within small molecules, scaffold classes are limited and so the orientation is rarely altered, leading to substituents determining interaction patterns of the ligand. If the amino acid sequence is known within the protein, and the orientation of the scaffold within the binding site is known, substituents can be selected that optimise binding interactions (Figure 1.7).³²

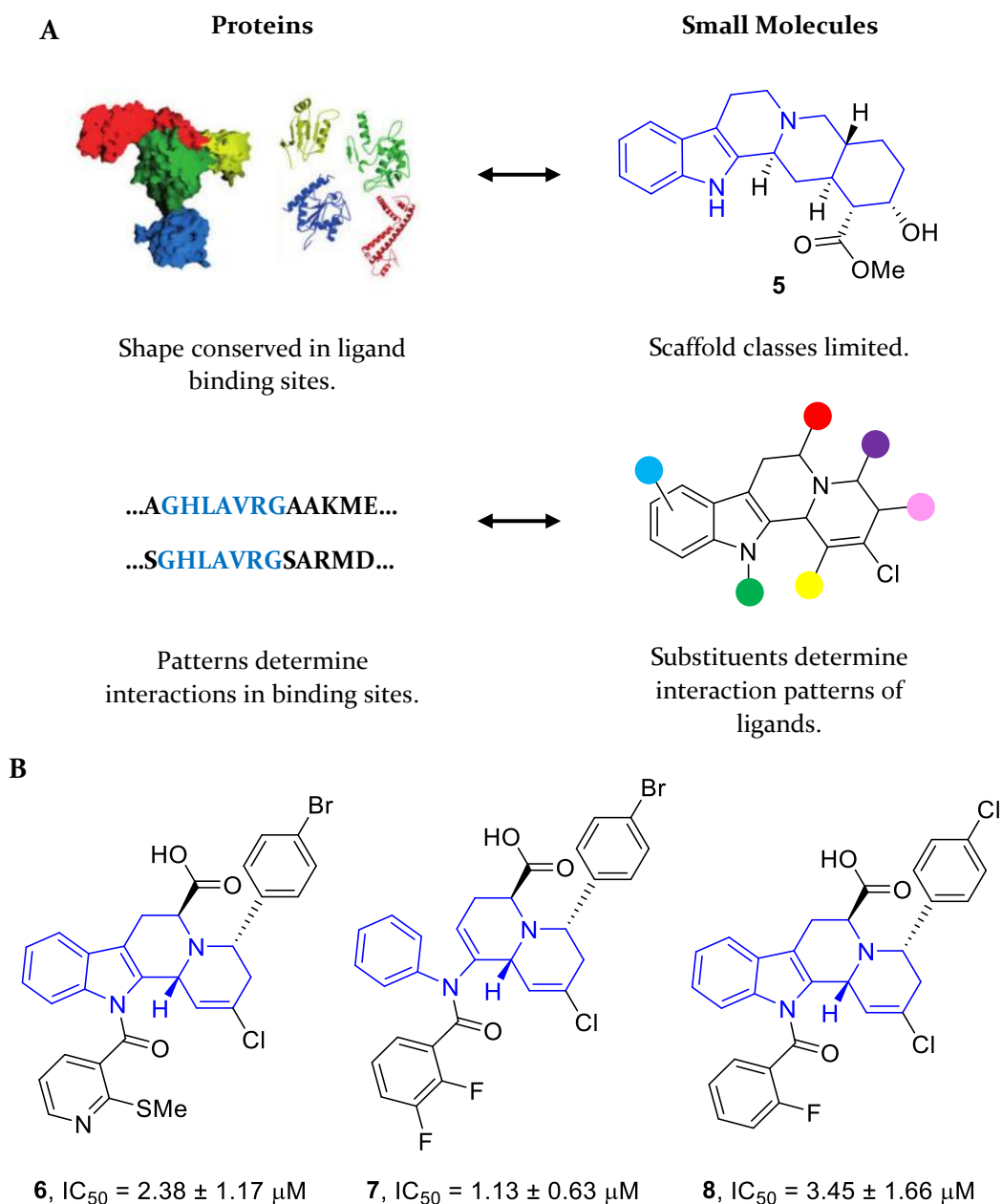


Figure 1.7 Analogy between small molecules and proteins as the inspiration for Biology-Oriented Synthesis (BIOS) - Panel A: The scaffold in the small-molecule determines the spatial orientation whereas the protein subfold arranges the amino acid chains. Binding occurs when molecule orientation matches the binding site. Both molecule structure and protein structure are investigated synergistically in BIOS.³² Panel B: Active *Mycobacterium tuberculosis* protein tyrosine phosphatase (MtpB) inhibitors, identified using the scaffold of compound 5. The scaffold has been indicated (blue) and IC_{50} values for each inhibitor against MtpB included.^{41,42}

Biological relevance (not to be confused with occurrence in nature) is the prime criteria for compound and scaffold selection in BIOS and all compounds within a BIOS-based compound library must prioritise this factor. Although synthesising a natural product-inspired library can be challenging, this is balanced out by the smaller (compared to traditional medicinal chemistry) number of compounds that need to be synthesised and the relatively high hit rate of BIOS. BIOS is one of the first methods that expands chemical diversity by focussing around areas of biologically relevant chemical space and can promote NPs in both medicinal chemistry and chemical biology research.³² In essence, BIOS offers an alternative to other strategies for library design (i.e. libraries focussed on chemical diversity or sequence or structure homology).³⁹ An example of some compound collections exploited and ligands that have been identified using BIOS are displayed in Figure 1.8.

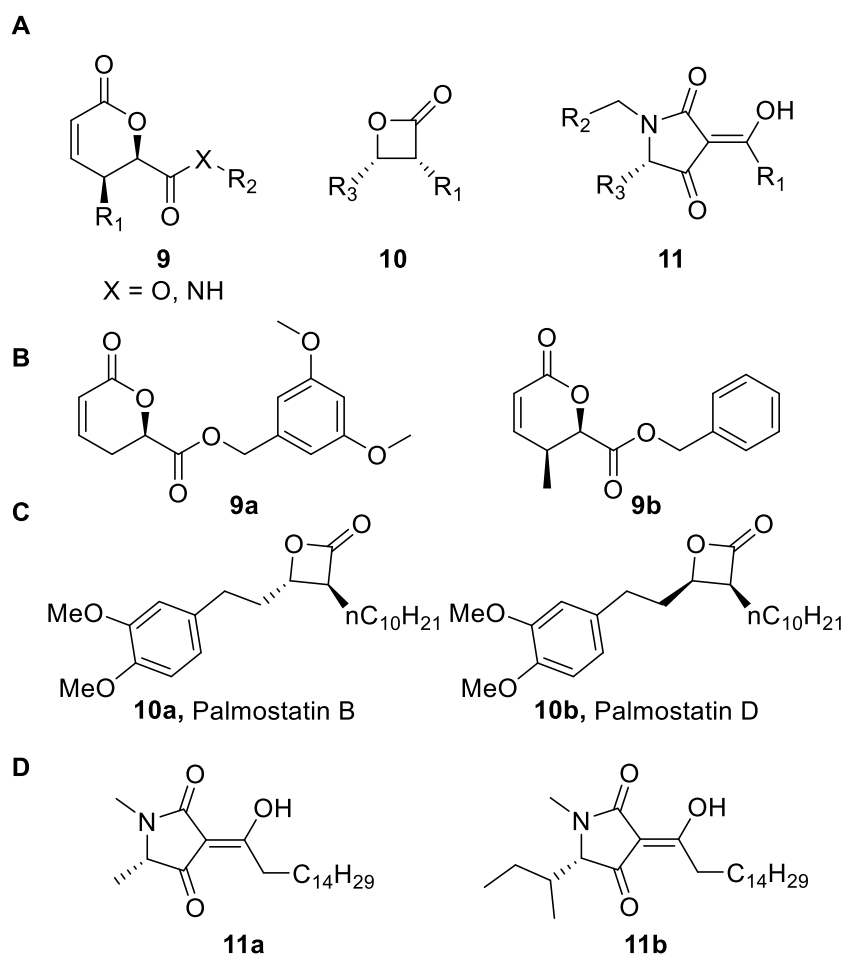


Figure 1.8 Compound collections based on the BIOS approach and ligands discovered from each library - Panel A: Three Compound collections based on the

BIOS approach. Panel B: A selection of α,β -unsaturated-lactones identified using BIOS, that inhibit viral entry into cells.⁴³ Panel C: The palmostatins were developed as APT₁ inhibitors. Palmostatin B, **10a**, inhibits APT₁ by forming a covalent enzyme-inhibitor complex ($IC_{50} = 670$ nM) at the Ser₁₁₄ residue in the active site. Palmostatin D, **10b**, is a weaker inhibitor ($IC_{50} = 1$ μ M) due to *syn*-configuration.^{32,44} Panel D: Ras Pathway probes identified using BIOS.⁴⁵

1.2.2 Activity-Directed Synthesis

Activity-directed synthesis (ADS) is a discovery approach where small bioactive molecules are discovered, together with an associated synthetic route.⁴⁶ ADS is a structure blind, function-driven² process whereby promiscuous reactions are exploited (by using various combinations of catalysts, solvents and substrates/co-substrates with multiple sites of reactivity) to increase the likelihood of multiple products forming and allows exploration of a diverse area of chemical space. ADS is iterative, somewhat mimicking concepts found in nature for the evolution of biosynthetic pathways and the formation of secondary metabolites. In each round, diverse reaction arrays are designed² and, after scavenging metal residue, product mixtures are screened directly, without purification, against a biological target (Figure 1.9).^{2,46} Promising reaction mixtures are scaled-up and purified to structurally elucidate the bioactive ligands. Substrates have traditionally been designed by analysing compounds (either synthetic or natural) known to interact with the target receptor and using a target-oriented approach. Key structural features are incorporated into the design and the scaffold is varied to discover more potent receptors and explore more areas of chemical space. So far, ADS has successfully been used to discover novel ligands with submicromolar activity against the androgen receptor.^{2,46} In order for ADS to work successfully, all substrates used must be inactive under the conditions of the assay and so these are tested and controlled for prior to performing reactions.

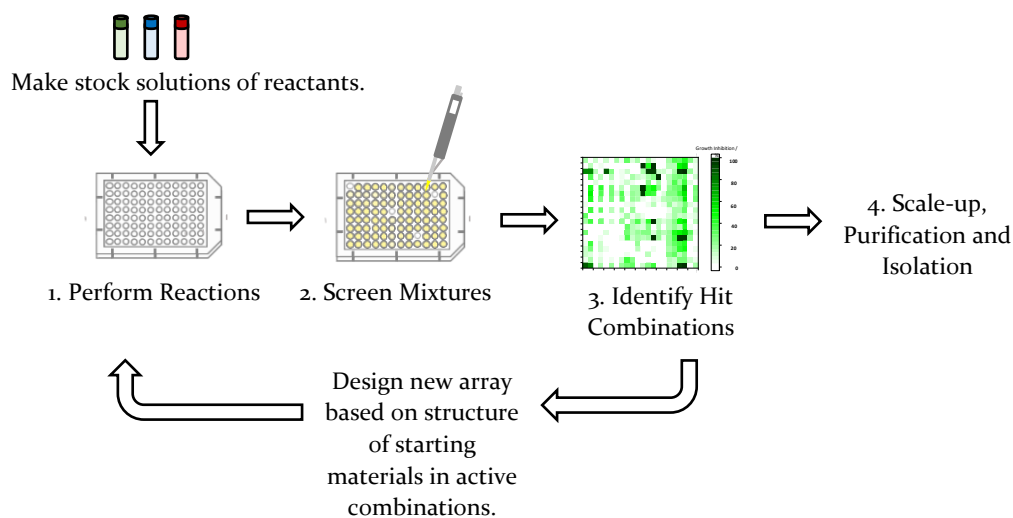


Figure 1.9 An overview of activity-directed synthesis - In each round, arrays of reactions are performed (assembled from stock solutions), screened against the chosen target and active product mixtures are used to inform the design of subsequent rounds. Afterwards, active product mixtures are scaled-up and product structures elucidated.^{2,46}

ADS was first used in the discovery and development of novel androgen receptor agonists⁴⁶ where intramolecular reactions of α -diazo amides containing a 4-cyano-3-trifluoromethyl phenyl group (a fragment found in various androgen receptor modulators) were exploited.^{2,46} Metal catalysed carbenoid reactions were used because alternative outcomes are possible depending on the functional groups that the substrates contain (i.e. O-H, C-H, N-H insertions, cyclopropanations, ylide formations and cycloadditions). This unpredictability can be controlled by the choice of catalyst and reaction conditions and so, from the same combination of substrate and co-substrate, it is possible to form multiple products in different ratios.

For this study,⁴⁶ α -diazo amides were prepared and designed to contain a variable R₁ position which increased scaffold diversity, thereby increasing the probability of cyclisation products (Figure 1.10). All bioactive product mixtures were identified using a Förster resonance energy transfer (FRET) readout and activity of the individual components in the mixture was checked to ensure active signals were not

caused by the starting materials.⁴⁶ Three rounds of ADS were performed, with the active combinations informing the design of subsequent rounds.

Most of the substrates for these reactions only formed active product mixtures when a specific catalyst and solvent was used showing the importance of reaction conditions. The most promising reaction mixtures that showed submicromolar activity were scaled up, purified, and had their products structurally elucidated (Table 1.1). From the eight reactions, three major products **13**, **14** and **15**, were identified and the most potent ligand was also synthesised via an alternative method to validate that the product identified was the cause of the activity.⁴⁶

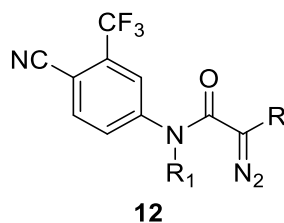


Figure 1.10 α -Diazoamides scaffold exploited in activity-directed synthesis intramolecular study of the androgen receptor - Substrates were chosen for rounds 2 and 3 based on the structure of the α -diazoamides within active combinations from the previous rounds.⁴⁶

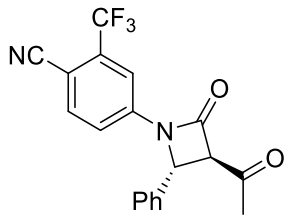
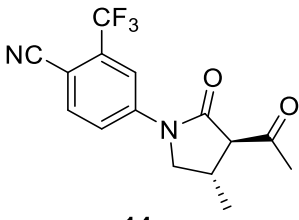
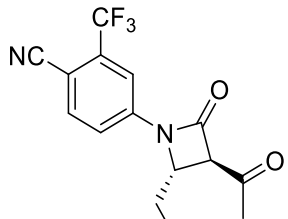
Active Product	Reaction conditions	EC ₅₀ / nM	Yield / %
 13	1 mol% Rh ₂ (esp) ₂ , EtOAc	340 ± 30 (agonist)	75
	1 mol% Rh ₂ (oct) ₄ , CH ₂ Cl ₂		71
	1 mol% Rh ₂ (OAc) ₄ , CH ₂ Cl ₂		68
β-lactam formation by C-H insertion			
 14	1 mol% Rh ₂ (esp) ₂ , CH ₂ Cl ₂	470 ± 40 (partial agonist)	90
	1 mol% Rh ₂ (oct) ₄ , CH ₂ Cl ₂		88
	1 mol% Rh ₂ (OAc) ₄ , CH ₂ Cl ₂		55
γ-lactam formation by C-H insertion			
 15	1 mol% Rh ₂ (esp) ₂ , EtOAc	440 ± 60 (agonist)	78
	1 mol% Rh ₂ (tpa) ₄ , PhMe		70
β-lactam formation by C-H insertion			

Table 1.1 Androgen receptor agonists discovered within active product mixtures from three rounds of activity-directed synthesis - The reaction components used during the array have been indicated for each product and were scaled-up to elucidate the structure of the active product within the reaction mixtures.⁴⁶

This approach was then exploited to explore intermolecular reactions of α -diazo amides bearing the same 4-cyano-3-trifluoromethyl core as used previously. This was performed in the same manner, with the introduction of co-substrates and aided in the discovery of two novel bioactive small molecules, **16** and **17**, with submicromolar activity (Figure 1.11).²

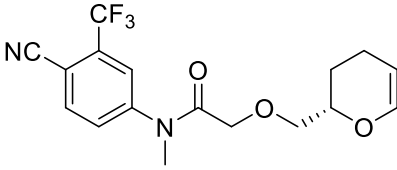
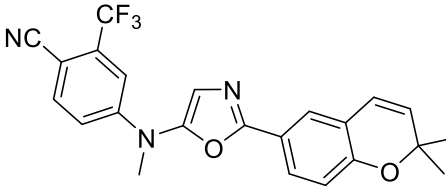
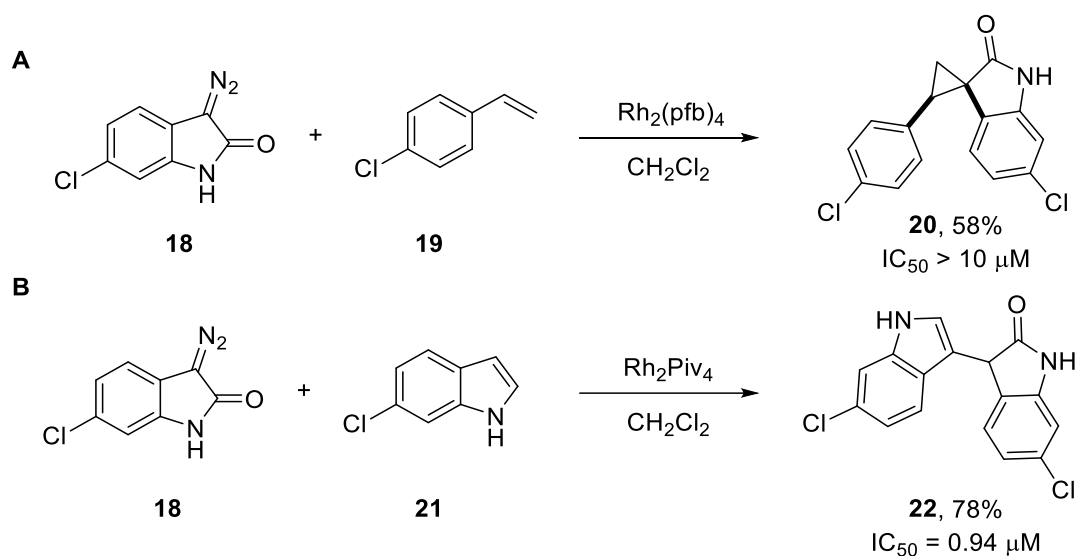
		
	16	17
EC₅₀ (nM)	860 ± 40	730 ± 30
Conditions	1 mol% Rh ₂ (<i>R</i> -DOSP) ₄ , CH ₂ Cl ₂	1 mol% Rh ₂ (OAc) ₄ , CH ₂ Cl ₂
Reaction Type	O-H insertion	Oxazole formation
Yield (%)	73	75

Figure 1.11 Androgen agonists identified from an intermolecular activity-directed synthesis protocol - Agonists **16** and **17** were identified after reaction mixtures, that had shown activity during screening, were scaled-up.²

More recently within the group, this technique was used to identify novel p53/*hDM2* PPI (Protein-Protein Interaction) inhibitors (Scheme 1.1).⁴⁷ Multiple different reaction combinations were explored allowing the identification of ‘hit’ reactions which were subsequently scaled-up to structurally elucidate the reaction products responsible for activity. For both intermolecular reactions of **18** with **19** and **21** respectively, alteration of the co-substrate and catalyst produced oxindole **20** and **22** via a cyclopropanation reaction and a C-H insertion, ultimately allowing the identification of two structurally related species, with **22** being significantly more active (IC₅₀ = 0.94 μM).⁴⁷



Scheme 1.1 Potential of Rh Chemistry to form multiple products from similar substrates - Panel A: Intermolecular reaction from common substrate **18** yielding **20**, a p53/hDM2 PPI inhibitor. Panel B: Intermolecular reaction from common substrate **18** yielding **22**, a compound that possessed higher activity against p53/hDM2 PPI.

1.3 The Discovery of Antibiotics

1.3.1 The Challenges of Antibacterial Drug Discovery

Upon the discovery of sulfonamides and penicillins in the early twentieth century, the once high mortality rate caused by bacterial infections experienced an incredible downturn and millions of lives were saved.^{48,49} By the 1970s, existing antibacterial therapies were deemed adequate and so there was a significant reduction in industrial support for the field of antibacterial research.⁴⁸ The lack of support created a 30 year stagnation where within that period, only two unique NMEs were discovered (linezolid and daptomycin).^{48,50,51} Since then, fidaxomicin⁵¹ and a group of diarylquinolines^{52,53} have been discovered but this cannot mask the fact that since the boom in the early twentieth century, there has been a significant decrease in the amount of unique antibiotics discovered.

The low rate of antibiotic discovery is alarming considering that infectious diseases are still a major cause of death worldwide and that some antibiotics are no longer effective due to the development of bacterial resistance.⁴⁸ Overuse of antibiotics, inadequate hygiene in hospitals, cosmopolitan travel, increased life expectancy and an immunocompromised population are all factors that are responsible for this problem.⁴⁸ Resistance to multiple antibiotics is spreading around the world and so the development of new, effective and safe antibiotics is crucial to avoid future global pandemics.^{48,54-56}

There are two main groups of bacteria, Gram-positive and Gram-negative, named after their positive or negative result during a Gram stain test.⁵⁷ Generally, Gram-positive and Gram-negative bacteria differ by the structure of their cell envelopes which leads to a purple stain and pink stain respectively (Figure 1.12). Gram-negative bacteria have two cell membranes, with the outer membrane composed of liposaccharides (LPS) that stack together very tightly with an overall negative charge, making passive

diffusion of small molecules challenging.⁵⁷⁻⁶⁰ Consequently, it has been hypothesised that small drug molecules can only either enter the bacteria through porins⁶¹ (with interiorly charged amino acids), by temporarily destabilising the LPS layer of the outer membrane,^{62,63} through a combination of both pathways or by self-promoted uptake.⁶⁴ The compounds are then subject to efflux pumps which can pump out compounds that cross the outer membrane.⁶⁵ Gram-positive only antibiotics that can cross the outer membrane, are often pumped out faster, stopping accumulation within Gram-negative cells and making these substrates inactive against them. This consequently makes the discovery of Gram-negative antibiotics more challenging than Gram-positive, leading to a rise in interest in converting Gram-positive to Gram-negative antibiotics.⁶⁰

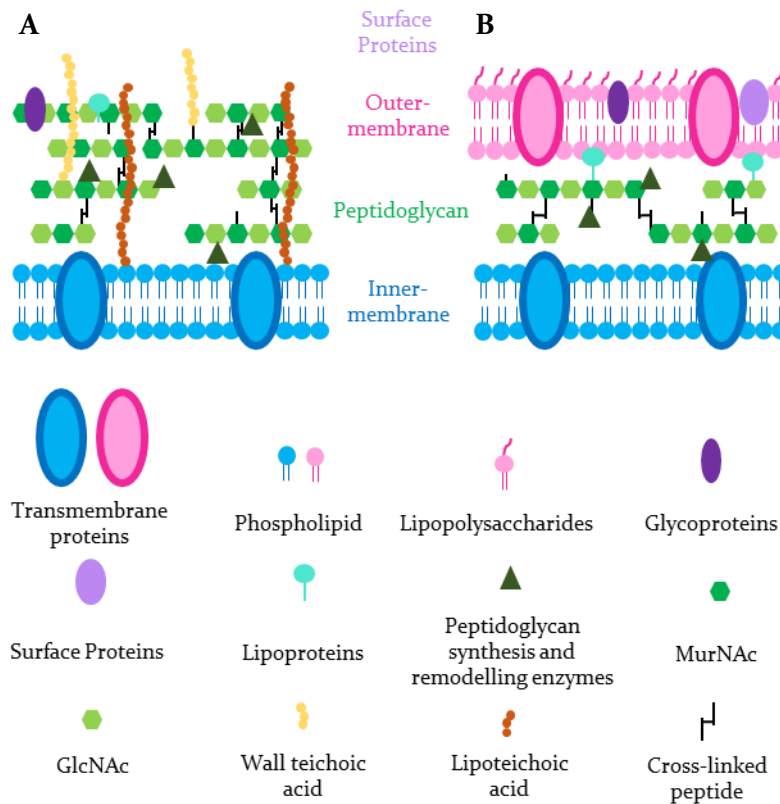
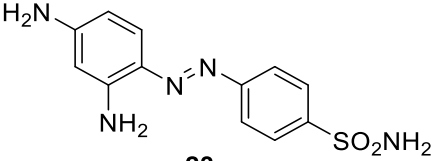
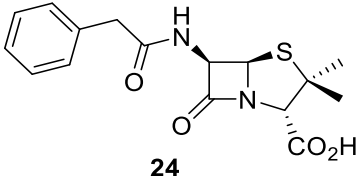
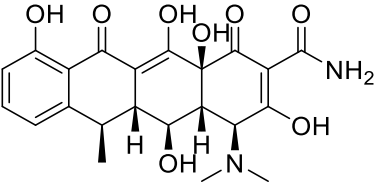
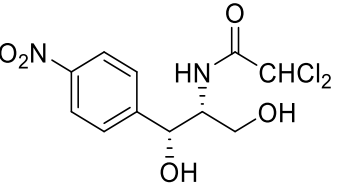


Figure 1.12 Schematic of the composition of the envelope within Gram-positive and Gram-negative bacteria - Panel A: The composition of the cell envelope within Gram-positive bacteria. Panel B: The composition of the cell envelope within Gram-negative bacteria.⁶⁶

1.3.2 A History of Antibacterial Drug Discovery

The majority of antibiotics discovered in the last 100 years have been extracted directly from natural products or are semisynthetic variations.⁴⁸ There are ten major classes of antibiotics, with the majority being discovered in the mid-20th century (Table 1.2).

Class	Year of Introduction	Year Resistance Observed	Target	Example	Structure
Sulfonamides	1936	1942	Folate pathway	Prontosil	 <p>23</p>
β -lactams	1938	1945	Cell wall	Benzylpenicillin	 <p>24</p>
Polyketides	1944	1950	Protein Biosynthesis	Doxycycline	 <p>25</p>
Phenylpropanoids	1948	1950	Protein Biosynthesis	Chloramphenicol	 <p>26</p>

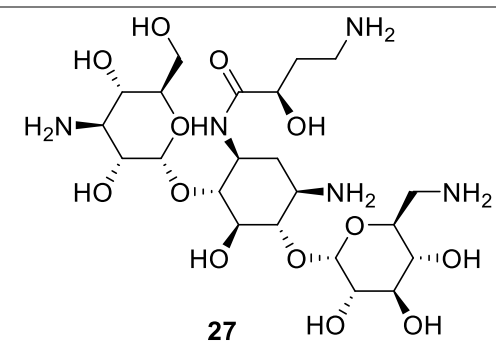
Aminoglycosides

1946

1946

Protein
Biosynthesis

Amikacin



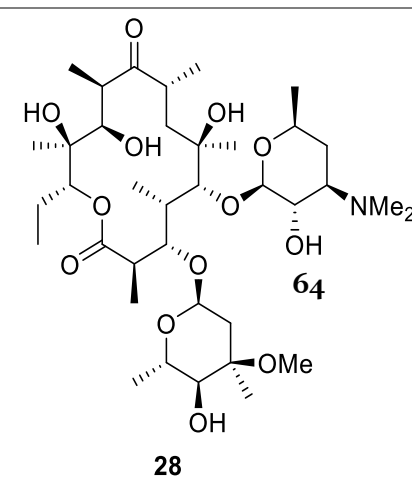
Macrolides

1951

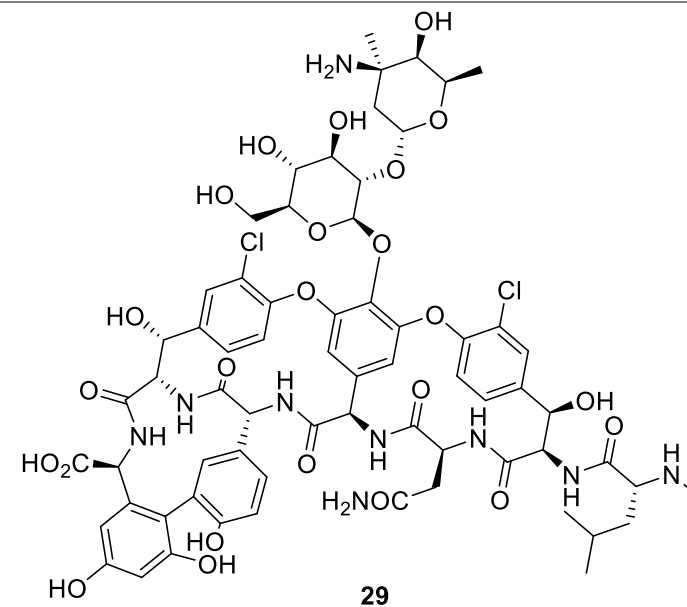
1955

Protein
Biosynthesis

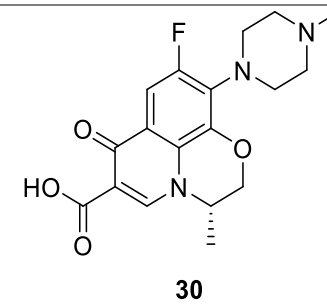
Erythromycin A



Glycopeptides 1958 1960 Cell wall Vancomycin



Quinolones 1968 1968 DNA Replication Levofloxacin



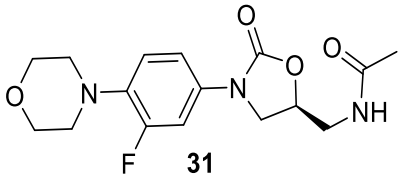
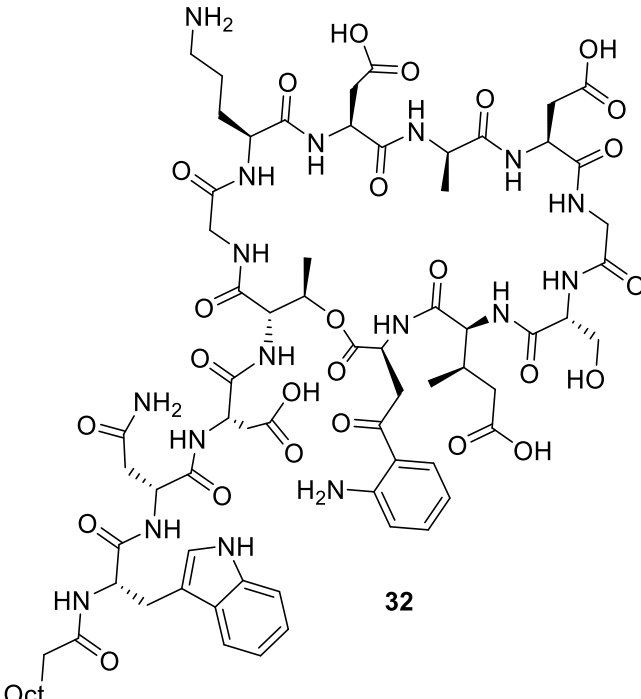
Oxazolidinones	2000	2001	Protein Biosynthesis	Linezolid	 <p style="text-align: center;">31</p>
Cyclic Lipopeptides	2003	1987	Cell Membrane Disruption	Daptomycin	 <p style="text-align: center;">32</p>

Table 1.2 Major classes of antibiotics - Major classes of antibiotics, their year of introduction in the clinic and the year resistance was first observed, their target and an example for each class.^{48,67}

Due to the misuse of antibiotics and the fast evolution of bacteria, antimicrobial resistance has been a growing concern within modern medicine and needs to be addressed. Usually, resistance is observed within a couple of years of the drugs introduction, concerning as this resistance can be readily passed on to different strains of bacteria.⁶⁷ Methicillin-resistant *Staphylococcus aureus* (MRSA), a Gram-positive strain of bacteria, is one of the leading public health concerns.⁶⁸ Resistance has arisen within this strain as it can replicate through 10 generations in under 12 hours, with each replication giving the cells the opportunity to mutate and gain resistance based on stress factors in its surrounding environment.⁶⁹ Vancomycin was originally the only effective therapy for MRSA infections, however, the discovery of daptomycin, linezolid and oritavancin has increased the number of treatments available against serious Gram-positive infections.⁶⁸ However, resistance has developed for all these alternatives and there is a continuous need for more innovative antibiotics with new modes of action to combat this.

1.3.3 Medicinal Chemistry Approaches to Antibacterial Drug Discovery

1.3.3.1 The Discovery of Linezolid

Phenotypic screening has been a common and successful screening technique since the beginning of modern medicinal chemistry and has aided in the discovery of a variety of bioactive compounds (i.e. Penicillin G, **24**). However, due to advances in molecular biology, genomics and combinatorial chemistry, molecular target-based drug discovery has generally been the favoured method within drug discovery.⁷⁰ Unlike target-based assays, phenotypic screens do not initially require target identification and validation, instead, a cell-based assay is developed which aids in identifying compounds that exhibit bioactivity by observing the amelioration of a phenotype, without knowing the part of the cell the compounds will target.⁷¹ By performing an assay this way, new mechanisms of disease action and targets can be discovered which would be completely overlooked using target-based methods.

Linezolid, **31** is an example of an oxazolidinone antibiotic which was discovered using a phenotypic bacterial cell assay and the target was subsequently found to be ribosomal ribonucleic acid (rRNA). Research into this class of antibiotic began when potent biological activity was observed in a select number of oxazolidinones in a variety of Gram-positive bacteria. The two lead compounds (Figure 1.13 – Panel A)⁷² were praised for their attractive antibacterial characteristics (potent *in vitro* activity, encouraging pharmacokinetic properties in rodents etc.), however, the project was ultimately cancelled (likely due to high toxicity in animal models).⁷³ The project was revisited and a SAR was performed which demonstrated that restricting rotational degrees of freedom of the aryl methyl ketone of **35** (incorporating into five- to six-membered benzo-fused cyclic ketones) and **36** (constructing a rigid [6,5,5]-tricyclic-fused oxazolidinone between the oxazolidinone nitrogen and aryl ring) increased antibacterial activity (Figure 1.13 – Panel B).⁷⁴

Many compounds were synthesised from these leads and were tested on mouse infection models, with many displaying good antibacterial activity. A month long rat toxicology study was performed early into the project to confirm that the lead compounds had no clinical signs or histopathological findings to avoid a repeat of the failed DuPont project.^{73,74} Further modifications to the lead compounds were performed to assess the effects of each structure on the growth rate of bacteria. Each compound was screened in *in vivo* and *in vitro* models with the growth rate of *S. aureus* and *S. pneumoniae* being chosen as the phenotype to observe.⁷⁴ Thousands of analogues of the original oxazolidinones were synthesised and evaluated, eventually leading to the discovery of linezolid, **31** and eperezolid, **37** (Figure 1.13 – Panel C).

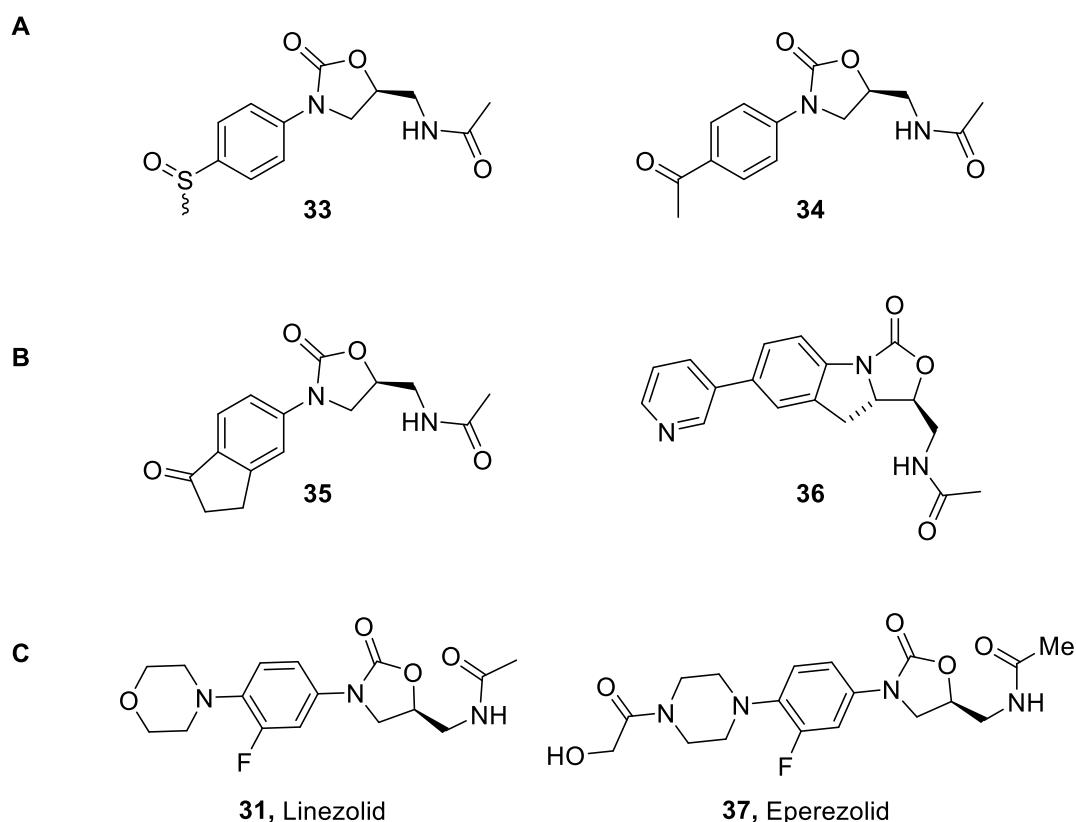


Figure 1.13 The Discovery of Linezolid - Panel A: Structures of the first oxazolidinone leads discovered.^{72,73} Panel B: Structures of oxazolidinones discovered from the SAR of leads **33** and **34**. Panel C: Linezolid, **31** and Eperezolid, **37**, the two oxazolidinones that made it through to clinical trials in the oxazolidinone research programme.⁷²⁻⁷⁴

Due to its far superior pharmacokinetic properties, linezolid, **31** was advanced through all three phases of clinical trials and eventually commercialised in the early 21st century for the treatment of *S. aureus* (methicillin-susceptible or MRSA), *S. pneumoniae* (penicillin-susceptible or multidrug-resistant strains) and vancomycin-resistant *E. faecium* as a last resort antibiotic.^{73,74} Both linezolid, **31** and eperezolid, **37** are solely used to treat resistant Gram-positive bacteria and display good activity against multiple different strains (Table 1.3). Most importantly, the MIC for linezolid, **31** against both methicillin-susceptible and methicillin-resistant *S. aureus* is identical when tested against 100 clinical isolates; $1-8 \mu\text{g mL}^{-1}$ (i.e. $2.9 - 23.7 \mu\text{M}$).

Strain (no. of clinical isolates)	MIC / $\mu\text{g mL}^{-1}$	
	Linezolid, 31	Eperezolid, 37
<i>S. aureus</i> (200)		
Methicillin susceptible (100)	1-8	1-8
Methicillin resistant (100)	1-8	1-8
<i>S. epidermidis</i> (59)		
Methicillin susceptible (24)	1-2	0.5-2
Methicillin resistant (35)	0.5-4	0.5-2
<i>Peptostreptococcus</i> (50)		
	0.25-2	0.25-1.0
<i>C. perfringens</i> (50)		
	1-4	1-2
<i>C. difficile</i> (50)		
	1-2	0.5-1
<i>B. fragilis</i> (50)		
	2-4	2-32
<i>Fusobacterium</i> (30)		
	0.25-8	0.125-2
<i>E. faecalis</i> (25)		
	1-4	1-4
<i>E. faecium</i> (25)		
	0.5-4	0.5-4

Table 1.3 Minimum inhibitory concentrations (MICs) of Linezolid, **31** and Eperezolid, **37** against different Gram-positive strains of bacteria - MIC values from all clinical isolates have been quoted as a range for each strain.^{75,76}

1.3.3.2 The Development of 4(3*H*)-Quinazolinones

The quinazolinones are a class of antibacterial compound discovered to possess Gram-positive activity against multiple strains of bacteria by inhibition of penicillin-binding proteins 1 and 2a (PBP1 and PBP2a).⁷⁷ Many SAR studies have been performed on this motif to expand the library of antibacterial quinazolinones.⁷⁸ Many of these SAR studies have been performed by altering the substituents in three different parts of the scaffold (Figure 1.14) and investigating the activity against *S. aureus* strain ATCC29213. Quinazolinones **38a**, **38b**, **38c**, **38e** and **38i** all contained a phenyl ring in the 3-position with a *m*-substituted phenol group. The positioning of a *m*-hydroxy substituent on the phenyl ring was shown to be important to obtain highly active quinazolinones and so, was incorporated into a wide range of the scaffolds investigated. It was also noted⁷⁹ that alteration of the hydroxy substituent with an alkyne, **38d** or a methoxy alkyne, **38f** yielded antibacterial quinazolinones with MICs of $1 \mu\text{g mL}^{-1}$ (i.e. $2.4 \mu\text{M}$) and $0.5 \mu\text{g mL}^{-1}$ (i.e. $1.3 \mu\text{M}$) respectively. The substitution on the 3-position was further studied⁸⁰

when investigating the effect of different amides in the *m*-position of the benzyl ring. The inclusion of an ⁱPr group attached to the amide in **38g** increased the activity to 0.25 $\mu\text{g mL}^{-1}$ (i.e. 0.58 μM), showing this area of the quinazolinone tolerated secondary amides. For **38h**, a pyrrolidine was also tolerated, however the ring system in this position increased the activity to 4 $\mu\text{g mL}^{-1}$ (i.e. 9.0 μM), approximately 16-fold higher than the secondary amide in **38g**.

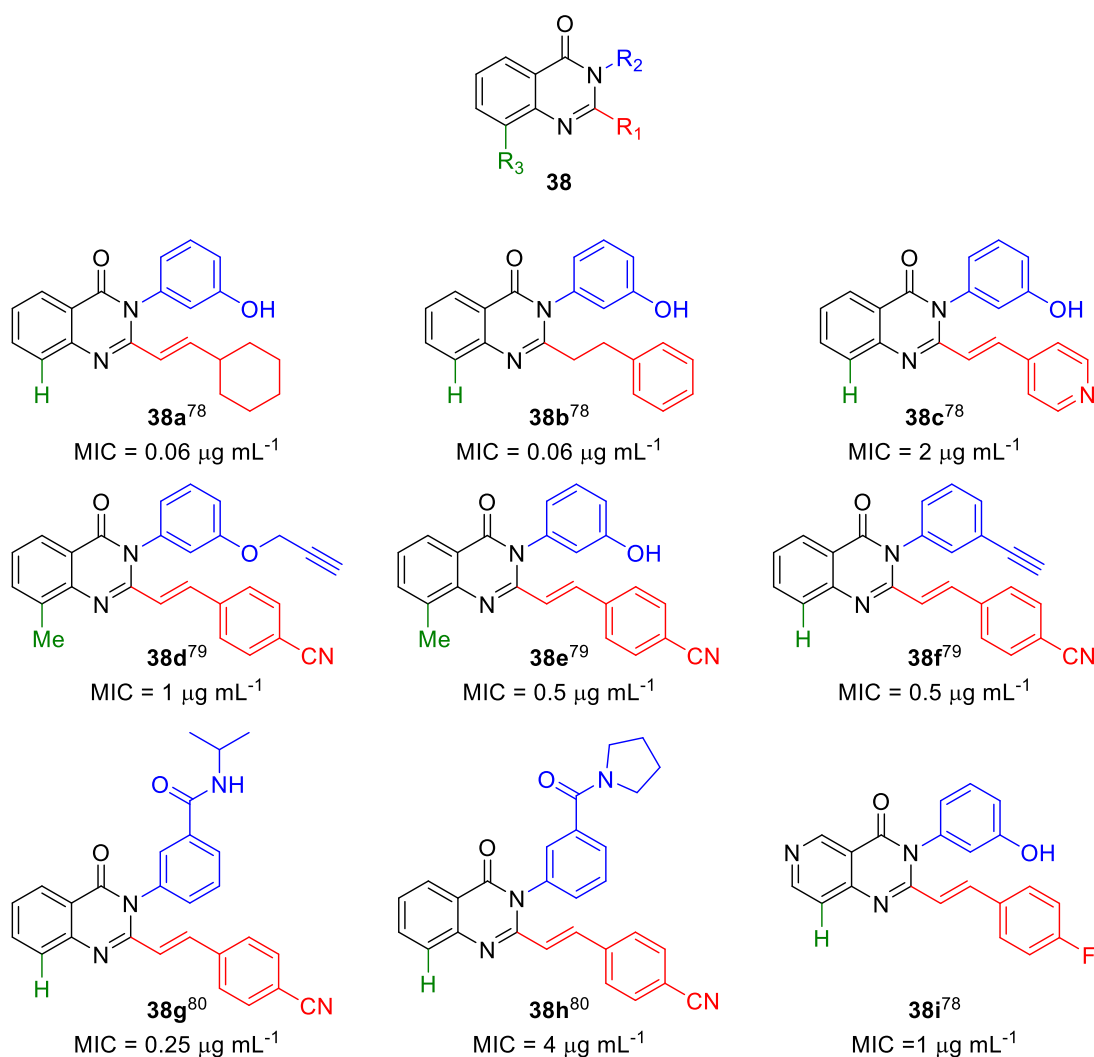


Figure 1.14 A selection of some structures of antibacterial quinazolinones, **38** and their corresponding minimum inhibitory concentrations (MIC) against *S. aureus* strain ATCC29213 - Diversification on the 2-position (red), 3-position (blue) and the 8-position (green) has been indicated.⁷⁸⁻⁸⁰

The 2-position on the quinazolinone was also acceptable of change however was less flexible than the 3-position. All ligands, **38a-38i**, contain a ring system attached to a 2-carbon linker in the 2-position. This was shown to be extremely important in obtaining activity within these types of scaffold. The quinazolinones tolerated changes to the benzyl ring in some cases, with a cyclohexane ring in **38a** producing an activity of $0.06 \mu\text{g mL}^{-1}$ (i.e. $0.17 \mu\text{M}$) against ATCC29213 and alterations to the 2-carbon linker, as in **38b** where the alkene was hydrogenated to the alkane, producing an activity of $0.06 \mu\text{g mL}^{-1}$ (i.e. $0.18 \mu\text{M}$) against ATCC29213. Substitution in the *p*-position of the phenyl ring, was also tolerated (**38c-38i**), showing significant activity against *S. aureus* strain ATCC29213 and showing this ring could be decorated with electron withdrawing groups. The SAR from these three studies have been summarised (Figure 1.15) along with the discoveries from two different investigations which altered the substituent on the 6-position of the quinazolinone, showing some antibacterial activity with chlorine, methyl, methoxy and NO_2 substituents.

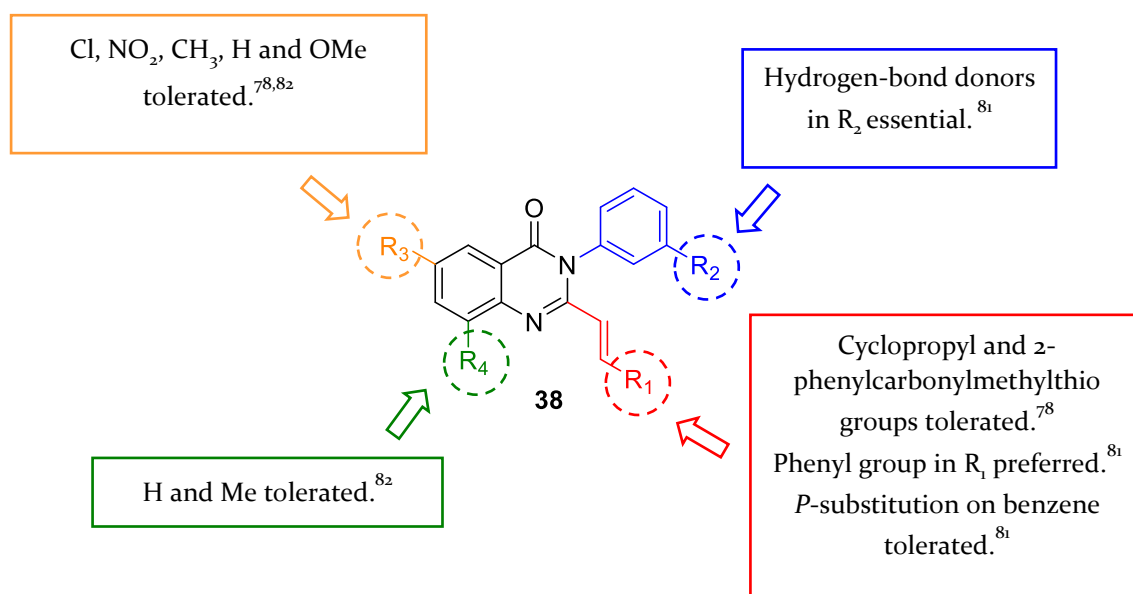


Figure 1.15 Structure-Activity Relationships (SAR) of a selection of reported antibacterial quinazolinones - The most commonly explored sites of diversification have been highlighted in circles.^{78,81,82}

1.3.3.3 Exploitation of High-Throughput Screening in Target-Based Discovery of Novel Antibiotics

High-throughput screening (HTS) is a powerful tool in medicinal chemistry which allows the screening of thousands of compounds from a library quickly to find hits and lead compounds for targets. HTS has been used on both phenotypic assay and target-based assays in the attempt to increase the speed of discovery of novel antibiotics and new scaffolds.⁸³

Target-based HTS are easy to perform as many of the enzymes within bacterial cells that have been identified as promising targets have existing assays and methodologies set up that are easy to access from the literature.⁸⁴⁻⁸⁹ One HTS campaign that began in 1995 and finished in 2001 ran 67 screens (each screen for a different target) against the SmithKline Beecham compound collection (260,000-530,000 compounds).⁸³ Out of all of these campaigns, only 16 screens gave rise to hits and only five resulted in lead compounds. The remainder of the hits were unable to be synthetically modified to produce lead compounds and were not investigated further.

The targets that were found to produce successful lead compounds were β -ketoacyl-acyl carrier protein synthase III (FabH), Enoyl-acyl carrier protein reductase (FabI), Peptide deformylase (PDF), methionyl tRNA synthetase (MetRS) and phenylalanyl-tRNA synthetase (PheRS). Although targeting Ribonuclease P (RNaseP) produced hits which showed promising bioactivity, the hits were found to indiscriminately destroy the cell membrane integrity of both bacterial and mammalian cells and thus were not suitable for clinical use. The most potent inhibitors for MetRS **41** and FabI **39** lacked activity for a suitable range of Gram-positive or Gram-negative bacteria and so were not investigated further (Table 1.4). FabH leads had significant antibacterial activity however were unable to be modified to possess drug-like properties. PDF leads were similar in structure to those identified by other research groups and so were not pursued by GSK. The PheRS leads were still being pursued at the time of publication and there is still no data available for these hits.

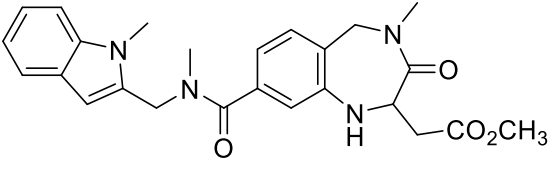
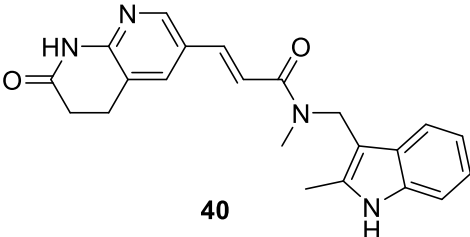
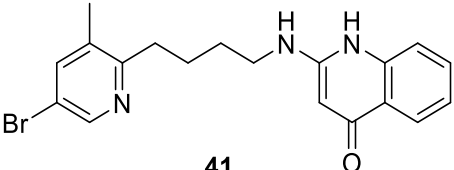
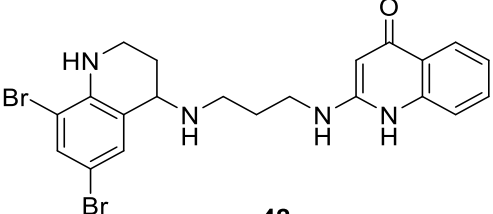
Target	Lead/Hit	Structure	Enzyme IC ₅₀ / μM	MIC / $\mu\text{g mL}^{-1}$
FabI	Hit	 39	17.1	>64
FabI	Optimised Lead	 40	0.047	0.06
MetRS	Hit	 41	0.35	>64
MetRS	Optimised Lead	 42	0.008	0.5

Table 1.4 Examples of hits and optimised leads obtained from GSK's high-throughput screen (HTS) against multiple different bacterial strains - These compounds only showed significant activity against *S. aureus* and were not pursued further.⁸³

Considering the time and money invested into the extensive target-based HTS, it is surprising that only one promising lead was discovered. This result shows that different approaches need to be developed and used in the discovery of novel antibiotics. Although this HTS was largely unsuccessful, there have been a few successes (i.e. Linezolid, **31**) and it is likely this failure was down to the diversity of the libraries used and the target-based approach that was employed.

1.3.4 Recent Advances in Gram-Negative Antibacterial Discovery

As most antibacterial targets are highly conserved across Gram-positive and Gram-negative bacteria, it has been suggested that cell entry and accumulation are the reasons for a lack of Gram-negative antibiotics. This has led researchers to investigate physical and chemical properties that can increase the speed of entry and accumulation of Gram-positive antibiotics through the outer membrane of Gram-negative bacteria.⁶⁰ Consequently, through accumulation studies of 100 compounds into *E. coli*, the “eNTRY Rules”, a set of principles that, if met by a compound, aid in Gram-negative cell accumulation, were defined (Figure 1.16 – Panel A and B).^{60,90} These rules state that compounds that contain a non-sterically encumbered basic nitrogen, have low three-dimensionality (globularity ≤ 0.25) and are relatively rigid (rotatable bonds (RB) ≤ 5) are more likely to accumulate.^{60,90} As most antibacterial targets are conserved within both Gram-positive and Gram-negative bacteria,⁶⁰ exploiting the “eNTRY” rules could aid in the formation of more Gram-negative antibiotics.⁶⁰ This hypothesis was investigated by the addition of primary amines onto Gram-positive antibiotics that had a globularity ≤ 0.25 and ≤ 5 rotatable bonds (Figure 1.16 – Panel C). Upon addition of a primary amine onto 6-DNM **44**, 6DNM-NH₃ **45** was synthesised, with activity against a broad range of multidrug resistant Gram-negative bacteria.⁹⁰ The group also investigated the literature to find examples of where addition of a primary amine repurposed the Gram-positive only antibiotic into a broad-spectrum antibiotic. One notable example found was REDXo4139 **46**, a DNA gyrase inhibitor developed by REDXPharma⁹¹, an analogue of linezolid, **31** synthesised to broaden the spectrum of oxazolidinones.⁹² Addition of a primary amine to REDXo4139 **46** to form REDXo5931 **47** significantly improved its activity against *E. coli* from a minimum inhibitory concentration (MIC) $> 128 \mu\text{g mL}^{-1}$ to $0.5 \mu\text{g mL}^{-1}$. REDXo5931 also displays some activity against *P. aeruginosa* ($16 \mu\text{g mL}^{-1}$) and *K. pneumoniae* ($8 \mu\text{g mL}^{-1}$).⁹¹ A similar improvement was noted in Ampicillin, **43** an analogue of benzylpenicillin, **24**.⁹³

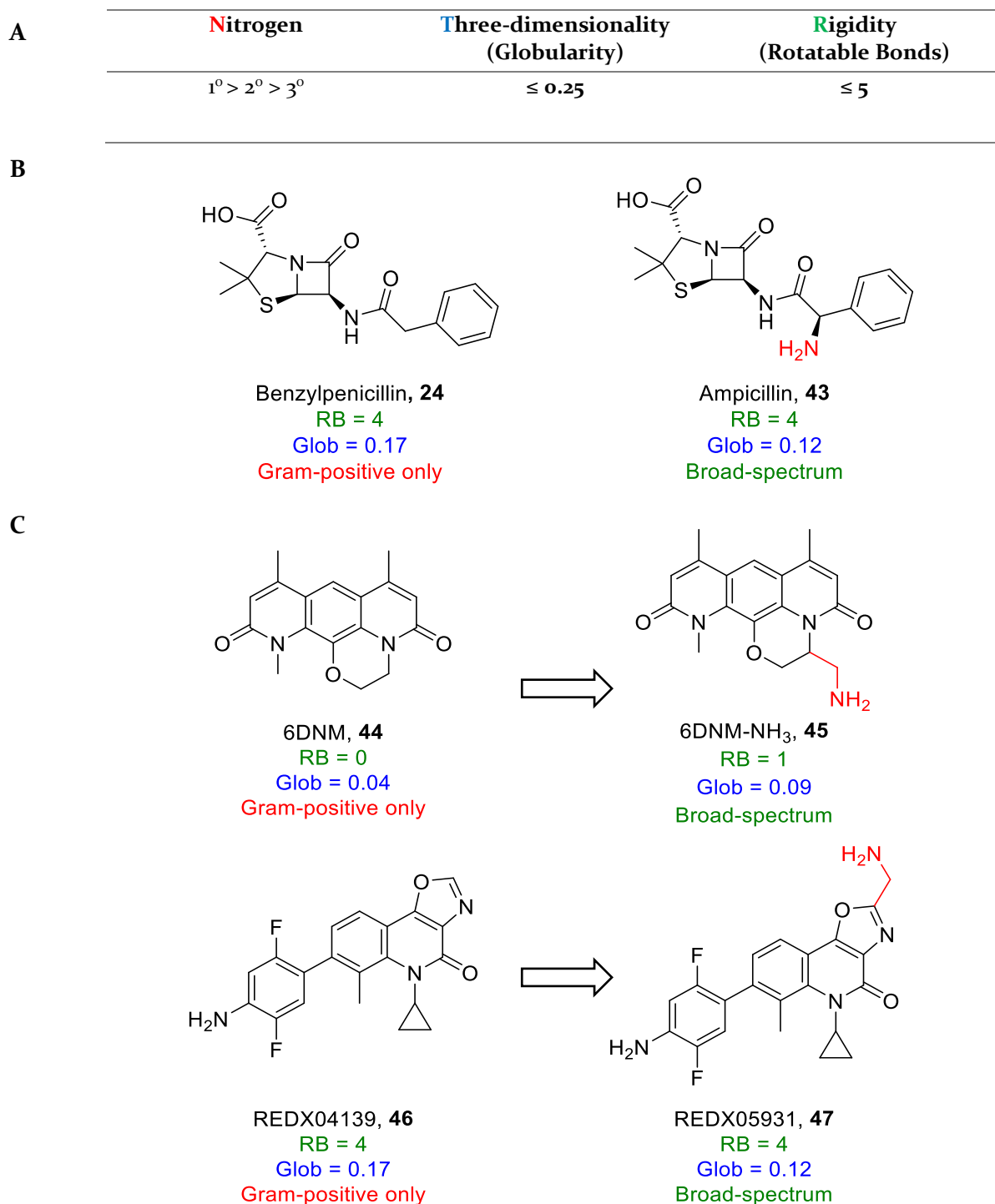


Figure 1.16 The eNTRY rules - Panel A: The rules identified that increase the likelihood of cell-accumulation into Gram-negative bacterial cells. Compounds with a non-sterically encumbered basic nitrogen, low three-dimensionality and mid-high rigidity were observed to accumulate better. Panel B: Penicillin G, **24** a Gram-positive only antibiotic that does not obey the eNTRY rules and Ampicillin, **43** a β -lactam with

a broad-spectrum of activity against both Gram-positive and Gram-negative strains of bacteria. This drug obeys the eNTRY rules (listed below the structure). Panel C: Before modification, compounds **44** and **46** possessed activity against only Gram-positive strains. Addition of a primary amine produced compounds **45** and **47** that possessed broad-spectrum antibacterial activity^{60,94}

The MICs of both Penicillin G, **24** and Ampicillin, **43** against a mixture of Gram-positive and Gram-negative strains shows that Ampicillin, **43** is active against a selection of Gram-negative bacteria, having been converted from Gram-positive only to a broad-spectrum antibiotic by addition of a primary amine (Table 1.5).

Strain	Gram-positive or Gram-negative?	MIC ₅₀ / µg mL ⁻¹	
		Penicillin, 24	Ampicillin, 43
<i>S. aureus</i> (blaZ positive)	Gram-positive	>32	>32
<i>Enterococcus sp.</i>	Gram-positive	2	0.5
<i>S. pneumoniae</i>	Gram-positive	0.01	0.02
<i>E. coli</i>	Gram-negative	64	2
<i>H. influenzae</i>	Gram-negative	0.4	0.25
<i>P. aeruginosa</i>	Gram-negative	>128 ^a	>500 ^{ab}

Table 1.5 MICs of β-lactams against six different strains of bacteria - The minimum inhibitory concentration has been reported for Penicillin, **24** and Ampicillin, **43** against a mixture of Gram-positive and Gram-negative strains to highlight Broad-spectrum toxicity of Ampicillin, **43**. *S. aureus* strain contains the blaZ gene that encodes for β-lactamases and so, MICs are higher than expected. ^a *P. aeruginosa* is resistant to both Penicillin, **24** and Ampicillin, **43**, hence no activity is observed. ^b Ampicillin, **43** was screened to a higher concentration than Penicillin, **24**.^{95,96}

1.4 Summary

Historically, medicinal chemists have tended to employ a narrow toolkit of robust reactions due to the high attrition rates of late-stage drug discovery and the need to get new molecular entities to market as quickly as possible. Consequently, only small areas of chemical space have been explored, reducing both the diversity of scaffolds discovered and creating libraries with undesirable molecular properties. Both the pharmaceutical industry and academics have noticed this problem and have implemented novel synthetic strategies (i.e. BIOS and ADS) that allow the development of a diverse range of scaffolds from highly decorated substrates and co-substrates. Activity-directed synthesis, for example, allows direct assessment of crude reaction mixtures, reducing the length of ligand discovery, as well as allowing the opportunity for diversity dependent on array design.

The lack of diverse NMEs commercialised is particularly alarming in the case of antibiotics, where a global resistance crisis has caused a sharp increase in the diversity of antibacterials required to treat both Gram-positive and Gram-negative strains of bacteria. The exploitation of HTS of compound collections has been largely unsuccessful within this field however, new strategies that assess the cell accumulation of antibacterials are being continuously assessed and may guide the discovery of a new class of antibiotic (i.e. the eNTRY rules). The efficiency of ADS, along with its ability to form a diverse range of products under the appropriate conditions, could be a useful tool to develop antibacterial ligands as starting points for drug discovery.

1.5 Project Outline

Activity-directed synthesis has been demonstrated as a powerful technique for the discovery of diverse, novel ligands against the androgen receptor. Due to its success, ADS was chosen to be exploited in antibiotic discovery, using a phenotypic screen, to identify novel antibacterial ligands. A series of project objectives was chosen which would allow the development and assessment of a phenotypic assay that could be utilised to analyse the products of an ADS array. The specific aims were:

Aim 1: To expand a series of antibacterials using activity-directed synthesis (Section 1.5.1).

Aim 2: Use ADS to discover novel antibacterial ligands with unique scaffolds (Section 1.5.2).

1.5.1 Aim 1: Activity-directed SAR Expansion

Previously, all ADS projects have focussed on using a protein-based assay (Section 1.2.2)^{2,46,47} and so there was an interest in assessing the feasibility of using this technique and screening all reaction mixtures against a phenotypic assay. The objective of this project was therefore, to harness an antibacterial growth assay, as a simple phenotypic assay, to expand the structure-activity relationship of a class of antibacterials. To do this, a set of specific objectives were chosen:

1. A suitable chemistry would be configured for use in micro-scale reactions.
2. An assay would be developed that could tolerate screening reaction mixtures and, could identify active compounds that were formed within these reaction mixtures.
3. A diverse array would be performed where both substrates and co-substrates were varied, to prepare a range of ligands, including quinazolinones (Section 1.3.3.2).
4. Active combinations would be purified, products would be structurally elucidated, and bioactive ligands characterised.

It was hoped that this approach would enable rapid expansion of a class of antibacterials and aid in the definition of key structure-activity relationships.

1.5.2 Aim 2: Activity-directed discovery of novel antibacterial classes

In all previous ADS projects that have been deployed, structures within reactions arrays have, in some way, been inspired by known ligands i.e. known active fragments have been incorporated into substrates (Section 1.2.2).^{2,46,47} Therefore, a more ambitious approach was envisioned, that would involve the discovery of chemotypes that were not based on any known antibacterial compounds. For this

project, Rh chemistry would be chosen as it has many possible outcomes and has been shown to tolerate micro-scale reactions (Section 3.1.1). It was proposed that an array of diverse substrates and co-substrates would be prepared and screened against the phenotypic assay developed in Aim 1, to identify promising 'hit' reactions. Promising reactions would be scaled-up, validated biologically and products would be structurally elucidated. Active products would be further assessed for eukaryotic toxicity and tested against multiple different strains of bacteria. For this to be possible, a set of specific objectives were chosen:

1. A diverse array would be performed, where substrates, co-substrates and catalysts were varied to prepare a range of chemotypes.
2. Products from hit reactions would be isolated and structurally elucidated.
3. These products would be validated and biologically evaluated.

It was hoped this approach would unlock new antibacterial chemotypes.

2 Chapter 2. Activity-Directed Expansion of the SAR of Antibacterials

Activity-directed synthesis (ADS) has been used in target-based ligand discovery against the androgen receptor^{2,46} by George Karageorgis (University of Leeds) to successfully aid in the discovery of diverse series of novel submicromolar agonists (Section 1.2.2). It was envisaged that ADS could be adapted to harness whole-cell assays, specifically, by measuring cell growth of *Staphylococcus aureus* (*S. aureus*), to discover novel bioactive compounds within reaction mixtures. A whole-cell antibacterial assay was chosen to be harnessed against a Gram-positive strain of *S. aureus*, ATCC29213 to investigate the feasibility of a phenotypic screening approach used in parallel with ADS.

Chapter two of this thesis focuses on studies to demonstrate the feasibility of using ADS to expand the structure-activity relationship (SAR) of a series of quinazolinones⁷⁸, thus allowing the feasibility of exploiting phenotypic screening in ADS to be assessed.⁹⁷

2.1 Rationale for the Selection of Pd⁰ Catalysed Chemistry to Underpin ADS

It was envisaged that Pd-catalysed chemistry could be used as an alternative to the metal carbenoid chemistry that had previously been harnessed for target-based ADS^{2,46} due to its potential to form a variety of scaffolds from one common substrate and its ability to form a quinazolinone core, in the presence of a carbon monoxide source.

2.1.1 The Potential of Pd⁰ Chemistry in Antibacterial Drug Discovery

For Pd-catalysed chemistry to be a promising contender for ADS, it needed to be able to form multiple scaffolds, including at least one with annotated antibacterial

activity (Figure 2.1). This chemistry, in the presence of a carbon monoxide source, can form a quinazolinone core (i.e. **38**), a scaffold which has previously been explored as an antibacterial ligand that targets penicillin-binding proteins (PBPs, Section 1.3.3.2).⁷⁸

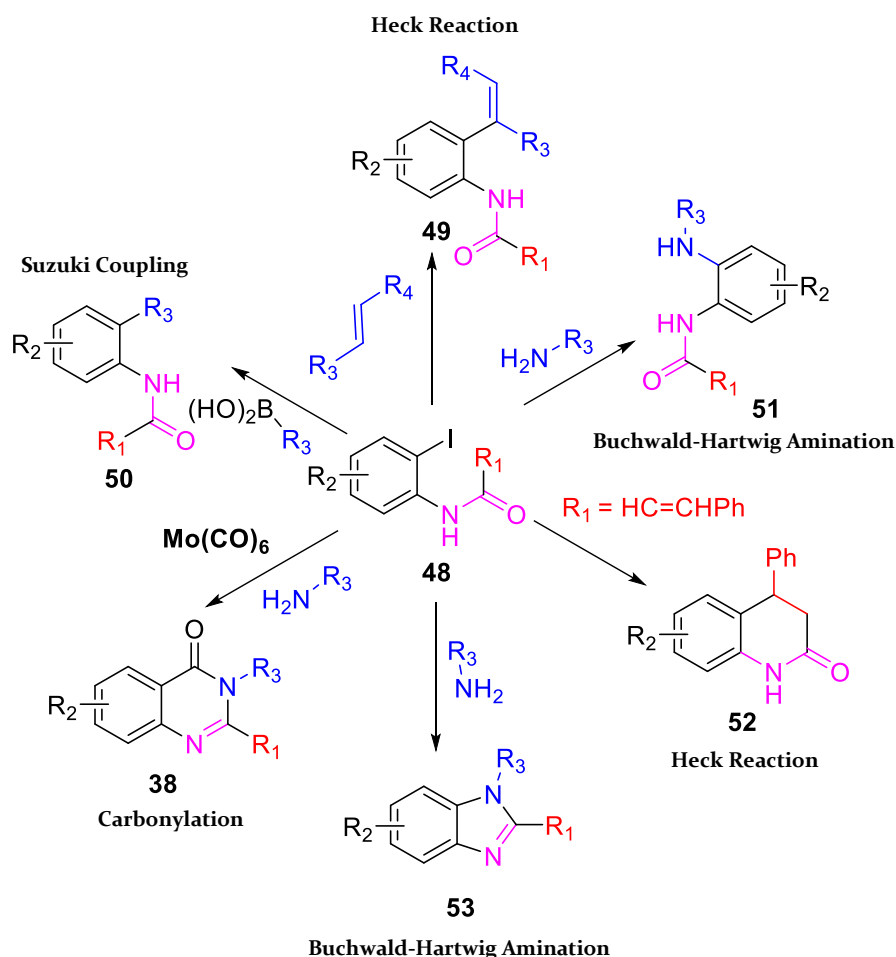
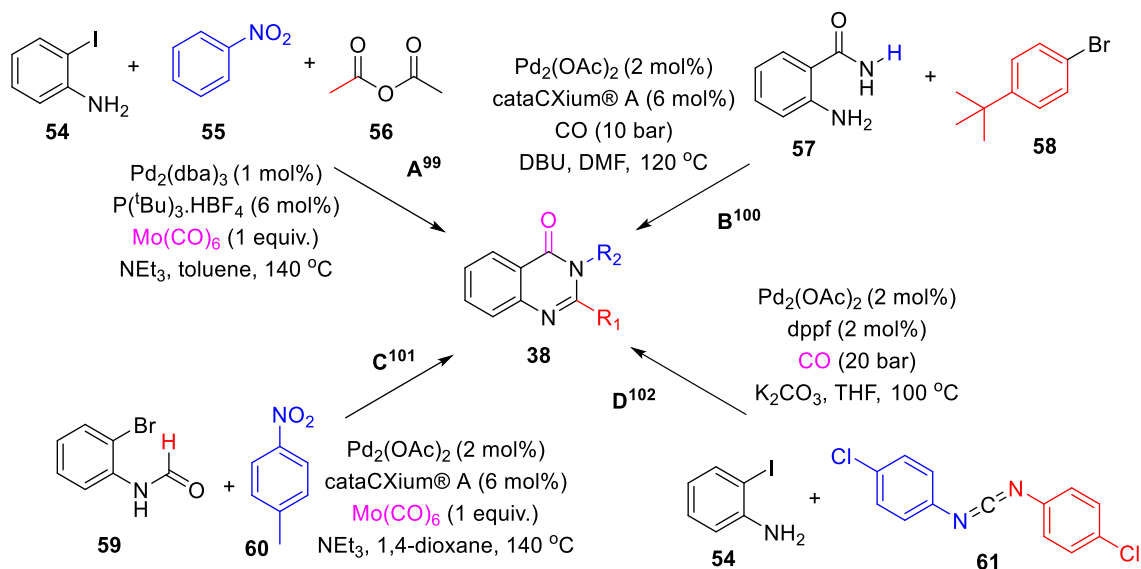


Figure 2.1 Potential of Pd-catalysed chemistry to yield alternative scaffolds from structurally related substrates and, in some cases, a carbon monoxide source - Groups derived from a co-substrate (blue) have been indicated. Reaction types accessible using this chemistry include carbonylation, amination, C-C coupling and cyclisation.⁹⁸

Alternative related substrates accessible using this chemistry include the Suzuki coupling, the Buchwald-Hartwig amination and the Heck cyclisation. Pd-catalysed aminations, without carbonylation, can yield anilines (e.g. **51**) or, with

subsequent cyclisation, benzimidazoles (e.g. **53**). An intramolecular Heck reaction could yield quinolinones (e.g. **52**) or in the presence of an alkene co-substrate and substrate, a new alkene (e.g. **49**). Finally, in the presence of a boronic acid, a new carbon-carbon bond could form via the Suzuki coupling reaction (e.g. **50**). All these reactions yield alternative scaffolds from similar substrates.⁹⁷

Quinazolinones are commonly synthesised from the amidation and cyclisation of 2-aminobenzoic acid derivatives;⁷⁸ however, there are multiple Pd-catalysed methods to synthesise the core scaffold in the presence of a carbon monoxide source (Scheme 2.1). Reaction **A** is a four-component synthesis of 4-(3*H*)-quinazolinones. This method uses acetic anhydride or other substituted alternatives to decorate the 2-position of the scaffold, Mo(CO)₆ as a carbon monoxide source and a Pd⁰ ligand. Similar conditions are used in reaction **C** to form a 2-H, 3-benzyl substituted quinazolinone, except this reaction no longer requires use of acetic anhydride and shows that replacement of the aniline and anhydride with a formamide is tolerated in the formation of quinazolinones. Both reactions **B** and **D** use CO gas as the carbonylating source, rather than forming it *in situ*. This allows the reaction temperature to be reduced but requires high pressures to yield products and so would not easily be possible for ADS. Reaction **B** produces a quinazolinone with no substitution in the 3-position and, in the 2-position, a 4-^tBu phenyl group whilst reaction **D** decorates both the 2 and 3-position with an identical substituent, obtained from the same co-substrate.



Scheme 2.1 Synthesis of the quinazolinone scaffold using palladium catalysed carbonylation - Groups derived from an amine co-substrate (blue), an additional co-substrate component (red) and carbon monoxide (pink) are indicated.^{99–102}

Pd-catalysed reactions all begin from the oxidative addition of the halogenated substrate (usually an iodine or a bromine) onto the Pd⁰ to form a Pd^{II} complex. For carbonylation (Figure 2.2, red) the oxidised Pd species is carbonylated in the presence of carbon monoxide to form acyl palladium species **63**. If a nucleophile, such as an amine or an alcohol, is added to the reaction mixture, it can attack into the complex to form the respective amide or ester, **65**. The Pd^{II} species is then reduced back to Pd⁰ and the catalytic cycle is repeated. Although not displayed in Figure 2.2, this product can undergo dehydration at high temperatures to form a quinazolinone. The Heck reaction (Figure 2.2, black) occurs in the presence of an alkene. The alkene co-ordinates with the Pd^{II} species formed from oxidative addition and undergoes migratory insertion, forming a bond with the Pd after abstracting the R group from the complex, **67**. A β -H elimination then occurs, dissociating the newly formed alkene from the complex with substitution by a hydrogen, **68**. The Pd^{II} is reduced back to Pd⁰ by reductive elimination and the catalytic cycle repeats.

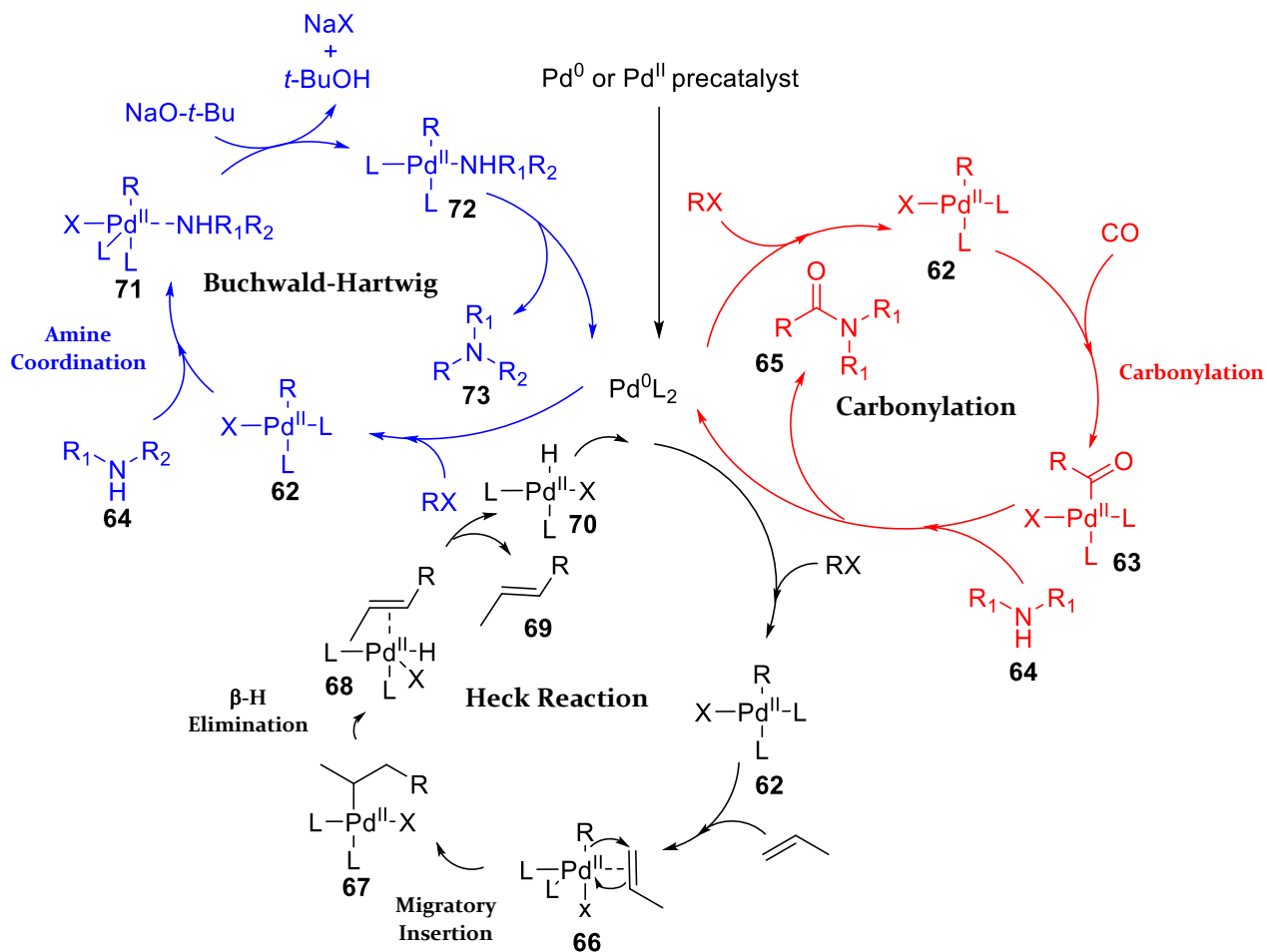


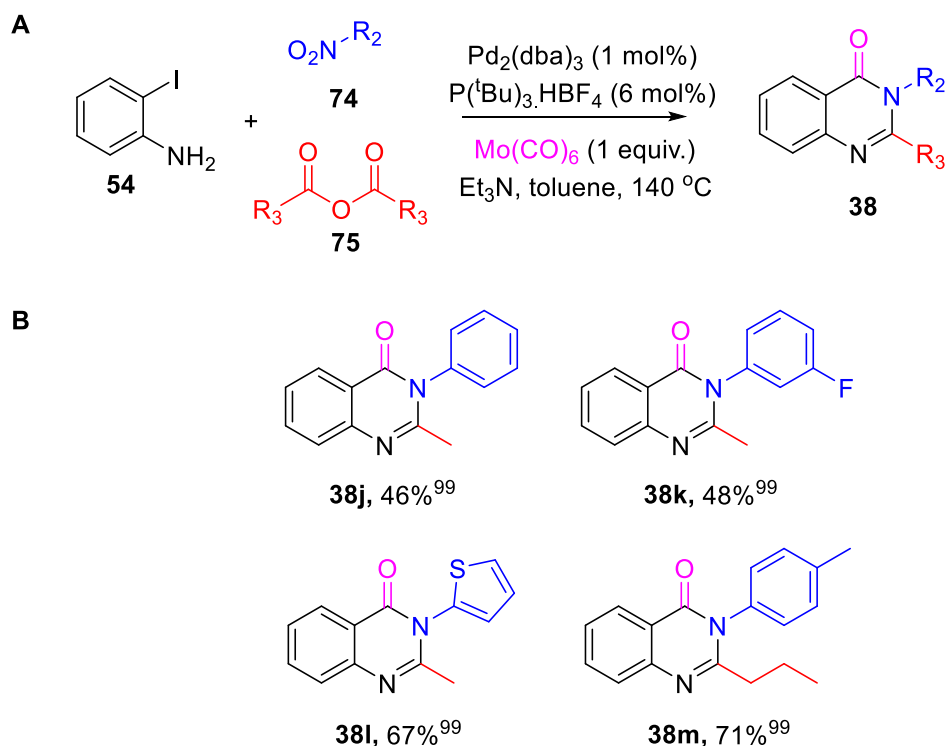
Figure 2.2 Outline mechanisms for aminocarbonylation (red)¹⁰³, the Heck catalytic cycle (black)¹⁰⁴ and the Buchwald-Hartwig Amination (blue)¹⁰⁵ - Oxidation states have been quoted on the relevant palladium species assuming two donor ligands (L) are attached to the metal complex.

The Buchwald-Hartwig amination (Figure 2.2, blue), occurs in the presence of an amine which can co-ordinate to the Pd^{II} complex to form a five-group substituted complex, **71**. The presence of a base allows the abstraction of the halogen from the complex to form a square planar Pd^{II} complex, **72**. This undergoes reductive elimination, releasing the newly formed amine and reforming Pd⁰. These three mechanisms may all be plausible under the same reaction conditions, depending on the functional groups available within the substrates and co-substrates. Careful selection of substrate and co-substrate using ADS may therefore allow a diverse range of scaffolds to be accessible under the reaction conditions and consequently explored

including a broad range of quinazolinones scaffolds. However, optimisation is still required to form disubstituted quinazolinones in significant yield that can be detected within reaction mixtures. As the chemistry allows both the formation of a known antibacterial scaffolds and still allows scaffold diversification, it is a good choice for activity-directed expansion of the known SAR and validation that phenotypic ADS is possible.

2.2 Configuration of Carbonylation Chemistry for Activity-Directed Synthesis

A known carbonylation reaction that could form quinazolinones was initially optimised for execution under conditions suitable for ADS.⁹⁷ The four-component reaction discussed in Section 2.1.1⁹⁹ allowed the formation of disubstituted quinazolinones, which could be modified to form a diverse range of quinazolinone substrates (Scheme 2.2). This reaction has been used to form quinazolinones with a broad range of diversity in the 3-position, with the 2-position commonly containing a methyl group. Quinazolinones with a phenyl ring as in **38j**, a *m*-substituted phenyl ring as in **38k**, a *p*-substituted phenyl ring as in **38m** and thiophene as in **38l** have all been successfully synthesised. Substitution in the 2-position is limited by the availability of the anhydride and most scaffolds discovered were formed from acetic anhydride, consequently substituting this position with a methyl group. It is important to note that **38m** contains a propyl substituent and forms the respective quinazolinone in good yield, allowing us to hypothesise substrates with a 2-carbon linker would yield product under these reaction conditions (Section 1.3.3.2).



Scheme 2.2 Synthesis (obtained from the literature)⁹⁹ of quinazolinones using a four-component carbonylative method - Panel A: General Synthetic Scheme. Panel B: Structures and yields of four quinazolinones reported⁹⁹ using this method. Groups derived from a co-substrate (blue), an additional co-substrate component (red) and carbon monoxide (pink) have been indicated.

Initially, the Pd-catalysed carbonylation reaction was adapted for use on a 3 mL scale (1 mmol substrate) in crimp-top vials (Table 2.1).⁹⁷ Accordingly, the *o*-iodo anilide **48a** or *o*-iodo aniline **54** (final concentration: 333 mM), nitrobenzene (1.2 equiv.), $\text{Mo}(\text{CO})_6$ (1 equiv.), $\text{Pd}_2(\text{dba})_3$ (0.1 mol%), $\text{P}(\text{tBu})_3 \cdot \text{HBF}_4$ (0.6 mol%) and NEt_3 (2.5 equiv.) were dissolved in toluene; after sealing, the vial was heated at the reported temperature for 48 h.⁹⁷ Reaction A, between aniline **54** and nitrobenzene **55**, was designed to investigate the feasibility of the four-component carbonylation reaction⁹⁹ when reducing the catalyst loading from 1 mol% to 0.1 mol% and performing the reactions under air. The reaction yielded the expected quinazolinone product in 11% yield (Table 2.1). The second reaction investigated, between acetanilide **48a** and nitrobenzene **55**, removed the anhydride component and replaced aniline **54** with

acetanilide **48a**. The suggested reaction mechanism hypothesised⁹⁹ that the anilide was formed *in situ* under the reaction conditions before undergoing a carbonylation and nucleophilic substitution and so, replacement of the anhydride with an anilide was believed to be tolerated under the reaction conditions. It had been shown that this reaction is possible with different catalysts and bromo-substrates which further supported this hypothesis (Scheme 2.1). The reaction was performed at 105 °C for 48 h, yielding a 19% yield of quinazolinone **38j**. It is important to note that the temperature was reduced to 105 °C due to the heating capabilities of the microvial equipment used for ADS. The seal used in the Optibloc™ would not be able to maintain a perfect seal at higher temperatures, which could adversely affect the yield of the carbonylation reaction. These experiments demonstrated that the chemistry had the potential to be suitable for ADS and was ready to be tested in a microvial format.

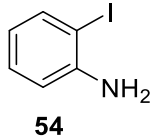
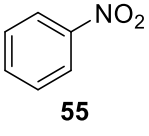
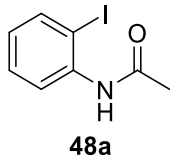
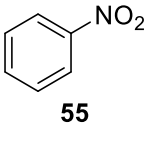
Substrate	Co-Substrate ^a	Solvent	Reactants	Temperature ^b / °C	Yield ^c / %
 54	 55	Toluene	Pd ₂ (dba) ₃ (0.1 mol%) P(^t Bu) ₃ .HBF ₄ (0.6 mol%) Mo(CO) ₆ , NEt ₃ Ac ₂ O Air	140	11
 48a	 55	Toluene	Pd ₂ (dba) ₃ (0.1 mol%) P(^t Bu) ₃ .HBF ₄ (0.6 mol%) Mo(CO) ₆ , NEt ₃ Air	105	19

Table 2.1 Configuration of Pd-catalysed chemistry for use in ADS - Reaction in row one is a replication of multi-component carbonylation⁹⁹ with the exception of using a lower catalyst loading and performing the reaction under air (indicated in bold). The reaction in row two has been altered by using an acetanilide in place of acetic anhydride. All crude mixtures were purified to determine yield. ^a Reactions performed

on a 1 mmol scale: substrate (final concentration: 333 mM), co-substrate (1.2 equiv.), $\text{Mo}(\text{CO})_6$ (1 equiv.) and NEt_3 (2.5 equiv.).^b Reaction performed in a sealed crimp-top vial. ^c Yield of purified product reported.

2.2.1 Configuration of Chemistry in Microscale Format

Converting the reactions to a microvial format required the exploitation of an Optibloc™ that has been designed to heat 96-wells, at a set temperature, in parallel (Figure 2.3). The block has slots available for borosilicate glass vials which are used commonly for ADS reactions and the plate comes with a seal which can be used during heating to prevent solvent loss.

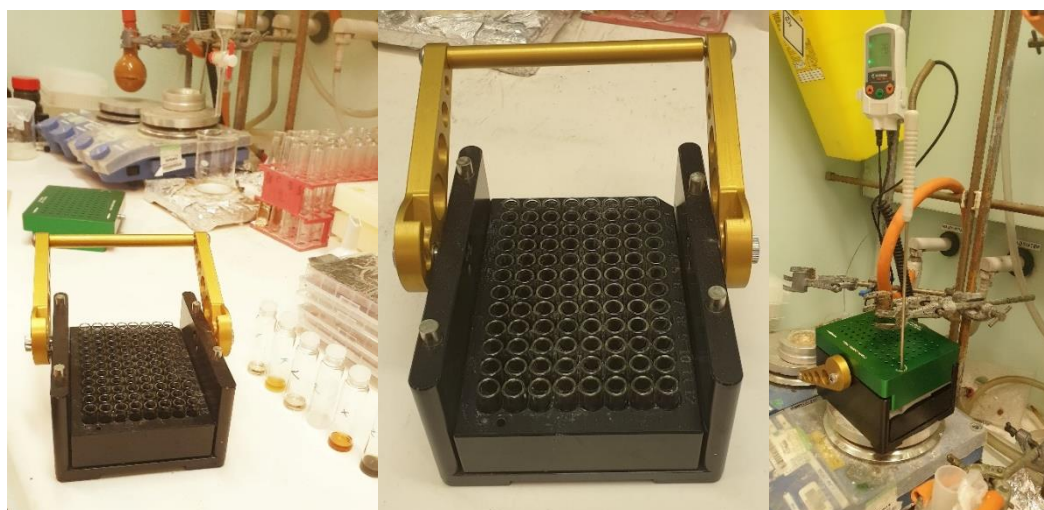


Figure 2.3 Photographs of the experimental set-up used to conduct heated microscale reactions - Reaction components are added to their respective vials from stock solutions, the plate is sealed and heated to the reaction temperature (right-hand photo).

The Pd-catalysed carbonylation reaction (Section 2.2) was adapted for execution on a 300 μL scale (100 μmol substrate) in a 96-well plate format. Reactants were not added as stock solutions during the initial experiments to ensure both microscale reactions from solids and then solutions were investigated separately. Individual reaction components were added to wells as described in Section 2.2 and

were dissolved in either toluene or *o*-xylene; after sealing, the plate was heated to 105 °C for 48 h.⁹⁷ After evaporating the *o*-xylene, dissolving in EtOAc and filtering the crude mixtures through silica, the solutions were left to evaporate.

The first microscale reaction investigated was between anilide **48a** and nitrobenzene **55** in toluene (Table 2.2). The solid residue formed during this reaction was no longer in the well, instead dispersed on the seal due to solvent evaporation and so, this crude product was not analysed. Consequently, it was decided the reaction between **48a** and **55** would be performed in *o*-xylene due to its chemical similarity to toluene and higher boiling point (*o*-xylene: 144 °C, toluene: 110 °C). Under these conditions, quinazolinone, **38j** was formed in an 18% yield, determined by quantitative NMR, with 333 mM of dichloromethane as a reference. The final two reactions were performed from stock solutions of reactants: anilide **48a** (1.00 M in THF), nitrobenzene/aniline **76** (1.20 M in THF), P(^tBu)₃.HBF₄ (2.00 mM in *o*-xylene) and tris(dibenzylideneacetone)dipalladium(o) (0.33 mM in *o*-xylene). Both triethylamine (35 μL) and MoCO₆ (26 mg) were added as a liquid and solid respectively.⁹⁷ Within this reaction, the yield dropped to 14%, however, assay optimisation would ensure active quinazolinones were detectable if yields were low. By replacing the nitrobenzene, **55** with aniline, **76**, the respective quinazolinone, **38j** was formed with a 20% yield, determined by quantitative NMR.

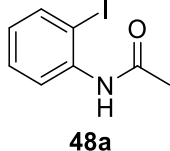
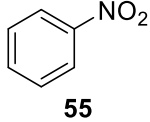
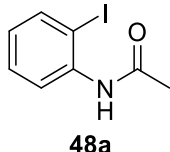
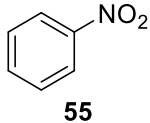
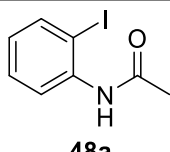
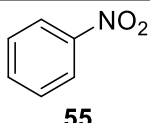
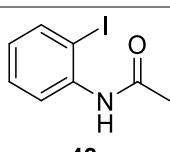
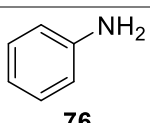
Substrate	Co-Substrate ^a	Solvent	Reactants	Assembled from stocks?	Temperature / °C	Yield / %
 48a	 55	Toluene	Pd ₂ (dba) ₃ (0.1 mol%) P(^t Bu) ₃ ·HBF ₄ (0.6 mol%) Mo(CO) ₆ , NEt ₃ Air	✘	105	0
 48a	 55	<i>o</i> -xylene	Pd ₂ (dba) ₃ (0.1 mol%) P(^t Bu) ₃ ·HBF ₄ (0.6 mol%) Mo(CO) ₆ , NEt ₃ Air	✘	105	18 ^b
 48a	 55	<i>o</i> -xylene	Pd ₂ (dba) ₃ (0.1 mol%) P(^t Bu) ₃ ·HBF ₄ (0.6 mol%) Mo(CO) ₆ , NEt ₃ Air	✓	105	14 ^b
 48a	 76	<i>o</i> -xylene	Pd ₂ (dba) ₃ (0.1 mol%) P(^t Bu) ₃ ·HBF ₄ (0.6 mol%) Mo(CO) ₆ , NEt ₃ Air	✓	105	20 ^b

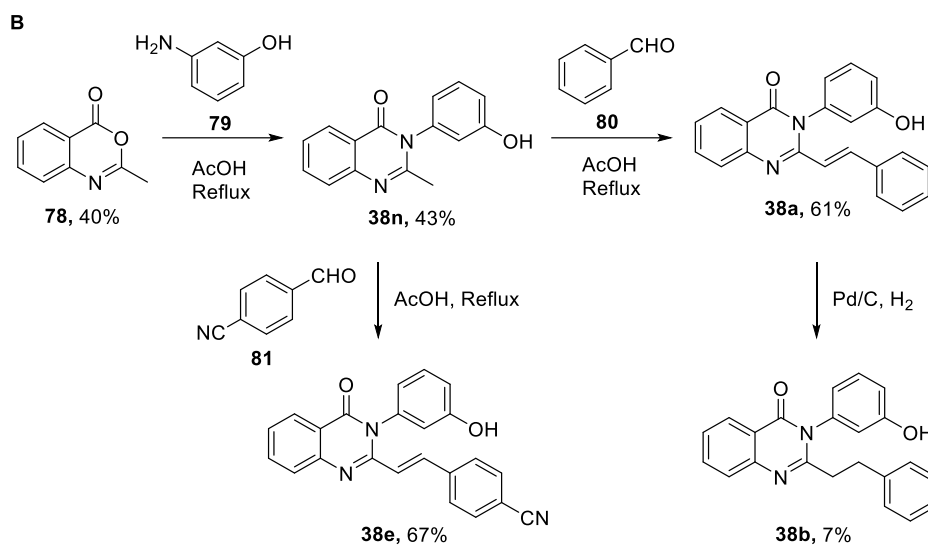
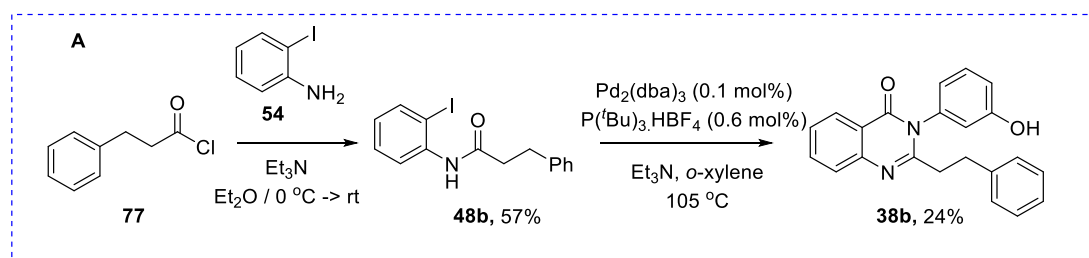
Table 2.2 Configuration of Pd-catalysed chemistry for use in ADS - ^a Reactions performed on 100 μmol scale: substrate (final concentration: 333 mM), co-substrate (1.2 equiv.), Mo(CO)₆ (1 equiv.) and NEt₃ (2.5 equiv.). ^b Quantitative NMR was used to calculate the respective yield. All reactions were performed in borosilicate vials using the experimental set-up displayed in Figure 2.3.

These experiments confirmed that the carbonylation chemistry was possible on a microscale format suitable for ADS, yielding between 14-20% quinazolinone in each case.⁹⁷ Although some quantities of reactants had to be altered for the reaction (i.e. the catalyst system) and yields were lower, the quinazolinone species were still detectable in a quantity which, after assay optimisation, would be visible within an antibacterial screen.

2.2.2 Demonstration of the Feasibility of Activity-Directed Antibacterial Discovery

Before an ADS array could be designed and performed, it was essential to demonstrate that a known antibacterial quinazolinone could be formed in a microscale reaction and its biological activity detected in the crude reaction mixture. Quinazolinone **38b** (Scheme 2.3)⁷⁸ was chosen as it was hypothesised that it would be synthetically accessible using the reaction conditions described in Section 2.2.1.

The carbonylation reaction was performed on a 3 mL scale to allow isolation of ample pure product that could then be screened against ATCC29213, the *S. aureus* strain used in the original SAR of the quinazolinones.⁷⁸ The Pd-catalysed carbonylation reaction was performed on a 3000 μ L scale (1 mmol substrate) in a crimp topped vial as described in Section 2.2. The resulting product was filtered through silica and purified using preparative LC-MS to afford quinazolinone **38b** in 24% yield. Both **38a** and **38e** were synthesised using the previously reported method⁷⁸ in 61% and 67% yield respectively. This method was a three-step synthetic route that firstly, involved the formation of oxazinone **78** by the cyclisation of anthranilic acid by heating triethyl orthoacetate. The recrystallised oxazinone **78** was dissolved in acetic acid by heating and, upon addition of a substituted aniline, refluxed for 4 h to afford quinazolinone **38n**. Addition of an aldehyde and further reflux overnight led to the formation of the respective quinazolinone. It was decided that both quinazolinones **38a** and **38e** would be isolated to provide two antibacterial quinazolinones for assay configuration. In order to confirm the structure, **38b** was also synthesised by Pd-catalysed hydrogenation of **38a**,⁷⁸ affording the expected product in 7% yield.



Scheme 2.3 Preparation of selected antibacterial quinazolinones - Panel A: Prepared using Pd-catalysed carbonylation method. **Panel B:** Prepared by condensation and in the case of **38b**, Pd-catalysed hydrogenation.⁷⁸

2.3 Establishment of Phenotypic Assay for Activity-Directed Antibacterial Discovery

An antibacterial assay was configured and tested against quinazolinone **38b** to ensure activity could be detected and bacterial growth inhibition could be quantified. A time-growth experiment (Figure 2.4) was performed to determine the length of time the bacteria needed to grow before reaching saturation. To investigate this time, three wells of 1% DMSO in Iso-Sensitest broth (ISB) were prepared, each containing a standardised amount of ATCC29213 culture (5×10^5 CFU mL⁻¹).⁹⁷ Two colonies of ATCC29213 were investigated to ensure results duplicated. Wells were incubated at 37 °C for 14 h and optical density (OD) at 600 nm was measured every two hours. It was found that cell growth was complete (OD > 1) for both duplicates after 10 h and so this time was chosen to be used for the reaction array. MIC determination would be performed on purified active species, incubating for a time of 18 h, according to CLSI guidelines.¹⁰⁶ The optimised screening time of 10 h was used whilst screening both the pure compounds and the reaction mixtures, reported within Section 2.3.1 and Section 2.3.2 respectively.

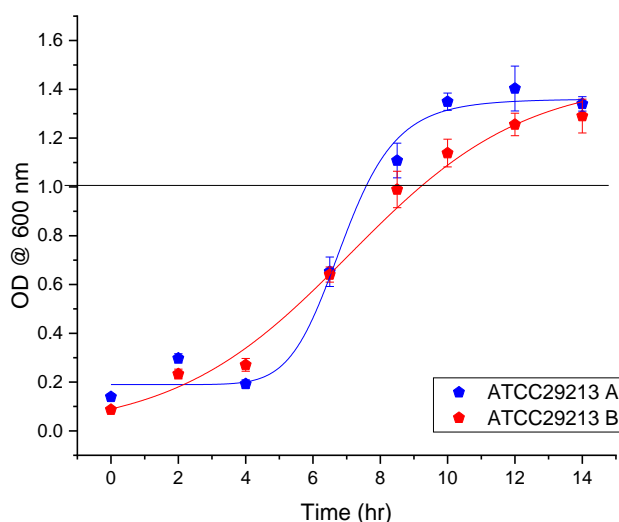


Figure 2.4 Configuration of *S. aureus* growth time in Iso-Sensitest Broth (ISB) - Wells containing 1% DMSO in ISB was incubated at 37 °C and optical density (OD) at 600 nm was measured every 2 hours. Each experiment was performed in triplicate using

two different colonies of ATCC29213. Results from both colonies have been indicated using the red and blue curves. OD = 1.0 is indicated by the black line.

2.3.1 Establishment of an Assay for the Determination of MICs

All isolated quinazolinones (Section 2.2.2) were screened against ATCC29213¹⁰⁷ and minimum inhibitory concentration (MIC) values against *S. aureus* were assessed in both ISB and cation-adjusted Mueller-Hinton Broth (MHB-II).⁹⁷ For **38b**, *S. aureus* strains SH1000,¹⁰⁸ and USA300 JE2¹⁰⁹, were also investigated in MHB-II.¹⁰⁶

For MICs, a 2-fold dilution series of the isolated compounds in DMSO was prepared, ranging from 800–0.8 $\mu\text{g mL}^{-1}$. Each dilution was transferred into a 96-well format at a final volume of 1 μL . Then, 99 μL of the standardised culture was added to each well to give final antibiotic concentrations of 8–0.008 $\mu\text{g mL}^{-1}$ (1% DMSO in ISB). Plates were incubated for 18 h at 37 °C and the MIC was determined visually as the lowest concentration at which growth was inhibited.⁹⁷ Although MICs had been quoted in growth media MHB-II within the literature,⁷⁸ it appeared from the initial screens that the quinazolinones were insoluble in this media and so MICs were not observed up to the highest screening concentration of 8 $\mu\text{g mL}^{-1}$ (Table 2.3). This trend was seen against all three different strains of *S. aureus* for compound **38b**. As the growth media was not reproducing MIC data,⁷⁸ it was switched to ISB, a buffered broth which solvated quinazolinones.

Compound	Strain of <i>S. aureus</i> ^a	Media ^b	MIC / $\mu\text{g mL}^{-1}$	EC ₅₀ / μM
38b	ATCC29213	MHB-II	> 8	> 23
38b	SH1000	MHB-II	> 8	> 23
38b	USA300 JE2	MHB-II	> 8	> 23
38a	ATCC29213	MHB-II	> 8	> 24
38e	ATCC29213	MHB-II	> 8	> 22
38b	ATCC29213	ISB	0.5-1.0	1.45-2.90
38a	ATCC29213	ISB	2-4	5.85-11.7
38e	ATCC29213	ISB	0.125-0.25	0.34-0.68

Table 2.3 Evaluation of the activity of reported quinazolinones against *S. aureus* strains ATCC29213, SH1000 and USA300 JE2 - The range of MICs observed obtained in duplicate on three different days is shown for each strain. ^a Three strains of *S. aureus* were tested in MHB-II to ensure lack of activity was not caused by mutations in ATCC29213. ^b The media used during screening was important due to the poor solubility of quinazolinones in MHB-II.

It was evident that switching the media allowed replication of activity and MICs were determined for **38b** and **38e** [**38b**: 0.5-1 $\mu\text{g mL}^{-1}$ (1.45-2.90 μM); **38e**: 0.125-0.25 $\mu\text{g mL}^{-1}$ (0.34-0.68 μM)].⁹⁷ A photograph of the MIC data obtained for **38e** and **38b** in both MHB-II and ISB has been displayed in Figure 2.5. These photographs show that within MHB-II, 100% cell growth is occurring within the four rows containing the dilution series of both quinazolinones and penicillin G, **24** is inhibiting ATCC29213 growth as expected. In ISB, both quinazolinones are inhibiting bacterial growth up to their MIC concentrations, showing that this media was essential for MIC determination. The darker yellow wells in the ISB photographs provide better contrast and occur due to faster cell growth of ATCC29213 over the same period (18 h).

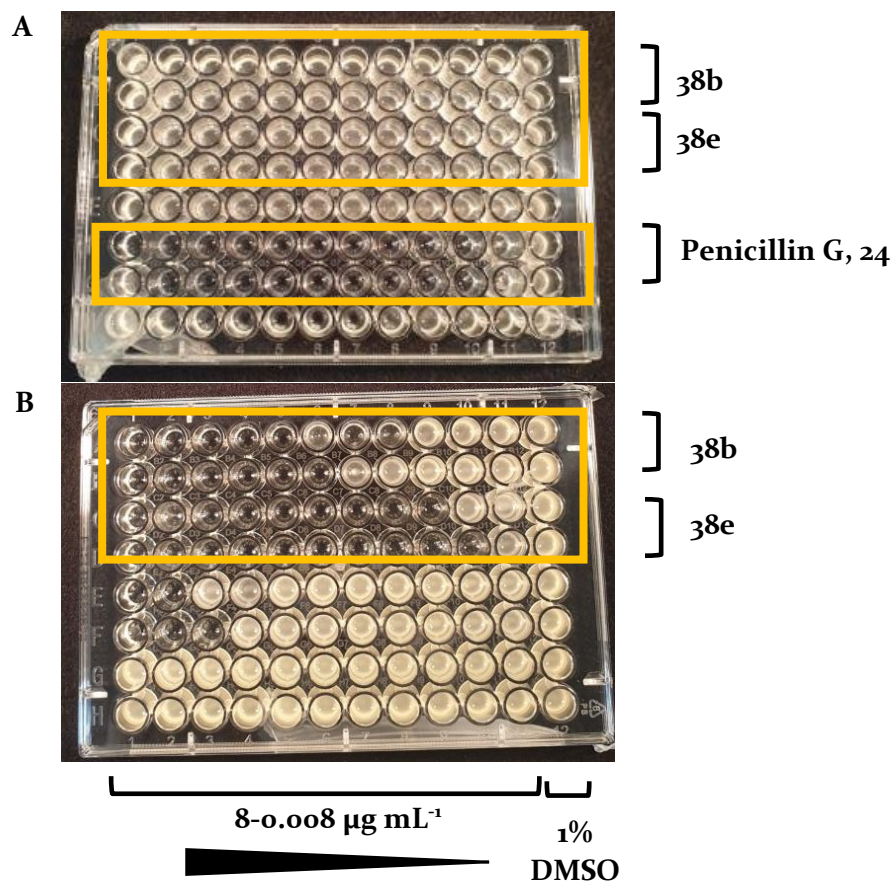


Figure 2.5 Comparison of MIC data obtained in MHB-II (A) and ISB (B) - Cloudy wells indicate 100% bacterial growth and clear wells indicate no growth. Each column is a different concentration within a 2-fold dilution series (8-0.008 $\mu\text{g mL}^{-1}$) with a blank containing 1% DMSO in column 12. Panel A: Rows 1-2: **38b** within a 2-fold dilution series performed in duplicate. Rows 3-4: **38e** within a 2-fold dilution series performed in duplicate. Rows 6-7: Penicillin G, **24** within a 2-fold dilution series performed in duplicate. Panel B: Rows 1-2: **38b** within a 2-fold dilution series performed in duplicate. Rows 3-4: **38e** within a 2-fold dilution series performed in duplicate. Wells not indicated (yellow box) were used for different experiments.

2.3.2 Detection of Activity of Reaction Components within Mixtures

To demonstrate that any unreacted starting material would not interfere with the assay, individual components were tested at the concentrations they would be used within each reaction mixture during the final array screen.⁹⁷ One mock reaction was performed for each component and four screening concentrations were investigated to inform the selection of an appropriate final screening concentration.⁹⁷ The following stock solutions were prepared: *o*-iodo anilide substrates **48a** and **48b** (1.0 M in THF); co-substrate **79** (1.20 M in THF); P(^tBu)₃·HBF₄ (2.00 mM in *o*-xylene); and tris(dibenzylideneacetone)dipalladium(*o*) (0.33 mM in *o*-xylene).

Wells were set up with the appropriate stock solutions and each well contained a final volume of 300 μL. Into well 1, a reaction known to form antibacterial quinazolinone was prepared from substrate **48b** and co-substrate **79** (Section 2.2.2). Initially, 100 μL of *o*-iodo anilide **48b** was added and after evaporation, 100 μL of co-substrate **79** was added. Upon evaporation, 26 mg of molybdenum hexacarbonyl was added using a scooper with a volume predetermined to correspond to that mass. Then, the well was redissolved in 300 μL of the P(^tBu)₃·HBF₄ and tris(dibenzylideneacetone)dipalladium(*o*) stock solution. Finally, 35 μL of concentrated triethylamine was added to the reaction mixture to give a final volume of 300 μL and a total product concentration of 333 mM.⁹⁷ Into well 2, a reaction known to form inactive quinazolinone was performed from substrate **48a** and co-substrate **79**. All reaction components were added as described above.⁹⁷

Wells 3-9 contained the individual substrates, co-substrates and reagents used within the reactions of well 1 and 2 to test whether they interfered with the assay. Each component was added at the same volume, from the same stock solution. The components of each well have been displayed in Table 2.4 along with their reaction concentration. All individual components were reacted as described in Section 2.2.1 and were dissolved in dimethyl sulfoxide (300 μL) to correspond to a final total product concentration of 333 mM (calculated from the limiting reagents from the reactions in wells 1 and 2, not for each individual component).⁹⁷ Well 10 contained **38b** a pure, *S. aureus* active quinazolinone, that did not undergo the carbonylation reaction.

Well	Substrate (333 mM)	Co-Substrate (400 mM)	Catalyst (0.33 mM)	Ligand (2.00 mM)	Mo(CO) ₆ (333 mM)	NEt ₃ (833 mM)	Quinazolinone 38b ^a
1	✓	✓	✓	✓	✓	✓	
2	✓	✓	✓	✓	✓	✓	
3	✓ ^b						
4	✓ ^c						
5		✓					
6			✓				
7				✓			
8						✓	
9					✓		
10							✓

Table 2.4 Configuration of control reactions used to determine compatibility of ADS protocol in an antibacterial assay - The components present in each reaction well have been indicated using a tick. Wells 1-9 were reacted at 105 °C for 48 h before preparation for screening. The concentration of each reaction component has been listed in the appropriate column. ^a Screening well 10 contained pure quinazolinone, **38b** to be used as a positive control for the experiment. ^b Substrate **48a**. ^c Substrate **48b**.

These stock solutions were subsequently further diluted with DMSO and screened at total product concentrations of 100 µM, 50 µM, 25 µM and 12.5 µM (1% DMSO in ISB) following the General Screening Procedure in ATCC29213 (Figure 2.6). Reaction wells were diluted in ISB containing standardised ATCC29213 as reported in Section 2.3.1.¹⁰⁶ Plates were incubated for 10 h at 37 °C and the optical density was measured using a plate reader ($\lambda = 600$ nm).

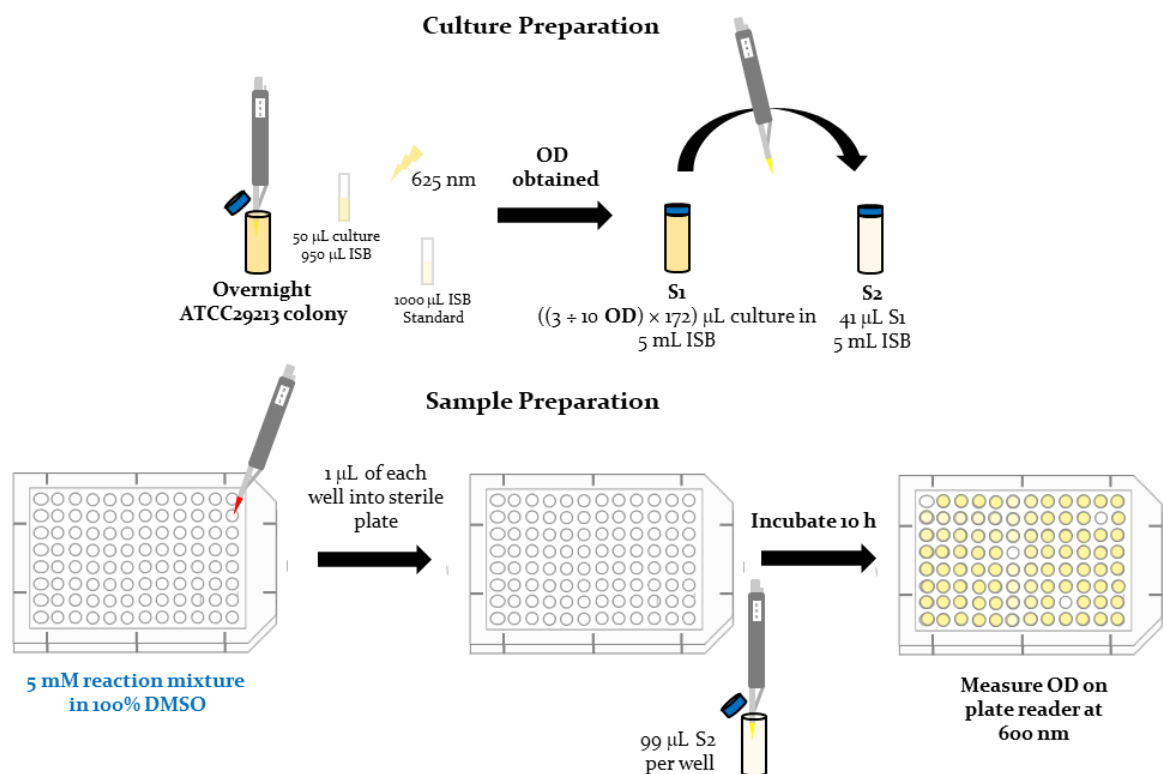


Figure 2.6 Schematic of the screening procedure used to determine activity within reaction mixtures -Total product concentrations of reaction mixtures are determined by using the limiting reagent (anilide substrate) as the maximum concentration of the reaction mixture. For this screen, a total product concentration of 50 μM was chosen. Culture preparation was performed according to CLSI guidelines.¹⁰⁶

Each reaction mixture/component was screened in triplicate against one colony of ATCC29213 and the average value was plotted (Figure 2.7).⁹⁷ At a total product concentration of 100 μM , all the individual reaction components showed no interference with the assay after heating and filtration through silica. Both quinazolinone **38b** and the reaction mixture between substrate **48b** and co-substrate **79** (known to form **38b** on scale) inhibited ATCC29213 growth visually (approximately above 75% growth inhibition), confirming quinazolinone, **38b** could be detected within reaction mixtures. No activity was detected from the reaction known to form inactive quinazolinone, **38j**. This trend was also observed at a total product concentration of 50 μM .⁹⁷ At a total product concentration of 25 μM , the reaction mixture known to form

quinazolinone **38b** no longer displayed significant activity whereas the pure quinazolinone retained its activity, expected as its MIC was between 1.45-2.90 μM . At a total product concentration of 12.5 μM , activity within the positive control reaction mixture disappeared. By screening at four different concentrations, a suitable assay screening concentration of 50 μM was selected.

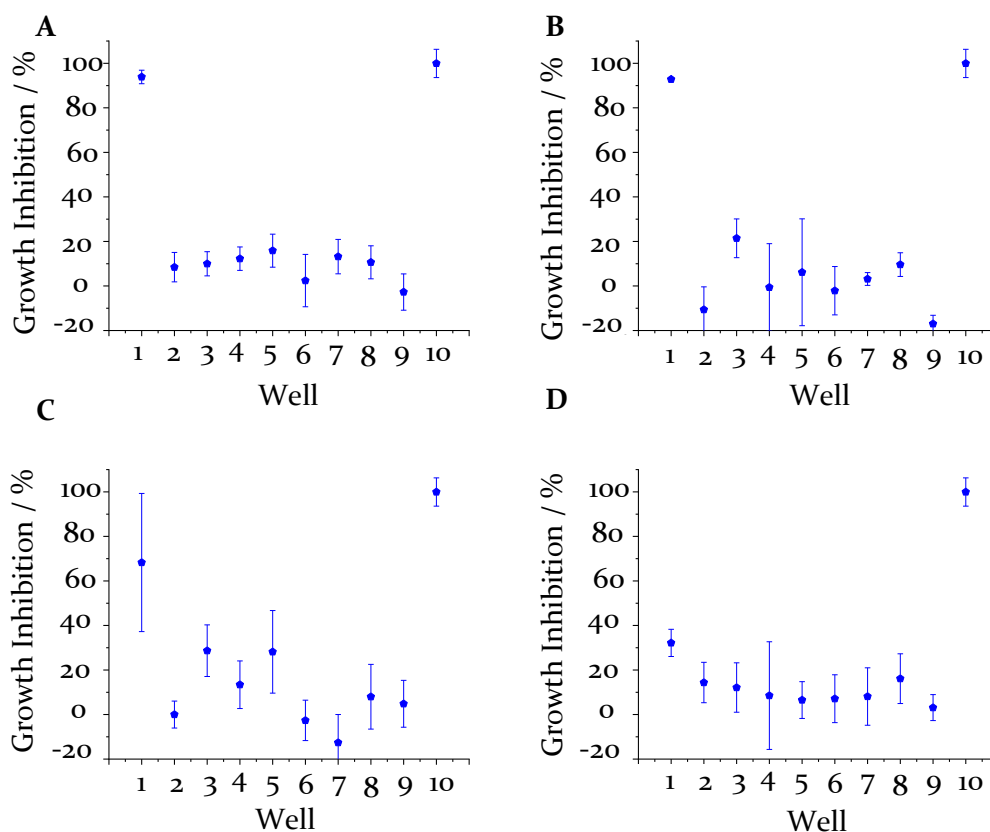


Figure 2.7 Growth inhibition values of individual reaction components, a reaction that forms a positive control and a reaction that forms a negative control against ATCC29213 - Reaction concentrations were based on the limiting reagent of the reaction mixtures, 333 mM. Screening concentrations were as follows: A = total product concentration, 100 μM , B = total product concentration, 50 μM , C = total product concentration, 25 μM and D = total product concentration, 12.5 μM . Well numbers correspond to those reported in Table 2.4.

2.4 Design and Synthesis of Substrates for Activity-Directed Synthesis

Both substrates and co-substrates needed to be carefully designed to allow expansion of the quinazolinone SAR whilst exploring productive areas of chemical space. The SAR of the quinazolinones (Section 1.3.4.2)⁷⁸ highlights the two areas of diversification chosen to be used in this activity-directed expansion study (Figure 2.8). By altering both substrate and co-substrate, which will contribute to the blue portion and red portion of the structure respectively, the SAR of the quinazolinones can be expanded significantly and efficiently using ADS.

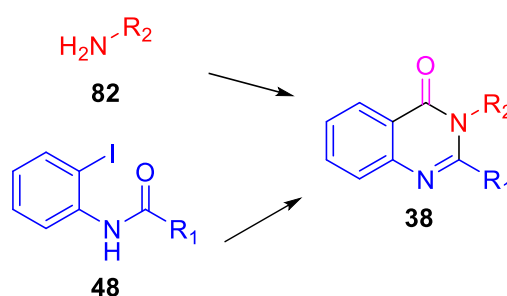


Figure 2.8 Design criteria to allow synthesis of quinazolinones⁷⁸ in an ADS reaction array - The section of the scaffold that can be derived from the substrate (blue), the co-substrate (red) and carbon monoxide (pink) have been indicated. This is one scaffold of many that can possibly be formed in the array (Section 2.1.1).

Co-substrate selection was decided using the software Pipeline Pilot (a scientific workflow system which allows the user to filter through an inputted data set and select criteria that each compound that is outputted should meet).¹⁰ Pipeline Pilot also allows the user to filter both structural data and molecular properties and provides an output of molecules that match the desired criteria. As co-substrates were chosen based on commercial availability, compounds from a commercial database were inputted and filtered by both molecular properties and designed to include structural groups that could undergo Pd-catalysed chemistry, including a minimum of one amine/aniline per compound to ensure quinazolinones could be formed (Figure 2.9).

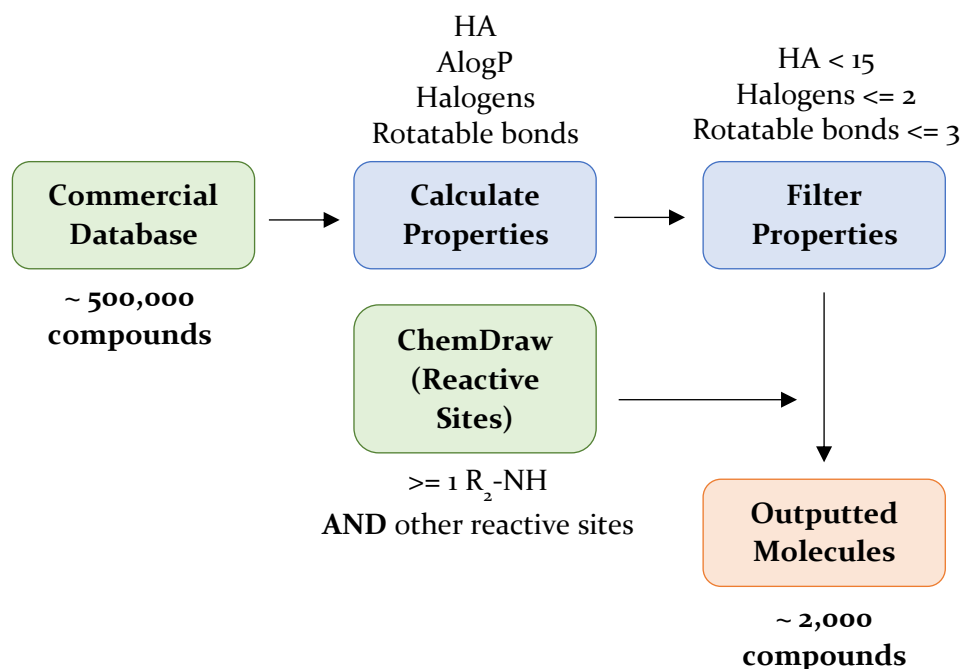


Figure 2.9 Summarised flow chart of the Pipeline Pilot filtering protocol - The commercial databases of Merck, Fluorochem and Alfa Aesar were inputted, and duplicate molecules were removed (~500,000 compounds inputted). The molecular properties of these compounds were calculated including heavy atoms (C, N, O, F, S, Cl, Br, I), molecular weight, number of rotatable bonds and AlogP. Compounds were filtered to limit HA < 15, halogens <= 2 and rotatable bonds <=3. Two ChemDraw files, one containing amine/aniline motifs and one containing other reactive sites were inputted and mapped on the molecules. Those containing both an amine and another reactive site were outputted (~2000 compounds outputted).

The outputted molecules were served as inspiration for co-substrate selection (Figure 2.10). The co-substrates have been split into three appropriate sections within the figure based on the selection criteria. Panel A are primarily analogues found in antibacterial quinazolinones that could form a substituent in the 3-position of any formed quinazolinones that has precedent to produce an active species. All anilines **C1**, **C5**, **C6**, **C14**, **C18** and **C19** have a substituent in the *m*-position which has been shown to significantly increase the bioactivity of quinazolinones that contain this structural feature. Compounds **C5** and **C6** also contain an alkene and an additional aniline

respectively which have the potential to undergo further Pd-catalysed reactions in the wells, this could expand the number of products that form in these wells, increasing the number of products this array explores. In Panel B, cyclohexane rings have also been included within the selection. The number of these has been limited to two, both **C2** and **C13**, as aliphatic rings in the 3-position have no precedent in the current quinazolinone SAR⁷⁸. It was hypothesised that the hydroxyl group on **C2** could yield an ester, rather than an amide, after carbonylation, a different scaffold that could be explored within the array. Panel C have little precedent within an antibacterial array, included to expand the known SAR by the inclusion of different aromatic rings and substituents. **C3**, **C8**, **C12**, **C15**, **C16** and **C17** also contain functional groups which can undergo different Pd-catalysed reactions which could allow further diversification within the products. It is also important to note that halogens were included as a second site for carbonylation and could form carboxylic acids during the reaction. A plot of AlogP against a number of heavy atoms has been included to show the distribution of the co-substates molecular properties (Panel D, Figure 2.10).

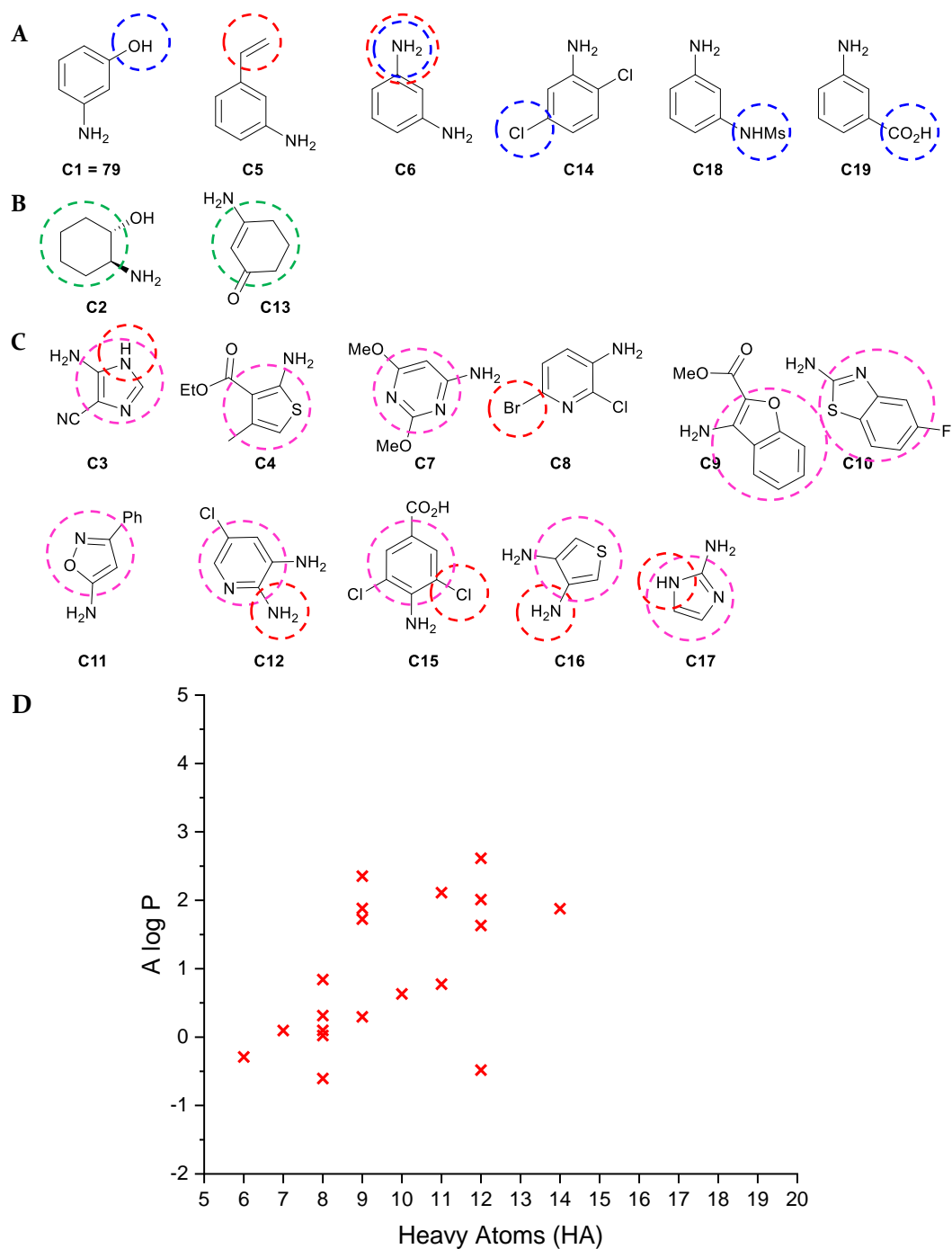


Figure 2.10 Set of 19 co-substrates chosen for the Pd-catalysed carbonylation array and their molecular properties – Panel A, B and C: Selected co-substrates where sites with a *m*-substituted aniline (blue), sites that might undergo alternative Pd reactions (red), contain an aliphatic ring (green) and sites that explore alternative aromatic structures (pink) have been indicated. Panel D: Plot of AlogP vs number of

heavy atoms for each co-substrate to show molecular property distribution of co-substrates.

As the substrates would need to be synthesised, the commercial database was filtered for carboxylic acids and acid chlorides. To aid in synthesis, acid chlorides were chosen preferentially, followed by carboxylic acids where necessary (Figure 2.11). All substrates contain an *o*-iodo amine/anilide moiety within them as this group is essential for quinazolinone formation. Substrates **S1** and **S3** were chosen as their 2-carbon linker in the 2-position (an alkane and alkene respectively) of antibacterial quinazolinones has been highlighted as important for *S. aureus* activity.⁷⁸ Substrates **S7**, **S8** and **S10** were selected as they allowed diversification of this linker with either a constrained ring system (as in **S7**) or a different functionality at the end of the linker (as in **S8** and **S10**, with an alkene and cyclopentane respectively). Compound **S9** was originally chosen in the hopes of diversifying the 5-8 portion of the quinazolinone with a five membered ring system, however, it was later found that substitution occurred on the secondary amine, making this the substrate chosen for the array (Scheme 2.4). Substrates **S4**, **S5** and **S6** were also chosen to expand the SAR of the 2-position beyond the literature.⁷⁸ Aniline **S2** was included as exposure to carbonylation conditions could form acyclic systems that could still possess antibacterial activity. A plot of AlogP against number of heavy atoms has also been included to show the distribution of the substrates molecular properties (Panel B, Figure 2.11).

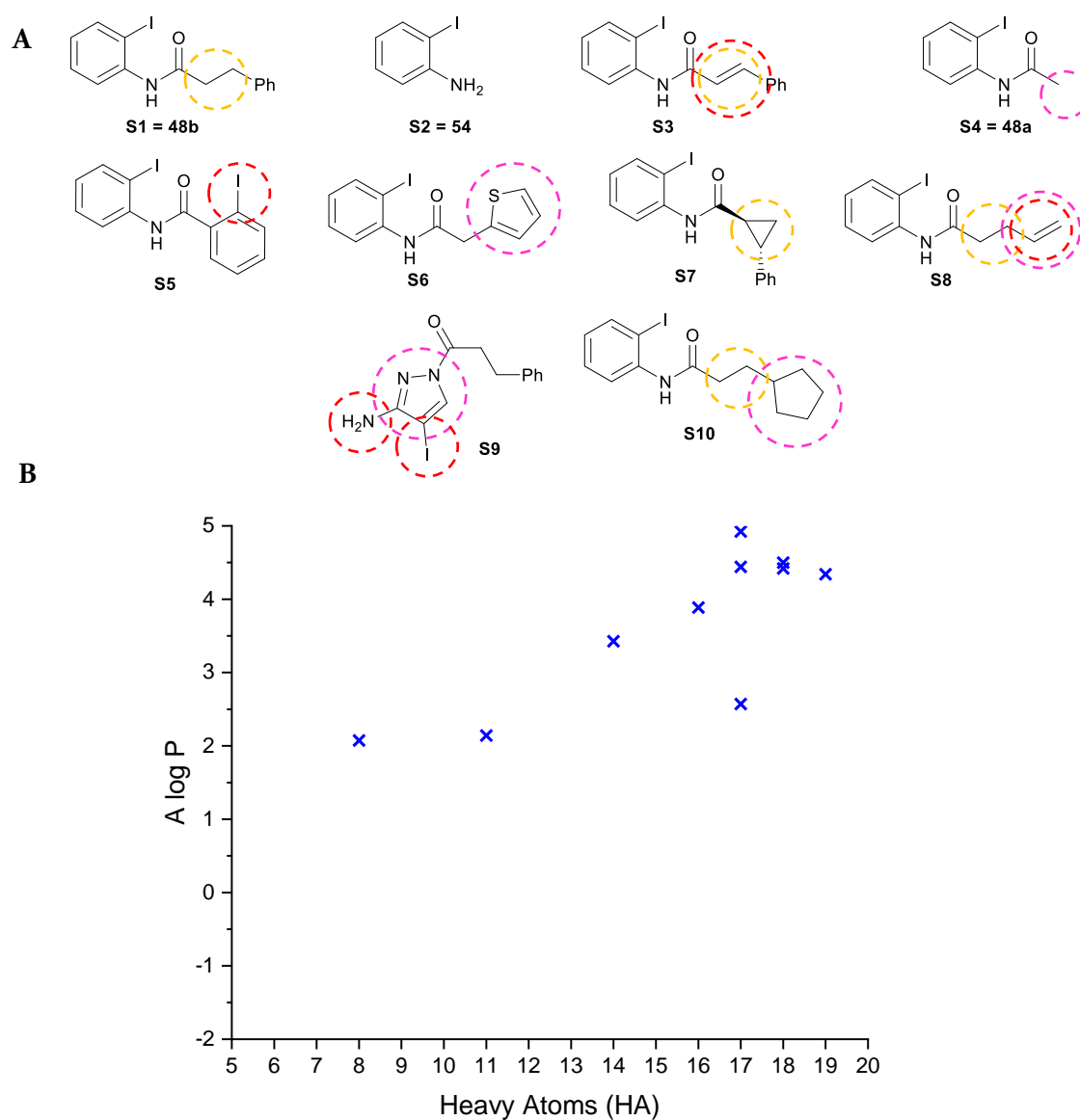


Figure 2.11 Set of 10 anilide substrates chosen for the Pd-catalysed carbonylation array and their molecular properties - Panel A: Selected substrates where sites with a 2-carbon linker (orange), sites that might undergo alternative Pd reactions (red) and sites that explore alternative ring systems (pink) have been indicated. Panel B: Plot of AlogP vs number of heavy atoms for each substrate to show the distribution of molecular properties of substrates.

As the project was focussed on using the activity-directed synthesis to expand the SAR of a known series of antibacterials, most substrates and co-substrates were chosen systematically and the resulting quinazolinone that could form from a reaction between the two was important in their selection. However, not all reactants would necessarily form this product, and mixtures of products were still possible within reaction wells. It was possible that some substrates could form multiple products from the same co-substrates, (Figure 2.12). Substrate **S3**, for example, could in principle, undergo an intramolecular Heck reaction to form quinolinone **85**, a Buchwald-Hartwig amination to form aniline **84**, a carbonylation followed by dehydration to form quinazolinone **38o** or a carbonylation reaction to form amide **83**.⁹⁷

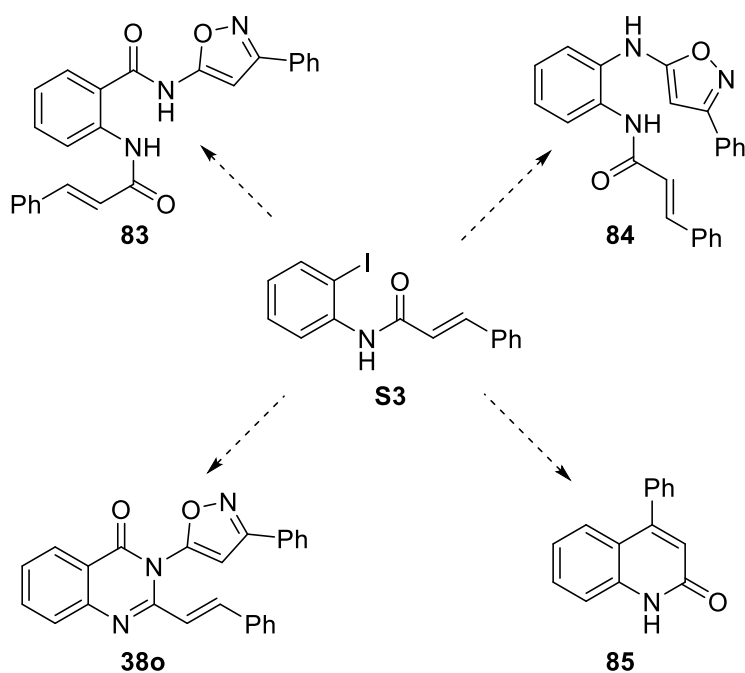
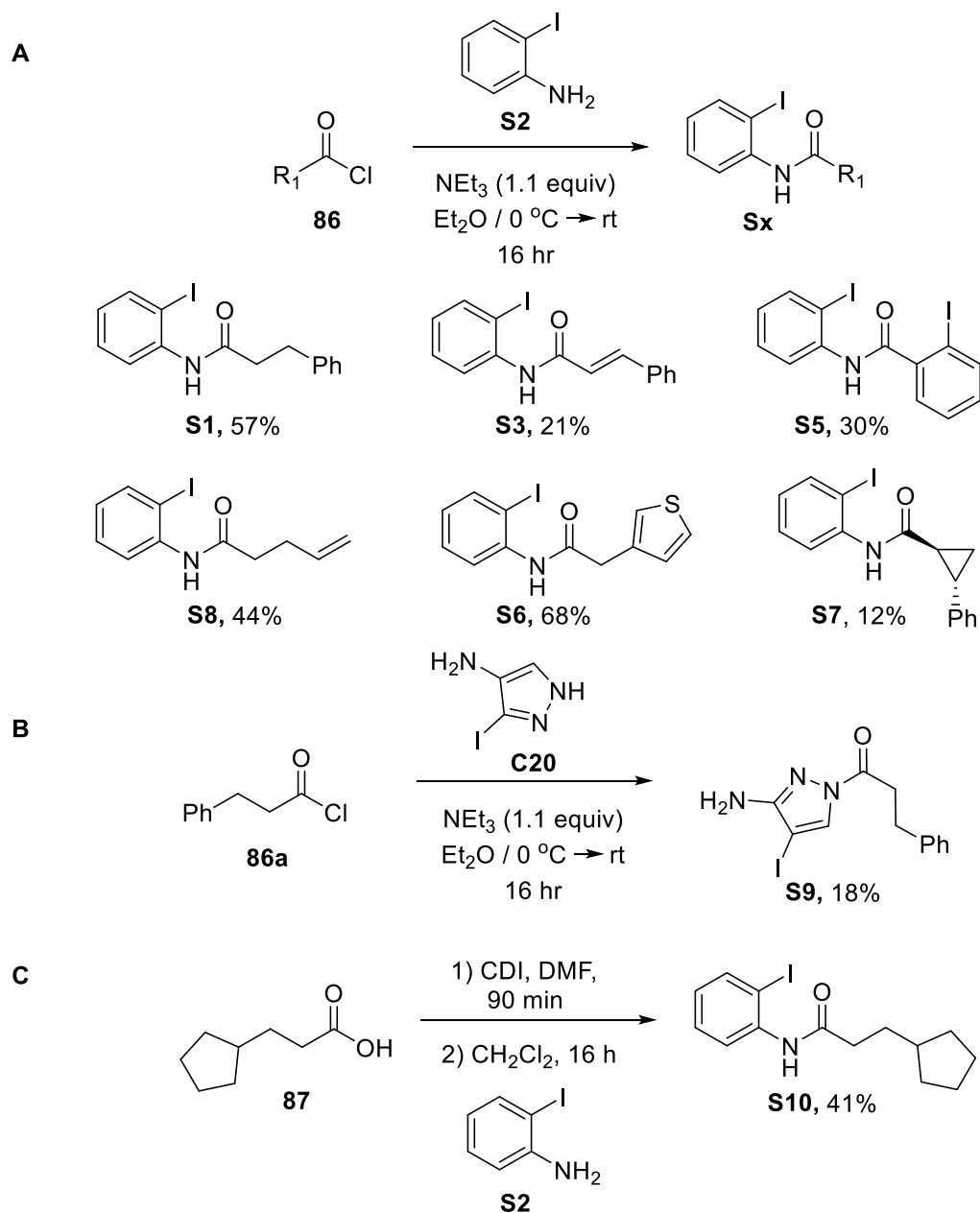


Figure 2.12 Potential of Pd-catalysed chemistry to yield alternative scaffolds from common substrates.

2.4.1 Preparation of 2-iodoanilide Substrates

Upon selection, the 2-iodoanilide substrates were prepared. The appropriate aniline (1 equiv.) and triethylamine (1.1 equiv.) were dissolved in diethyl ether and cooled to 0 °C. A solution of the appropriate acid chloride (1.1 equiv.) in diethyl ether was added dropwise. The reaction was heated to rt and stirred overnight until completion (Scheme 2.4, Panel A).¹¹¹ This method was chosen as it could afford reasonable yields of *o*-iodo anilides from structurally diverse acid chlorides and most substrates only needed to be recrystallised, simplifying purification. Substrate **S10** was synthesised from the corresponding carboxylic acid and so a different approach to the synthesis was required. The carboxylic acid (1.1 equiv) was dissolved in DMF and CDI (1.1 equiv) was added. The reaction mixture was stirred at rt for 90 mins. Afterwards, the aniline (1.0 equiv) was added and the reaction was stirred for a further 16 h at rt (Scheme 2.4, Panel B).¹¹²

The reaction forming **S9** yielded 18% product, which was low due to the different regioisomers that could form within the reaction mixture. The mass of both the mono-substituted and di-substituted product were also identified by LC-MS and only **S9** was isolated during purification. The structure of **S9** was determined by X-ray crystallography and confirmed the reaction product isolated was the regioisomer drawn (Section 5.2.4).



Scheme 2.4 Synthesis of anilide substrates - Panel A: Synthesis by coupling with an acid chloride.¹¹¹ Panel B: Synthesis of **S9** by coupling with an acid chloride. Panel C: Synthesis by coupling with a carboxylic acid. Structures and yields of all anilides have been included.¹¹²

2.5 Carbonylation Reaction Arrays

2.5.1 Reaction Array Design

For the ADS array, borosilicate glass vials were set up in 96-well plate layout, using the Optibloc™ apparatus (Figure 2.3, Section 2.2.1). The outer wells contained *o*-xylene and the central wells contained reaction mixtures. Addition of both the substrate and co-substrate was from stock solutions of the same concentration to reduce the amount of compound measurements that needed to be performed within the reaction array.⁹⁷ Multiple volatile solvents were tested for the stock solutions including acetone, ethyl acetate, diethyl ether and THF and, most substrates and co-substrates tested dissolved in THF and only partially or not at all in the other solvents; therefore, THF was chosen for stock solutions. In cases where dissolution was not possible at the desired concentration, additional solvent was added to the stock solution to make it less concentrated. This was possible as all solvent was removed before the addition of other reaction components. In cases where this did not dissolve the substrate or co-substrate, suspensions were added. To ensure even loading, these were stirred vigorously prior to each addition. Reactions were assembled to give a final reaction concentration of 333 mM, based on the limiting anilide reactant, in 300 µL of *o*-xylene.

2.5.2 Reaction Array Execution and Product Analysis

Having established appropriate synthetic procedure for ADS, a reaction array was executed based on ten substrates **S1-S10** (and no substrate) and nineteen co-substrates **C1-C19** (and no co-substrate). The array of 220 reactions was designed to enable formation of a diverse range of quinazolinones, some related to known analogues,⁷⁸ as well as other products of Pd-catalysed processes (Section 2.4). An exhaustive array of all components was performed and due to equipment availability (one Optibloc™), only one plate could be performed at a time. The array was performed in a 96-well Optibloc™; assembled from stock solutions using multi-

channel pipettes. Stock solutions were prepared, and components were added as described in section 2.3.2. To minimise the potential for side reactions occurring at room temperature, the catalyst and ligand in a *o*-xylene were added in the penultimate step. As the reactions relied on the release of carbon monoxide from molybdenum hexacarbonyl via a base, the triethylamine was added concentrated using a multichannel pipette and plates were sealed as quickly as possible. Each plate contained 60 reactions and a total of four reaction plates were required for the entirety of the array and controls. After 48 h at 105 °C, the crude reaction mixtures were filtered through silica, evaporated, and dissolved in DMSO (total product concentration: 333 mM). DMSO stocks of product mixtures were stored at -20 °C and screened in parallel once all reactions were complete.

LC-MS was performed to investigate the productivity of the chemistry on twenty-three randomly selected product mixtures (approximately 10% of the total number of reactions).⁹⁷ Masses that matched that of the respective the quinazolinone and intermolecular carbonylation product were identified and reported (Table 2.5). Sixteen of these contained carbonylated intermolecular products, 13 of which had been dehydrated. In the case of the reaction between **S5** and **C13** the quinazolinone formed, however, the second iodo-group on the substrate was carbonylated into a carboxylic acid. In some of the cases, where the reaction showed no intermolecular product, either the mass of the carbonylated substrate or the de-halogenated substrate was found, having formed a carboxylic acid or proton in the *o*-position of the anilide. Multiple products were also observed in some reaction wells (i.e. **S10** and **C2**). One of the product mixtures (from **S3** and **C1**), also contained the product of an intramolecular reaction of **S3**, which was later shown to stem from a reductive Heck reaction, forming a quinolinone. Within the twenty-three reaction wells tested, no intermolecular products formed from a Buchwald-amination were found suggesting that carbonylation is faster than amination under these conditions.⁹⁷

Substrate	Co-Substrate	Mass corresponding to quinazolinone product ^a	Mass corresponding to intermolecular carbonylation product ^b
S5	C1		
S3	C1		
S2	C12		✓
S4	C8		
S3	C6	✓	
S1	C18	✓	
S2	C17		
S4	C9	✓	
S1	C4	✓	
S5	C13	✓ ^c	
S2	C15		✓
S4	C15	✓	
S8	C14	✓	
S8	C18	✓	
S7	C1	✓	
S7	C10		
S8	C7		✓
S7	C12	✓	
S10	C12	✓	
S10	C2	✓	✓
S10	C19	✓	
S9	C17		
S9	C12		

Table 2.5 Results of the LC-MS screen performed on a random ~10% of wells -

^aTick indicates that the mass corresponding to a quinazolinone product was observed

^bTick indicates that the mass corresponding to an intermolecular carbonylation product was observed. ^cThe observed mass corresponded to a quinazolinone in which

the second iodo group in the product had undergone a carbonylation reaction to form a carboxylic acid.

From the masses obtained during this study, it is possible to predict some products that could have formed within this reaction array (Figure 2.13). Most of the reaction mixtures displayed the mass of quinazolinone product (labelled **38p**, **38q**, **38r** and **38s**). Each of these quinazolinones has different decorations in the 2 and 3 positions, showing how many different quinazolinone scaffold that were explored within this reaction array. Some reaction wells also showed the mass of a carbonylation product without dehydration and most likely contained the corresponding amide (labelled **88** and **89**). At this stage of the array, none of these reactions were scaled up and only mass was used to determine reaction success. It is estimated that from 220 reactions, over half yielded at least one product, therefore most of the reactions productively gave an intermolecular product.

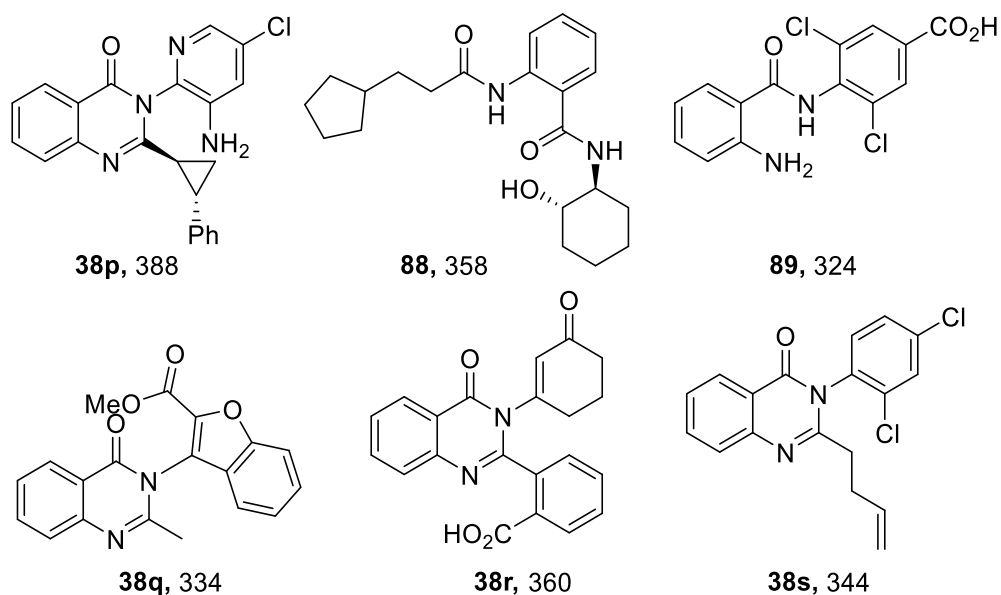


Figure 2.13 Possible products, with masses that were observed, that could have formed within in the reactions listed in Table 2.5 - Masses were obtained from the LCMS screen and matched the theoretical mass values for all six compounds.

2.5.3 Reaction Array Results and Hit Validation

The crude reaction mixtures were screened in duplicate against *S. aureus* ATCC29213 (final product concentration of 50 μM in 1% DMSO in ISB). Initially, reaction wells containing 100% DMSO at 333 mM total product concentration were diluted to 5 mM total product concentration in 100% DMSO (100-fold higher than the screening concentration). Then, 1 μL of each of the 5 mM reaction wells was pipetted into the sterile plate and were diluted in 99 μL ISB containing the standardised ATCC29213 ($5 \times 10^5 \text{CFU mL}^{-1}$)¹⁰⁶ to ensure each screening well contained 1% DMSO and a final total product concentration of 50 μM . Plates were incubated for 10 h at 37 °C using both a growth control (antibacterial free, 1% DMSO in ISB) and Penicillin G, **24** (50 μM in 1% DMSO in ISB) as a positive control. In addition to visual observation, the optical density was measured using a plate reader at 600 nm and converted to growth inhibition (Section 2.3.2). A photograph of a plate after 10 h incubation has been displayed in Figure 2.14.



Figure 2.14 Photograph of a reaction array plate of ATCC29213 after incubation for 10 h at 37 °C.- The positive control (Penicillin G, **24**, is in the bottom right corner of the plate).

Areas of 0% growth inhibition are indicated by the cream (not black) wells within the photograph and 100% growth inhibition is indicated by areas on the plate which appear black (due to the background of the photograph, broth within wells is

clear). For this screen, quantitative data was desired to allow easy identification of hits graphically and so percentage growth inhibition was chosen to determine activity. All wells were screened in duplicate against two different colonies of ATCC29213 and mixtures that were active in duplicate were considered hits. In certain cases, some mixtures did not duplicate, and these wells were rescreened against a further two colonies of ATCC29213. By comparing percentage growth values to visual analysis of the plates, 75% growth inhibition was chosen as the criteria for an active combination.

From all the 220 crude reaction mixtures that were screened, six displayed significant antibacterial activity in both replicate cultures: Substrate **S1** (with **C1** or **C18**); substrate **S7** (with **C18**) and substrate **S10** (with **C1**, **C6** or **C18**).⁹⁷ The combination of **S1** and **C1** that had previously validated in the method development work, also displayed activity. Substrates and co-substrates have been plotted within a heat map to display the growth inhibition of all combinations (Figure 2.15).

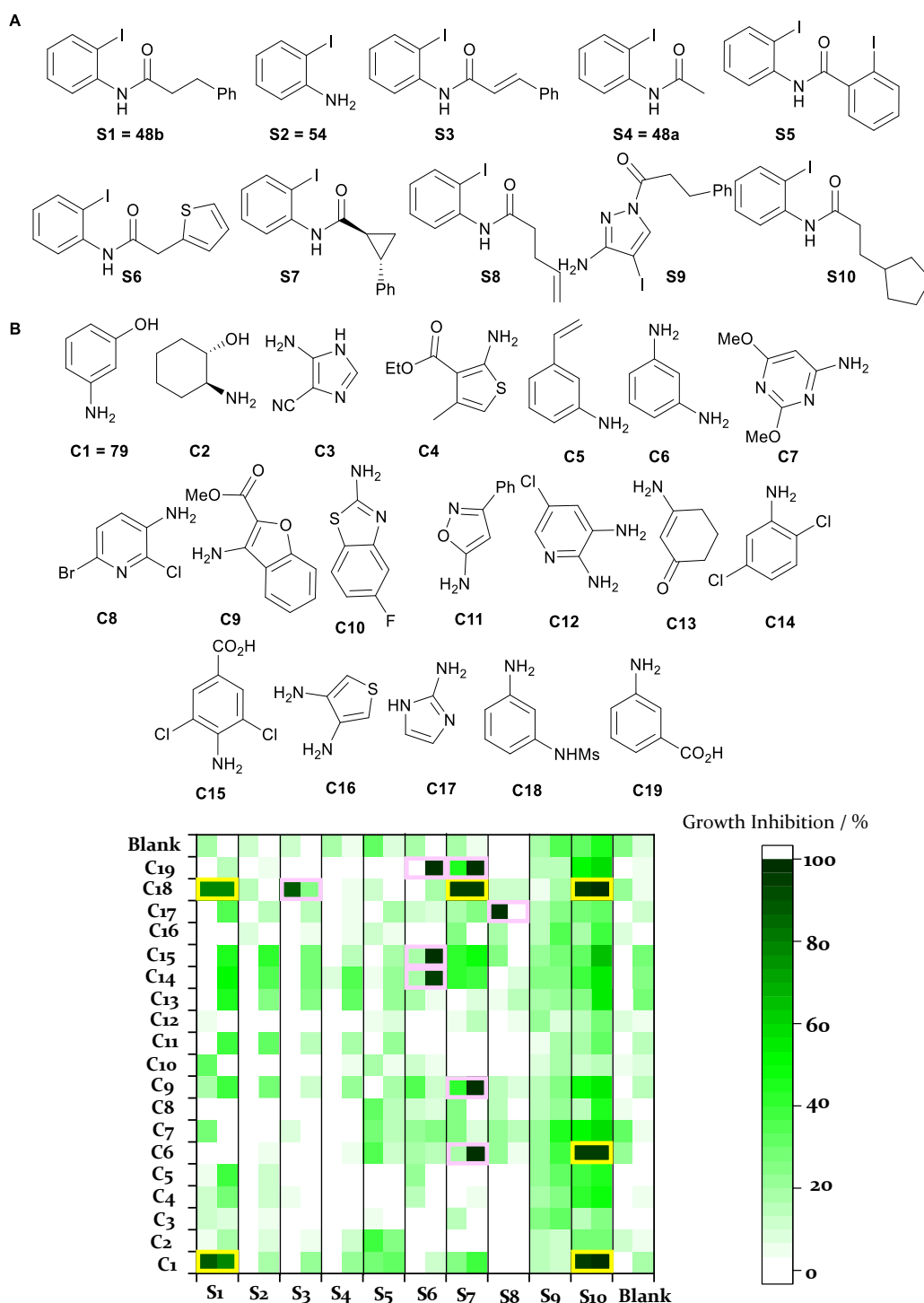


Figure 2.15 Activity-directed antibacterial discovery (see table 2.2 for reaction conditions)- Panels A and B: Structures of substrates (A) and co-substrates (B). Panel C: Activity against *S. aureus* ATCC29213 (total product concentration: 50 μ M), with active combinations that were scaled up shown (yellow box). On the x-axis, the

substrates have been plotted and duplicate screens have been placed adjacent to each other. On the y-axis, co-substrates have been plotted. For a reaction to be deemed a hit, both must be dark green (> 75% growth inhibition). Product mixtures that displayed activity against only one colony have been indicated (pink box). Control wells (with either blank substrate or blank co-substrate) have been plotted on the outside of the heat map and display no activity.

A few reactions resulted in hits against only one of the two colonies (indicated by the pink squares in Figure 2.15). These combinations needed to be retested against two more colonies of ATCC29213 to reinvestigate their activity, using the same approach as described above. Reaction mixtures were screened at a total product concentration of 50 μM in ISB containing 1% DMSO and the screen was performed identically. The results were plotted, and each combination has been labelled on the x-axis (Figure 2.16). Although there appears to be a lot of noise within the data, none of the reaction mixtures inhibited bacterial growth greater than 75% (indicated by the black line on the graph) and growth inhibition was not visually observed. These combinations were therefore not validated and were not investigated further during scale-up.⁹⁷

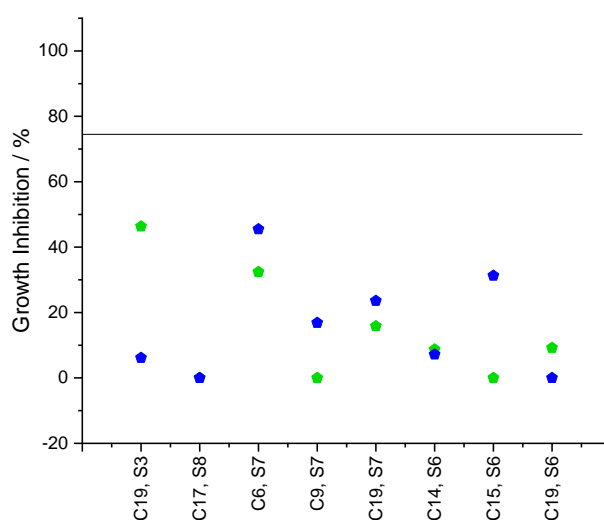


Figure 2.16 Reinvestigation of reaction hits that had been active against one colony- Reaction combinations that did not show duplicated biological activity (see figure 2.15) at total product concentration: 50 μM against ATCC29213 were re-screened in duplicate.

2.6 Scale-up and Structural Elucidation of Antibacterial Ligands

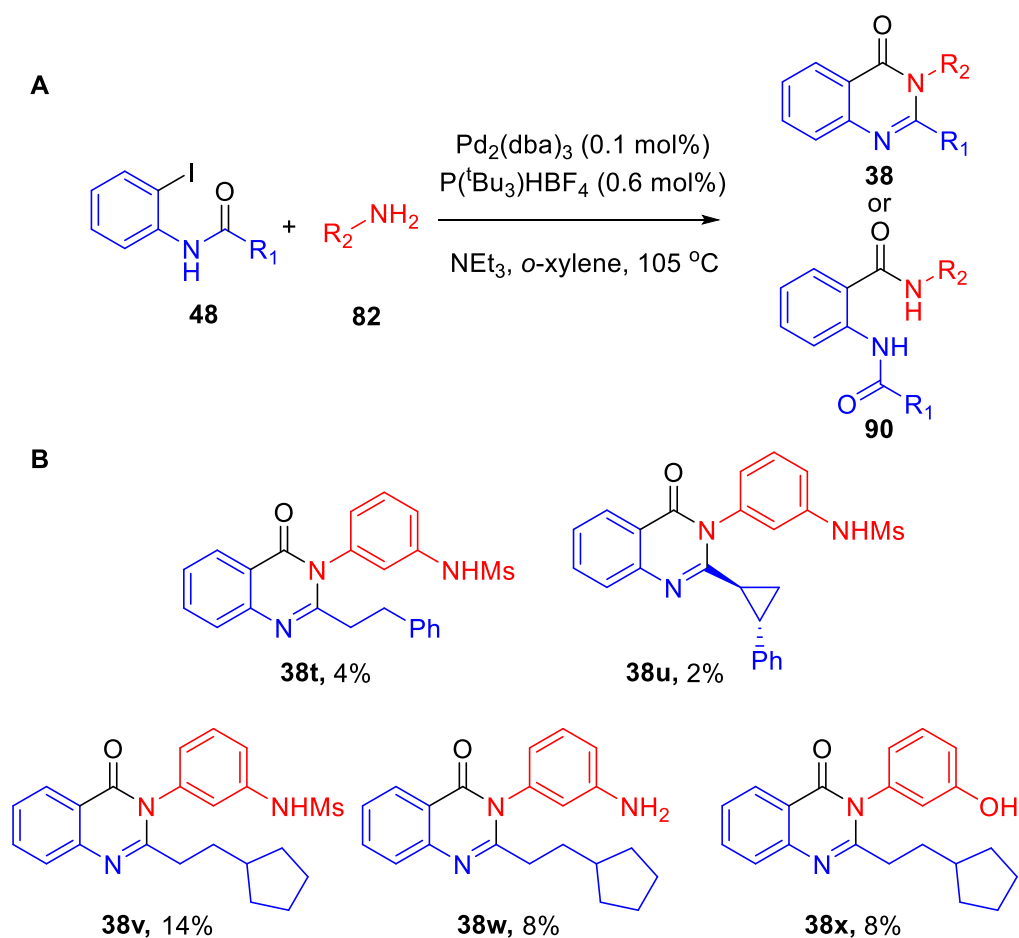
Active combinations were scaled-up to elucidate the active products within the reaction mixtures. These products were purified and screened against three different strains of *S. aureus*. In addition, inactive combinations from the reaction array were also scaled-up to validate that the assay was effectively identifying active combinations and not reporting false negatives.

2.6.1 Scale-up and Isolation of Products within Active Combinations

Reaction combinations highlighted by yellow squares (Figure 2.15, section 2.5.3) were scaled-up as they inhibited bacterial growth in duplicate. These combinations were between substrate **S1** (with **C18**); substrate **S7** (with **C18**) and substrate **S10** (with **C1**, **C6** and **C18**). The appropriate aniline (1.2 equiv.) and 2-iodophenylanilide (1 equiv.) were added to a crimp-top vial containing molybdenum hexacarbonyl (1 equiv.), $P(tBu)_3 \cdot HBF_4$ (0.6 mol%) and tris(dibenzylideneacetone)dipalladium(o) (0.1 mol%) and the mixture was dissolved in *o*-xylene (3.0 mL per mmol). Then, triethylamine (2.5 equiv) was added at rt.⁹⁷ After heating to 105 °C for 48 h, the crude mixture was filtered through silica followed by purification by preparative LC-MS to afford the product. In each case, LC-MS analysis of the crude mixtures had shown that quinazolinone had formed in each of these wells and therefore, this mass was chosen for isolation. Yields likely suffered from poor recovery possible with preparative LC-MS however, this was accepted as purity was preferred over yield for MIC determination (Scheme 2.5).

Product **38t** contained a methanesulfonylamino group on the phenyl ring in the 3-position of the quinazolinone which was expected from current SAR⁷⁸ to display significant bioactivity against ATCC29213. The saturated 2-carbon linker in the 2-position of the quinazolinone within substrate **S1** in combination with the *m*-substitution in the 3-position of co-substrate **C18** yielded a novel quinazolinone from a one-step reaction in 4% yield.⁹⁷ Product **38u**, isolated in 2% yield, also contained the mesylate substituent on the benzyl ring in the 3-position of the quinazolinone,

however, it had a cyclopropane ring instead of the 2-carbon linker in the 2-position.⁹⁷ If activity was conserved in the MIC screen, this discovery would confirm that this position tolerated constrained ring systems, not just linear 2-carbon linkers. The ¹H NMR of this substrate was more complex than anticipated and appeared to contain diastereotopic protons, so an analogue without substitution of the phenyl ring in the 3-position needed to be synthesised to determine whether HPLC would be required to separate the diastereomers prior to purification (Section 2.6.3). Products **38v**, **38w** and **38x** were all formed from substrate **S10** with different co-substrates in 14%, 8% and 8% yield, respectively. If activity was conserved within these structures, it would confirm a 5-membered ring at the end of the 2-carbon linker was tolerated for growth inhibition of ATCC29213.

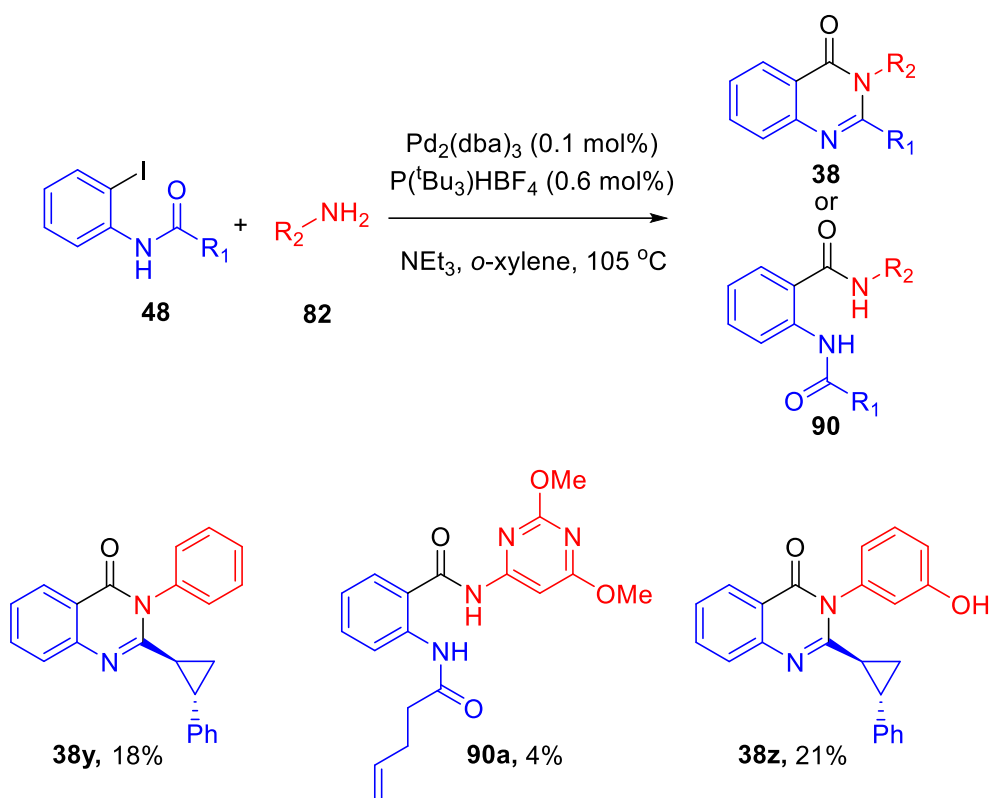


Scheme 2.5 Scale-up reactions of active combinations found in the array screen against ATCC29213- Panel A: General Synthetic Scheme. Panel B: Structures and yields of the intermolecular species isolated from the reaction mixture. The section of the scaffold that can be derived from the substrate (blue) and the co-substrate (red) have been indicated.

2.6.2 Scale-up and Isolation of Products within Inactive Combinations

Additional quinazolinones were also prepared from inactive combinations within the reaction array (Scheme 2.6). These combinations were between substrate **S7** (with aniline and **C1**) and substrate **S8** (with **C7**) and reactions were performed as described in Section 2.6.1. Quinazolinones **38y** and **38z** were obtained from their

respective reaction as expected. The reaction between **S8** and **C7** yielded amide **90a**, an acyclic carbonylation product that confirmed that the reaction array was not only forming quinazolinones, but alternative scaffolds as well.⁹⁷



Scheme 2.6 Scale-up reactions of inactive combinations found in the array screen against ATCC29213 - Panel A: General Synthetic Scheme. Panel B: Structures and yields of the intermolecular species isolated from the reaction mixture. Species **38y** was included in this selection for NMR experiments and was not a combination within the reaction array. The section of the scaffold that can be derived from the substrate (blue) and the co-substrate (red) have been indicated.

2.6.3 Identification of Rotamers Within Cyclopropyl Containing Quinazolinones

After isolation, **38y** was analysed to determine whether the 2 and 6 positions on the phenyl ring substituent in the 3-position of the quinazolinone were within the same

chemical environment or not. If these two protons were not within the same environment, slow rotation around the cyclopropane ring could be confirmed and the cause of the diastereomers within active quinazolinone **38u** (Scheme 2.5, Section 2.6.1) could be identified as rotamers (Figure 2.17). The ^1H and ^{13}C NMR were assigned and it was found that the protons in the 2 and 6 positions were diastereotopic, appearing in two different chemical environments, indicated by the ^{13}C NMR chemical shifts. It was also observed that the 3 and 5 positions were similarly diastereotopic, indicated by the ^1H NMR chemical shifts.

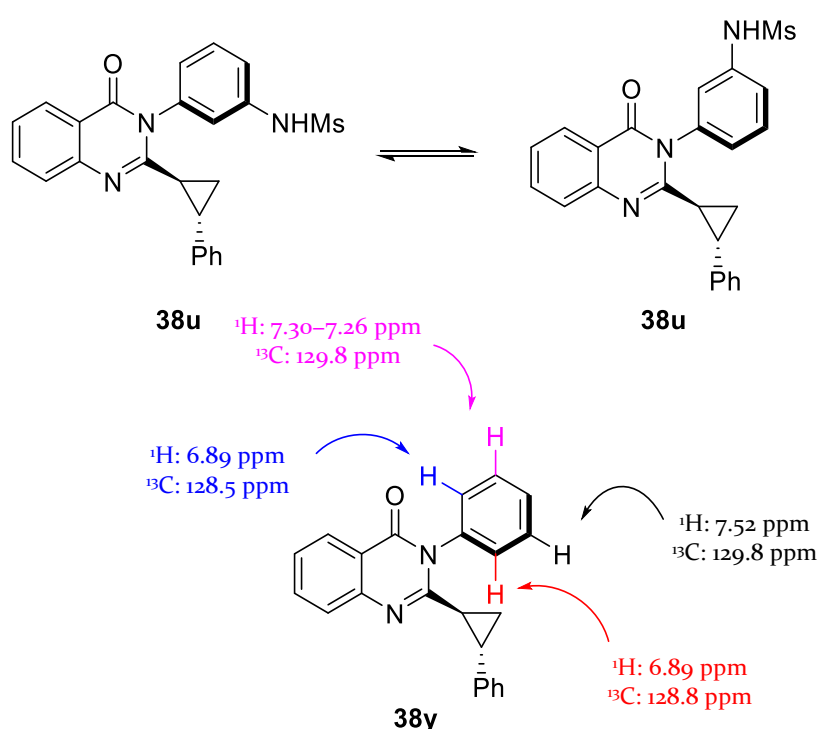


Figure 2.17 The two rotamers of quinazolinone **38u** and the diastereotopic protons identified in **38y** - The key ^1H NMR and ^{13}C NMR peak used in determining that the protons in both the 2 and 6 position and the 3 and 5 positions were diastereotopic have been indicated in their respective colour. NMR data has been provided in Appendix B.1.

2.6.4 Minimum Inhibitory Concentration and IC_{50} Determination of Isolated Species

After isolation of all the species, MIC determination could be performed against all of the quinazolinones **38t-38z** and product **90a**. Minimum inhibitory concentration (MIC) values for selected compounds were determined by broth microdilution against *S. aureus* strains SH1000, ATCC29213 and USA300 JE2, according to CLSI guidelines¹⁰⁶ for low solubility compounds except for using Iso-Sensitest Broth (ISB) in place of cation-adjusted Mueller-Hinton Broth (MHB-II). A 2-fold dilution series of the isolated compounds in DMSO was prepared, ranging from 1600–1.6 $\mu\text{g mL}^{-1}$. Each dilution was transferred into a 96-well format at a final volume of 1 μL and 99 μL of the standardised culture was added to each well to give final antibiotic concentrations of 16–0.016 $\mu\text{g mL}^{-1}$ (1% DMSO in ISB). Plates were incubated for 16 h at 37 °C and the MIC was determined visually as the lowest concentration at which growth was inhibited. Higher concentration ranges (128–0.128 $\mu\text{g mL}^{-1}$) were used for MIC determinations where no growth inhibition was observed at concentrations up to 16 $\mu\text{g mL}^{-1}$.⁹⁷ The results from this assay have been summarised in Table 2.6. Each compound was screened in duplicate over three different days for the three strains, including the known literature compound, **38b**.⁷⁸ On each plate, a serial dilution of Penicillin G, **24** was also performed to ensure that each *S. aureus* strain was performing as expected with a known antibiotic.⁹⁷ As quinazolinones were known to target PBP1 and PBP2a, it was expected that MIC values would be similar against all three strains. PBP1 was present in all three strains whereas PBP2a is only present in *mecA* (methicillin-resistant) containing strains of *S. aureus*, in this case USA300 JE2.

The products have MIC values against ATCC29213 ranging from 0.016 $\mu\text{g mL}^{-1}$ (i.e. 38 nM) for quinazolinone **38t** to 2–4 $\mu\text{g mL}^{-1}$ (i.e. 6–12 μM) for **38w**. Quinazolinone **38b** displayed activity approximately 10-fold higher than previously reported. Compounds **38x**, **38u** and **38v** all displayed significant activity against methicillin susceptible ATCC29213.⁹⁷ In addition, quinazolinones **38y** and **38z** displayed significantly lower (or no detectable) activity, as expected as they were isolated from non-hit reactions. The activity of **38z** was higher than the other quinazolinones at 4–8 $\mu\text{g mL}^{-1}$ (i.e. 11–22 μM), explaining why it was not detected at the screening concentration of 50 μM when screened as a mixture. The uncyclised amide **90a** also displayed no activity against ATCC29213, confirming it was not detected within the reaction array as it was inactive.⁹⁷ All quinazolinones were also screened against *S.*

aureus strains SH1000 and USA300 JE2. Compounds **38t-38x** all showed significant activity against methicillin-resistant USA300 JE2, however activity against the laboratory strain SH1000 was less active.⁹⁷ Quinazolinones **38z** and **38y** showed a similar trend within USA300 JE2 and SH1000, with significantly lower activity than the quinazolinones isolated from active combinations. Uncyclised amide **90a** also showed no activity against USA300 JE2 and SH1000.

Substrates	Product ^a	Found in 'hit' reaction?	MIC / $\mu\text{g mL}^{-1}$		
			ATCC29213	USA300 JE2	SH1000
S1, C1 ^b	38b	✓	0.5-1	0.5	4
S1, C18	38t	✓	0.016	0.016	0.5-1
S7, C18	38u	✓	1-2	2	32-64
S10, C1	38x	✓	1	0.5-1	4-8
S10, C6	38w	✓	2-4	2-4	16
S10, C18	38v	✓	0.5	0.5	1-2
S7, C1	38z		4-8	4-8	16
S4, C9	90a		>128	64	32-64
S7, aniline	38y		>128	>128	>128

Table 2.6 Evaluation of the activity of products against three *S. aureus* strains (ATCC29213, USA300 JE2 and SH1000) - The range of MICs observed in duplicate on three different days is shown for each strain. Penicillin G, **24, used as a positive control in all experiments, displayed MIC values as expected. ^a Co-substrate (1.2 equiv.), Mo(CO)₆ (1 equiv.), 0.1 mol% Pd₂dba₃, 0.6 mol% P(^tBu)₃.HBF₄, NEt₃, o-xylene. ^bRefer to Scheme 2.3, Section 2.2.2.**

2.7 Summary

The feasibility of ADS has been demonstrated within this chapter, showing that Pd-catalysed chemistry can be implemented within an ADS workflow to aid in the

discovery of new antibacterial compounds. It has been shown that under the reaction conditions, multiple different scaffolds can form, maintaining some level of diversity within reaction arrays. This method has consequently enabled significant expansion of the SAR of a known series of antibacterials, the quinazolinones, without the need to synthesise and purify every compound formed within the reaction array (Figure 2.18).^{78,97} From a total number of 220 reactions, six combinations displayed significant bioactivity in duplicate without purification. LC-MS analysis of a random 10% of the reaction wells confirmed significant conversion to product, with 16 of the 23 reactions showing an intermolecular carbonylated mass. After scale-up and structural elucidation, new submicromolar 4(3*H*)-quinazolinones antibacterials, ranging from 38 nM (i.e. 0.016 $\mu\text{g mL}^{-1}$) for **38t** to 6-12 μM (i.e. 2-4 $\mu\text{g mL}^{-1}$) for **38w** were identified.⁹⁷ From these structures, it was surmised that the key structural features needed for good activity included a *meta* substituted hydrogen bond donor on the phenyl ring in the 3-position and a two-atom tether in the 2-position that was connected to an aryl/hydrophobic group. This project has shown the capabilities of phenotypic ADS and, that when the appropriate substrates, co-substrates and chemistries are chosen, formation and detection of antibacterial compounds within mixtures is possible.

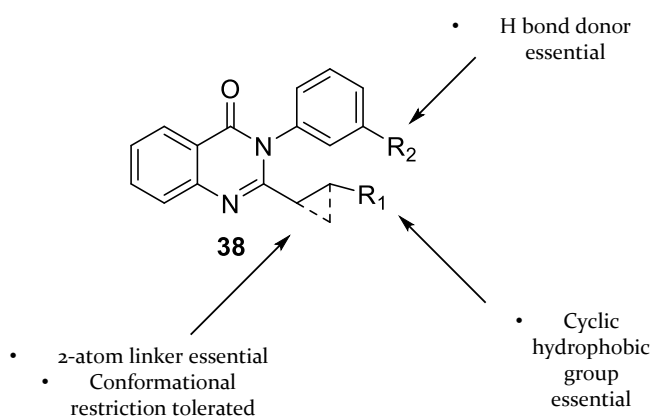


Figure 2.18 SAR expanded using ADS.⁹⁷

3 Chapter 3.

Activity-Directed Discovery of Novel Antibacterial Classes

The feasibility of using Activity-directed synthesis (ADS) in parallel with a phenotypic screening approach has proven successful when targeting *S. aureus* ATCC29213 (Chapter 2). So far, an assay has been developed that tolerates screening reaction mixtures to allow the detection of combinations containing ‘hit’ compounds. Consequently, ADS has aided in the expansion of the structure-activity relationship (SAR) of a series of quinazolinones.⁷⁸ Therefore, it was envisaged that the technique could be exploited to assess its feasibility in the discovery of a novel antibacterial series with unknown mechanisms of action.

Chapter three of this thesis shows the discovery of new chemotypes that are not based on any known antibacterial compounds. This section explores the use of Rh chemistry in an ADS reaction array of diverse substrates and co-substrates and the identification of active compounds from ‘hit’ reactions. These new chemotypes are biologically assessed and the chemistry leading to their formation is discussed.

3.1 Rationale for the Selection of Rh Catalysed Chemistry to Underpin Target-Agnostic ADS

It was envisaged that Rh-catalysed carbenoid chemistry could be used as a platform for target-agnostic ADS, in parallel with phenotypic screening, to aid in the discovery of novel chemotypes. This chemistry had already been optimised to work effectively in the ADS format and within previous target-based ADS (Section 1.2.2), had been shown to produce a diverse range of scaffolds from common substrates and co-substrates. Product diversity was also modified by both alteration of both the catalyst and the reaction solvent.^{2,46,47}

3.1.1 The Potential of Rh(II) Chemistry to generate diverse chemotypes

For Rh-catalysed carbenoid chemistry to be a promising contender for ADS, it needs to be able to form multiple scaffolds from a series of substrates when executed using a common format (Figure 3.1). Using an α -diazo carbonyl (**91**) as the starting substrate, and in the presence of a rhodium catalyst, a diverse set of intermolecular and intramolecular products can be formed. Functional group that can be synthesised include secondary/tertiary amines (**92**),¹¹³⁻¹¹⁷ ethers (**96**),¹¹⁸⁻¹²⁰ new alkane chains (**94**)¹²¹⁻¹²³ and sulfides (**93**)¹²⁴⁻¹²⁶ via insertion reactions, cyclopropane rings (**97**) via cyclopropanation reactions¹²⁷⁻¹³⁰ and oxazoles (**95**)^{2,131-133} via cyclisation reactions from the carbene precursor. If a starting substrate or co-substrate was designed to contain multiple of these reaction sites, one can alter the reaction outcome by careful selection of catalyst and solvent, ultimately allowing multiple products to be explored from one combination of substrate and co-substrate.¹³⁴

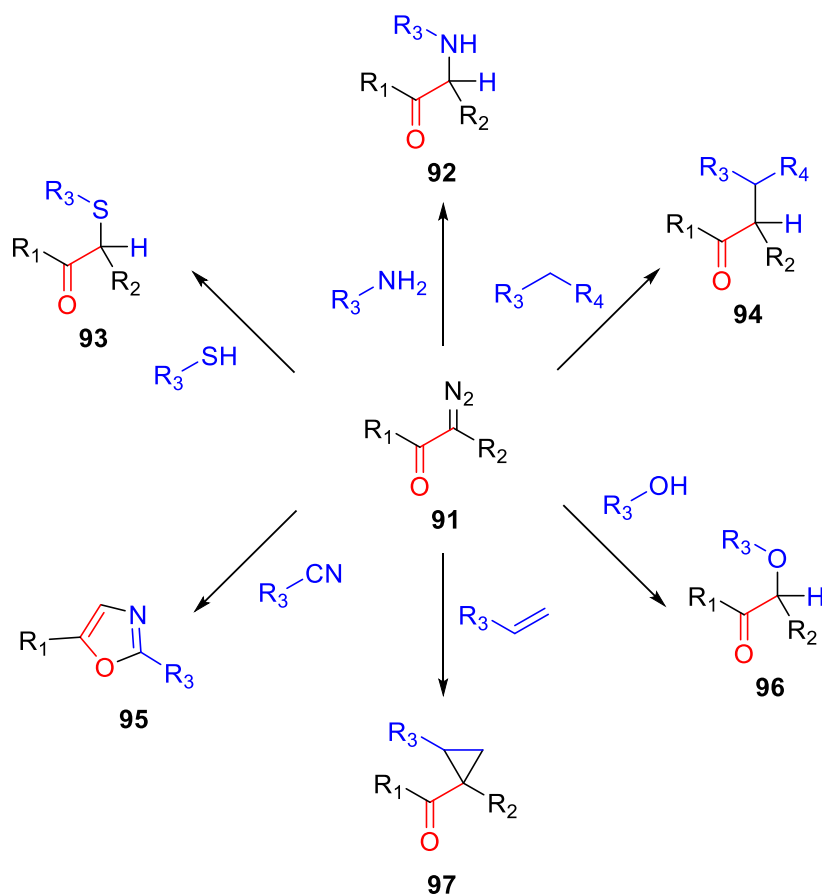


Figure 3.1 Alternative Rh-catalysed carbenoid reactions that yield different chemotypes - Groups derived from co-substrate (blue) have been indicated. Reactions

have been shown to be possible using multiples different Rh catalysts.¹¹⁵

By careful selection of all these components within an ADS reaction array, multiple different products can be formed from the same starting substrates, allowing the exploration of a diverse range of chemical structures, which can be exploited in the discovery of novel chemotypes (Section 1.2.2).

3.2 Design and Synthesis of Substrates for Activity-Directed Synthesis

Both substrates and co-substrates needed to be carefully designed to allow discovery of novel antibacterial scaffolds and, by inclusion of multiple catalysts in the reaction array, allow the exploration of a wide area of chemical space. As diversity was the driving force in the selection of these reaction components, molecular weight, number of heavy atoms (C, N, O, F, S, Cl, Br), AlogP, the diversity of heterorings in the species and commercial availability were all considered in their selection.

3.2.1 Selection of Substrates and Co-Substrates

Co-substrate selection was informed using Pipeline Pilot (Section 2.4).¹¹⁰ Compounds from the commercial database were both filtered by molecular properties and designed to contain at least two reactive groups to limit the number of co-substrates to select from (Figure 3.2).

The outputted molecules served as inspiration for co-substrate selection (Figure 3.3). Some examples of the alternative potentially reactive groups present in each of the co-substrates have been highlighted. Some example sites include alkene motifs present in co-substrates **C1**, **C2**, **C10**, **C12** and **C16** that under the correct conditions, could form new cyclopropane rings. In co-substrates **C5**, **C18** and **C21**, nitrile groups were included that could undergo a cyclisation reaction to form oxazoles, allowing the introduction of new heterocycle rings into the products. Other groups included were, but not limited to, amines/anilines, benzylic and aromatic carbons, and

alcohols/phenols. Although reactivity was a key driving force for co-substrate selection, molecular properties also had a large weighting on the final selection. Heavy atom count, AlogP and the type of ring systems present were important in the final selection to ensure a diverse scope of products could potentially be synthesised within the reaction array. A plot of AlogP against number of heavy atoms has been included to show the distribution of the co-substates molecular properties (Panel B, Figure 3.3).

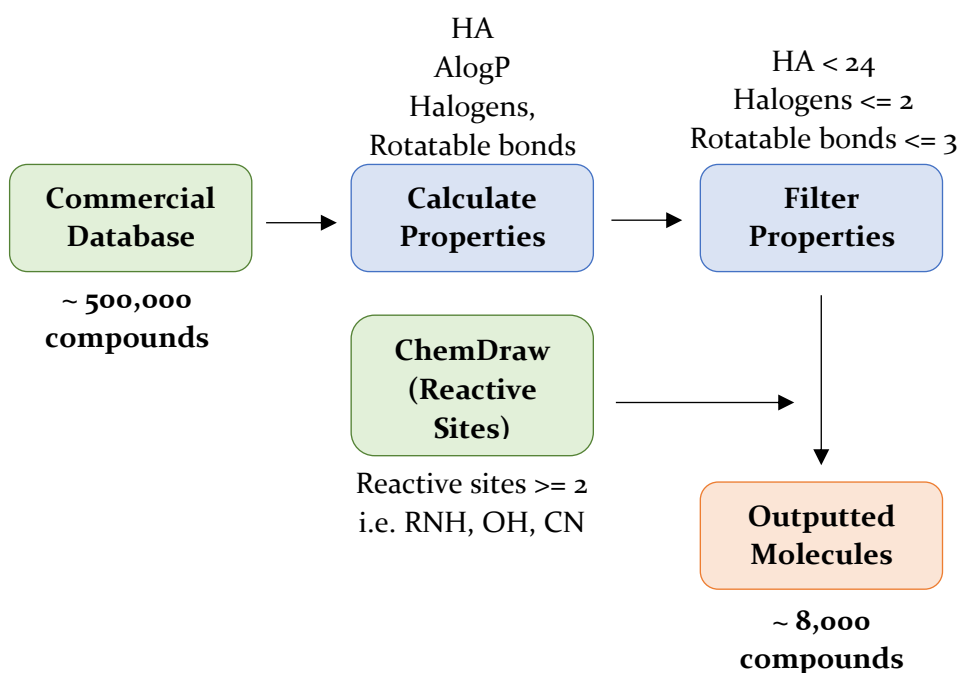


Figure 3.2 Summarised flow chart of the Pipeline Pilot filtering protocol - The commercial databases of Merck, Fluorochem and Alfa Aesar were inputted, and duplicate molecules were removed (~500,000 compounds inputted). The molecular properties of these compounds were calculated including heavy atoms (C, N, O, F, S, Cl, Br, I), molecular weight, number of rotatable bonds and AlogP. Compounds were filtered to limit HA < 24, halogens <= 2 and rotatable bonds <=3. One ChemDraw file, containing possible reactive sites, was inputted, and mapped onto the molecules. Compounds were filtered to ensure that they had at least 2 potentially reactive sites (Section 5.2.1). Those containing at least two reactive sites were outputted and a list of potential co-substrates was created (~8000 compounds outputted). These were filtered by eye and interesting compounds were chosen.

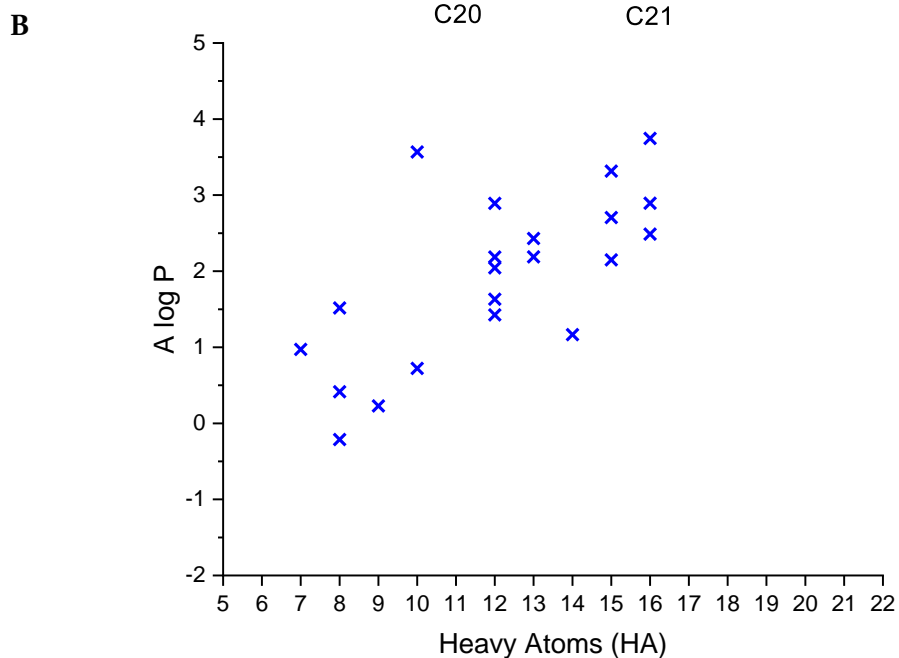
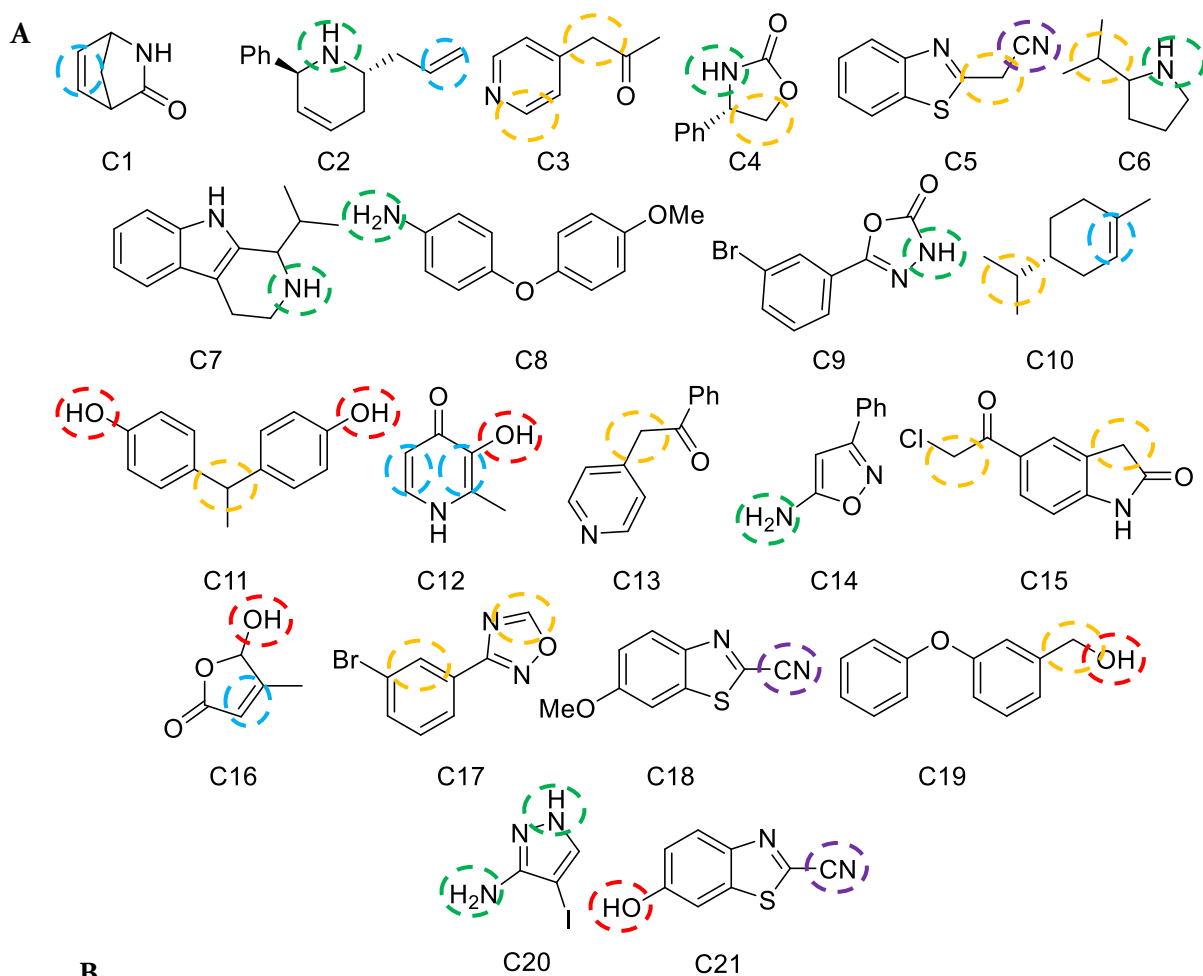


Figure 3.3 Set of 21 co-substrates chosen for the Rh-catalysed array and their molecular property distribution - Panel A: Co-substrates selected with examples of sites that can undergo cyclopropanation (blue), N-H insertion (green), O-H insertion

(red), C-H insertion (yellow) and oxazole formation (purple) have been indicated. Panel B: A plot of AlogP versus heavy atom count to show the molecular property distribution of co-substrates.

As all substrates required synthesis prior to use, diazo compounds were selected based on compounds that had been synthesised before within the Nelson group (Figure 3.4). The six substrates chosen were designed to contain different heterorings. As before, a plot of AlogP vs. number of heavy atoms has been produced.

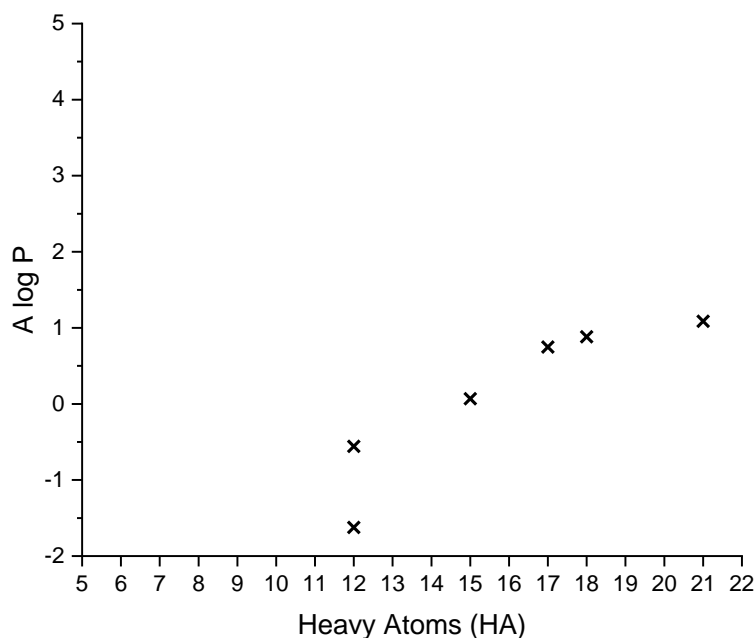
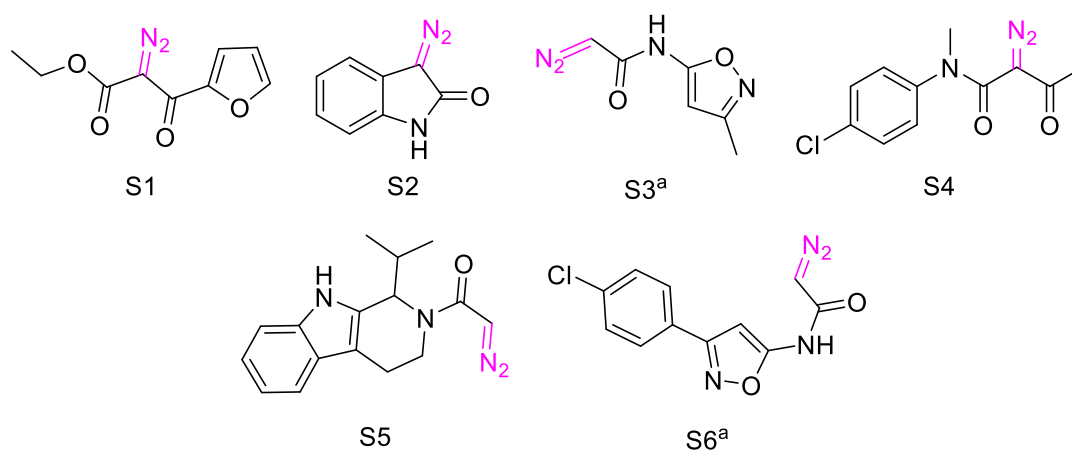


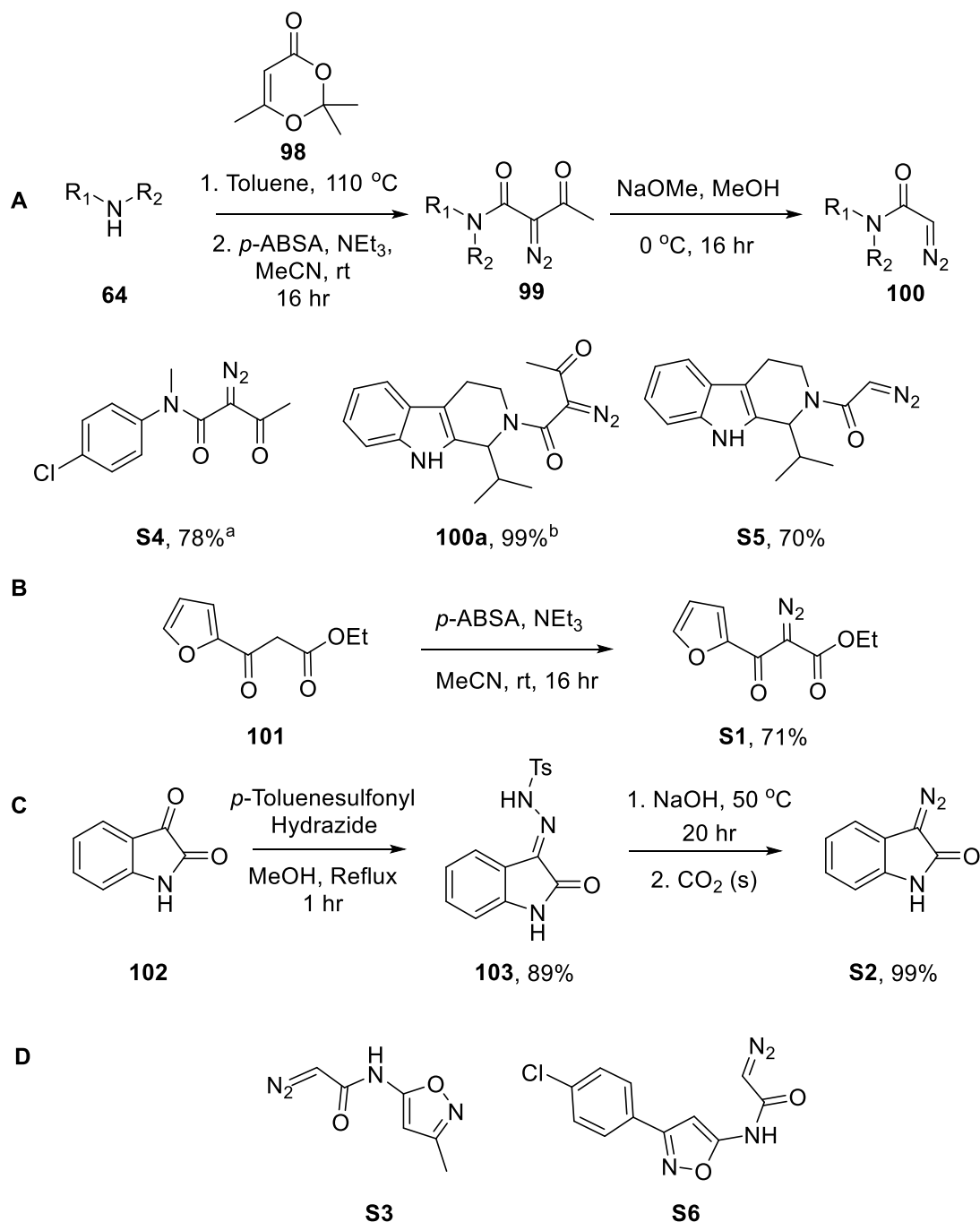
Figure 3.4 Set of 6 substrates chosen for the Rh-catalysed array and their molecular property distribution - Panel A: The six chosen diazo compounds with their reactive sites indicated (pink). ^a Compounds were obtained from research group

inventory and did not require synthesis.⁴⁷ Panel B: A plot of AlogP versus number of heavy atoms for all six substrates.

3.2.2 Preparation of Diazo Substrates

Substrate were prepared, firstly, from their corresponding amine or aniline via a *N*-acetylation and subsequent diazo transfer (Scheme 3.1, Panel A). The appropriate amine/aniline (1 equiv.) and 2,2,6-trimethyl-4H-1,3-dioxin-4-one, **98** (1.2 equiv.) were dissolved in toluene and were either irradiated by microwave radiation at 110 °C for 4 h (**S4**) or heated under reflux for 16 h (**99a**). The resulting reaction mixtures were concentrated under reduced pressure and the crude product was redissolved in ethyl acetate, washed with brine, and concentrated. The crude intermediate and triethylamine (2 equiv.) were dissolved in acetonitrile and 4-acetamidobenzenesulfonyl azide (*p*-ABSA) (1.1 equiv.) was added portion-wise. The reaction mixture was stirred at rt overnight until completion, affording **S4** in 71% yield and **99a** in 80% yield. To synthesise **S5**, intermediate **99a** was then dissolved in methanol at 0 °C and NaOMe (1.1 equiv.) was added. The reaction mixture was stirred for 16 h to afford **S5** in 70% yield.¹³⁵ This method was chosen as it could afford reasonable yields of α -diazo amides from amine or aniline substrates. Substrate **S1** was synthesised via a diazo transfer onto the corresponding dicarbonyl species as described above (Scheme 3.1, Panel B).

Substrate **S2** was synthesised by the formation of the corresponding hydrazone followed by decomposition.^{136,137} Isatin (1 equiv.) was dissolved in methanol and *p*-toluenesulfonyl hydrazide (1.02 equiv.) was added portion-wise. The reaction was stirred at rt for 1 h to afford **103** in 71% yield. Hydrazone **103** was dissolved in NaOH and heated to 50 °C for 20 h. Dry ice was added to acidify the solution and afford **S2** in 99% yield (Scheme 3.1, Panel C). Both diazo compounds **S3** and **S6** were obtained from research group inventory and were synthesised by Adam Green (Scheme 3.1, Panel D).⁴⁷



Scheme 3.1 Synthesis of diazo substrates - Panel A: Synthesis via *N*-acetylation and diazo transfer followed by deacetylation.¹³⁵ ^a *N*-acetylation performed for 4 h under microwave irradiation ^b for 16 h under reflux. Panel B: Synthesis via diazo transfer of starting material **101**. Panel C: Synthesis of hydrazone followed by conversion to diazo compound **S2**.^{136,137} Panel D: Compounds did not require synthesis and were obtained from the Nelson inventory.⁴⁷

3.3 Rh Catalysed Reaction Arrays

After all diazo compounds were synthesised, the reaction arrays were executed. Unlike Pd reaction arrays (Section 2.5), Rh arrays do not require heating and thus were performed in borosilicate glass vials organised in a custom-made PTFE block. Substrates, co-substrates, and catalysts were added from stock solutions therefore solubility in CH_2Cl_2 needed to be assessed. Most compounds were found to be soluble. In cases where dissolution was not possible at the desired concentration, additional CH_2Cl_2 was added to the stock solution to make it less concentrated. In cases where this did not dissolve the substrate or co-substrate, suspensions were added. To ensure even loading, these were stirred vigorously prior to each addition. All catalysts were selected based on both on their complementary reactivity and their ability to dissolve in CH_2Cl_2 .¹³⁸⁻¹⁴²

All Rh reaction arrays were performed using methodology previous developed within the group.^{2,46} The diazo substrates (8 μL ; typically 1.25 M in CH_2Cl_2) were added to the appropriate vials and the solvent was evaporated. Then, co-substrates (8 μL , 2.5 M in CH_2Cl_2) were added, and the solvent was evaporated. Finally, the appropriate catalyst (100 μL , 1 mM in CH_2Cl_2) was added to give a final reaction concentration of 100 mM in 100 μL of CH_2Cl_2 based on the limiting diazo reagent. After sealing, the vials were reacted at rt for 24 h. Upon reaction completion, CH_2Cl_2 was evaporated, and wells were redissolved in DMSO to a total product concentration of 100 mM.

3.3.1 Detection of Activity of Individual Reaction Components

Prior to screening the reaction mixtures, the individual substrates, co-substrates, and catalysts were screened to test whether they inhibited bacterial growth. Individual components were tested at the same concentration in these control reactions, as the corresponding components were in the reaction array. One mock reaction was performed for each component and set up as they would be in a reaction array, assuming a total product concentration of 100 mM (Section 3.3).

For screening, all individual components were treated as they would be in the array. The screening assay used previously was adapted to more closely represent CLSI guidelines,¹⁴³ as, unlike in chapter 2, it was not assumed that the products would have

low solubility (Section 2.3). The stock solutions were diluted with DMSO to a total product concentration of 10 mM (100% DMSO), dissolved in water to 1 mM (10% DMSO) and subsequently screened at a total product concentration of 100 μ M (1% DMSO in MHB-II) following General Screening Procedure B (Chapter 5, Section 5.3), with 1 mM stocks being diluted in MHB-II containing standardised ATCC29213. Plates were incubated for 16 h at 37 $^{\circ}$ C and the optical density was measured using a plate reader ($\lambda = 600$ nm). The positive control used to assess the validity of this experimental was Penicillin G, **24**. Each reaction mixture/component was screened against two colonies of ATCC29213 and the values were plotted (Figure 3.6). At a total product concentration of 100 μ M, Penicillin G, **24** inhibited ATCC29213 growth visually and most individual reaction components did not inhibit bacterial growth, although significant background activity was observed. From the compounds tested, only one co-substrate, α -chloro ketone **C15**, and Rh₂Piv₄ showed >75% growth inhibition (visual growth inhibition threshold), therefore, combinations containing these compounds were removed from the array.

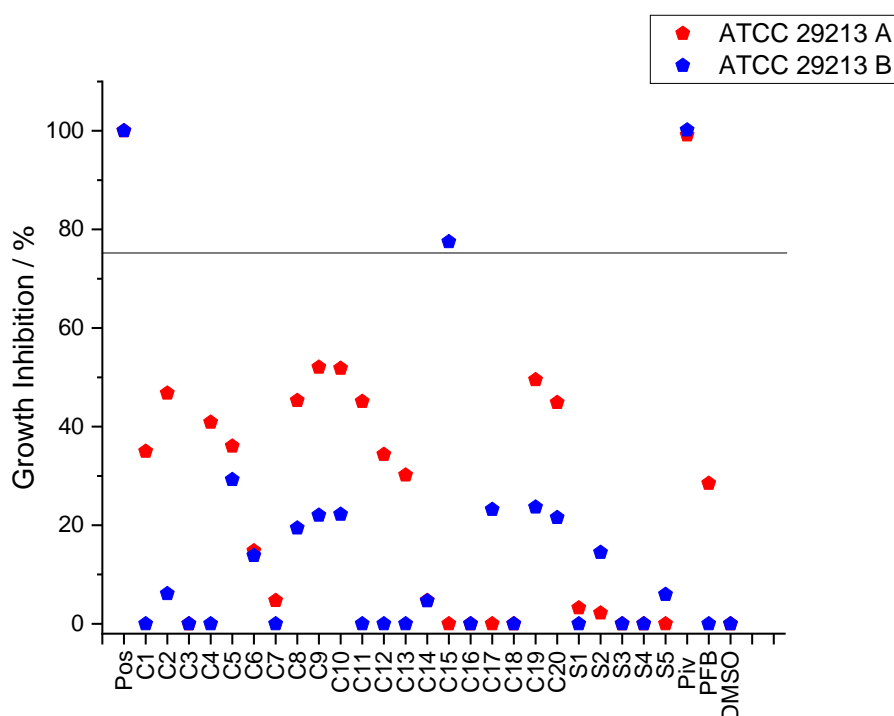


Figure 3.5 Growth inhibition values of individual reaction components in Rh reaction array without catalyst scavenging, Penicillin G, **24** (Pos) and a 1% DMSO Control against *S. aureus* ATCC29213 - Reaction concentrations were based on the limiting reagent of the reaction mixtures, 100 mM. Screening was performed at a total

product concentration of 100 μM . Within this assay, significant background activity was observed.

3.3.2 Reaction Array Execution and Product Analysis

Having assessed the toxicity of all the individual reaction components in array **a**, a reaction array was executed based on five substrates **S1-S5** (and no substrate), twenty co-substrates **C1-C14, C16-C20** (and no co-substrate) and one catalyst, Rh_2pfb_4 . The array of 120 reactions was designed to enable formation of multiple scaffolds which could potentially possess antibacterial properties (Section 3.2.1). An exhaustive array was performed as described in Section 3.3.

Analytical LC-MS was performed to investigate the productivity of the chemistry on twelve randomly selected product mixtures (approximately 10% of the total number of reactions). Masses that matched that of the respective intermolecular product were identified and recorded (Table 3.1). In addition, masses that corresponded to an intermolecular product followed by oxidation by formal dehydrogenation and those masses of a plausible alternative product, formed without the loss of dinitrogen, were also included. Three of the explored reactions, contained intermolecular products, three contained the mass of the intermolecular product followed by subsequent loss of two hydrogens and two contained the mass of an alternative product: **S2, C7** displayed the mass of the intermolecular product, plus dinitrogen, with the loss of two hydrogens and **S1, C13** displayed the mass of the intermolecular product plus dinitrogen.

Combination	Intermolecular Mass	Mass corresponding to intermolecular product ^a	Mass corresponding to intermolecular product with oxidation ^b	Mass corresponding to alternative product
S2, C4	294		✓ (292)	
S2, C7	345			✓ (371) ^c
S2, C18	321			
S3, C19	338	✓		

S1, C13	377		✓ (405) ^d
S2, C14	291	✓	
S5, C8	469	✓	
S1, C6	293		
S1, C8	395		
S2, C8	346		
S5, C5	428		✓ (426)
S3, C10	276		✓ (274)

Table 3.1 Results of the LC-MS screen performed on a random ~10% of wells from Rh reaction array without catalyst scavenging - ^aTick indicates that the mass corresponding to an intermolecular product was observed ^bTick indicates that the mass corresponding to an intermolecular product followed by oxidation was observed. ^c Corresponds to mass of intermolecular product, plus dinitrogen, minus two hydrogens. ^d Corresponds to mass of intermolecular product, plus dinitrogen.

From the masses obtained during this study, it is possible to predict some products that could have formed within this reaction array (Figure 3.6). Three of the reaction mixtures displayed the mass of the intermolecular product (labelled **104**, **105** and **106**) and so it can be assumed these reactions would have reacted at one of the expected reaction sites. In some examples, the mass of the intermolecular product plus formal dehydrogenation was also observed (labelled **107**). As with the previous ADS array, none of these reactions were scaled up and only mass was used to determine reaction success. It is estimated that from 100 reactions, over half yielded at least one product.

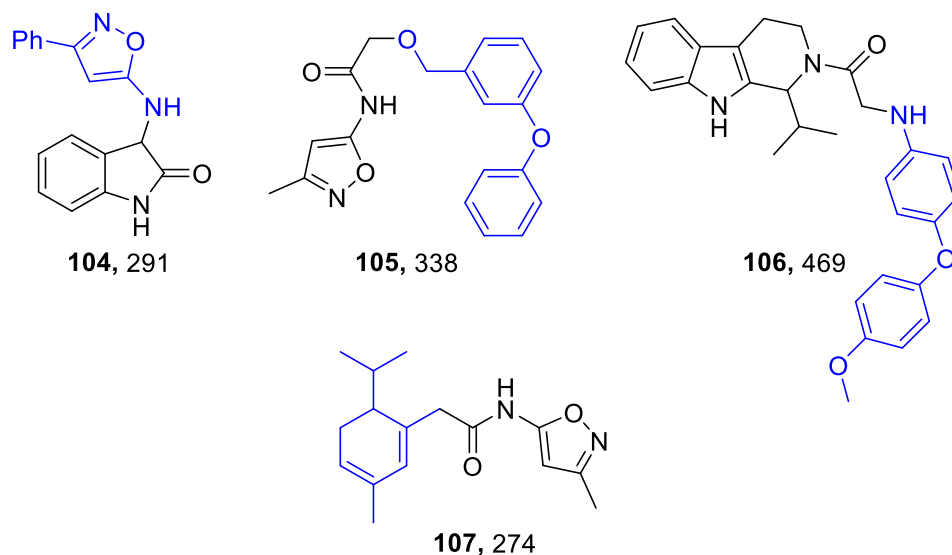


Figure 3.6 Possible products, with masses that were observed, that could have formed within the reactions listed in Table 3.1- Masses were obtained from the LCMS screen and matched the theoretical mass values for all four compounds.

3.3.3 Reaction Array Results

The crude reaction mixtures were screened in duplicate against *S. aureus* ATCC29213 (final product concentration of 100 μM in 1% DMSO in MHB-II). Initially, reaction wells containing 100% DMSO at 100 mM total product concentration were diluted to 10 mM total product concentration in 100% DMSO (100-fold higher than the screening concentration). Then, 10 μL of each of the 10 mM reaction wells were pipetted into the sterile plate and were diluted in 90 μL water to a total product concentration of 1 mM. Afterwards, 10 μL of each of the 1 mM reaction wells were diluted in 90 μL of MHB-II containing the standardised ATCC29213 ($5 \times 10^5 \text{ CFU mL}^{-1}$)¹⁰⁶ to ensure each screening well contained 1% DMSO and a final total product concentration of 100 μM . Plates were incubated for 16 h at 37 $^\circ\text{C}$ using both a growth control (antibacterial free, 1% DMSO in MHB-II) and Penicillin G, **24** (100 μM in 1% DMSO in MHB-II) as a positive control. In addition to visual observation, the optical density was measured using a plate reader at 600 nm and converted to growth inhibition. All wells were screened in duplicate against two different colonies of ATCC29213 and mixtures that were active in duplicate were considered hits.

From the 100 crude reaction mixtures that were screened, two displayed significant antibacterial activity against both cultures: Substrate **S2** (with **C5**) and substrate **S5** (with **C20**). Substrates and co-substrates have been plotted within a heat map to display the growth inhibition of all combinations (Figure 3.7). For a reaction to be deemed a hit, both must exhibit growth inhibition. Control wells (with either blank substrate or blank co-substrate with catalyst) display no activity, indicating that reaction combinations that displayed activity had not been influenced by either starting materials, intramolecular diazo reaction products or co-operative effects between the catalyst and co-substrate. Reactions involving components (Rh_2Piv_4 and **C15**) possessing antibacterial activity prior to reaction (Section 3.3.1), have been excluded from the data set.

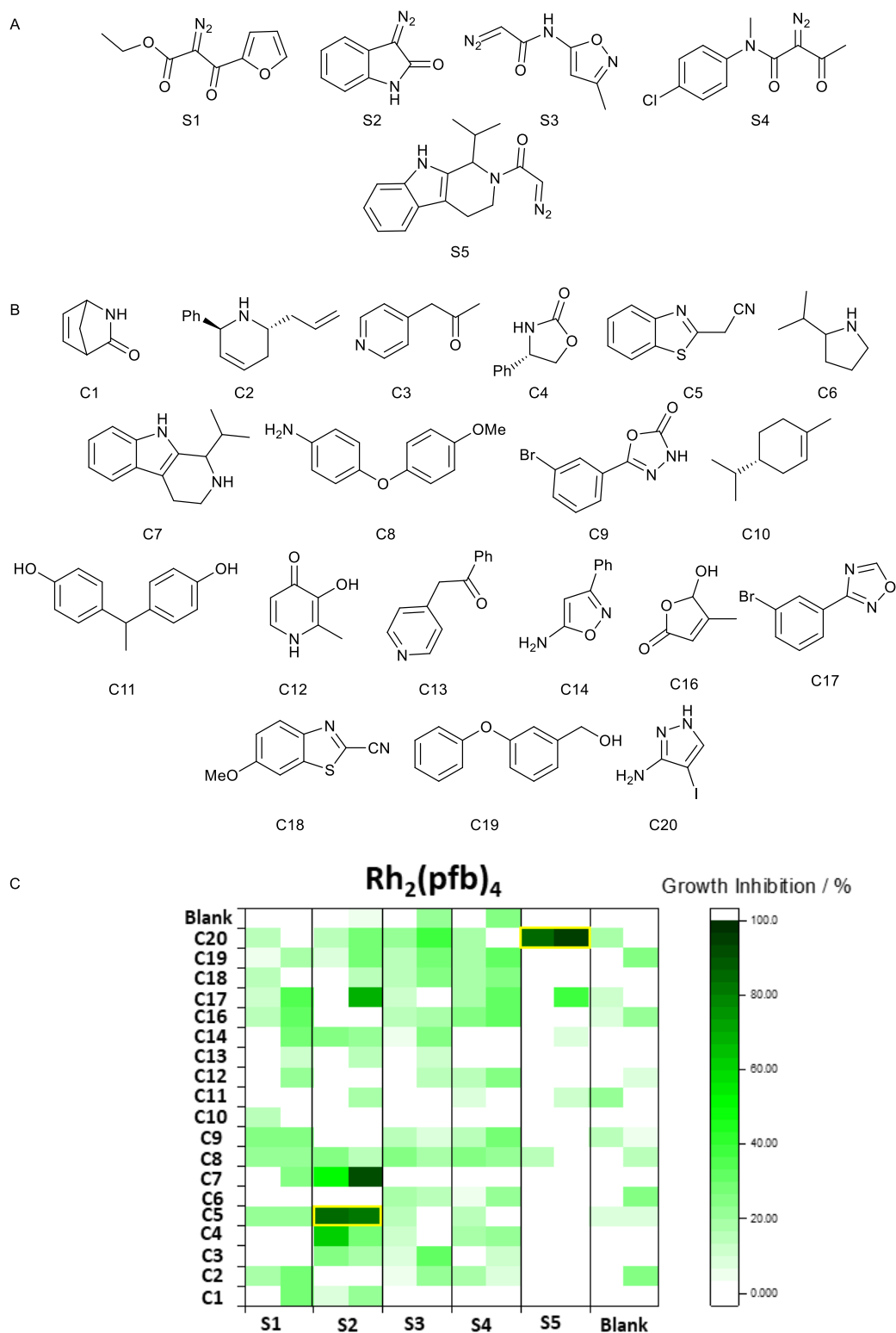


Figure 3.7 Activity-directed antibacterial discovery using Rh Carbenoid Chemistry without catalyst scavenging - Panels A and B: Structures of substrates (A) and co-substrates (B). Panel C: Activity against *S. aureus* ATCC29213 (total product concentration: 100 μ M), with active combinations shown (yellow box). On the x-axis,

the substrates have been plotted and duplicate screens have been placed adjacent to each other. On the y-axis, co-substrates have been plotted and labelled accordingly.

3.4 Scale-up and Structural Elucidation of Antibacterial Ligands

Active combinations were scaled-up to structurally elucidate the active products within the reaction mixtures. These products were purified and screened against ATCC29213 to detect whether they were responsible for the activity.

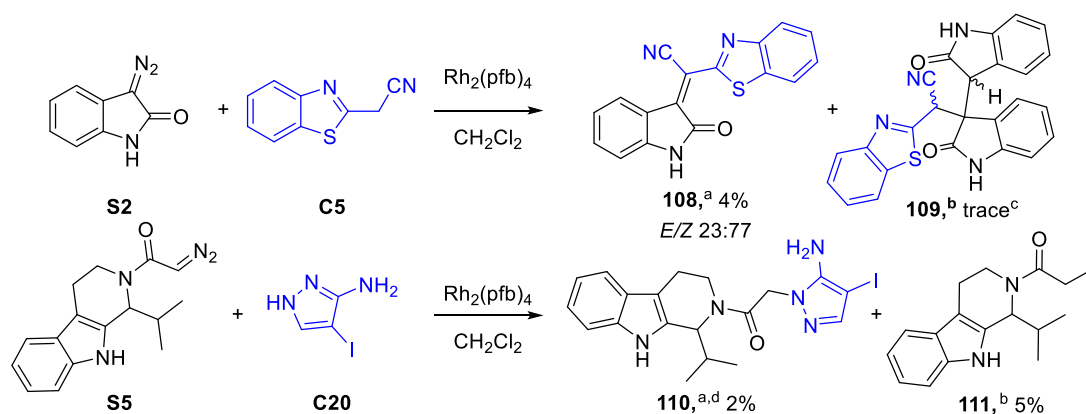
3.4.1 Scale-up and Isolation of Products within Active Combinations

Prior to scale-up, reaction combinations highlighted by yellow squares (Figure 3.8, Section 3.3.3) that possessed antibacterial activity in duplicate were investigated to see whether they possessed a plausible product mass by LC-MS. In both the active combinations between substrate **S2** (with **C5**) and substrate **S5** (with **C20**), the mass of an intermolecular product was identified (Table 3.2). For the reaction between **S2** and **C5**, the product mass corresponded to an intermolecular reaction followed by formal dehydrogenation of the product.

Combination	Intermolecular Mass	Mass corresponding to intermolecular product ^a	Mass corresponding to intermolecular product with oxidation
S2, C5, Rh ₂ (pfb) ₄	305		✓ (303) ^b
S5, C20, Rh ₂ (pfb) ₄	463	✓	

Table 3.2 Results of the LC-MS screen performed on active combinations - ^aTick indicates that the mass corresponding to an intermolecular product was observed ^bTick indicates that the mass corresponding to an intermolecular product followed by formal dehydrogenation was observed. Reaction combinations and intermolecular masses have been indicated.

Upon identification of an intermolecular mass, both reactions were scaled-up to allow structural elucidation of the product. Typically, reactions were performed on a 50-fold scale, with 0.5 mmol of substrate. The appropriate diazo substrate (1 equiv.) and co-substrate (2 equiv.) were added to a crimp-top vial containing $\text{Rh}_2(\text{pfb})_4$ (1 mol%) and the mixture was dissolved in CH_2Cl_2 (10 mL per mmol). After stirring at rt for 24 h, the crude mixture was filtered through silica followed by purification by UV-directed HPLC to afford the reaction products (Scheme 3.2). Reaction mixtures were complex and product isolation was non-trivial. For the reaction between **S2** and **C5**, two products of interest were isolated: **108**, the intermolecular product identified by LC-MS analysis; and **109**, a product with a mass of 436, identified via peptide LCMS-MS within a mixture of co-substrate **C5**. It was hypothesised that **109** had likely formed from the conjugate addition of the co-substrate into the dimer of **S2**. The structures of **108** and **109** were later confirmed by independent synthesis (Section 3.4.3). For the reaction between **S5** and **C20**, two products of interest were also identified, including the intermolecular product **110** and product **111**, a product with a mass of 382, likely to be an iodine insertion product. The structure of **111** was confirmed by detailed characterisation (Section 3.4.2).



Scheme 3.2 Scale-up reactions of active combinations found in the array screen against ATCC29213- Panel A: Scale-up reaction of **S2** (**C5**) and **S5** (**C20**) with the products isolated from the mixture: Substrate (1 equiv.), Co-substrate (2 equiv.) and catalyst (1 mol%). ^a The suspected intermolecular product responsible for the mass on LC-MS. ^b Compounds other than the intermolecular product isolated from the reaction mixture. ^c A possible structure for compound **109**, identified using LCMS-MS, present

within a mixture of itself and **C5**. Functionality obtained from the co-substrate has been indicated (blue). The structure of compounds **109** and **111** were determined by detailed characterisation and independent synthesis (Section 3.4.2 and Section 3.4.3).^d Compound **110** is one of two possible regioisomers (from HMBC evidence), the other has been reported in Section 5.2.3.

3.4.2 Confirmation of the Structure of Compound **111**

Although scale-up yielded the expected intermolecular products, other unexpected products were also isolated by HPLC. Of particular interest was the reaction between **S5** and **C20** to yield **111** as it was an unexpected product under the reaction conditions described (Section 3.4.1). The structure of **111** was validated by the identification of characteristic peaks by both ¹H NMR and ¹³C NMR (Figure 3.8) and by identification of its corresponding mass (382).

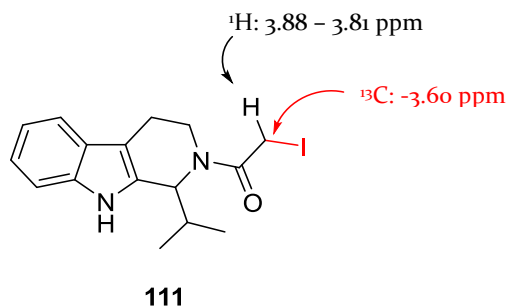


Figure 3.8 Key NMR peaks used in the identification of **111** - The ¹³C NMR of **111** possessed a peak at -3.60 ppm, that lies within the region commonly associated with saturated carbon-iodine bonds (red).^{144,145} From the HSQC, it was evident that on this carbon, lies two protons which are shifted to around 3.85 ppm. On the HMBC spectra, this peak did not see any other carbons in the compound as no carbons lie within 3-bonds of these protons which would not be observed in any other products with the mass of 382. NMR data has been provided in Appendix B.2.

Two possible mechanism that could account for such a reaction has been described (Figure 3.9). Firstly, within the first mechanism, it is hypothesised that a HI source is responsible for the formation of **111**. This HI could have been present in the

purchased starting material or conversely, could have formed via decomposition pathways of the iodoaminopyrazole, potentially via a ring fragmentation of **C20** to give alkyl iodide **114**. If a nucleophilic species is present within the reaction mixture, **114** could subsequently be substituted by H-Nu to get HI. These decomposition pathways are preceded with isoxazoles in the presence of base¹⁴⁶⁻¹⁴⁹ and have some precedent in photochemical reactions of pyrazoles.¹⁵⁰ The resulting HI can then react with the carbene to form product **111**, as has been observed within the literature.¹³² Alternatively, it is possible that **116** could insert directly into the iodine lone pair on pyrazole **C20** to give a iodonium ylide **117**.¹⁵¹⁻¹⁵³ Addition of an X⁻ source within the reaction mixture to the iodine would produce a trivalent species that, following a reductive elimination,^{154,155} would give product **111**. Without further mechanistic studies, neither mechanism can be confirmed. From both spectral and mechanistic analysis, the structure of **111** could be confidently assigned.

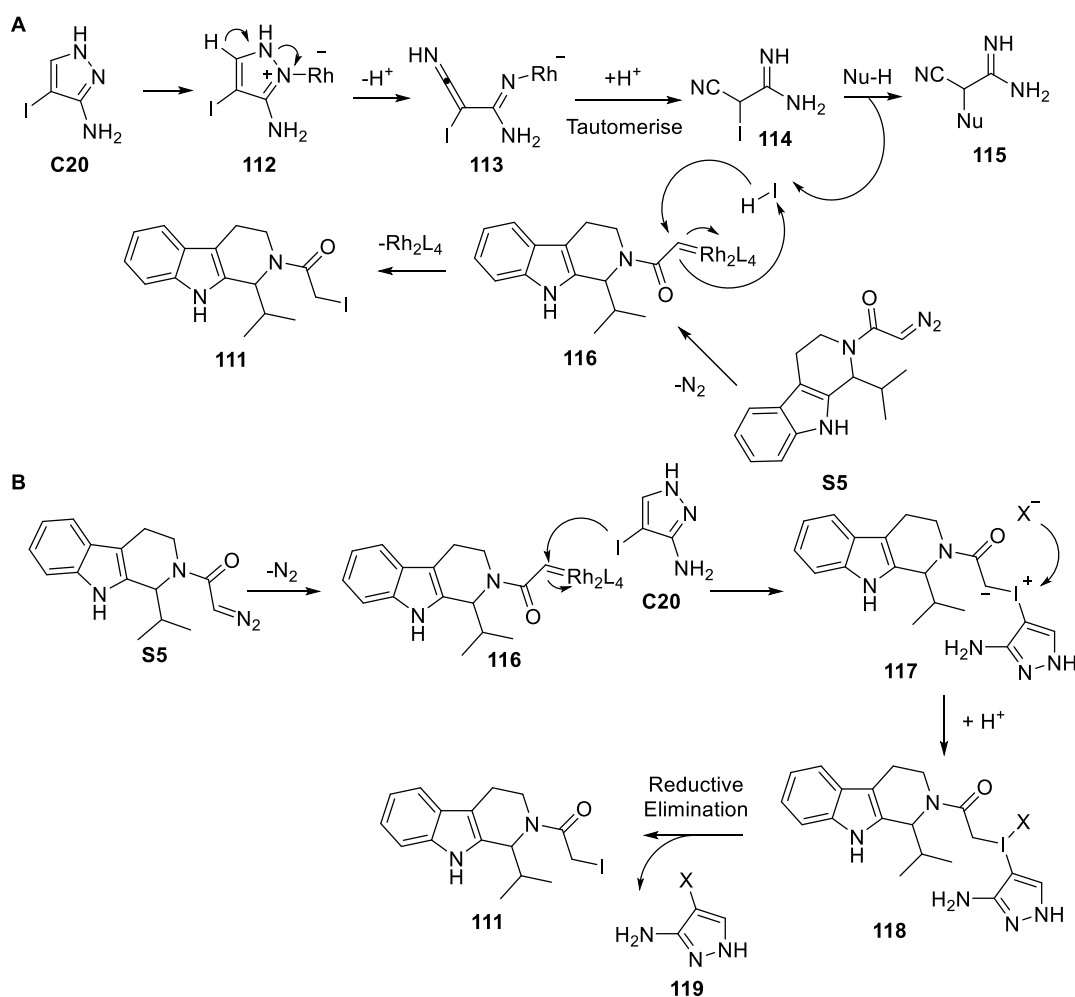
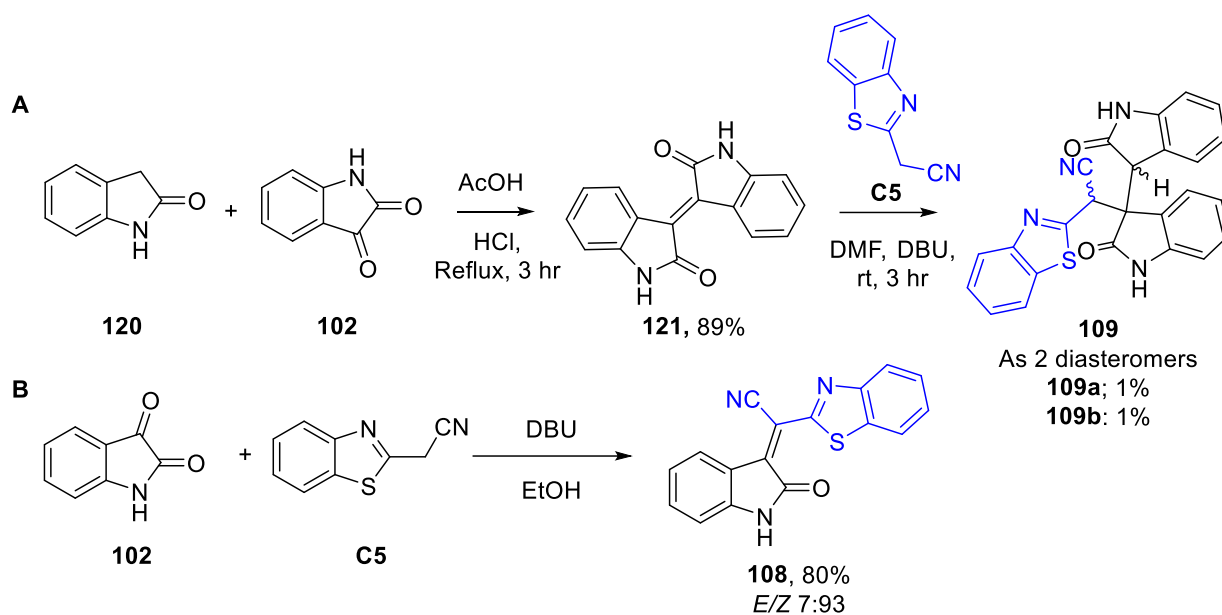


Figure 3.9 Possible mechanism for the synthesis of **111** from **S5** and **C20**- Panel A: This hypothesised mechanism begins via the formation of HI from the decomposition

of **C20**. The carbene produced via the loss of nitrogen from **S5** reacts with this to produce product **111**. Panel B: Alternatively, it is possible **116** could insert into the lone pair of iodine to form iodonium ylide **117**. Addition of an X^- source followed by reductive elimination could lead to compound **111**.

3.4.3 Confirmation of Structures via Independent Synthesis

Two of the products had been formed in low yield, and it was decided to synthesise them by independent routes to confirm their structures (Scheme 3.4). For determination of the trace product isolated from the reaction between **S2** and **C5**, the dimer **121** was firstly synthesised from isatin (1 equiv.) and oxindole **120** (1 equiv.) in the presence of concentrated hydrochloric acid via a dehydration reaction.¹⁵⁶ Afterwards, **121** was added to a solution of **C5** (1 equiv.) and DBU (1.1 equiv.) in DMF and stirred until completion to afford **109** as a complex mixture. Two diastereomers were isolated from the reaction mixture via UV-directed HPLC, **109a** and **109b**, whose relative configuration could not be confirmed by NOESY NMR. Interestingly, the benzothiazole motif appears to be important for Gram-positive activity in some reported antibacterials.¹⁵⁷⁻¹⁶² Compound **108** was also synthesised via a Knoevenagel condensation of isatin **102** (1 equiv.) with **C5** (1 equiv.) to validate antibacterial screen and assess whether the different ratios of E/Z isomers caused different activities.¹⁶³



Scheme 3.3 Synthesis of 109a and 109b via an alternative conjugate addition reaction between the dimer and co-substrate - Panel A: Synthesis of **109a** and **109b**, isolated as two diastereomers. Yields of the products have been displayed.¹⁵⁶ Relative configuration could not be confirmed using NOESY NMR. Panel B: An alternative synthetic route for **108** to validate antibacterial screen and control for *E/Z* isomers with differing activities. A ratio has been reported for *E/Z* isomers, determined by ¹H NMR, however, crystals could not be grown for true conformational assignment and X-Ray crystal structures could not be found in the literature.

To confirm that both isolated diastereomers had indeed formed within the original reaction array, the retention times of both isolated diastereomers were compared with those found within the impure reaction mixture between **S2** and **C5** using peptide LCMS-MS (Figure 3.10). Peaks, with the mass of 436, were identified within the original mixture; with an adduct of 263, equivalent to the dimer portion of the molecule, being primarily observed. The spectra was overlaid with the purified diastereomers. Both products **109a** and **109b** had retention times identical to those found within the Rh reaction mixture and it was concluded that the isolated compounds were the same as those that had formed within the reaction array. From the peak retention time, it was likely not all possible diastereomers had been isolated. It was believed that **109a** and **109b** could undergo a reversible reaction to form dimer **121**, however, product quantities were not large enough to investigate this in detail. In the future, the nitrile in both diastereomers will be reduced into an amine, and

products will be biologically tested, to confirm whether any activity is caused by reformation of dimer **121** or the product.

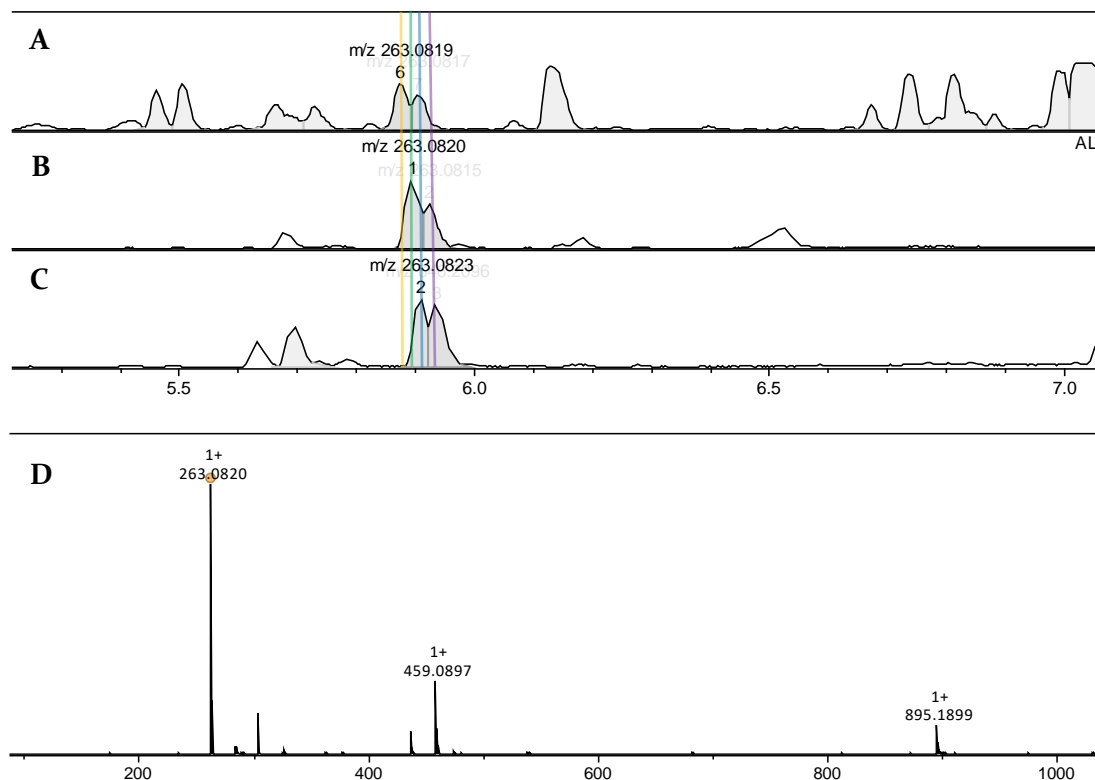


Figure 3.10 Comparison of the retention times of **109a and **109b** with the crude reaction mixture between **S2** and **C5** - Panel A: LC-MS trace of crude reaction mixture between **S2** and **C5** catalysed by $\text{Rh}_2(\text{pfb})_4$. Panel B: LC-MS trace of **109a**. Panel C: LC-MS trace of **109b**. Panel D: MS trace of **109a**, confirming presence of 436 as $\text{M}+\text{Na}$. Peaks of interest have been indicated, with each possible diastereomer peak indicated with different colours (orange, green, blue and purple).**

3.4.4 MIC Determination of Isolated Products Against ATCC29213

All of the isolated compounds were then tested in duplicate against three different colonies of ATCC29213 according to CLSI guidelines.¹⁰⁶ MICs were performed with MHB-II as the media and with two 10-fold dilutions, unlike those described in Section 2.6.4. Accordingly, a 2-fold dilution series of the isolated compounds in DMSO was prepared, ranging from 6400–6.4 $\mu\text{g mL}^{-1}$. Each dilution was transferred into 96-well format, diluted 10-fold in water and diluted again to obtain a final volume of 10 μL

sample (10% DMSO) and 90 μL of the standardised culture in MHB-II. Final antibiotic concentrations range from 64–0.064 $\mu\text{g mL}^{-1}$ (1% DMSO in MHB-II). Plates were incubated for 16 h at 37 °C and the MIC was determined visually as the lowest concentration at which growth was inhibited. The results from this assay have been summarised in Table 3.3.

From the seven isolated products, four displayed activities against ATCC29213. For the reaction between **S5** and **C20**, compound **111** displayed a MIC of 16 $\mu\text{g mL}^{-1}$ and from the combination between **S2** and **C5**, dimer **121**, conjugate addition product **109a** and **109b**, all isolated from an independent synthesis (Section 3.4.3), displayed MIC values of 2 $\mu\text{g mL}^{-1}$, 4–8 $\mu\text{g mL}^{-1}$ and 2–4 $\mu\text{g mL}^{-1}$ respectively. Dimer **121** was a known compound, whose MIC against ATCC29213 could not be found online. No growth inhibition was observed for either intermolecular product (**108** and **110**) or the control product **108**, formed via an independent synthesis and it was concluded these were not responsible for the activity within the reaction mixtures.

Product	Product Mass	MIC / $\mu\text{g mL}^{-1}$	MIC / μM
		ATCC29213	
108^a	303	> 64	> 211
110^a	463	> 64	> 138
111^a	382	16	42
108^b	303	> 64	> 211
121^{bc}	262	2	7.6
109a^b	436	4–8	9.2 – 18.3
109b^b	436	2–4	4.6 – 9.2

Table 3.3 Evaluation of the activity of isolated products against *S. aureus* strains ATCC29213 - The MIC value observed in duplicate on three different days for ATCC29213 is shown. Penicillin G, **24**, used as a positive control in all experiments, displayed MIC values as expected. ^a Substrate (1 equiv.), co-substrate (2 equiv.), 1 mol% Rh catalyst, CH_2Cl_2 . ^b Compounds prepared via independent synthesis. ^c The dimer of diazo **S2**, purified as **121**.

3.5 Rh Catalysed Reaction Array with Scavenging

Within the array described in Section 3.3, the reaction array had been limited to one catalyst (Section 3.3.1), therefore, the possibility of scavenging was investigated. A thiourea (TU) resin was chosen to scavenge away rhodium catalyst as it had been optimised under these array conditions previously.⁴⁶ Reactions were prepared as described in Section 3.3, with the exception that after reacting at rt for 24 h, TU resin (30 mg) was added and the reactions were left for a further 24 h at rt. The reaction wells were filtered to remove the resin, the solvent was evaporated, and the wells were dissolved in DMSO to give a total product concentration of 100 mM.

3.5.1 Detection of Activity of Individual Reaction Components

As described previously (Section 3.3.1), individual substrates, co-substrates and catalysts needed to be evaluated against ATCC29213 to check for assay interference. Although compounds had already been tested, a slight change to the array methodology to include a TU resin meant it was essential to re-evaluate the activities against ATCC29213. Stock solutions were created to the concentrations described in Section 3.3 and mock reactions were performed with each compound as described in Section 3.5, using the TU resin to scavenge for 24 h after reaction completion. Individual components were tested at the concentrations they would be used within each reaction mixture during the final array screen. Each compound was screened at a total product concentration of 100 μ M.

For screening, all individual components were treated as they would be in the array. The screening assay performed as described in Section 3.3.1. The positive control used to assess the validity of this experimental was Penicillin G, **24**. Each reaction mixture/component was screened against two colonies of ATCC29213, and the values were plotted (Figure 3.11). At a total product concentration of 100 μ M, Penicillin G, **24** inhibited ATCC29213 growth visually and all individual reaction components did not inhibit bacterial growth. Unlike the array without scavenging, there was much less variability in the growth inhibition and, as none of the individual reaction components inhibited bacterial growth, all reaction combinations could be explored in the reaction array.

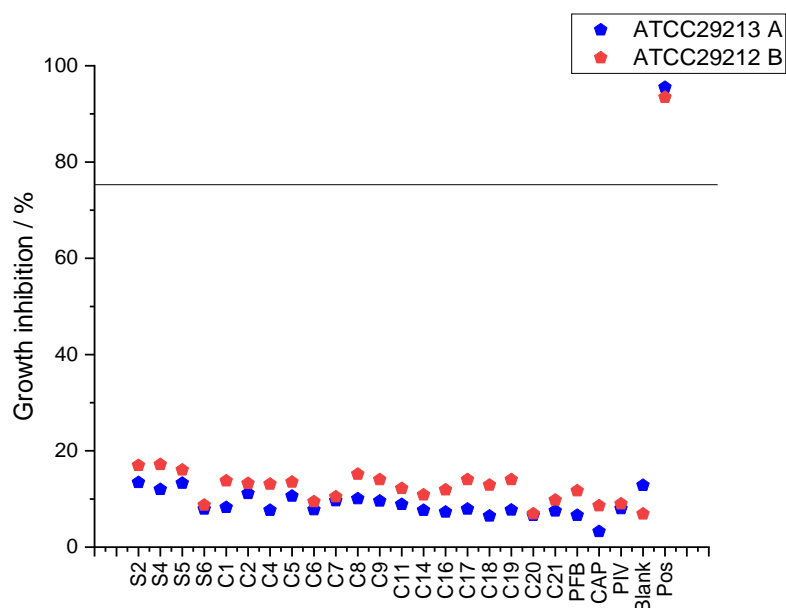


Figure 3.11 Growth inhibition values of individual reaction components in Rh reaction array with catalyst scavenging, Penicillin G, 24 (Pos) and a 1% DMSO Control (Blank) against *S. aureus* ATCC29213 - Reaction concentrations were based on the limiting reagent of the reaction mixtures, 100 mM. Screening was performed at a total product concentration of 100 μ M. Within this assay, there was less noise, a likely consequence of using a resin as a scavenger.

3.5.2 Reaction Array Execution and Product Analysis

Having assessed the toxicity of all the individual reaction components in the array, a reaction array was executed based on four substrates **S2, S4-S6** (and no substrate), sixteen co-substrates **C1, C2, C4-C9, C11, C14, C16-C21** (and no co-substrate) and three catalysts: $\text{Rh}_2(\text{pfb})_4$, $\text{Rh}_2(\text{Piv})_4$ and $\text{Rh}_2(\text{Cap})_4$. An exhaustive array of 255 reactions was performed with components assembled from stock solutions using multi-channel pipettes. Reactions were performed as described in Section 3.5, using the TU resin to scavenge for 24 h after reaction completion.

As with the array without scavenging (Section 3.3.2), analytical LC-MS was performed to investigate the productivity of the chemistry on 25 randomly selected product mixtures (approximately 10% of the total number of reactions) and allow

comparison between the two reaction arrays. Masses that matched that of the respective the intermolecular product were identified and recorded (Table 3.4). In addition, masses that corresponded to an intermolecular product followed by formal dehydrogenation and those masses of a plausible alternative product, formed without the loss of dinitrogen, were also included. Six of these contained intermolecular products, one contained the mass of the intermolecular product followed by subsequent loss of two hydrogens and one contained the mass of the intermolecular product plus dinitrogen. Compared to the array without scavenging, it appeared fewer alternative products had been identified, with most masses identified being from intermolecular product.

Combination	Intermolecular Mass	Mass corresponding to intermolecular product ^a	Mass corresponding to intermolecular product with oxidation	Mass corresponding to plausible alternative product
S2, C2, Rh ₂ (Piv) ₄	330	✓		
S2, C5, Rh ₂ (Piv) ₄	305		✓ (303) ^b	
S4, C2, Rh ₂ (Piv) ₄	422			
S4, C4, Rh ₂ (Piv) ₄	386			
S4, C14, Rh ₂ (Piv) ₄	428	✓		
S6, C4, Rh ₂ (pfb) ₄	397			
S6, C18, Rh ₂ (Piv) ₄	424			
S5, C19, Rh ₂ (pfb) ₄	454			
S6, C21, Rh ₂ (Piv) ₄	410			
S2, C14, Rh ₂ (pfb) ₄	291	✓		
S4, C16, Rh ₂ (cap) ₄	337			
S6, C12, Rh ₂ (cap) ₄	359	✓		
S2, C1, Rh ₂ (pfb) ₄	240	✓		
S4, C9, Rh ₂ (pfb) ₄	462	✓		
S4, C17, Rh ₂ (cap) ₄	446			
S2, C12, Rh ₂ (Piv) ₄	256			
S2, C16, Rh ₂ (pfb) ₄	245			✓ (273) ^c
S6, C19, Rh ₂ (pfb) ₄	434			

S5, C17, Rh ₂ (pfb) ₄	478	
S2, C4, Rh ₂ (Piv) ₄	294	✓
S6, C9, Rh ₂ (Piv) ₄	473	
S4, C12, Rh ₂ (pfb) ₄	348	
S2, C5, Rh ₂ (pfb) ₄	305	
S5, C9, Rh ₂ (Piv) ₄	494	
S5, C12, Rh ₂ (cap) ₄	379	

Table 3.4 Results of the LC-MS screen performed on a random ~10% of wells from Rh reaction array with catalyst scavenging - ^aTick indicates that the mass corresponding to an intermolecular product was observed ^bTick indicates that the mass corresponding to an intermolecular product followed by formal dehydrogenation was observed (Mass - 2). ^cTick indicates mass of intermolecular product plus nitrogen was observed.

Some possible structures of products were predicted based on the intermolecular masses found (Figure 3.12). Within this reaction array, a diverse set of products appear to have formed from different substrates and co-substrates including **122** from **S2** with **C1**, **123** from **S6** with **C12** and **124** from **S2** with **C4**. These products were not isolated, and structures are predicted based on reactive sites within the co-substrates. Of course, it is possible multiple different intermolecular products had also formed within the wells. Within this array, around 40% of the reactions were productive, confirming the chemistry was successful in many reaction wells. Analysis of the masses found in all the reaction wells would be required to confidently compare the productivity of both arrays, but from a selection of 10% reactions, the array without a TU resin appears to have yielded a larger percentage of productive reactions, perhaps as electrophilic products had been generated that are now being scavenged (Section 3.3.2).

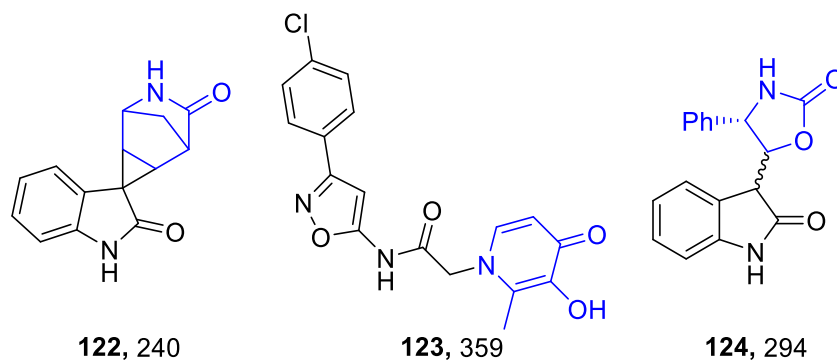


Figure 3.12 A selection of possible products, with masses that were observed, that could have formed within in the reactions listed in Table 3.4- Masses were obtained from the LCMS screen and matched the theoretical mass values for all three compounds.

3.5.3 Reaction Array Results and Validation

The crude reaction mixtures were screened in duplicate against *S. aureus* ATCC29213 as described in Section 3.3.3. From all the 192 crude reaction mixtures that were screened, seven displayed significant antibacterial activity against both cultures: Substrate **S2** (with **C7** and $\text{Rh}_2(\text{Piv})_4$); substrate **S4** (with **C7** and **C18** and $\text{Rh}_2(\text{Piv})_4$) and substrate **S5** (with **C4**, **C5**, **C17** and **C18** and $\text{Rh}_2(\text{Piv})_4$). Substrates and co-substrates have been plotted within a heat map to display the growth inhibition of all combinations (Figure 3.13). Control wells (with either blank substrate or blank co-substrate with catalyst) have been plotted on the outside of the heat map and the majority display no activity. In the case of **C2** with $\text{Rh}_2(\text{Piv})_4$, antibacterial activity was observed in duplicate and so this row was not investigated further. For the combination between **C18** and $\text{Rh}_2(\text{Piv})_4$, the well was rescreened against two colonies of ATCC29213 and found to be inactive. Active combinations that duplicated have been highlighted in a yellow box. Combinations between **C2** (with **C5**) and **S5** (with **C20**) in the presence of $\text{Rh}_2(\text{pfb})_4$, that possessed activity when resin was not used (Section 3.3.3), no longer possessed activity, likely caused by the active products being scavenged away within the reaction mixtures upon addition of the TU resin.

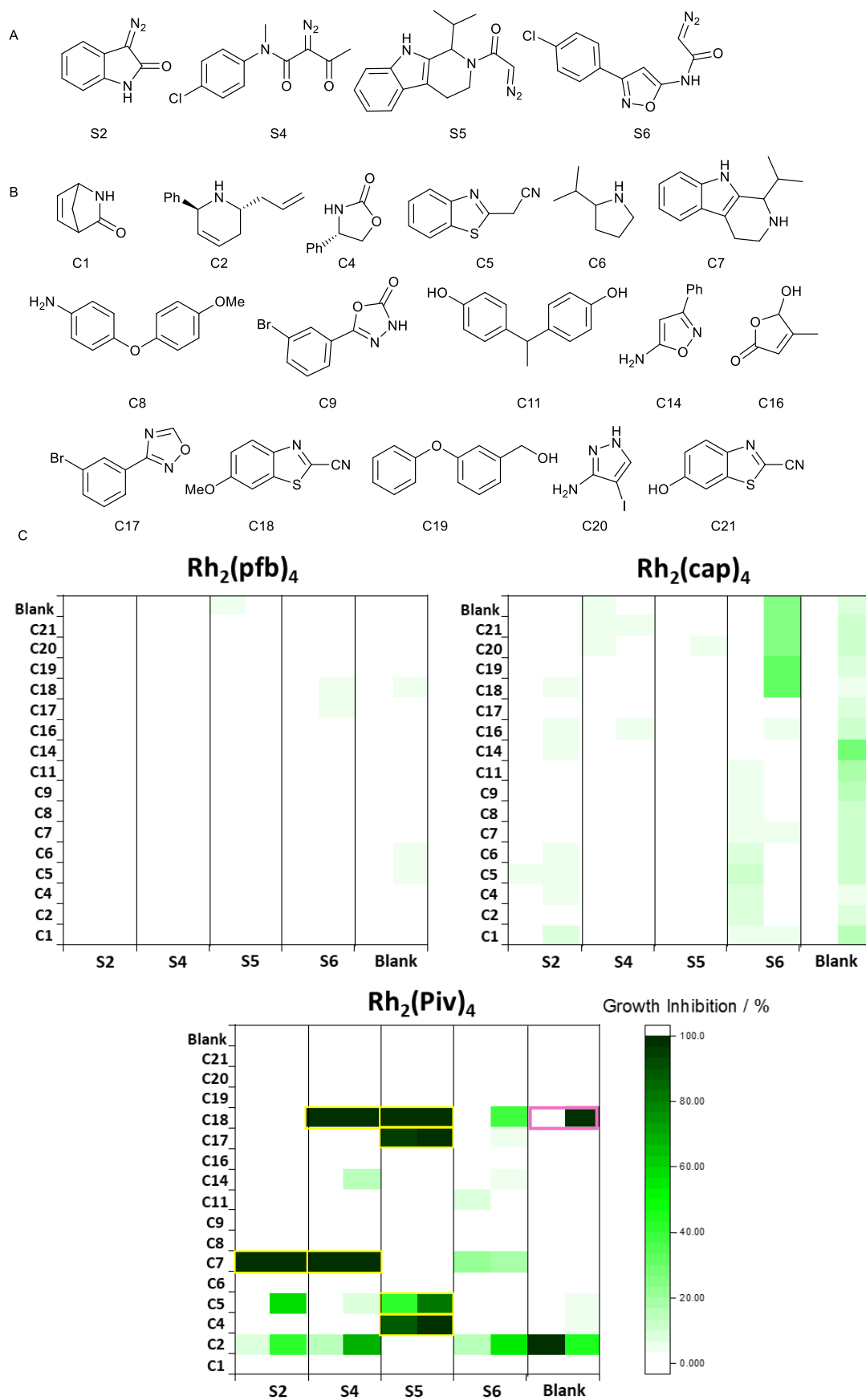


Figure 3.13 Activity-directed antibacterial discovery using Rh Carbenoid Chemistry with catalyst scavenging - Panels A and B: Structures of substrates (A)

and co-substrates (B). Panel C: Activity against *S. aureus* ATCC29213 (total product concentration: 100 μ M), with active combinations that were scaled up shown (yellow box). Product mixtures that displayed activity against only one colony (pink box) were re-assayed, but none of these combinations were validated as hits. On the x-axis, the substrates have been plotted and duplicate screens have been placed adjacent to each other. On the y-axis, co-substrates have been plotted and labelled accordingly.

3.6 Scale-up and Structural Elucidation of Antibacterial Ligands

Active combinations were scaled-up to structural elucidate the active products within the reaction mixtures. These products were purified and screened against ATCC29213 to detect whether they were responsible for the activity.

3.6.1 Scale-up and Isolation of Products within Active Combinations

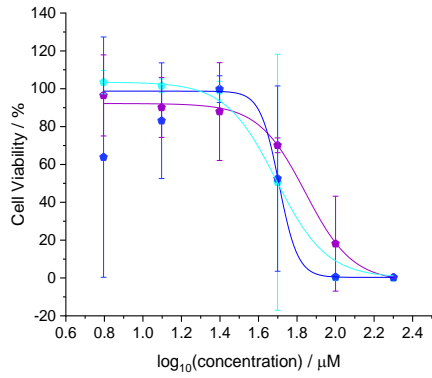
As described in section 3.4.1, LC-MS analysis was initially performed on all active combinations to assess whether the reaction was productive and prioritise the seven reactions for scale-up (Table 3.5). From this analysis, reactions between **S5** (with **C4**, **C5** and **C18**) were all found to possess the mass of an intermolecular product. In addition to finding intermolecular product, in the reaction combinations of both **S2** (with **C7**) and **S4** (with **C7**), masses that corresponded to an intermolecular product plus nitrogen were identified. For the reactions between **S4** (with **C18**) and **S5** (with **C17**), where no intermolecular mass was identified, reactions were de-prioritised for scale-up. In addition to performing a LC-MS screen, a six-point dose response curve was created from the crude reaction mixtures to further aid in work prioritisation. A two-fold dilution series ranging from a total product concentration of 20 – 0.625 mM was created for each active combination and diluted 100-fold following the methodology reported in section 3.5.3 to create screening concentration of 200 – 6.25 μ M. Wells were incubated for 16 h at 37 °C and the optical density of each well was read at 600 nm. Each concentration was tested against three colonies of ATCC29213 in duplicate and cell viability has been calculated for each value, using Penicillin G, **24** as

a positive control (0% cell viability) and 1% DMSO as a negative control (100% cell viability) (Figure 3.14).

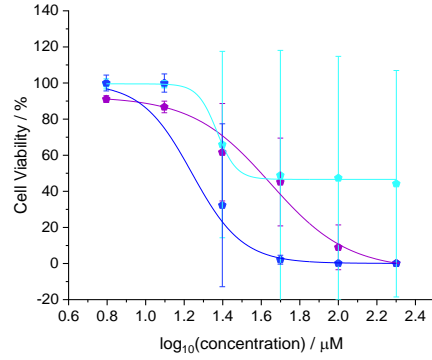
Combination	Intermolecular Mass	Mass corresponding to intermolecular product ^a	Mass corresponding to plausible alternative product
S2, C7, Rh ₂ (Piv) ₄	345		✓ (371) ^b
S4, C7, Rh ₂ (Piv) ₄	437		✓ (463) ^b
S4, C18, Rh ₂ (Piv) ₄	413		
S5, C4, Rh ₂ (Piv) ₄	417	✓	
S5, C5, Rh ₂ (Piv) ₄	428	✓	
S5, C17, Rh ₂ (Piv) ₄	478		
S5, C18, Rh ₂ (Piv) ₄	444	✓	

Table 3.5 Results of the LC-MS screen performed on active combinations - ^aTick indicates that the mass corresponding to an intermolecular product was observed ^bTick correspond to mass of intermolecular product plus dinitrogen with loss of two hydrogens. Reaction combinations and intermolecular masses have been indicated.

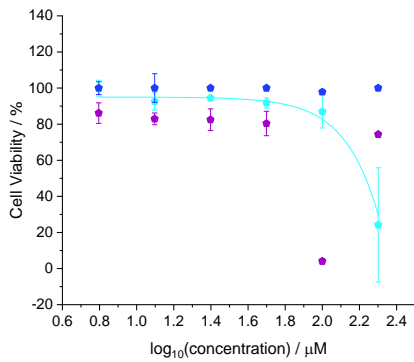
For the crude product combinations from the reaction array between **S2** (with **C7**), **S4** (with **C7**), **S5** (with **C5** and **C18**), a dose response curve was plotted and an IC₅₀ calculated. Values varied from 14 μM (for **S5** with **C18**), 26 μM (for **S5** with **C5**), 28 μM (for **S4** with **C7**) and 56 μM (for **S2** with **C7**). For those mixtures where curves could not be plotted, an estimated IC₅₀ value has been calculated. For **S5** with **C17**, poor solubility amounted to the curve increasing at 200 μM, evident from a solid in the screening wells at this value. Although curves possess a large error, as is the nature of optical density measurements on bacteria, they served as a guide for reaction prioritisation along with LC-MS data. Those combinations whose IC₅₀ was greater than 100 μM and had no obvious product mass by LC-MS were not investigated further (**S4** with **C18**; **S5** with **C17**).



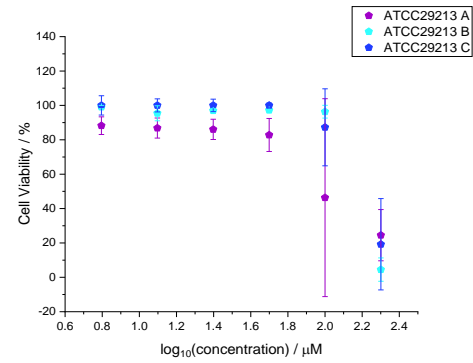
S2, C7; $I_{C50} = 56 \pm 3.5 \mu\text{M}$



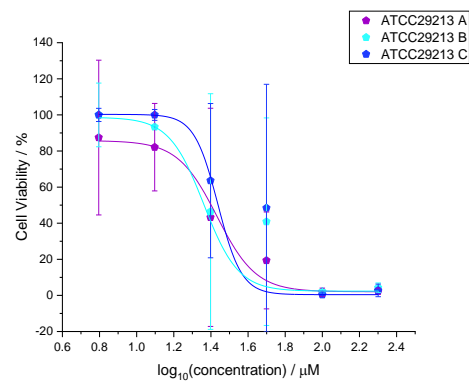
S4, C7; $I_{C50} = 28 \pm 2.4 \mu\text{M}$



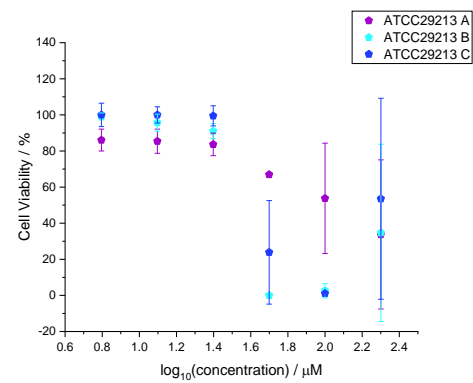
S4, C18; $I_{C50} = \sim 200 \mu\text{M}$



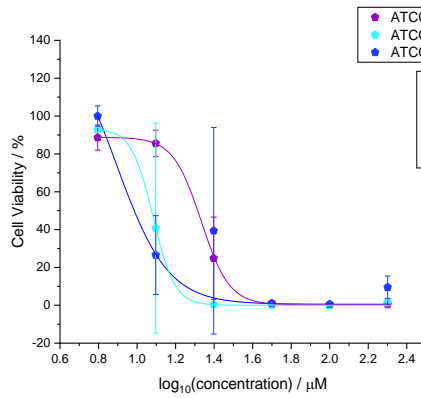
S5, C4; $I_{C50} = \sim 150 \mu\text{M}$



S5, C5; $I_{C50} = 26 \pm 4.3 \mu\text{M}$



S5, C17; $I_{C50} = \sim 100 \mu\text{M}$



S5, C18; $I_{C50} = 14 \pm 3.4 \mu\text{M}$

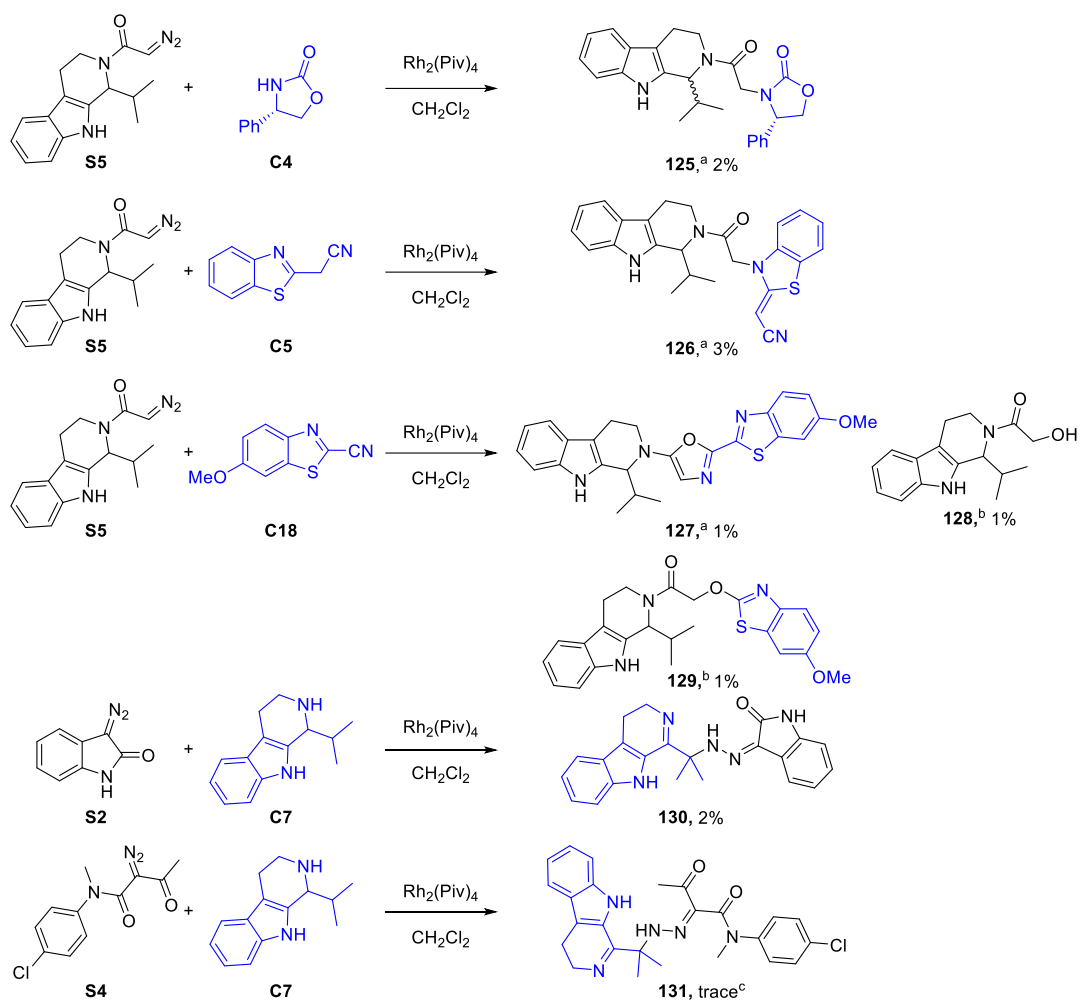
Figure 3.14 6-Point dose Response values (total product concentration: 200 –

6.25 μM) of active combinations against ATCC29213 - Combinations and average IC_{50} values have been indicated. Testing was performed against three different colonies. in duplicate. Curves were plotted to prioritise reactions for elucidation.

Reactions that displayed an intermolecular mass and whose crude activity was significant were scaled-up to allow structural elucidation of the products. The appropriate diazo substrate (1 equiv.) and co-substrate (2 equiv.) were added to a crimp-top vial containing $\text{Rh}_2(\text{Piv})_4$ (1 mol%) and the mixture was dissolved in CH_2Cl_2 (10 mL per mmol). After stirring at rt for 24 h, TU resin was added, and the reaction was stirred for a further 24 h. The resulting mixture was filtered through silica followed by purification by mass directed HPLC to afford the reaction products (Scheme 3.4). For reactions between **S5** (with **C4**, **C5** and **C18**), intermolecular products were isolated from the reaction mixtures that had formed via a N-H insertion reaction for **S5** with **C4** to yield **125**; ylide formation followed by hydrogen abstraction for **S5** and **C5** to yield **126**; and cyclisation of the nitrile group for **S5** and **C18** to afford oxazole **127**. In the case of **S5** with **C18**, two other interesting masses were identified on analytical HPLC and isolated: compound **128** from a reaction between the carbene and residual water present in either the atmosphere or the solvent; and compound **129**, likely formed via an $\text{S}_{\text{N}}\text{Ar}$ type reaction of **128** with either **C18** or a modified version of **C18** that possessed an altered nitrile group to increase its potential as a leaving group. For the reaction between **S2** (with **C7**), product was isolated with the intermolecular mass plus nitrogen. Similarly, for the reaction between **S4** (with **C7**), trace product was isolated with the intermolecular mass plus nitrogen and therefore, could not be identified structurally.

From NMR analysis of **130**, it was hypothesised that the product in both reactions was a hydrazone, formed via the imine of **C7**. The presence of the imine in the product was confirmed via HR-MS analysis, where an adduct with the mass of 212 was identified. Although crystals could not be formed from the oil to allow full structural characterisation of **130**, a few key peaks from the NMR support the theory that **130** and by extension, **131** are indeed the hydrazone (Figure 3.15). Primarily, in **130**, there is no longer two peaks for the isopropyl methyl protons, instead, one peak with an integration of six is found. This no longer couples to any protons on the COSY NMR, indicating the adjacent proton is no longer present, and allowing us to propose this could be the reaction site. Similar compounds have been synthesised by other groups

from the reaction between alkenes or alkynes and diazo compounds, however, have only been shown with a cobalt catalyst or under catalyst-free conditions.^{164,165}



Scheme 3.4 Scale-up reactions of active combinations found in the array screen against ATCC29213 - Scale-up reactions of **S5** (with **C4**, **C5** and **C18**), **S2** (with **C7**) and **S4** (with **C7**) with the products isolated from the mixture: Substrate (1 equiv.), Co-substrate (2 equiv.) and catalyst (1 mol%). ^a The suspected intermolecular product responsible for the mass on LC-MS. ^b Compounds other than the intermolecular product isolated from the reaction mixture. ^c Trace compound isolated with mass identified by HR-MS, structural elucidation of product not possible at this stage. Functionality obtained from the co-substrate has been indicated (blue). The confirmation of the alkene on **126** was confirmed as *Z* by NOESY NMR (Appendix B.4).

Protons pairs no longer diastereotopic.

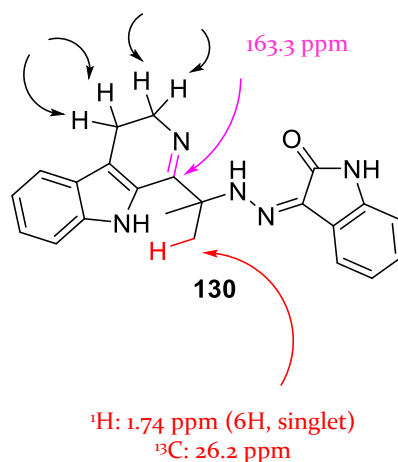


Figure 3.15 Key NMR peaks used in the identification of **130** - Full data can be seen in Section 5.2.3. The isopropyl in both **130** is now a single peak integrating to six protons. The four protons in the 3 and 4 positions of the pyridoindole are now triplets, indicating they are no longer diastereotopic. The 1 position is now quaternary, with a high shift of 163.3 ppm. NMR data has been provided in Appendix B.3.

3.6.2 MIC Determination of Isolated Products Against ATCC29213

All the isolated compounds were then tested in duplicate against three different colonies of ATCC29213 as described in Section 3.4.4. The results from this assay have been summarised in Table 3.6. From the six isolated products, two displayed activities against ATCC29213. For the reaction between **S5** and **C18**, compound **127** displayed a MIC of 4-8 $\mu\text{g mL}^{-1}$. From the reaction between **S2** and **C7**, **130**, displayed a MIC value of 16-32 $\mu\text{g mL}^{-1}$. It should be noted that some isatin hydrazones (related to **130**) have been shown to possess *S. aureus* activity, therefore, it is unsurprising that activity was observed for compound **130**.¹⁶⁸⁻¹⁷¹ No growth inhibition was observed for either intermolecular product (**125** and **126**) isolated from **S5** (with **C4**) and **S5** (with **C5**) or products **128** and **129**, found within the reaction mixture of **S5** (with **C18**). For those reactions where active product was not identified, further analysis of reaction wells is necessary to identify the true cause of antibacterial activity. In these cases, either cooperative effects between two or more components within the reaction mixture are possible causes of bioactivity, or alternative intermolecular products not yet identified, whose low yield could have influenced identification during purification.

Product ^a	Product Mass	MIC / $\mu\text{g mL}^{-1}$	MIC / μM
		ATCC29213	
125	417	> 64	> 153
126	428	> 64	> 150
127	444	4-8	9-18
128	272	> 64	> 235
129	435	> 64	> 147
130	371	16-32	43-86

Table 3.6 Evaluation of the activity of isolated products against *S. aureus* strains ATCC29213 - The MIC value observed in duplicate on three different days for ATCC29213 is shown. Penicillin G, **24**, used as a positive control in all experiments, displayed MIC values as expected. ^a Substrate (1.0 equiv.), Co-substrate (2.0 equiv.), 1 mol% Rh catalyst, CH₂Cl₂.

It is evident from the diversity of the chemical reactions identified from only seven different reactions that the arrays performed were exploring large areas of chemical space which has consequently allowed the identification of antibacterial compounds. Interestingly, the hydrazone reaction yielding active compound **130** has been less frequently identified within ADS projects^{2,46,47,134} and arguably, future co-substrate and catalyst selection within antibacterial ADS projects involving Rh-catalysed carbenoid chemistry should incorporate this chemistry as well as the more common transformations (Section 3.1.1), to aid in the discovery of more interesting and structurally diverse compounds. This could be done by either careful co-substrate selection or incorporation of Fe, Ag or Co catalysts which have more precedent for these transformations in the literature.^{165,166,172}

3.7 Biological Evaluation of Active Compounds

3.7.1 Minimum Inhibitory Concentration and IC₅₀ Determination of Isolated Species

After isolation of all the species, MIC determination was performed for all the isolated compounds. Minimum inhibitory concentration (MIC) values for selected compounds were determined by broth microdilution against *S. aureus* strains SH1000 and ATCC29213 according to CLSI guidelines.¹⁴³ MIC determinations were performed as described in Section 3.4.4 and Section 3.6.3 and the results of the active compounds have been summarised in Table 3.7. Each compound was screened in duplicate over three different days for the three strains.

The products have MIC values against ATCC29213 ranging from 16 $\mu\text{g mL}^{-1}$ for compound **111**, found within the reaction between **S5**, **C20** and Rh_2pfb_4 ; 2 $\mu\text{g mL}^{-1}$, 4-8 $\mu\text{g mL}^{-1}$ and 2-4 $\mu\text{g mL}^{-1}$ for **121**, **109a** and **109b** respectively, found from the combination between **S2**, **C5** and Rh_2pfb_4 ; 4-8 $\mu\text{g mL}^{-1}$ for compound **127**, found from the reaction between **S5**, **C18** and Rh_2Piv_4 and 16-32 $\mu\text{g mL}^{-1}$ for **130** found from the reaction between **S2**, **C7** and Rh_2Piv_4 . All active compounds also possessed similar activity against SH1000, another strain of *S. aureus*.

Product	Product Mass	MIC / $\mu\text{g mL}^{-1}$	
		ATCC29213	SH1000
111	382	16	8-16
121	262	2	2-4
109a	436	4-8	8
109b	436	2-4	4
127	444	4-8	4-8
130	371	16-32	32

Table 3.7 Evaluation of the activity of products against two *S. aureus* strains (ATCC29213 and SH1000) - The range of MICs observed in duplicate on three different days is shown for each strain. Penicillin G, **24**, used as a positive control in all

experiments, displayed MIC values as expected. ^a Substrate (1.0 equiv.), co-substrate (2.0 equiv.), 1 mol% Rh catalyst, CH₂Cl₂.

3.7.2 Evaluation of Eukaryotic Toxicity Against HeLa Cells

Once antibacterial activity was confirmed for all isolated compounds, products were tested by Jack White (University of Leeds, Megan Wright Research Group) against HeLa cells to determine if they possessed eukaryotic toxicity using an MTT assay.¹⁷³⁻¹⁷⁵ For each compound, an eight point two-fold dilution series in 100% DMSO was prepared at 100-fold higher concentration to the screening concentrations. Concentrations were chosen around the MIC value and repeat screens were performed, where necessary, if curves could not be plotted from the data. For the screen, HeLa cells (2×10^4 cells mL⁻¹) were prepared and diluted with medium (Dulbecco's Modified Eagle Medium (DMEM) with 4.5 g L⁻¹ glucose, 10% fetal bovine serum (FBS), 1% penicillin/streptomycin and without L-Glutamine) into a 96-well flat plate to obtain a concentration of 4000 cells per well. Plates were incubated (37 °C, 5% CO₂) for 24 h. The medium was removed from the incubated cells and stock solutions of each compound (1 µL), dissolved in medium (99 µL) were added to give a dilution series with a final DMSO concentration of 1% and a total volume of 100 µL. All compounds were tested in triplicate. Plates were incubated (37 °C, 5% CO₂) for 48 h. To each well, MTT solution (20 µL, 5 mg mL⁻¹ in PBS buffer) was added, and the plate was shaken (5 mins, 300 rpm). Plates were incubated for a further 4 h (37 °C, 5% CO₂) and the medium was removed. Each well was redissolved in DMSO (200 µL), shaken (5 mins, 300 rpm) and the optical density was measured at 570 nm to determine cell viability. Wells containing only 1% DMSO without compound were used as a 100% growth control and wells containing doxorubicin were used as a positive control.

The results of the MTT screen for compounds **111**, **121**, **109a**, **109b** and **127** have been presented (Table 3.8). Average cell viability values were plotted for triplicate screens and IC₅₀ values have been indicated for each compound. For conjugate addition products **109a** and **109b**, IC₅₀ values were found to be 89 µM and 66 µM, respectively. These values were approximately ten times higher than the MIC values against ATCC29213 (9.2 – 18.3 and 4.6 – 9.2 µM) and therefore, compounds were deemed to be non-toxic. For dimer **121**, the IC₅₀ was found to be 35 µM. When compared to the MIC

of 7.6 μM , dimer **121** was deemed to be slightly toxic and was not investigated further. Compound **111**, found from the reaction between **S5** and **C20** had an unexpected activity against HeLa cells, with an IC_{50} of 1.0 μM compared to an MIC of 42 μM against ATCC29213. It is possible that this compound possesses some anti-cancer properties but evaluation against mammalian cells would be required to confirm if selectivity were present. Compound **130** could not have its toxicity assessed due to limited sample. Finally, oxazole **127** had an IC_{50} of 38 μM against HeLa cells compared to an MIC of 9 μM against ATCC29213 and was also deemed to possess too much eukaryotic toxicity compared to antibacterial activity and were not investigated further. From six isolated antibacterial compounds, two were found to possess antibacterial activity approximately ten times higher than their equivalent eukaryotic toxicity and were deemed the most interesting hits identified.

Product	Product Mass	IC_{50} / μM
		HeLa Cells
111	382	1.0 \pm 0.4
121	262	35 \pm 7
109a	436	89 \pm 27
109b	436	66 \pm 4
127	444	38 \pm 6
130	371	- ^a

Table 3.8 IC_{50} of isolated compounds against HeLa cells to assess eukaryotic toxicity - For a compound to be deemed non-toxic, eukaryotic toxicity should be less than ten times the MIC. Data for compound **130** has not been included due to limited sample quantity. Dose response curves are presented in Appendix C. This screen was performed by Jack White (University of Leeds). ^a Tests not performed due to limited sample.

3.7.3 Activity Against an ESKAPE panel

Compounds that possessed activity against ATCC29213 but were deemed non-toxic were then tested against an ESKAPE panel of pathogens (*Enterococcus faecium*, *Staphylococcus aureus*, *Klebsiella pneumoniae*, *Acinetobacter baumannii*, *Pseudomonas aeruginosa*, and *Enterobacter spp.*). The ESKAPE panel is a group of both Gram-positive and Gram-negative strains that are multidrug resistant and therefore, are prioritised when researching new antibacterial compounds.¹⁷⁶ All six bacteria were investigated, with the addition of *E. coli*, a second *Enterobacter* species. A 2-fold dilution series of both **109a** and **109b** in 100% DMSO was prepared, ranging from 6400–6.4 $\mu\text{g mL}^{-1}$. Each dilution was transferred into a 96-well format, diluted 10-fold in water and diluted again to obtain a final volume of 100 μL . Final antibiotic concentrations range from 64–0.064 $\mu\text{g mL}^{-1}$ (1% DMSO in MHB-II). All of the isolated compounds were then tested in duplicate against three different colonies of each strain according to CLSI guidelines.¹⁰⁶ Plates were incubated for 16 h at 37 °C and the MIC was determined visually as the lowest concentration at which growth was inhibited. The results from this assay have been summarised in Table 3.9. For all strains, ciprofloxacin was used as a positive control to ensure the assay was valid and wells were not contaminated with different strains.

It was found from this screen that both **109a** and **109b** possessed selective activity against SH1000 (*S. aureus*) with activities of 8 $\mu\text{g mL}^{-1}$ (i.e. 18 μM) and 4 $\mu\text{g mL}^{-1}$ (i.e. 9.2 μM) respectively. No growth inhibition was observed against any of the other strains including ATCC700603 (*K. pneumoniae*),¹⁷⁷ ATCC19606 (*A. baumannii*),¹⁷⁸ PA01 (*P. aeruginosa*),¹⁷⁹ 051255 (*E. cloacae*) and BW25113 (*E. coli*).¹⁸⁰ Compounds could not be tested against VSE19579 (*E. faecium*) as cells did not grow up in overnight media. Although broad-spectrum activity was desired, this result was not surprising as discovering antibacterials with Gram-negative activity is challenging due to their second membrane (Section 1.3.1). Further investigations into the mode of action and accumulation of both **109a** and **109b** would confirm why these compounds are selective for *S. aureus* and would confirm whether these compounds inhibit bacterial growth via a known or unknown pathway within the cell.

Strain	MIC / $\mu\text{g mL}^{-1}$	
	109a	109b
<i>S. aureus</i> (ATCC29213)	4-8	2-4
<i>E. faecium</i> (VSE19579)	- ^a	- ^a
<i>S. aureus</i> (SH1000)	8	4
<i>K. pneumoniae</i> (ATCC700603)	>64	>64
<i>A. baumannii</i> (ATCC19606)	>64	>64
<i>P. aeruginosa</i> (PA01)	>64	>64
<i>E. cloacae</i> (051255)	>64	>64
<i>E. coli</i> (BW25113)	>64	>64

Table 3.9 Evaluation of activity of 109a and 109b against an ESKAPE panel of pathogens- The MIC value observed in duplicate on three different days for each strain is shown. Ciprofloxacin, used as a positive control in all experiments, displayed MIC values as expected. ^a MIC values could not be determined for this strain as cells did not grow up in overnight media.

3.8 Chemistry Leading to Active Compounds

Within this project, a diverse range of products have been explored, a consequence of the diverse range of chemistry that has happened within both reaction arrays. Consequently, new chemosynthetic pathways to antibacterials have emerged via activity-directed synthesis. This workflow is somewhat analogous to the emergence of biosynthetic pathways for secondary metabolites; with an active compound only being identified from two inactive fragments when a specific reaction pathway was taken.¹⁸¹ By varying the synthesis (controlled by the catalyst), inactive products were produced instead. The active products isolated within this project were in most cases, not the expected intermolecular product under the reaction conditions, but an analogue of this, and highlights the advantage of using catalytic reactions, in combination with screening reaction mixtures. A summary diagram of all the chemistries identified within active combinations is shown in Figure 3.16. From three

different diazo substrates (**S2**, **S4** and **S5**) and five co-substrates (**C4**, **C5**, **C7**, **C18** and **C20**), nine different reaction types have been explored. For diazo **S2**, this includes a C-H insertion reaction followed by subsequent oxidation to form **108**,¹⁸² a dimerization of the diazo followed by a conjugate addition of the co-substrate into the dimer to form **109** and the formation of hydrazone **130** without loss of nitrogen.¹⁷² For diazo **S4**, the formation of a hydrazone **131** was also observed. For diazo **S5**, six different reaction types were observed including: formation of oxazole **127** via a cyclisation of a diazocarbonyl and a nitrile;^{2,183,184} an O-H insertion reaction between **S5** and trace water present in either the solvent or the atmosphere to form **128**,^{140,185} an S_NAr reaction, possibly between product **128** and **C18** or a modified version of **C18**, whereby the lone pair on the nitrogen has reacted with another component of the mixture to create a better leaving group; a formal iodine transfer;¹⁸⁶ two N-H insertion reactions to form **110** and **125**;¹⁸⁷ and the formation of carbonyl ylide by addition of the lone pair of nitrogen into the substrate, followed by hydrogen abstraction of a benzylic proton.¹¹⁵

From all the reaction types identified, four different classes yielded an active product (hydrazone formation, conjugate addition, oxazole formation and I-H insertion). It is possible, that in those active combinations where an active product has not been identified (Section 3.5), new reaction pathways, not currently listed, could be responsible for the activity. Alternatively, products in low yield, formed via these four pathways, could be present but unidentified. By using the pathways as a guide, new arrays could be designed that target these chemotypes, aiding in the identification of more antibacterial compounds. It is also possible, that by performing arrays on more substrates and co-substrates, not used in this project, more chemosynthetic pathways will emerge. By exploiting this workflow in antibacterial drug discovery, new chemosynthetic pathways can be identified that lead to antibacterial compounds. These molecules could possess new modes of action that can ultimately help alleviate the pressure caused by the antibacterial crisis.

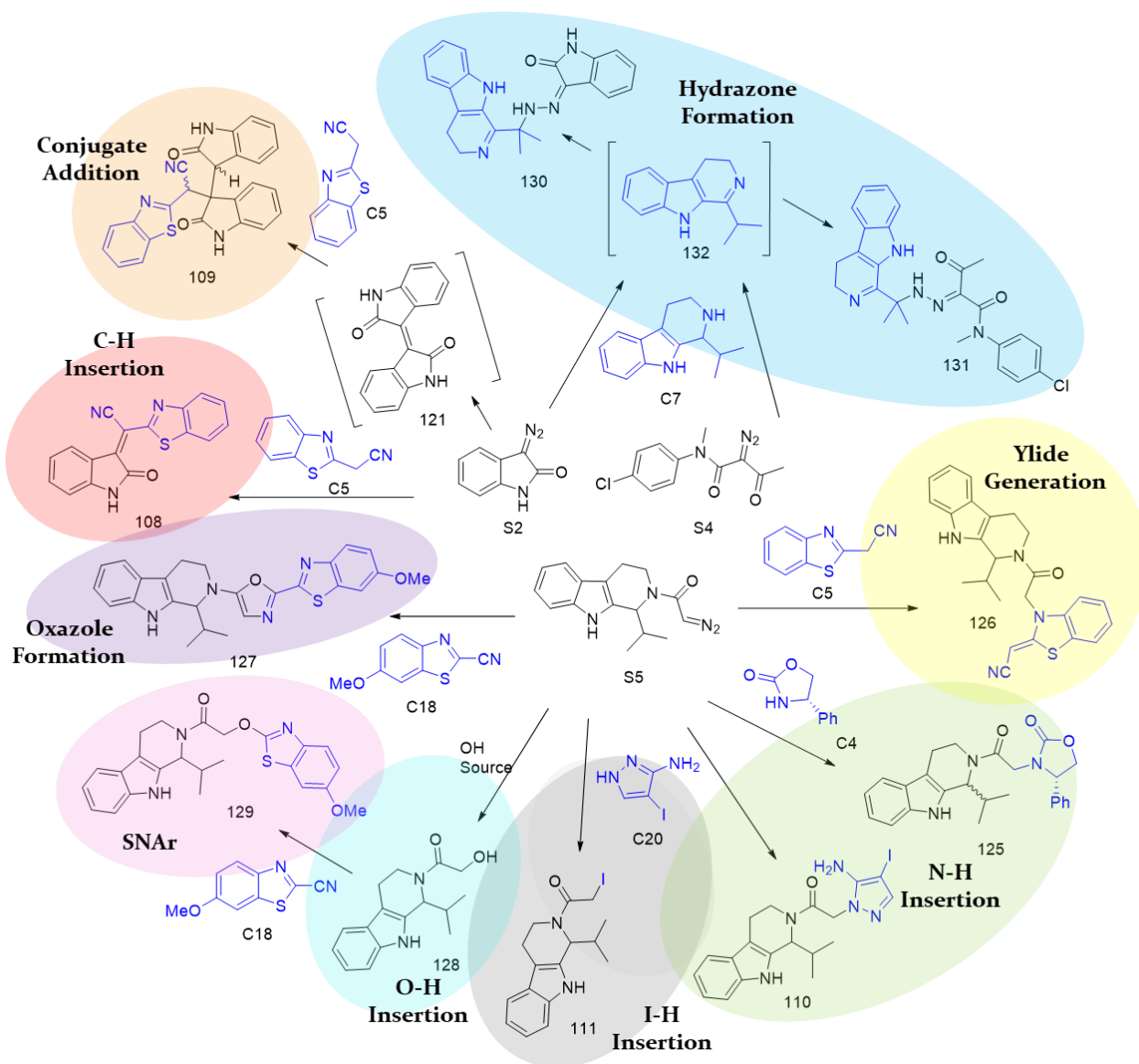


Figure 3.16 Activity-directed emergence of chemosynthetic pathways to antibacterials - Substrates, co-substrates have been indicated and have been organised based on reaction class. From three substrates (**S2**, **S4** and **S5**) and five co-substrates (**C4**, **C5**, **C7**, **C18** and **C20**), nine different reaction types have been explored including: N-H, I-H, O-H and C-H insertions, ylide generation and subsequent reaction with co-substrate, oxazole formation, hydrazone formation, S_NAr reactions and conjugate additions. Reaction types leading to active products include hydrazone formation to yield **130**, conjugate addition to yield **109**, I-H insertion to yield **111** and oxazole formation to yield **127**.

3.9 Summary and Conclusions

The feasibility of target-agnostic ADS in parallel with phenotypic screening has been demonstrated within this chapter, showing that Rh-catalysed carbenoid chemistry can be used with the ADS workflow to aid in the discovery of new antibacterial compounds. It has been shown that under the reaction conditions, many different types of reactions can occur, including for example insertion reactions, oxazole formations and conjugate additions (Section 3.8) ensuring that in one reaction array, a diverse range of chemical space is being explored. LC-MS analysis of a random 10% of the reaction wells from both arrays confirmed significant conversion to product, with 8 of the 12 reactions in the array without scavenging showing either an intermolecular mass, an intermolecular mass plus formal dehydrogenation or an intermolecular mass plus nitrogen and 9 of the 25 reactions in the array with scavenging showing either intermolecular mass or intermolecular mass plus nitrogen. These results allow us to estimate that around 50% of reactions formed some type of intermolecular product. From two arrays, and a total of 375 reactions, nine combinations displayed significant bioactivity in duplicate without purification. After scale-up, a total of twelve products were identified within the reaction mixtures, with six possessing antibacterial activity, ranging from 16 $\mu\text{g mL}^{-1}$ (i.e. 42 μM) for compound **111**, found within the reaction between **S5** and **C20**; 2 $\mu\text{g mL}^{-1}$ (i.e. 7.6 μM), 4-8 $\mu\text{g mL}^{-1}$ (i.e. 9.2 – 18.4 μM) and 2-4 $\mu\text{g mL}^{-1}$ (i.e. 4.6 – 9.2 μM) for **121**, **109a** and **109b** respectively, found from the combination between **S2** and **C5**; 4-8 $\mu\text{g mL}^{-1}$ (i.e. 9-18 μM) for compound **127**, found from the reaction between **S5** and **C18** and 16-32 $\mu\text{g mL}^{-1}$ (i.e. 43 – 86 μM) for **130** found from the reaction between **S2** and **C7** (Figure 3.19). From these six products, two (**109a** and **109b**) possessed eukaryotic toxicity approximately 10-times less than their antibacterial activity. These two compounds were then tested against an ESKAPE panel of pathogens, with selective activity against *S. aureus* being observed. This project has shown the capabilities of target-agnostic ADS and, that when the appropriate substrates, co-substrates and catalyst are chosen, formation and detection of antibacterial compounds within mixtures is possible. Further biological analysis of **109a** and **109b** are still required to determine their mode of action within the cell.

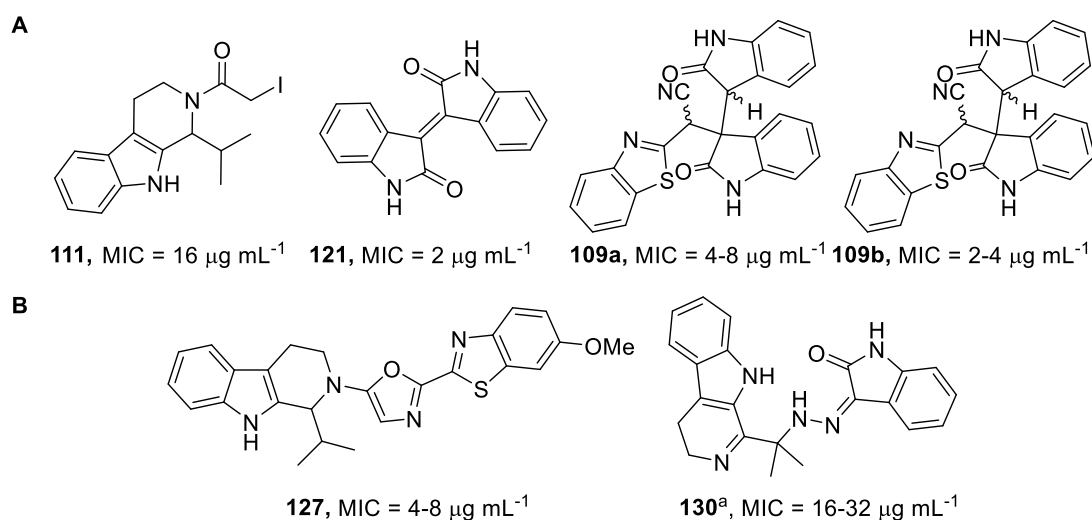


Figure 3.17 Six compounds identified with antibacterial activity- Panel A: Compound isolated from the array without a TU resin, from these four, compounds **109a** and **109b** were the only two deemed non-toxic against HeLa cells. Panel B: Compounds isolated from the array with a TU resin. MICs against ATCC29213 have been indicated for all compounds. ^a Compounds have not been structurally elucidated by X-Ray crystallography and structures are based on the NMR, IR and MS evidence available.

4 Future Work

Activity-directed synthesis (ADS) was shown to be a feasible early-stage drug discovery technique to use in combination with a phenotypic assay, in this case, a bacterial assay. Initially, activity-directed synthesis was used to expand the structure-activity relationship (SAR) of a known class of antibacterials (Chapter 2). Within this project, Pd chemistry was configured for use in micro-scale reactions, an assay was developed that could tolerate screening mixtures and after performing over 200 reactions, six products from active combinations were structurally elucidated. From these structures, the SAR was expanded, with key structural features needed for good activity identified as a *meta* substituted hydrogen bond donor on the phenyl ring in the 3-position of the quinazolinone and a two-atom tether in the 2-position, connected to a hydrophobic group. These products were shown to possess significant activity against *S. aureus*.

Due to this project's success, the feasibility of using ADS to identify active compounds found in a target-agnostic array where no known antibacterial chemotypes were incorporated into the array design was assessed (Chapter 3). Two arrays of reactions were performed, using a range of substrates, co-substrates and catalysts and products from hit reactions were isolated. Eight products were identified with promising activity against *S. aureus*, with two possessing no eukaryotic toxicity. From analysis of all the isolated compounds, it was confirmed that a wide range of chemotypes could be explored in the ADS workflow to allow identification of novel antibacterial compounds.

4.1 Future work: Investigation of Mechanism of Action of Novel Antibacterials

Although many compounds have been identified, some active combinations have still not had their active product structurally elucidated; allowing the conclusion that the isolated intermolecular product is not responsible for activity. It is plausible that when screening mixtures, a combination effect, either between two or more products or reactants, could be responsible for the activity and so this could be why active product was not found. Although combination therapies can be used to treat

multi-drug resistant infections,¹⁸⁸⁻¹⁹⁰ identification of the components responsible in the complex mixtures within this project would be non-trivial and, it is unlikely that one reaction would yield two compounds that could act in combination. From the products isolated, further biological evaluation of diastereomers **109a** and **109b** is of interest as they were the only active compounds to possess eukaryotic toxicity greater than ten times their MIC against ATCC29213 (Section 3.7.2). So far, these two compounds have been assessed against an ESKAPE panel of pathogens (Section 3.7.3) but require further analysis to truly understand how they work within the cell. Firstly, time-kill assays need to be performed to confirm whether the compounds are bactericidal or bacteriostatic and thus, confirm whether **109a** and **109b** kill the cells or inhibit growth.¹⁹¹ Minimum biofilm eradication concentration assays (MBEC) would then be performed to determine if **109a** and **109b** were also effective against biofilms due to the clinical difficulties associated with treating them.¹⁹² Afterwards, mode of action studies¹⁹³ would be performed to identify the compounds target. Initially, testing would be focused to see if **109a** and **109b** disrupted biosynthetic pathways targeted by known antibiotics. Finally, compounds mutation frequencies¹⁹⁴ would be determined to assess resistance development in the strain and compounds would be evaluated against the target in an *in vitro* assay.

4.2 Future work: Extension of the Scope of ADS

ADS has now been shown to aid in the discovery of novel scaffolds that target the androgen receptor,^{2,46} p53/hDM2⁴⁷ and *S. aureus*.⁹⁷ Both Pd catalysed and Rh catalysed chemistry have shown to be feasible chemistries for use in microscale format. This high-throughput approach has the potential to be an important technique in the development of novel scaffolds for many other druggable targets and cells, especially when used in combination with a robust assay. Currently, reaction arrays are performed in an exhaustive manner, by hand and therefore, there is an opportunity to further expand the capabilities of ADS by automating the process. Automation of both reaction set-up and substrate selection would both be plausible areas to develop. In addition, different chemistries, such as photoredox catalysis,¹⁹⁵ could be harnessed to either expand the areas of chemical space that can be explored in a reaction array, or for late-stage functionalisation of known compounds (Figure 4.1).

This late-stage functionalisation approach could be of particular interest in antibacterial drug discovery as, by using the eNTRY rules as a guide (Section 1.3.4), one could envisage selecting a series of known Gram-positive antibacterial compounds with a globularity ≤ 0.25 and rotatable bonds ≤ 5 and modifying them by addition of a primary amine. If photoredox chemistry was exploited, *N*-methylphthalimide, for example, could be added to heteroaromatic rings in known antibacterials and deprotected prior to screening. Due to the promiscuity of this chemistry, it is feasible that addition could occur at multiple different sites or more than once, to yield products with primary amines in different positions. These compounds could then be tested against Gram-negative strains to assess their activity.



PG: Boc, Fmoc, CBz, Tf, Phthalimide

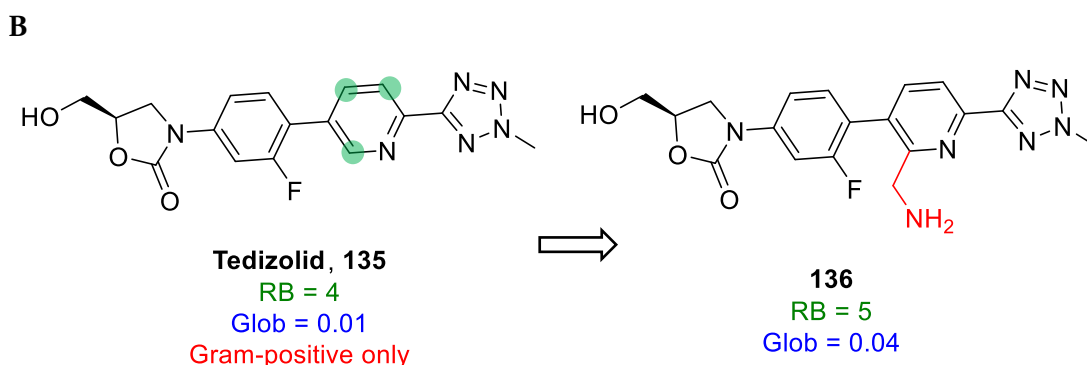


Figure 4.1 The Potential for a Late-Stage Functionalisation approach to be harnessed within an ADS workflow- Panel A: Photoredox catalysis could be exploited in late-stage functionalisation to add hydrogen donors to heterocycles. This could be useful in Gram-negative antibacterial discovery. Addition of a protected methylamine to known Gram-positive antibacterials, followed by deprotection, could decorate the antibiotic with a primary amine to make it meet the eNTRY rule criteria. All products could be screened against *E. coli* to determine if broad-spectrum activity had been developed. Panel B: Tedizolid **135**, a Gram-positive only antibiotic, is one heterocycle containing antibiotic that could be modified. Some possible reaction sites

have been indicated (green circles) and one possible product, **136**, shown. The globularity and rotatable bonds have been shown to confirm both compounds meet the eNTRY rule criteria. Tedizolid, **135** would need protecting prior to decoration.

Although ADS is still in development, it has the potential to be an important technique in drug discovery. It has shown to be a plausible technique in antibacterial discovery and could continue to be used to provide novel scaffolds for early drug discovery programmes. Ultimately, ADS could help speed up the rate of antibiotic discovery and contribute towards alleviating the antibacterial crisis.

5 Experimental

5.1 General Information and Instrumentations

All reactions were carried out under air and at room temperature unless stated otherwise. Solvents were removed under reduced pressure using a Büchi rotary evaporator and a Vacuubrand PC2001 Vario diaphragm pump. Anhydrous dimethylsulfoxide (DMSO) was obtained from SureSeal bottles from Sigma–Aldrich. All other solvents used were of chromatography or analytical grade. Petrol refers to petroleum spirit (b.p. 40-60 °C). Commercially available starting materials were obtained from Alfa Aesar, Enamine BB (EU), Fluorochem or SigmaAldrich.

Flash column chromatography was carried out using silica gel 60 (35-70 µm particles) supplied by Merck. Thin layer chromatography was carried out using commercially available pre-coated aluminium plates (Merck silica gel 60 F254) from Merck. Ultraviolet lamp ($\lambda_{\text{max}} = 254 \text{ nm}$) and KMnO_4 were used for visualisation. Perkin-Elmer One FT-IR spectrometer was used to analyse the infrared spectra. Melting points (m.p.) were determined using Stuart melting point apparatus SMP3. X-ray measurements were carried out at 120 K on an Agilent SuperNova diffractometer equipped with an Atlas CCD detector and connected to an Oxford Cryostream low temperature device using mirror monochromated $\text{Cu K}\alpha$ radiation ($\lambda = 1.54184 \text{ \AA}$) from a Microfocus X-ray source. The structure was solved by intrinsic phasing using SHELXT and refined by a full matrix least squares technique based on F^2 using SHELXL2014.

Analytical LC-MS was performed using a Thermo Ultimate 3000 HPLC instrument with a UV diode array detector and an MS detector Bruker Amazon Speeds with electrospray ionisation run positive and negative switching mode. The system used a Phenomenex Kinetex C18 $2.1 \times 50 \text{ mm } 2.6 \text{ micron}$ column, two solvent systems: MeCN/H₂O + 0.1% Formic acid or MeCN/H₂O and a run time of 1.7 minutes.

A Bruker Daltonics micrOTOF spectrometer with electrospray (ES) ionisation source was used for high-resolution mass spectrometry (HRMS).

Proton (¹H) and carbon (¹³C) NMR data was collected on a Bruker 400 (AV3HD NMR spectrometer operating at 9.4 T and equipped with a 5 mm BBO probe) or 500 (AV-NEO NMR spectrometer operating at 11.7 T and equipped with a 5 mm DCH

cryoprobe) MHz spectrometer. Data was collected at 298 K unless otherwise stated. Chemical shifts (δ) are given in parts per million (ppm) and they are referenced to the residual solvent peak. Coupling constants (J) are reported in Hertz (Hz) and splitting patterns are reported in an abbreviated manner: app (apparent), s (singlet), d (doublet), t (triplet), q (quartet), m (multiplet), br (broad). Many assignments were made using COSY, DEPT, HSQC, HMBC or NOESY experiments.

Preparative LC-MS was performed using an Agilent Technologies Infinity (1260) instrument with a UV diode array detector and an Agilent 6100 series Single Quad MS detector. The system used a Phenomenex Kinetex C18 EVO 21.2 \times 250 mm 5 micron column. The general preparation method used a solvent system of MeCN/H₂O (5–95%) + 0.1% Formic acid and a run time of 15 minutes.

Preparative HPLC was performed using a Water (2767) instrument with a Water SQ detector 2. The system used an XBridge C18 19.0 \times 100 mm 5 micron OBD column. The general preparation method used a solvent system of MeCN/H₂O (5–95%) + 0.1% Formic acid.

5.2 Chemistry

5.2.1 General Procedures

General Procedure A: Synthesis of 4(3*H*)-Quinazolinones using Carbonylation Chemistry

By modification of an existing procedure,⁹⁹ the appropriate aniline/amine/nitroarene (1.2 equiv.) and 2-iodophenylanilide (1 equiv.) were added to a crimp-top vial containing molybdenum hexacarbonyl (1 equiv.), tri-tert-butylphosphine (0.6 mol%) and tris(dibenzylideneacetone)dipalladium(o) (0.1 mol%) and purged with nitrogen for 5 minutes. The mixture was dissolved in *o*-xylene (3.0 mL per mmol) and triethylamine (2.5 equiv.) was added at rt. The reaction was stirred vigorously and heated to 105 °C for 48 hours and the resulting mixture was concentrated under reduced pressure to afford the crude product. Reactions were typically performed on a 0.5 mmol scale and scaled appropriately where necessary.

General Procedure B: Synthesis of iodoanilide substrates

By modification of an existing procedure,^m the appropriate aniline (1 equiv.) and triethylamine (1.1 equiv.) were dissolved in diethyl ether (4.4 mL per mmol) and cooled to 0 °C. A solution of the appropriate acid chloride (1.1 equiv.) in diethyl ether (2.2 mL per mmol) was added dropwise. The reaction was heated to rt and stirred until complete. The reaction mixture was concentrated under reduced pressure to afford a crude product.

General Procedure C: Synthesis of diazo substrates via *N*-acetylation followed by diazo transfer

By modification of an existing procedure,^{135,196} the appropriate amine (or aniline) (1 equiv.) and 2,2,6-trimethyl-4H-1,3-dioxin-4-one (1.2 equiv.) were dissolved in toluene (3.2 mL per mmol). The solution was irradiated under microwave radiation (110 °C, max 200 W, max 300 psi) for 4 h and the resulting reaction mixture was concentrated under reduced pressure. The crude product was dissolved in EtOAc (60 mL), washed with brine (3 × 20 mL) and dried (MgSO₄). The organic layer was concentrated under reduced pressure to afford the intermediate. Triethylamine (2.0 equiv.) was added to a stirred solution of the intermediate in anhydrous MeCN (3.2 mL per mmol) and 4-acetamidobenzenesulfonyl azide (1.1 equiv.) was added portion-wise. The reaction mixture was stirred at rt overnight and the resulting mixture was concentrated to afford the crude diazo substrate.

General Procedure D: Scale-up synthesis of intermolecular products from diazo reactions (without scavenging)

By modification of an existing procedure,² the appropriate diazo substrate (1 equiv.) and co-substrate (2 equiv.) were added to a crimp-top vial containing the appropriate catalyst (1 mol%) and purged with nitrogen for 5 minutes. The mixture was dissolved in anhydrous CH₂Cl₂ (10 mL per mmol) and the reaction was stirred for 24 h at rt. The resulting mixture was concentrated under reduced pressure to afford the crude product. Reactions were typically performed on a 0.5 mmol scale and altered where necessary.

General Procedure E: Scale-up synthesis of intermolecular products from diazo reactions (with scavenging)

By modification of an existing procedure,² the appropriate diazo substrate (1 equiv.) and co-substrate (2 equiv.) were added to a crimp-top vial containing the appropriate catalyst (1 mol%) and purged with nitrogen for 5 minutes. The mixture was dissolved in anhydrous CH₂Cl₂ (10 mL per mmol) and the reaction was stirred for 24 h at rt. Then, thiourea (TU) resin (3000 mg per mmol) was added and the resulting mixture was stirred at rt for a further 24 h. The reaction mixture was filtered and concentrated under reduced pressure to afford the crude product. Reactions were typically performed on a 0.5 mmol scale and altered where necessary.

5.2.2 Implementation of Reaction Arrays

5.2.2.1 Carbonylation Reaction Arrays

By modification of an existing procedure,² the reaction arrays were carried out in a 96-well plate (8 × 12) custom made out of PTFE in borosilicate glass vials (vial volume = 750 μL, vial dimensions = 8 × 30 mm, CV-2100-0830 Chemglass). 2-Iodophenylanilide substrates were dissolved in THF to give 1.0 M stock solutions. Amine/aniline co-substrates were dissolved in THF to give 1.20 M stock solutions. A stock solution of the catalyst system was prepared that was 2.00 mM in tri-tert-butylphosphine and 0.33 mM in tris(dibenzylideneacetone)dipalladium(o) in *o*-xylene. 100 μL of the appropriate substrate stock solution was added to the appropriate well and the solvent was evaporated. Then, 100 μL of the appropriate co-substrate stock solution was added and evaporated. This was followed by the addition of 26 mg of molybdenum hexacarbonyl as a solid and 300 μL of the catalyst stock solution. Then, 35 μL of triethylamine was added to each well and the plate was quickly sealed (silica layer and rubber Optibloc™ seal). The final volume of the reaction mixture was 300 μL; with final concentrations of catalyst (0.3 mM), substrate (333 mM), co-substrate (400 mM), ligand (2.0 mM), triethylamine (833 mM) and molybdenum hexacarbonyl (333 mM). The wells were left to react at 105 °C for 48 h and the crude mixture was concentrated under pressure overnight to remove residual *o*-xylene (EZ-2 Plus

Genevac). The wells were re-dissolved in EtOAc (150 μ L) and filtered through silica (30 mg) using filter microplates (96-well polypropylene with 0.45 μ m polypropylene membrane, 800 μ L/well, long drip, Agilent Technologies 200933-100) into new borosilicate glass vials. The crude wells were washed with EtOAc (2 \times 150 μ L) and the washes also transferred to the corresponding wells. The product mixtures were left to evaporate under reduced pressure overnight (EZ-2 Plus Genevac). The product mixtures were dissolved in 300 μ L of DMSO to give a total product concentration of 333 mM and transferred to a 96-well plate for screening.

5.2.2.2 Rh Reaction Arrays (without scavenging agent)

By modification of an existing procedure,² the reaction arrays were carried out in a 96-well plate (8 \times 12) custom made out of PTFE in borosilicate glass vials (vial volume = 750 μ L, vial dimensions = 8 \times 30 mm, CV-2100-0830 Chemglass). Diazo substrates were typically dissolved in CH₂Cl₂ to give 1.25 M stock solutions. Co-substrates were dissolved in CH₂Cl₂ to give 2.50 M stock solutions. A stock solution of the catalysts was prepared that was 1.00 mM in CH₂Cl₂. 8 μ L of the appropriate substrate stock solution was added to the appropriate well and the solvent was evaporated. Then, 8 μ L of the appropriate co-substrate stock solution was added and evaporated. This was followed by the addition of 100 μ L of the catalyst stock solution. Then, the plate was capped. The final volume of the reaction mixture was 100 μ L; with final concentrations of catalyst (1 mM), substrate (100 mM) and co-substrate (200 mM). The wells were left to react at rt for 24 h and the crude mixtures were concentrated under pressure overnight to remove residual CH₂Cl₂. The wells were re-dissolved in 100 μ L of DMSO to give a total product concentration of 100 mM and transferred to a 96-well plate for screening.

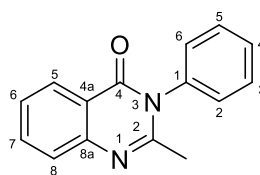
5.2.2.3 Rh Reaction Arrays (with scavenging agent)

By modification of an existing procedure,² the reaction arrays were carried out in a 96-well plate (8 \times 12) custom made out of PTFE in borosilicate glass vials (vial volume = 750 μ L, vial dimensions = 8 \times 30 mm, CV-2100-0830 Chemglass). Diazo substrates were typically dissolved in CH₂Cl₂ to give 1.25 M stock solutions. Co-

substrates were dissolved in CH₂Cl₂ to give 2.50 M stock solutions. A stock solution of the catalysts was prepared that was 1.00 mM in CH₂Cl₂. 8 μL of the appropriate substrate stock solution was added to the appropriate well and the solvent was evaporated. Then, 8 μL of the appropriate co-substrate stock solution was added and evaporated. This was followed by the addition of 100 μL of the catalyst stock solution. Then, the plate was capped. The final volume of the reaction mixture was 100 μL; with final concentrations of catalyst (1 mM), substrate (100 mM) and co-substrate (200 mM). The wells were left to react at rt for 24 h and a thiourea (TU) resin (30 mg) was added to each well. The wells were left to scavenge for a further 24 h at rt. The reaction mixtures were filtered through filter microplates (96-well polypropylene with 0.45 μm polypropylene membrane, 800 μL/well, long drip, Agilent Technologies 200933-100) into new borosilicate glass vials to remove the resin. The crude wells were washed with CH₂Cl₂ (2 × 150 μL) and the washes also transferred to the corresponding wells. The crude mixtures were concentrated under pressure overnight to remove residual CH₂Cl₂. The wells were re-dissolved in 100 μL of DMSO to give a total product concentration of 100 mM and transferred to a 96-well plate for screening.

5.2.3 Compound Data

2-Methyl-3-phenylquinazolin-4-one, **38j**

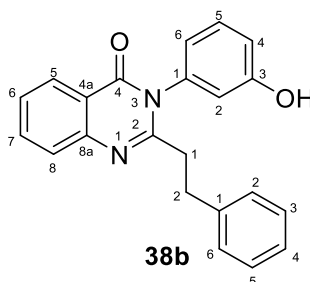


38j

By general procedure A using 2-iodophenylacetamide (0.26 g, 1.00 mmol) and nitrobenzene (0.12 mL, 1.20 mmol) followed by purification by flash column chromatography, eluting with 70:30 petrol–EtOAc gave the quinazolinone⁷⁸ **38j** (0.044 g, 19%) as a colourless amorphous solid, *R_f* 0.20 (70:30 Petrol–EtOAc); *v*_{max}/cm⁻¹ (film); 3270, 1657, 1525 and 1253; *δ*_H (400 MHz, CDCl₃); 8.27 (1H, dd, *J* 7.9, 1.1, 5-H), 7.77 (1H, td, *J* 8.3, 1.5, 7-H), 7.68 (1H, br d, *J* 8.0, 8-H), 7.56 (2H, app t, *J* 7.3, phenyl 3-H and 5-H), 7.51 – 7.47 (1H, m, phenyl 4-H), 7.46 (1H, app t, *J* 7.6, 6-H), 7.27 (2H, d, *J* 6.8, phenyl 2-H and phenyl 6-H), 2.25 (3H, s, 2-methyl); *δ*_c (101 MHz, CDCl₃); 162.2 (4-C), 154.3 (2-C),

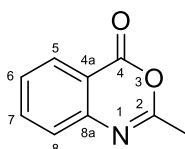
147.5 (8a-C), 137.8 (phenyl 1-C), 134.7 (7-C), 130.0 (phenyl 3-C and 5-C), 129.4 (phenyl 4-C), 128.1 (phenyl 2-C and 6-C), 127.1 (5-C), 126.8 (8-C), 126.7 (6-C), 120.9 (4a-C), 24.5 (2-methyl); HRMS found MH^+ 237.1031. $C_{15}H_{12}N_2OH$ requires MH^+ 237.1029.

3-(3-Hydroxyphenyl)-2-(2-phenylethyl)quinazolin-4-one, **38b**



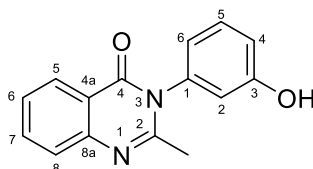
By general procedure A using *N*-(2-iodophenyl)-3-phenylpropanamide, **S1** (=48b) (0.25 g, 1.00 mmol) and 3-aminophenol (0.13 g, 1.20 mmol) followed by purification by flash column chromatography, eluting with 50:50 hexane–EtOAc, gave the quinazolinone⁷⁸ **38b** (0.086 g, 24%) as a colourless amorphous solid, R_f 0.55 (50:50 hexane–EtOAc); ν_{max}/cm^{-1} (film); 3361, 2945, 1667, 1585 and 1460; δ_H (501 MHz, d_6 -DMSO); 9.85 (1H, s, OH), 8.11 (1H, dd, J 7.9, 1.2, 5-H), 7.86 (1H, ddd, J 8.6, 7.3, 1.5, 7-H), 7.72 (1H, d, J 7.8, 8-H), 7.53 (1H, td, J 8.1, 1.0, 6-H), 7.33 (1H, app t, J 8.0, hydroxyphenyl 5-H), 7.22 (2H, app t, 7.4, phenyl 3-H and phenyl 5-H), 7.14 (1H, t, J 7.3, phenyl 4-H), 7.07 (2H, d, J 7.0, phenyl 2-H and phenyl 6-H), 6.90 (1H, ddd, J 8.3, 2.2, 0.9, hydroxyphenyl 6-H), 6.80–6.78 (2H, m, hydroxyphenyl 4-H and hydroxyphenyl 2-H), 2.98 (2H, t, J 7.5, ethyl 1-H₂), 2.64 (2H, t, J 7.5, ethyl 2-H₂); δ_C (126 MHz, d_6 -DMSO); 161.2 (4-C), 158.3 (hydroxyphenyl 5-C), 156.0 (2-C), 147.1 (8a-C), 140.9 (phenyl 1-C), 138.1 (hydroxyphenyl 1-C), 134.6 (7-C), 130.2 (hydroxyphenyl 3-C), 128.4 (phenyl 3-C and phenyl 5-C), 128.2 (phenyl 2-C and phenyl 6-C), 126.9 (8-C), 126.6 (6-C), 126.3 (5-C), 126.0 (phenyl 4-C), 120.6 (4a-C), 119.0 (hydroxyphenyl 6-C), 116.0 (hydroxyphenyl 4-C), 115.6 (hydroxyphenyl 2-C), 37.0 (ethyl 1-C), 32.2 (ethyl 2-C); HRMS found MH^+ 343.1441. $C_{22}H_{18}N_2O_2H$ requires MH^+ 343.1447.

2-Methyl-4*H*-benzo[*d*][1,3]oxazin-4-one, **78**

**78**

Anthranilic acid (8.00 mL, 0.08 mol) was dissolved in triethyl orthoacetate (25.33 mL, 0.14 mol) and the reaction mixture was heated under reflux for 2 h. The crude product was crystallised by cooling the reaction mixture on ice-water for 4 h. The solid precipitate was isolated by vacuum filtration and washed liberally with hexanes to yield the oxazinonone⁷⁸ **78** (5.220 g, 40%) as a colourless amorphous solid, R_f 0.10 (50:50 Hexane–EtOAc); $\nu_{\max}/\text{cm}^{-1}$ (film); 3070, 2931, 1753 and 1688; δ_{H} (400 MHz, CDCl_3); 8.19 (1H, dd, J 7.9, 1.4, 5-H), 7.79 (1H, ddd, J 8.1, 7.4, 1.5, 7-H), 7.54 (1H, d, J 8.1, 8-H), 7.50 (1H, td, J 7.7, 1.0, 6-H), 2.47 (3H, s, methyl); δ_{C} (101 MHz, CDCl_3); 160.3 (4-C), 159.8 (2-C), 146.6 (8a-C), 136.7 (7-C), 128.6 (5-C), 128.3 (8-C), 126.5 (6-C), 116.8 (4a-C), 21.5 (methyl); HRMS found MH^+ 162.0543. $\text{C}_9\text{H}_7\text{NO}_2\text{H}$ requires MH^+ 162.0555.

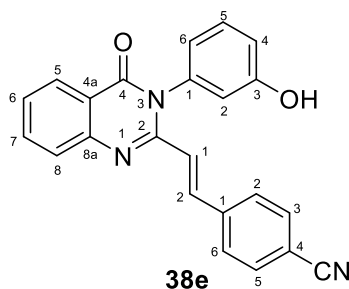
3-(3-Hydroxyphenyl)-2-methylquinazolin-4-one, **38n**

**38n**

2-Methyl-4H-benzo[*d*][1,3]oxazin-4-one, **78** (2.10 g, 13.00 mmol) and 3-aminophenol (1.50 g, 13.70 mmol) were suspended in glacial acetic acid (5 mL) and the reaction mixture was heated under reflux for 4 h. The reaction mixture was cooled and water (10 mL) was added. The resulting precipitate was filtered, washed with water, cold EtOH and hexanes to yield the quinazolinone⁷⁸ **38n** (1.420 g, 43%) as a colourless amorphous solid, R_f 0.37 (50:50 hexane–EtOAc); $\nu_{\max}/\text{cm}^{-1}$ (film); 3522, 3164, 1650, 1597 and 1292; δ_{H} (501 MHz, d_6 -DMSO); 9.84 (1H, s, OH), 8.09 (1H, dd, J 7.9, 1.2, 5-H), 7.83 (1H, ddd, J 8.6, 7.2, 1.5, 7-H), 7.65 (1H, d, J 7.8, 8-H), 7.51 (1H, ddd, J 8.0, 7.9, 1.0, 6-H), 7.34 (1H, app t, J 8.0, hydroxyphenyl 5-H), 6.91 (1H, ddd, J 8.3, 2.3, 0.8, hydroxyphenyl 6-H), 6.83 (1H, ddd, J 7.8, 1.9, 0.8, hydroxyphenyl 4-H), 6.79 (1H, app t, J 2.1, hydroxyphenyl 2-H), 2.16 (3H, s, methyl); δ_{C} (126 MHz, d_6 -DMSO); 161.0 (4-C), 158.1 (hydroxyphenyl 3-C), 154.3 (2-C), 147.2 (8a-C), 138.6 (hydroxyphenyl 1-C), 134.4 (7-C),

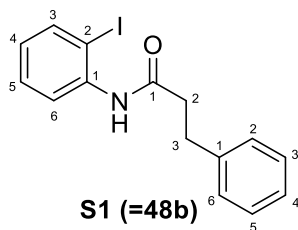
130.1 (hydroxyphenyl 5-C), 126.5 (8-C), 126.2 (6-C), 126.1 (5-C), 120.3 (4a-C), 118.6 (hydroxyphenyl 6-C), 115.8 (hydroxyphenyl 4-C), 115.2 (hydroxyphenyl 2-C), 23.6 (methyl); HRMS found MH^+ 253.0979. $C_{15}H_{12}N_2O_2H$ requires MH^+ 253.0977.

3-(3-Hydroxyphenyl)-2-((1E)-2-(4-cyanophenyl)ethenyl)quinazolin-4-one, 38e



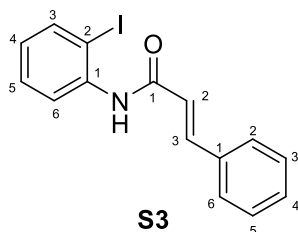
3-(3-Hydroxyphenyl)-2-methylquinazolin-4-one, **38n** (0.50 g, 1.98 mmol) was suspended in glacial acetic acid (5 mL) and dissolved upon heating. 4-Cyanobenzaldehyde (0.26 g, 1.98 mmol) was added and the reaction mixture was heated under reflux for 18 h. The reaction mixture was cooled and water (10 mL) was added. The resulting precipitate was filtered, washed with water, cold EtOH and hexanes to yield the quinazolinone⁷⁸ **38e** (0.475 g, 66%) as a yellow amorphous solid, R_f 0.56 (50:50 hexane–EtOAc); ν_{max}/cm^{-1} (film); 3339, 2227, 1655, 1553 and 1286; δ_H (501 MHz, d_6 -DMSO); 9.92 (1H, s, OH), 8.14 (1H, dd, J 8.0, 1.2, 5-H), 7.91 (1H, d, J 15.6, ethenyl 2-H), 7.88 (1H, ddd, J 8.6, 7.2, 1.5, 7-H), 7.82 (2H, d, J 8.4, 2-phenyl 2-H and 2-phenyl 6-H), 7.78 (1H, d, J 7.7, 8-H), 7.57–7.54 (3H, m, 2-phenyl 3-H, 2-phenyl 5-H and 6-H), 7.39 (1H, app t, J 8.0, hydroxyphenyl 5-H), 6.97 (1H, ddd, J 8.2, 2.3, 1.0, hydroxyphenyl 6-H), 6.88–6.84 (2H, m, hydroxyphenyl 4-H and hydroxyphenyl 2-H) and 6.53 (1H, d, J 15.6, ethenyl 1-H); δ_C (126 MHz, d_6 -DMSO); 161.2 (4-C), 158.5 (2-C), 151.0 (2-phenyl 1-C), 147.4 (8a-C), 139.6 (hydroxyphenyl 3-C), 137.8 (hydroxyphenyl 1-C), 136.8 (ethenyl), 135.0 (8-C), 133.1 (2-phenyl 2-C and 2-phenyl 6-C), 130.6 (hydroxyphenyl 5-C), 128.3 (2-phenyl 3-C and 2-phenyl 6-C), 127.5 (7-C), 127.1 (5-C), 126.7 (6-C), 123.7 (hydroxyphenyl 4-C), 121.0 (4a-C), 119.5 (ethenyl 1-C), 118.8 (CN), 116.6 (hydroxyphenyl 2-C), 116.0 (hydroxyphenyl 6-C), 111.7 (2-phenyl 4-C); HRMS found MH^+ 366.1232. $C_{23}H_{15}N_3O_2H$ requires MH^+ 366.1243.

N-(2-Iodophenyl)-3-phenylpropanamide, S1 (=48b)



By general procedure B using 2-iodoaniline (1.50 g, 7.17 mmol) and hydrocinnamoyl chloride (1.17 mL, 7.89 mmol) followed by with recrystallisation using hot EtOH to yield 2-iodoanilide¹⁹⁷ **S1** (=48b) (0.943 g, 37%) as a long colourless needles, m.p (from EtOH) 129.2–130.0 °C, R_f 0.19 (90:10 hexane–EtOAc); $\nu_{\max}/\text{cm}^{-1}$ (film); 3266, 3024, 1659, 1521 and 1184; δ_{H} (501 MHz, CDCl_3); 8.22 (1H, d, J 7.4, iodophenyl 3-H), 7.76 (1H, d, J 7.2, iodophenyl 6-H), 7.36–7.27 (5H, m, iodophenyl 4-H, phenyl 2-H, phenyl 3-H, phenyl 5-H and phenyl 6-H), 7.23 (1H, t, J 7.1, phenyl 4-H), 6.84 (1H, app t, J 7.2, iodophenyl 5-H), 3.09 (2H, t, J 7.7, 3-H₂), 2.75 (2H, t, J 7.7, 2-H₂); δ_{C} (126 MHz, CDCl_3); 170.4 (1-C), 140.5 (iodophenyl 1-C), 138.9 (iodophenyl 5-C), 138.2 (phenylpropanamidyl 1-C), 129.4 (iodophenyl 4-C), 128.8 (phenyl 2-C and phenyl 6-C), 128.5 (phenyl 3-C and phenyl 5-C), 126.6 (phenyl 4-C), 126.1 (iodophenyl 6-C), 122.1 (iodophenyl 3-C), 90.1 (iodophenyl 2-C), 39.8 (2-C), 31.6 (3-C); HRMS found MNa^+ 374.0013. $\text{C}_{15}\text{H}_{14}\text{INa}$ requires MNa^+ 374.0019.

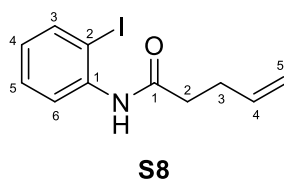
(2E)-N-(2-iodophenyl)-3-phenylprop-2-enamide, **S3** (Chapter 2)



By general procedure B using 2-iodoaniline (1.50 g, 7.17 mmol) and cinnamoyl chloride (1.32 g, 7.90 mmol) followed by purification with recrystallisation using hot EtOH to yield 2-iodoanilide¹⁹⁸ **S3** (1.152 g, 46%) as small colourless needles, m.p (EtOH) 149.1–150.7 °C, R_f 0.81 (50:50 hexane–EtOAc); $\nu_{\max}/\text{cm}^{-1}$ (film); 3218, 3025, 1657, 1529 and 1182; δ_{H} (400 MHz, CDCl_3); 8.39 (1H, d, J 7.7, iodophenyl 3-H), 7.81 (1H, dd, J 7.9, 1.4, iodophenyl 6-H), 7.79 (1H, d, J 15.5, 3-H), 7.59 (2H, dd, J 7.1, 2.4, phenyl 3-H and phenyl 5-H), 7.43–7.36 (4H, m, iodophenyl 4-H, phenyl 2-H, phenyl 4-H and phenyl 6-H), 6.87 (1H, td, J 7.8, 1.6, iodophenyl 5-H), 6.59 (1H, d, J 15.5, 2-H); δ_{C} (101 MHz, CDCl_3); 164.0

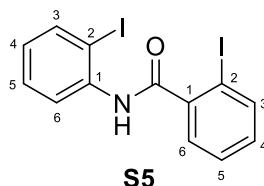
(1-C), 143.2 (3-C), 139.0 (iodophenyl 6-C), 138.5 (iodophenyl 1-C), 134.6 (phenyl 1-C), 130.3 (phenyl 4-C), 129.5 (iodophenyl 4-C), 129.1 (phenyl 3-C and phenyl 5-C), 128.2 (phenyl 2-C and phenyl 6-C), 126.2 (iodophenyl 5-C), 122.2 (iodophenyl 3-C), 120.8 (2-C), 83.3 (iodophenyl 2-C); HRMS found MH^+ 350.0033. $C_{15}H_{12}INO$ requires MH^+ 350.0042.

N-(2-iodophenyl)pent-4-enamide, **S8** (Chapter 2)



By general procedure B using 2-iodoaniline (1.50 g, 6.83 mmol) and 4-pentenyl chloride (0.83 mL, 7.51 mmol) followed by purification by flash column chromatography, eluting with 80:20 hexane–EtOAc to yield 2-iodoanilide¹⁹⁹ **S8** (0.906 g, 44%) as a colourless amorphous solid, R_f 0.37 (80:20 hexane–EtOAc); ν_{max}/cm^{-1} (film); 3269, 3070, 1657, 1519 and 1287; δ_H (501 MHz, d_6 -DMSO); 9.41 (1H, s, NH), 7.94–7.81 (1H, m, iodophenyl 3-H), 7.46–7.29 (2H, m, iodophenyl 5-H and iodophenyl 6-H), 7.09–6.88 (1H, m, iodophenyl 4-H), 6.04–5.72 (1H, m, 4-H), 5.11 (1H, br d, J 16.9, 5-H_a), 5.00 (1H, br d, J 9.4, 5-H_b), 2.46–2.40 (2H, m, 2-H), 2.40–2.33 (2H, m, 3-H); δ_C (126 MHz, d_6 -DMSO); 170.4 (1-C), 139.4 (iodophenyl 1-C), 138.7 (iodophenyl 3-C), 137.4 (4-C), 128.4 (iodophenyl 5-C), 127.4 (iodophenyl 6-C), 127.4 (iodophenyl 4-C), 115.1 (5-C), 96.6 (iodophenyl 2-C), 34.7 (2-C) and 29.0 (3-C); HRMS found MH^+ 302.0034. $C_{11}H_{12}INO$ requires MH^+ 302.0042.

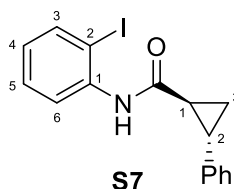
2-Iodo-*N*-(2-iodophenyl)benzamide, **S5** (Chapter 2)



By general procedure B using 2-iodoaniline (1.50 g, 6.83 mmol) and 2-iodobenzoyl chloride (2.00 g, 7.51 mmol) followed with purification by flash column chromatography, eluting with 50:50 hexane–EtOAc to yield 2-iodoanilide²⁰⁰ **S5** (0.917

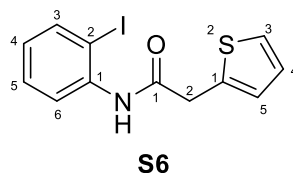
g, 30%) as a colourless amorphous solid, R_f 0.81 (50:50 hexane–EtOAc); $\nu_{\max}/\text{cm}^{-1}$ (film); 3243, 3017 and 1651; δ_{H} (501 MHz, d_6 -DMSO); 10.09 (1H, s, NH), 7.94 (2H, m, iodophenyl 3-H and 3-H), 7.58 (1H, dd, J 7.8, 1.2, iodophenyl 5-H), 7.54 (1H, app t, J 7.4, iodophenyl 6-H), 7.52–7.45 (2H, m, 5-H, 6-H), 7.25 (1H, td, J 7.8, 1.5, iodophenyl 4-H), 7.08 (1H, td, J 8.0, 1.6, 4-H); δ_{C} (126 MHz, d_6 -DMSO); 167.6 (carbonyl), 142.5 (1-C), 139.4 (iodophenyl 3-C), 139.4 (iodophenyl 1-C), 139.2 (3-C), 131.3 (iodophenyl 4-C), 129.0 (6-C), 128.6 (4-C), 128.3 (iodophenyl 6-C), 128.2 (iodophenyl 5-C), 128.2 (5-C), 98.1 (iodophenyl 2-C) and 93.8 (2-C); HRMS found MH^+ 449.8841. $\text{C}_{13}\text{H}_9\text{I}_2\text{NO}$ requires MH^+ 449.8846.

(1*R,2*R**)-*N*-(2-iodophenyl)-2-phenylcyclopropane-1-carboxamide, **S7****
(Chapter 2)



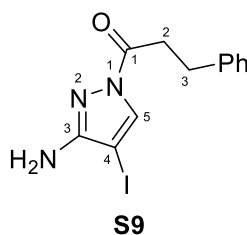
By general procedure B using 2-iodoaniline (1.00 g, 4.57 mmol) and (1*R**,2*R**)-2-phenylcyclopropane-1-carbonyl chloride (0.75 mL, 5.02 mmol) followed by purification with recrystallisation using hot EtOH to yield 2-iodoanilide **S7** (0.200 g, 12%) as long colourless needles, m.p (EtOH) 150.7–151.2 °C, R_f 0.83 (50:50 hexane–EtOAc); $\nu_{\max}/\text{cm}^{-1}$ (film); 3232, 3025, 1649, 1573 and 1283; δ_{H} (501 MHz, MeOD); 9.58 (1H, s, NH), 7.89 (1H, dd, J 7.9, 1.3, iodophenyl 3-H), 7.49 (1H, d, J 7.7, iodophenyl 6-H), 7.38 (1H, td, J 7.8, 1.3, iodophenyl 5-H), 7.28 (2H, app t, J 7.5, phenyl 3-H and phenyl 5-H), 7.22–7.17 (3H, m, phenyl 2-H, phenyl 4-H and phenyl 6-H), 6.98 (1H, td, J 7.8, 1.5, iodophenyl 4-H), 2.50 (1H, ddd, J 9.4, 6.4, 4.2, cyclopropane 2-H), 2.15 (1H, dt, J 7.0, 4.8 cyclopropane 1-H), 1.61 (1H, ddd, J 9.5, 5.2, 4.4, cyclopropane 3- H_a), 1.38 (1H, ddd, J 10.9, 7.3, 4.0, cyclopropane 3- H_b); δ_{C} (126 MHz, MeOD); 173.4 (carbonyl), 141.9 (iodophenyl 1-C), 140.6 (phenyl 1-C), 140.5 (iodophenyl 3-C), 129.9 (iodophenyl 5-C), 129.5 (phenyl 3-C and phenyl 5-C), 129.0 (iodophenyl 4-C), 128.4 (iodophenyl 6-C), 127.4 (phenyl 4-C), 127.3 (phenyl 2-C and phenyl 6-C), 27.0 (cyclopropane 1-C), 26.6 (cyclopropane 2-C) and 16.6 (cyclopropane 3-C); HRMS found MH^+ 364.0194. $\text{C}_{16}\text{H}_{14}\text{INO}$ requires MH^+ 364.0198.

***N*-(2-iodophenyl)-2-(thiophen-2-yl)acetamide, **S6** (Chapter 2)**



By general procedure B using 2-iodoaniline (1.00 g, 4.57 mmol) and 2-(thiophen-2-yl)acetyl chloride (0.62 mL, 1.1 mmol) followed by purification by flash column chromatography, eluting with 80:20 hexane–EtOAc and recrystallisation using hot EtOH to yield 2-iodoanilide **S6** (1.067 g, 68%) as a small, brown, flat crystals, m.p (EtOH) 125.1–126.6 °C, R_f 0.33 (80:20 hexane–EtOAc); $\nu_{\max}/\text{cm}^{-1}$ (film); 3237, 2912, 1660, 1574 and 1282; δ_{H} (501 MHz, CDCl_3); 8.27 (1H, d, J 8.0, iodophenyl 3-H), 7.75 (1H, s, NH), 7.70 (1H, dd, J 7.9, 0.9, iodophenyl 6-H), 7.35–7.29 (2H, m, iodophenyl 4-H and thiophenyl 3-H), 7.13 (1H, d, J 2.8, thiophenyl 5-H), 7.08 (1H, dd, J 5.0, 3.5, thiophenyl 4-H), 6.81 (1H, td, J 7.9, 1.2, iodophenyl 5-H), 3.99 (2H, s, 2- H_2); δ_{C} (126 MHz, CDCl_3); 168.3 (1-C), 139.0 (iodophenyl 6-C), 138.0 (iodophenyl 1-C), 135.2 (thiophenyl 1-C), 129.4 (thiophenyl 3-C), 128.8 (thiophenyl 5-C), 128.0 (thiophenyl 4-C), 126.6 (iodophenyl 4-C), 126.2 (iodophenyl 5-C), 121.5 (iodophenyl 3-C), 89.3 (iodophenyl 2-C), 38.8 (2-C); HRMS found MH^+ 365.9418. $\text{C}_{12}\text{H}_{10}\text{INOS}$ requires MH^+ 365.9425.

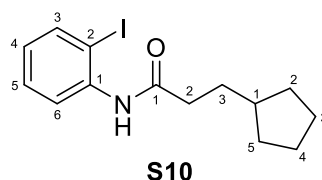
1-(3-Amino-4-iodopyrazol-1-yl)-3-phenylpropan-1-one, **S9** (Chapter 2)



By general procedure B using 3-amino-4-iodo-1H-pyrazole (2.00 g, 9.57 mmol) and hydrocinnamoyl chloride (1.56 mL, 10.53 mmol) followed by purification by flash column chromatography, eluting with 100% CH_2Cl_2 and recrystallisation using hot EtOH to yield to yield pyrazole **S9** (0.581 g, 18%) as long colourless needles, m.p (EtOH) 110.2–111.5 °C, R_f 0.59 (100% CDCl_3); $\nu_{\max}/\text{cm}^{-1}$ (film); 3428, 3303, 3124 and 1718; δ_{H} (500 MHz, CDCl_3); 8.03 (1H, s, pyrazoyl 5-H), 7.23–7.19 (2H, m, phenyl 3-H and 5-H), 7.18–7.15 (2H, m, phenyl 2-H and 6-H), 7.12 (1H, t, J 7.1, phenyl 4-H), 4.01 (2H, br s, NH_2), 3.18 (2H, t, J 7.8, 2- H_2), 2.98 (2H, t, J 7.8, 3- H_2); δ_{C} (126 MHz, CDCl_3); 169.5 (1-C), 157.2 (pyrazoyl 3-C), 140.5 (phenyl 1-C), 134.0 (pyrazoyl 5-C), 128.6 (phenyl 2-C and 6-C), 128.5

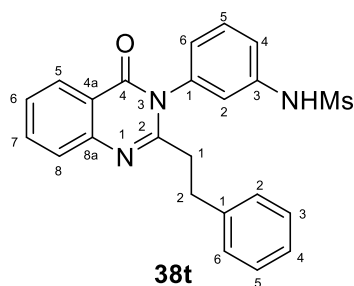
(phenyl 3-C and 5-C), 126.4 (phenyl 4-C), 57.6 (pyrazoyl 4-C), 35.01 (3-C), 30.3 (2-C); HRMS found MNa^+ 363.9924. $C_{12}H_{12}IN_3O$ requires MNa^+ 363.9917. The structure was determined by X-ray crystallography (Section 6.2.4).

3-Cyclopentyl-*N*-(2-iodophenyl)propanamide, **S10** (Chapter 2)



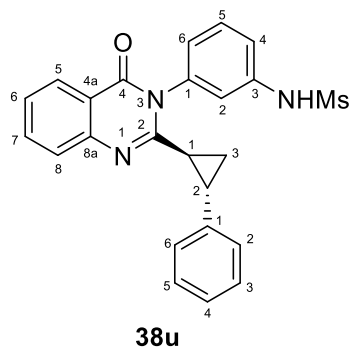
Following known procedure,¹² 3-Cyclopentylpropanoic acid (1.44 g, 10.04 mmol) was dissolved in DMF (25 mL) and CDI (1.68 g, 10.04 mmol) was added. The reaction mixture was stirred at rt for 90 mins. Afterwards, 2-iodoaniline (2.00 g, 9.13 mmol) was added and the reaction was stirred for a further 16 h at rt. CH_2Cl_2 (25 mL) was added to the reaction mixture and the resulting solution was washed with water (5 × 30 mL), dried with $MgSO_4$ and concentrated under reduced pressure to give a crude product. The crude product was purified by flash column chromatography, eluting with 100% CH_2Cl_2 to yield 2-iodoanilide **S10** (1.399 g, 41%) as a colourless amorphous solid, R_f 0.42 (80:20 hexane–EtOAc); ν_{max}/cm^{-1} (film); 3267, 2947 and 1656; δ_H (501 MHz, $CDCl_3$) 8.24 (1H, d, J 7.7, iodophenyl 3-H), 7.77 (1H, dd, J 8.0, 1.3, iodophenyl 6-H), 7.46 (1H, br s, NH), 7.34 (1H, td, J 8.1, 1.3, iodophenyl 4-H), 6.83 (1H, td, J 7.5, 1.3, iodophenyl 5-H), 2.45 (2H, t, J 7.6, 2-H₂), 1.90–1.81 (3H, m, cyclopentyl 1-H and cyclopentyl 3-H), 1.81–1.75 (2H, dd, J 14.8, 7.2, 3-H₂), 1.67–1.60 (2H, m, cyclopentyl 4-H), 1.58–1.50 (2H, m, cyclopentyl 5-H), 1.20–1.09 (2H, m, cyclopentyl 2-H); δ_c (126 MHz, $CDCl_3$); 171.6 (1-C), 138.9 (iodophenyl 6-C), 138.4 (iodophenyl 1-C), 129.4 (iodophenyl 4-C), 125.9 (iodophenyl 5-C), 122.1 (iodophenyl 3-C), 90.0 (iodophenyl 2-C), 39.7 (cyclopentyl 1-C), 37.5 (2-C), 32.7 (cyclopentyl 2-C), 32.5 (cyclopentyl 3-C), 32.0 (3-C), 25.3 (cyclopentyl 4-C and cyclopentyl 5-C); HRMS found MNa^+ 366.0322. $C_{14}H_{18}INO$ requires MNa^+ 366.0325.

3-(3-(*N*-Phenylmethanesulfonamide))-2-(2-phenylethyl)quinazolin-4-one, **38t**



By general procedure A using *N*-(2-iodophenyl)-3-phenylpropanamide, **S1** (=48b) (0.13 g, 0.50 mmol) and *N*-(3-aminophenyl)methanesulfonamide (0.11 g, 0.60 mmol) followed by purification by flash column chromatography, eluting with 50:50 hexane–EtOAc and purification using preparative LC-MS eluting with gradient elution: 5:95 → 95:5 MeCN–water to yield *quinazolinone* **38t** (0.008 g, 4%) as a colourless amorphous solid. R_f 0.36 (50:50 petrol–EtOAc); $\nu_{\max}/\text{cm}^{-1}$ (film); 3241, 3018, 1651, 1570 and 1302; δ_{H} (501 MHz, CDCl_3); 8.26 (1H, dd, J 8.0, 1.1, 5-H), 7.81 (1H, ddd, J 8.4, 7.0, 1.5, 7-H), 7.76 (1H, dd, J 8.1, 0.7, 8-H), 7.49 (1H, ddd, J 8.1, 7.1, 1.3, 6-H), 7.46 (1H, br d, J 8.3, 3-phenyl 6-H), 7.28 (1H, ddd, J 8.3, 2.0, 0.9, 3-phenyl 5-H), 7.22 (2H, app t, J 7.2, 2-phenyl 3-H and 2-phenyl 5-H), 7.17 (1H, t, J 7.3, 2-phenyl 4-H), 7.05–7.01 (2H, m, 2-phenyl 2-H and 2-phenyl 6-H), 6.95–6.93 (2H, m, 3-phenyl 4-H and 3-phenyl 2-H), 3.07 (2H, t, J 7.5, 2-ethyl 1-H), 2.97 (3H, s, Me) and 2.72 (2H, t, J 7.5, 2-ethyl 2-H); δ_{C} (126 MHz, CDCl_3); 162.8 (4-C), 155.6 (2-C), 147.6 (8a-C), 140.7 (2-phenyl 1-C), 138.9 (3-phenyl 3-C), 138.3 (3-phenyl 1-C), 135.0 (7-C), 131.3 (3-phenyl 6-C), 128.7 (2-phenyl 2-C and 2-phenyl 6-C), 128.6 (2-phenyl 3-C and 2-phenyl 5-C), 127.4 (8-C), 127.1 (5-C), 127.1 (6-C), 126.5 (2-phenyl 4-C), 124.7 (3-phenyl 4-C), 120.7 (4a-C), 120.1 (3-phenyl 2-C), 120.1 (3-phenyl 5-C), 39.9 (Me), 37.6 (2-ethyl 2-C) and 33.3 (2-ethyl 1-C); HRMS found MH^+ 420.1387. $\text{C}_{23}\text{H}_{21}\text{N}_3\text{O}_3\text{S}$ requires MH^+ 420.1376.

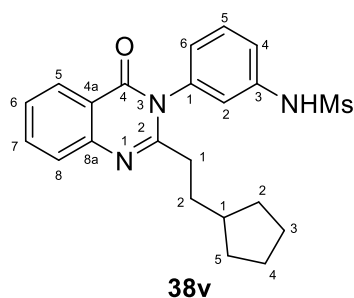
3-(3-(*N*-Phenylmethanesulfonamide))-2-((1*R, 2*R**)-2-phenylcyclopropyl)quinazolin-4-one, 38u**



By general procedure A using (*1R*^{*}, *2R*^{*})-*N*-(2-iodophenyl)-2-phenylcyclopropane-1-carboxamide, **S7** (0.18 g, 0.50 mmol) and *N*-(3-aminophenyl)methanesulfonamide (0.11 g, 0.60 mmol) followed by purification by flash column chromatography, eluting with 50:50 hexane–EtOAc and purification using preparative LC-MS eluting with gradient elution: 5:95 → 95:5 MeCN–water to yield *quinazolinone* **38u** (0.004 g, 2%, *rotamers* 56:44 by ¹H NMR) as a colourless amorphous solid. *R*_f 0.11 (50:50 hexane–EtOAc); $\nu_{\max}/\text{cm}^{-1}$ (film); 3213, 2926, 1662, 1584 and 1153; δ_{H} (501 MHz, CDCl₃); 8.25 (2H, ddd, *J* 7.9, 3.7, 1.3, 5-*H*^{maj} and 5-*H*^{min}), 7.77 (2H, td, *J* 8.4, 1.4, 7-*H*^{maj} and 7-*H*^{min}), 7.66 (2H, d, *J* 8.1, 8-*H*^{maj} and 8-*H*^{min}), 7.51–7.46 (2H, m, 3-phenyl 5-*H*^{maj} and 3-phenyl 5-*H*^{min}), 7.47–7.43 (2H, m, 6-*H*^{maj} and 6-*H*^{min}), 7.25–7.20 (4H, m, 2-phenyl 4-*H*^{maj}, 2-phenyl 4-*H*^{min}, 3-phenyl 6-*H*^{maj} and 3-phenyl 6-*H*^{min}), 7.20–7.18 (4H, m, 2-phenyl 3-*H*^{maj}, 2-phenyl 3-*H*^{min}, 2-phenyl 5-*H*^{maj} and 2-phenyl 5-*H*^{min}), 7.17–7.14 (2H, m, 3-phenyl 4-*H*^{maj} and 3-phenyl 4-*H*^{min}), 6.95–6.88 (6H, m, 2-phenyl 2-*H*^{maj}, 2-phenyl 2-*H*^{min}, 2-phenyl 6-*H*^{maj}, 2-phenyl 6-*H*^{min}, 3-phenyl 2-*H*^{maj} and 3-phenyl 2-*H*^{min}), 3.02 (3H, s, methyl^{min}), 2.66 (3H, s, methyl^{maj}), 2.59 (1H, ddd, *J* 9.2, 6.4, 4.4, cyclopropane 2-*H*^{min}), 2.53 (ddd, *J* 9.2, 6.4, 4.3, cyclopropane 2-*H*^{maj}), 2.16 (1H, ddd, *J* 9.1, 5.5, 4.7, cyclopropane 3-*H*_a^{maj}), 2.07 (1H, ddd, *J* 9.2, 5.4, 4.7, cyclopropane 3-*H*_a^{min}), 1.65 (2H, m, cyclopropane 1-*H*^{maj} and cyclopropane 1-*H*^{min}) and 1.34 (2H, m, cyclopropane 3-*H*_b^{maj} and cyclopropane 3-*H*_b^{min}); δ_{C} (126 MHz, CDCl₃); 162.6 (4-*C*^{min}), 162.5 (4-*C*^{maj}), 156.1 (2-*C*^{min}), 156.0 (2-*C*^{maj}), 147.9 (8a-*C*^{min}), 147.9 (8a-*C*^{maj}), 140.4 (2-phenyl 1-*C*^{maj}), 140.2 (2-phenyl 1-*C*^{min}), 138.5 (3-phenyl 3-*C*^{maj}), 138.4 (3-phenyl 3-*C*^{min}), 138.3 (3-phenyl 1-*C*^{maj}), 138.3 (3-phenyl 1-*C*^{min}), 134.5 (7-*C*), 131.1 (3-phenyl 5-*C*^{maj}), 131.0 (3-phenyl 5-*C*^{min}), 128.8 (2-phenyl 3-*C*^{maj} and 2-phenyl 5-*C*^{maj}), 128.5 (2-phenyl 3-*C*^{min} and 2-phenyl 5-*C*^{min}), 127.3 (5-*C*^{min}), 127.3 (5-*C*^{maj}), 127.2 (8-*C*^{maj}), 127.2 (8-*C*^{min}), 126.8 (2-phenyl 4-*C*^{min}), 126.6 (2-phenyl 4-*C*^{maj}), 126.6 (6-*C*^{min}), 126.5 (6-*C*^{maj}), 126.0 (2-phenyl 2-*C*^{min} and 2-phenyl 6-*C*^{min}), 126.0 (2-phenyl 2-*C*^{maj} and 2-phenyl 6-*C*^{maj}), 125.2 (3-phenyl 4-*C*^{min}), 125.1 (3-phenyl 4-*C*^{maj}), 120.8 (3-phenyl 2-*C*^{min}), 120.7 (4a-*C*^{maj}), 120.6 (4a-*C*^{min}), 120.5 (3-phenyl 2-*C*^{maj}), 120.3 (3-phenyl 6-*C*^{maj}), 120.0 (3-

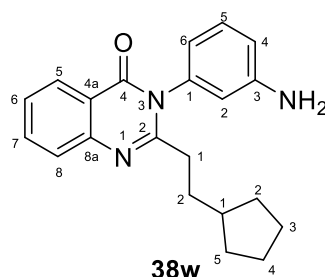
phenyl 6-C^{min}), 39.9 (methyl^{min}), 39.3 (methyl^{maj}), 29.7 (cyclopropane 2-C^{maj}), 29.3 (cyclopropane 2-C^{min}), 26.6 (cyclopropane 1-C^{maj}), 26.4 (cyclopropane 1-C^{min}), 18.1 (cyclopropane 3-C^{min}), 17.9 (cyclopropane 3-C^{maj}); HRMS found MH^+ 432.1378. $C_{24}H_{21}N_3O_3S$ requires MH^+ 432.1376. It was noted that two diastereomeric rotamers were observed.

3-(3-(*N*-Phenylmethanesulfonamide))-2-(2-cyclopentylethyl)quinazolin-4-one, 38v



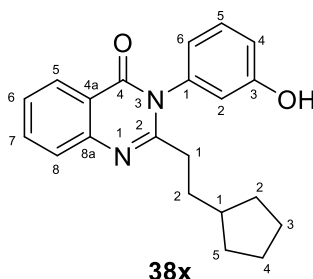
By general procedure A using 3-cyclopentyl-*N*-(2-iodophenyl)propenamide, **S10** (0.17 g, 0.50 mmol) and *N*-(3-aminophenyl)methanesulfonamide (0.11 g, 0.60 mmol) followed by purification followed by purification by flash column chromatography, eluting with 50:50 hexane–EtOAc and purification using preparative LC-MS eluting with gradient elution: 5:95 → 95:5 MeCN–water to yield *quinazolinone* **38v** (0.029 g, 14%) as a colourless amorphous solid. R_f 0.31 (50:50 hexane–EtOAc); ν_{max}/cm^{-1} (film); 3221, 2944, 1656, 1570 and 1472; δ_H (501 MHz, $CDCl_3$); 8.25 (1H, dd, J 8.0, 1.3, 5-H), 7.92 (1H, s, NH), 7.78 (1H, td, J 8.3, 1.5, 7-H), 7.71 (1H, d, J 8.0, 8-H), 7.47 (1H, app t, J 8.0, 3-phenyl 5-H), 7.47 (1H, td, J 8.0, 1.0, 6-H), 7.28 (1H, dd, J 8.2, 1.4, 3-phenyl 4-H), 7.08 (1H, br t, J 2.0, 3-phenyl 2-H), 7.06–7.02 (1H, m, 3-phenyl 6-H), 2.98 (3H, s, Me), 2.43 (2H, t, J 7.5, ethyl 1-H), 1.70–1.62 (3H, m, cyclopentyl 1-H and cyclopentyl 2-H), 1.61–1.57 (2H, m, ethyl 2-H), 1.53–1.46 (2H, m, cyclopentyl 4-H), 1.46–1.39 (2H, m, cyclopentyl 5-H), 0.96–0.82 (2H, m, cyclopentyl 2-H); δ_C (126 MHz, $CDCl_3$); 163.1 (4-C), 156.9 (2-C), 147.6 (8_a-C), 139.1 (3-phenyl 3-C), 138.2 (3-phenyl 1-C), 135.0 (7-C), 131.2 (3-phenyl 5-C), 127.2 (6-C), 127.1 (8-C), 126.9 (5-C), 124.4 (3-phenyl 6-C), 120.9 (3-phenyl 4-C), 120.4 (4_a-C), 120.3 (3-phenyl 2-C), 39.7 (cyclopentyl 1-C), 39.6 (ethyl 1-C), 35.3 (cyclopentyl 2-C), 33.7 (cyclopentyl 3-C), 32.4 (ethyl 2-C), 32.3 (cyclopentyl 5-C), 25.1 (cyclopentyl 4-C); HRMS found MH^+ 412.1691. $C_{22}H_{25}N_3O_3S$ requires MH^+ 412.1689.

3-(3-Aminophenyl)-2-(2-cyclopentylethyl)quinazolin-4-one, 38w



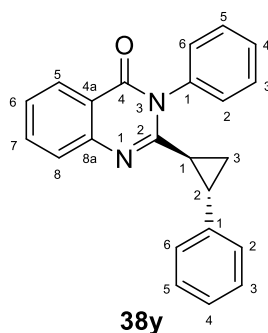
By general procedure A using 3-cyclopentyl-*N*-(2-iodophenyl)propenamide, **S10** (0.09 g, 0.26 mmol) and *m*-phenylenediamine (0.03 g, 0.31 mmol) followed by purification by flash column chromatography, eluting with 50:50 hexane–EtOAc and purification using preparative LC-MS eluting with gradient elution: 5:95 → 95:5 MeCN–water to yield quinazolinone **38w** (0.007 g, 8%) as a colourless amorphous solid. R_f 0.50 (50:50 hexane–EtOAc); $\nu_{\max}/\text{cm}^{-1}$ (film); 3267, 2947, 2920 and 1656; δ_{H} (501 MHz, CDCl_3); 8.27 (1H, dd, J 7.9, 0.9, 5-H), 7.77–7.73 (1H, m, 7-H), 7.69 (1H, d, J 8.1, 8-H), 7.44 (1H, td, J 7.8, 0.8, 6-H), 7.30 (1H, app t, J 7.9, 3-phenyl 5-H), 6.79 (1H, dd, J 8.1, 2.1, 3-phenyl 6-H), 6.62 (1H, dd, J 7.7, 1.0, 3-phenyl 4-H), 6.54 (1H, br t, J 2.0, 3-phenyl 2-H), 3.87 (2H, s, NH_2), 2.51 (2H, t, J 7.5, ethyl 1-H), 1.74–1.67 (3H, m, cyclopentyl 1-H and cyclopentyl 3-H), 1.67–1.59 (2H, m, ethyl 2-H), 1.56–1.51 (2H, m, cyclopentyl 4-H), 1.48–1.41 (2H, m, cyclopentyl 5-H), 1.00–0.90 (2H, m, cyclopentyl 2-H); δ_{C} (126 MHz, CDCl_3); 162.9 (4-C), 158.0 (2-C), 148.3 (3-phenyl 3-C), 148.0 (8a-C), 138.7 (3-phenyl 1-C), 134.8 (7-C), 130.9 (3-phenyl 5-C), 127.4 (8-C), 127.3 (5-C), 126.8 (6-C), 121.1 (4a-C), 118.4 (3-phenyl 4-C), 116.2 (3-phenyl 2-C), 115.0 (3-phenyl 6-C), 40.1 (cyclopentyl 1-C), 35.4 (ethyl 1-C), 34.2 (cyclopentyl 2-C), 32.7 (cyclopentyl 3-C), 32.7 (ethyl 2-C), 25.5 (cyclopentyl 4-C and cyclopentyl 5-C); HRMS found MH^+ 334.1912. $\text{C}_{21}\text{H}_{23}\text{N}_3\text{O}$ requires MH^+ 334.1914.

2-(2-Cyclopentylethyl)-3-(3-hydroxyphenyl)quinazolin-4-one, 38x



By general procedure A using 3-cyclopentyl-*N*-(2-iodophenyl)propenamide, **S10** (0.17 g, 0.50 mmol) and 3-aminophenol (0.07 g, 0.60 mmol) followed by purification by preparative LC-MS followed by purification by flash column chromatography, eluting with 50:50 hexane–EtOAc and purification using preparative LC-MS eluting with gradient elution: 5:95 → 95:5 MeCN–water to yield *quinazolinone* **38x** (0.014 g, 8%) as a colourless amorphous solid. R_f 0.60 (50:50 hexane–EtOAc); $\nu_{\max}/\text{cm}^{-1}$ (film); 3244, 2946 and 1655; δ_{H} (501 MHz, CDCl_3); 8.28 (1H, dd, J 7.9, 0.9, 5-H), 7.78 (1H, td, J 8.0, 1.4, 7-H), 7.73 (1H, d, J 8.0, 8-H), 7.47 (1H, td, J 8.3, 1.1, 6-H), 7.32 (1H, app t, J 8.1, 3-phenyl 5-H), 6.83 (1H, dd, J 8.3, 1.7, 3-phenyl 4-H), 6.71–6.68 (1H, m, 3-phenyl 6-H), 6.56 (1H, br t, J 2.1, 3-phenyl 2-H), 2.48 (2H, t, J 7.5, ethyl 1-H), 1.72–1.54 (5H, m, cyclopentyl 1-H, ethyl 2-H and cyclopentyl 3-H), 1.55–1.48 (2H, m, cyclopentyl 4-H), 1.46–1.38 (2H, m, cyclopentyl 5-H), 0.97–0.85 (2H, m, cyclopentyl 2-H); δ_{C} (126 MHz, CDCl_3); 163.3 (4-C), 158.8 (2-C), 157.8 (3-phenyl 3-C), 147.6 (8a-C), 137.3 (3-phenyl 1-C), 135.2 (7-C), 130.9 (6-C), 127.2 (8-C), 127.0 (5-C and 3-phenyl 5-C), 120.2 (4a-C), 118.9 (3-phenyl 6-C), 117.5 (3-phenyl 4-C), 115.8 (3-phenyl 2-C), 39.8 (cyclopentyl 1-C), 35.0 (ethyl 1-C), 33.9 (cyclopentyl 2-C), 32.4 (cyclopentyl 3-C), 32.3 (ethyl 2-C), 25.1 (cyclopentyl 5-C), 25.1 (cyclopentyl 4-C); HRMS found MH^+ 335.1757. $\text{C}_{21}\text{H}_{23}\text{N}_2\text{O}_2$ requires MH^+ 335.1754.

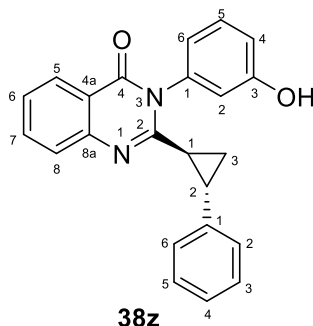
3-Phenyl-2-[(1*R**,2*R**)-2-phenylcyclopropyl]quinazolin-4-one, **38z**



By general procedure A using (1*R**,2*R**)-*N*-(2-iodophenyl)-2-phenylcyclopropane-1-carboxamide, **S7** (0.130 g, 0.31 mmol) and aniline (0.03 mL, 0.37 mmol) followed by purification by flash column chromatography, eluting with 50:50 hexane–EtOAc and purification using preparative LC-MS eluting with gradient elution: 5:95 → 95:5 MeCN–water to yield *quinazolinone* **38y** (0.019 g, 18%) as a colourless amorphous solid. R_f 0.19 (80:20 hexane–EtOAc); $\nu_{\max}/\text{cm}^{-1}$ (film); 3306, 3056, 1674, and 1586; δ_{H} (501 MHz, CDCl_3); 8.28 (1H, dd, J 8.0, 1.1, 5-H), 7.76 (1H, td, J 8.3, 1.4, 7-H), 7.67 (1H, d, J 8.1, 8-H),

7.52 (1H, app t, J 7.7, 3-phenyl 5-H), 7.44 (1H, app t, J 7.5, 6-H), 7.38 (1H, d, J 7.5, 3-phenyl 4-H), 7.35 (1H, br d, J 7.8, 3-phenyl 2-H), 7.30–7.26 (1H, m, 3-phenyl 3-H), 7.22–7.15 (4H, m, 3-phenyl 2-H, 2-phenyl 3-H, 2-phenyl 4-H and 2-phenyl 5-H), 6.89 (2H, d, J 7.0, 2-phenyl 2-H and 2-phenyl 6-H), 2.67–2.61 (1H, m, cyclopropane 2-H), 2.05 (1H, dt, J 9.7, 5.0, cyclopropane 3-H_a), 1.69 (1H, dt, J 8.5, 4.9, cyclopropane 1-H), 1.29 (1H, ddd, J 8.2, 6.3, 4.5, cyclopropane 3-H_b); δ_c (126 MHz, CDCl₃); 162.5 (4-C), 156.7 (2-C), 148.0 (8_a-C), 140.3 (2-phenyl 1-C), 137.2 (3-phenyl 1-C), 134.6 (7-C), 129.8 (3-phenyl 3-C and 3-phenyl 5-C), 129.1 (3-phenyl 4-C), 128.8 (3-phenyl 6-C), 128.5 (3-phenyl 2-C), 128.4 (2-phenyl 3-C and 2-phenyl 5-C), 127.2 (5-C), 127.1 (8-C), 126.5 (2-phenyl 4-C), 126.3 (6-C), 126.1 (2-phenyl 2-C and 2-phenyl 6-C), 120.9 (4_a-C), 29.1 (cyclopropane 2-C), 25.9 (cyclopropane 1-C), 18.3 (cyclopropane 3-C); HRMS found MH⁺ 339.1504. C₂₃H₁₉N₂O requires MH⁺ 339.1497. The two sides of the *N*-phenyl ring were revealed to be diastereotopic, indicating slow rotation around the *N*-phenyl bond.

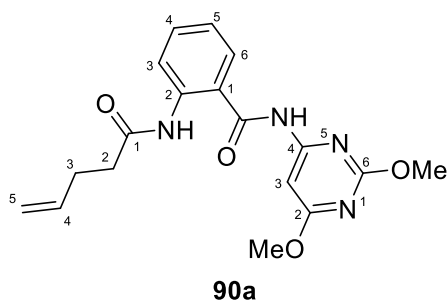
3-(3-Hydroxyphenyl)-2-[(1*R**,2*R**)-2-phenylcyclopropyl]quinazolin-4-one, **38z**



By general procedure A using (1*R**,2*R**)-*N*-(2-iodophenyl)-2-phenylcyclopropane-1-carboxamide, **S7** (0.12 g, 0.28 mmol) and 3-aminophenol (0.04 g, 0.33 mmol) followed by purification by flash column chromatography, eluting with 50:50 hexane–EtOAc and purification using preparative LC-MS eluting with gradient elution: 5:95 → 95:5 MeCN–water to yield *quinazolinone* **38z** (0.021 g, 21%, *rotamers* 55:45 by ¹H NMR) as a colourless amorphous solid. R_f 0.65 (50:50 hexane–EtOAc); δ_H (501 MHz, CDCl₃); 8.29 (2H, dd, J 7.2, 1.5, 5-H^{maj} and 5-H^{min}), 7.76 (2H, td, J 8.5, 1.4, 7-H^{maj} and 7-H^{min}), 7.67 (2H, dd, J 8.0, 2.8, 8-H^{maj} and 8-H^{min}), 7.44 (2H, app t, J 7.5, 6-H^{maj} and 6-H^{min}), 7.29 (1H, br d, J 8.0, 3-phenyl 5-H^{min}), 7.24–7.13 (6H, m, 2-phenyl 3-H^{maj}, 2-phenyl 3-H^{min}, 2-phenyl 4-H^{maj}, 2-phenyl 4-H^{min}, 2-phenyl 5-H^{maj} and 2-phenyl 5-H^{min}), 7.03 (1H, app t, J 8.0, 3-

phenyl 5-H^{maj}), 6.94 (2H, d, *J* 7.3, 2-phenyl 2-H^{min} and 2-phenyl 6-H^{min}), 6.88 (2H, d, *J* 7.1, 2-phenyl 2-H^{maj} and 2-phenyl 6-H^{maj}), 6.76 (1H, dd, *J* 7.7, 0.9, 3-phenyl 4-H^{min}), 6.72–6.65 (3H, m, 3-phenyl 6-H^{min}, 3-phenyl 4-H^{maj} and 3-phenyl 2-H^{maj}), 6.60–6.57 (2H, m, 3-phenyl 6-H^{maj} and 3-phenyl 2-H^{min}), 2.67 (1H, ddd, *J* 11.1, 7.8, 4.7, cyclopropane 2-H^{min}), 2.58 (1H, ddd, *J* 9.4, 6.3, 4.4, cyclopropane 2-H^{maj}), 2.03 (1H, dd, *J* 9.4, 5.1, cyclopropane 3-H_a^{maj}), 1.94 (1H, dt, *J* 9.4, 4.9 cyclopropane 3-H_a^{min}), 1.77 (2H, td, *J* 9.8, 4.7, cyclopropane 1H^{maj} and cyclopropane 1H^{min}), 1.30 (2H, dddd, *J* 16.9, 8.2, 6.4, 4.4, cyclopropane 3-H_b^{maj} and cyclopropane 3-H_b^{min}); δ_c (126 MHz, CDCl₃); 163.3 (4-C^{maj}), 163.3 (4-C^{min}), 158.5 (3-phenyl 3-C^{min}), 158.5 (3-phenyl 3-C^{maj}), 156.8 (2-C^{maj}), 156.8 (2-C^{min}), 148.2 (8_a-C^{maj}), 148.1 (8_a-C^{min}), 140.2 (2-phenyl 1-C^{maj}), 140.1 (2-phenyl 1-C^{min}), 137.2 (3-phenyl 1-C^{min}), 137.2 (3-phenyl 1-C^{maj}), 135.0 (7-C^{maj}), 135.0 (7-C^{min}), 130.8 (3-phenyl 5-C^{min}), 130.8 (3-phenyl 5-C^{maj}), 128.5 (2-phenyl 2-C^{maj}, 2-phenyl 2-C^{min}, 2-phenyl 6-C^{maj}, 2-phenyl 6-C^{min}), 127.3 (8-C^{maj}), 127.2 (8-C^{min}), 126.6 (5-C^{maj}), 126.5 (5-C^{min}), 126.5 (6-C^{maj}), 126.4 (6-C^{min}), 126.4 (2-phenyl 4-C^{min}), 126.4 (2-phenyl 4-C^{maj}), 126.1 (2-phenyl 3-C^{maj}, 2-phenyl 3-C^{min}, 2-phenyl 5-C^{maj} and 2-phenyl 5-C^{min}), 120.4 (4_a-C^{min}), 120.3 (4_a-C^{maj}), 119.5 (3-phenyl 4-C^{maj}), 119.0 (3-phenyl 4-C^{min}), 117.4 (3-phenyl 6-C^{maj}), 117.2 (3-phenyl 6-C^{min}), 116.2 (3-phenyl 2-C^{min}), 115.8 (3-phenyl 2-C^{maj}), 29.7 (cyclopropane 2-C^{maj}), 28.9 (cyclopropane 2-C^{min}), 25.6 (cyclopropane 1-C^{min}), 25.5 (cyclopropane 1-C^{maj}), 18.5 (cyclopropane 3-C^{maj}), 18.5 (cyclopropane 3-C^{min}); HRMS found MH^+ 355.1437. C₂₃H₁₉N₂O₂ requires MH^+ 355.1441. It was noted that two rotamers were observed.

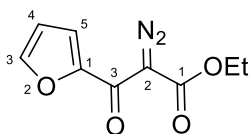
N-(2,6-dimethoxypyrimidin-4-yl)-2-(pent-4-enamido)benzamide, 90a



By general procedure A using *N*-(2-iodophenyl)pent-4-enamide, **S8** (0.15 g, 0.5 mmol) and 4-amino-2,6-dimethoxypyrimidine (0.09 g, 0.6 mmol) followed by purification by flash column chromatography, eluting with 50:50 hexane–EtOAc and purification using preparative LC-MS eluting with gradient elution: 5:95 → 95:5 MeCN–water to yield *benzamide* **90a** (0.08 g, 4%) as a colourless amorphous solid; $\nu_{\max}/\text{cm}^{-1}$ (film); 3540,

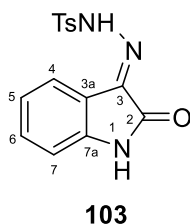
3223, 2920, 1708, 1669, 1583 and 1384; δ_{H} (501 MHz, CDCl_3); 10.72 (1H, s, N-H), 8.66 (1H, d, J 8.4, 6-H), 8.50 (1H, s, pyrimidinyl N-H), 7.63 (1H, d, J 7.7, 3-H), 7.54 (1H, app t, J 7.7, 5-H), 7.30 (1H, s, pyrimidinyl 3-H), 7.14 (1H, app t, J 7.6, 4-H), 5.88 (1H, ddt, J 17.1, 10.3, 4.0, pentenyl 4-H), 5.11 (1H, d, J 17.1, pentenyl 5-H_a), 5.02 (1H, d, J 10.3, pentenyl 5-H_b), 4.00 (3H, s, 6-methoxy methyl), 3.96 (3H, s, 2-methoxy methyl), 2.56–2.47 (4H, m, pentenyl 2-C and pentenyl 3-C); δ_{C} (126 MHz, CDCl_3); 173.60 (pyrimidinyl 5-C), 171.36 (pentenyl 1-C), 167.97 (carbonyl), 164.82 (pyrimidinyl 3-C), 158.61 (pyrimidinyl 1-C), 140.34 (1-C), 136.81 (pentenyl 4-C), 134.05 (5-C), 126.85 (3-C), 123.09 (4-C), 122.17 (6-C), 119.51 (2-C), 115.87 (pentenyl 5-C), 89.28 (pyrimidinyl 3-C), 54.98 (2-methoxyl methyl), 54.45 (6-methoxyl methyl), 37.68 (pentenyl 2-C), 29.42 (pentenyl 3-C); HRMS found MH^+ 357.1566. $\text{C}_8\text{H}_{21}\text{N}_4\text{O}_4$ requires MH^+ 357.1563.

Ethyl 2-diazo-3-(furan-2-yl)-3-oxopropanoate, **S1** (Chapter 3)

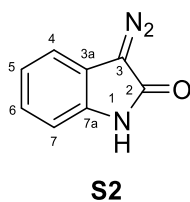


S1

1-(Furan-2-yl)pentane-1,3-dione, **101** (0.40 g, 2.20 mmol) and triethylamine (0.92 mL, 6.6 mmol) were dissolved in anhydrous MeCN (10 mL) and 4-acetamidobenzenesulfonyl azide (0.58 g, 2.4 mmol) was added portion-wise. The reaction mixture was stirred at rt overnight and then concentrated under reduced pressure. The resulting crude product was purified by flash column chromatography, eluting with 80:20 Petrol–EtOAc, to yield *diazo S1* (0.32 g, 71%) as an amorphous yellow solid; R_f 0.30 (80:20 Petrol–EtOAc); δ_{H} (501 MHz, Acetone- d_6); 7.83 (1H, dd, J 1.7, 0.7, furan 5-H), 7.49 (1H, dd, J 3.6, 0.7, furan 3-H), 6.67 (1H, dd, J 3.6, 1.7, furan 4-H), 4.29 (2H, q, J 7.1, ethyl CH_2), 1.29 (3H, t, J 7.1, ethyl CH_3); δ_{C} (126 MHz, Acetone- d_6); 171.2 (3-C), 161.5 (1-C), 151.3 (furan 2-C), 147.4 (furan 5-C), 119.7 (furan 3-C), 113.0 (furan 4-C), 75.0 (2-C), 62.1 (ethyl CH_2), 14.5 (ethyl CH_3); unable to obtain HR-MS.

Bis(4-methyl-N'-[(3E)-2-oxo-1H-indol-3-ylidene]benzenesulfonylhydrazide, 103

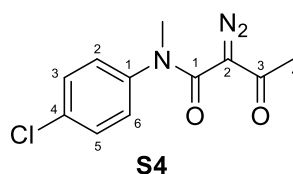
p-Toluene sulfonyl hydrazide (1.29 g, 6.94 mmol) was added in one portion to a solution of isatin (1.00 g, 6.80 mmol) in MeOH (30 mL) and the reaction was stirred at rt for 1 h. The resulting precipitate was filtered, washed with ice-cold MeOH and dried under reduced pressure to yield hydrazone²⁰¹ **103** (1.91 g, 89%) as a yellow amorphous solid; R_f 0.62 (1:99 MeOH-CH₂Cl₂); δ_H (501 MHz, DMSO-d₆); 7.86 (2H, d, J 8.3, tosyl 2-H and 6-H), 7.47–7.40 (3H, m, tosyl 3-H, 4-H and 5-H), 7.35 (1H, t, J 7.7, indoylidene 6-H), 7.04 (1H, td, J 7.6, 0.7, indoylidene 7-H), 6.89 (1H, d, J 7.8, indoylidene 5-H), 2.38 (3H, s, Me); δ_C (126 MHz, DMSO-d₆); 161.8 (indoylidene 2-C), 144.5 (tosyl 4-C), 142.5 (indoylidene 7a-C), 137.4 (indoylidene 3-C), 135.0 (tosyl 1-C), 131.9 (indoylidene 6-C), 130.0 (tosyl 3-C and 5-C), 127.6 (tosyl 2-C and 6-C), 122.6 (indoylidene 7-C), 120.7 (indoylidene 4-C), 119.3 (indoylidene 3a-C), 111.1 (indoylidene 5-C), 21.1 (Me). All data is consistent with known literature values.²⁰¹

3-(λ⁵-diazonylidene)-1H-indol-2-one, S2 (Chapter 3)

Bis(4-methyl-N'-[(3E)-2-oxo-1H-indol-3-ylidene]benzenesulfonylhydrazide, **103** (0.78 g, 2.48 mmol) was dissolved in a solution of NaOH (0.18 g, 4.96 mmol) in water (30 mL) and the reaction mixture was stirred for 20 h at rt. Solid CO₂ was added to the mixture until pH 7 was reached and the resulting precipitate was filtered and dried under reduced pressure to yield diazo²⁰¹ **S2** (0.39 g, 99%) as an orange amorphous solid; R_f 0.15 (1:99 MeOH-CH₂Cl₂); δ_H (501 MHz, CDCl₃); 9.11 (1H, s, NH), 7.19 (1H, d, J 7.6, 4-H), 7.15 (1H, td, J 7.7, 1.1, 6-H), 7.08 (1H, td, J 7.6, 0.9, 5-H), 7.01 (1H, d, J 7.8, 7-H);

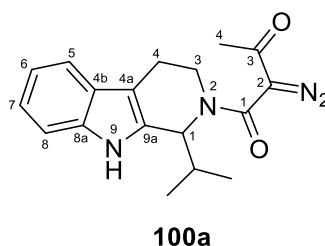
δ_c (126 MHz, CDCl_3); 169.22 (2-C), 131.96 (7_a-C), 125.71 (6-C), 122.34 (5-C), 118.50 (4-C), 117.40 (3_a-C), 110.83 (7-C), 61.6 (3-C). All data is consistent with known literature values.²⁰¹

***N*-(4-Chlorophenyl)-2-diazo-*N*-methyl-3-oxobutanamide, S4 (Chapter 3)**



By general procedure C using, 4-chloro-*N*-methylaniline (0.50 mL, 4.13 mmol) followed by purification by flash column chromatography, eluting with 1:1 Petrol–EtOAc to yield diazo¹³⁵ **S4** (0.81 g, 78%) as a yellow amorphous solid; R_f 0.50 (1:1 Petrol–EtOAc); δ_H (501 MHz, CDCl_3); 7.38 – 7.35 (2H, m, phenyl 3-H and phenyl 5-H), 7.15 – 7.11 (2H, m, phenyl 2-H and phenyl 6-H), 3.32 (3H, s, *N*-methyl), 2.43 (3H, s, 4-H); δ_c (126 MHz, CDCl_3); 190.4 (3-C), 161.0 (1-C), 141.6 (phenyl 1-C), 133.8 (phenyl 4-C), 130.5 (phenyl 3-C and phenyl 5-C), 127.5 (phenyl 2-C and phenyl 6-C), 74.5 (2-C), 38.5 (*N*-methyl), 28.4 (4-C). All data is consistent with known literature values.¹³⁵

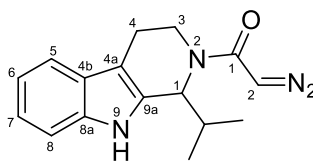
2-Diazo-1-{1-isopropyl-1H,3H,4H,9H-pyrido[3,4-b]indol-2-yl}butane-1,3-dione, 100a



By general procedure C using, 1-isopropyl-2,3,4,9-tetrahydro-1H- β -carboline (1.33 g, 6.21 mmol); with the exception of reacting the starting amine under reflux for 20 h instead of irradiating with MW radiation; followed by purification by flash column chromatography, eluting with 1:99 MeOH– CH_2Cl_2 to yield diazo **100a** (2.00 g, 99%) as a yellow fluffy solid, R_f 0.26 (1:99 MeOH– CH_2Cl_2); $\nu_{\text{max}}/\text{cm}^{-1}$ (film); 3304, 2962, 2101, 1610 and 1588; δ_H (501 MHz, CDCl_3); 8.05 (1H, s, NH), 7.47 (1H, d, J 7.8, pyridoindole 5-H),

7.33 (1H, dt, *J* 8.1, 0.8, pyridoindole 8-H), 7.18 (1H, ddd, *J* 8.2, 7.1, 1.2, pyridoindole 7-H), 7.11 (1H, ddd, *J* 8.0, 7.1, 1.0, pyridoindole 6-H), 5.30 (1H, s, pyridoindole 1-H), 4.09 – 3.95 (1H, m, pyridoindole 3-H_a), 3.72 – 3.60 (1H, m, pyridoindole 3-H_b), 2.95 – 2.79 (2H, m, pyridoindole 4-H_{a+b}), 2.35 (3H, s, 4-H), 2.20 (1H, m, CH(Me)₂), 1.16 (3H, d, *J* 6.7, isopropyl), 1.04 (3H, d, *J* 6.8, isopropyl); δ_c (126 MHz, CDCl₃); 160.9 (1-C), 136.1 (pyridoindole 8_a-C), 132.8 (pyridoindole 9_a-C), 129.2 (3-C), 126.6 (pyridoindole 4_b-C), 122.3 (pyridoindole 7-C), 119.8 (pyridoindole 6-C), 118.2 (pyridoindole 5-C), 111.1 (pyridoindole 8-C), 108.1 (pyridoindole 4_a-C), 56.7 (2-C), 53.6 (pyridoindole 1-C), 42.9 (pyridoindole 3-C), 33.9 (CH(Me)₂), 27.3 (4-C), 22.3 (pyridoindole 4-C), 20.1 (isopropyl CH₃), 19.9 (isopropyl CH₃); HRMS found MNa 347.1476. C₁₈H₂₀N₄O requires *MNa* 347.1484.

2-diazo-1-{1-isopropyl-1H,3H,4H,9H-pyrido[3,4-b]indol-2-yl}ethenone, S5
(Chapter 3)

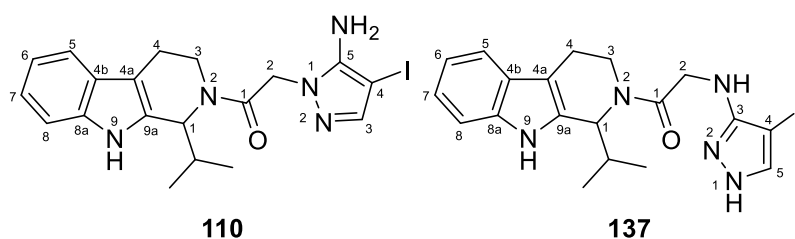


S5

2-Diazo-1-{1-isopropyl-1H,3H,4H,9H-pyrido[3,4-b]indol-2-yl}butane-1,3-dione, **100a** (0.66 g, 2.07 mmol) was dissolved in MeOH (3 mL) and cooled to 0 °C. Sodium methoxide (0.12 g, 2.28 mmol) was added portion-wise, and the reaction mixture was stirred for 16 h. The solution was poured into ice-water (10 mL), the aqueous layer was saturated with NaCl, extracted with Et₂O (4 × 20 mL), dried (MgSO₄) and concentrated at reduced pressure. The resulting crude product was purified by flash column chromatography, eluting with 1:99 MeOH–CH₂Cl₂, to yield diazo¹³⁵ **S5** (0.41 g, 70%) as a yellow amorphous solid; *R_f* 0.28 (1:99 MeOH–CH₂Cl₂); $\nu_{\max}/\text{cm}^{-1}$ (film); 3194, 2967, 2103, 1580, 1467, 1428 and 1349; δ_H (501 MHz, CDCl₃); 8.48 (1H, s, NH), 7.44 (1H, d, *J* 6.8, pyridoindole 5-H), 7.32 (1H, dt, *J* 8.1, 0.9, pyridoindole 8-H), 7.18 – 7.13 (1H, m, pyridoindole 7-H), 7.09 (1H, t, *J* 7.4, pyridoindole 6-H), 5.44 (1H, br s, pyridoindole 1-H), 5.18 (1H, br s, 2-H), 3.93 – 3.43 (2H, m, pyridoindole 3-H_{a+b}), 2.80 (1H, d, *J* 3.6, pyridoindole 4-H_a), 2.76 – 2.69 (1H, m, pyridoindole 4-H_b), 2.13 (1H, br s, CH(Me)₂), 1.16 (3H, d, *J* 6.7, isopropyl CH₃), 1.01 (3H, d, *J* 5.7, isopropyl CH₃); δ_c (126 MHz, CDCl₃); 165.4

(1-C), 136.1 (pyridoindole 8_a-C), 134.1 (pyridoindole 9_a-C), 126.6 (pyridoindole 4_b-C), 121.8 (pyridoindole 7-C), 119.4 (pyridoindole 6-C), 117.9 (pyridoindole 5-C), 111.1 (pyridoindole 8-C), 104.3 (pyridoindole 4_a-C), 55.8 (pyridoindole 1-C), 46.9 (2-C), 40.9 (pyridoindole 3-C), 33.2 (CH(Me)₂), 22.0 (pyridoindole 4-C), 20.1 (isopropyl CH₃); HRMS found M-N₂, 254.1486 . C₁₆H₁₈N₂O requires M-N₂, 254.1419.

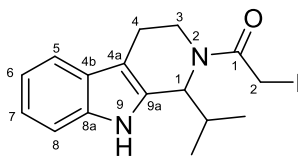
2-(5-amino-4-iodo-1H-pyrazol-1-yl)-1-[1-(propan-2-yl)-1H,2H,3H,4H,9H-pyrido[3,4-b]indol-2-yl]ethan-1-one, 110 or **2-[(4-iodo-1H-pyrazol-3-yl)amino]-1-[1-(propan-2-yl)-1H,2H,3H,4H,9H-pyrido[3,4-b]indol-2-yl]ethan-1-one, 137**



By general procedure D using, 2-diazo-1-{1-isopropyl-1H,3H,4H,9H-pyrido[3,4-b]indol-2-yl}ethenone, **S5** (0.11 g, 0.40 mmol), 3-amino-4-iodo-1H-pyrazole (0.17 g, 0.80 mmol) and Rh₂(pfb)₄ (4.23 mg, 0.004 mmol) followed by purification using preparative HPLC with gradient elution: 30:70 → 95:5 MeCN–water to yield *pyridoindole* **110** (2.84 mg, 2%, *rotamers* 75:25 by ¹H NMR) as a colourless amorphous solid; *R_f* 0.67 (1:99 MeOH–CH₂Cl₂); δ_H (501 MHz, CDCl₃); 8.06 (1H, s, pyridoindole N-H^{maj}), 7.98 (1H, s, pyridoindole N-H^{min}), 7.45 (2H, m, pyridoindole 5-H^{maj} and pyridoindole 5-H^{min}), 7.37 – 7.28 (3H, m, pyrazole 3-H^{maj}, pyridoindole 8-H^{maj} and pyridoindole 8-H^{min}), 7.21 – 7.15 (3H, m, pyrazole 3-H^{min}, pyridoindole 7-H^{maj} and pyridoindole 7-H^{min}), 7.09 (2H, m, pyridoindole 6-H^{maj} and pyridoindole 6-H^{min}), 5.46 (1H, d, *J* 8.2, pyridoindole 1-H^{maj}), 5.36 (1H, d, *J* 8.5, pyridoindole 1-H^{min}), 5.21 – 5.09 (2H, m, 2-H_a^{maj} and 2-H_a^{min}), 5.07 (1H, d, *J* 15.7, 2-H_b^{maj}), 4.98 (1H, d, *J* 15.7, 2-H_b^{min}), 4.29 (1H, dd, *J* 14.5, 4.9, pyridoindole 3-H_a^{min}), 3.66 – 3.58 (3H, m, pyridoindole 3-H_a^{maj}, pyridoindole 3-H_b^{maj} and pyridoindole 3-H_b^{min}), 2.88 – 2.80 (2H, m, pyridoindole 4-H_a^{maj} and pyridoindole 4-H_a^{min}), 2.75 (2H, d, *J* 15.3, pyridoindole 4-H_b^{maj} and pyridoindole 4-H_b^{min}), 2.19 – 2.11 (2H, m, CH(Me)₂^{maj} and CH(Me)₂^{min}), 1.18 (3H, d, *J* 6.7, Me_a^{maj}), 1.14 (3H, d, *J* 6.7, Me_a^{min}), 1.04 (3H, d, *J* 7.2, Me_b^{maj}), 0.96 (3H, d, *J* 6.8, Me_b^{min}); δ_c (126 MHz, CDCl₃); 166.4 (1-C^{min}), 165.6 (1-C^{maj}), 147.4 (pyrazole 5-C^{maj+min}), 142.7 (pyrazole 3-C^{maj}), 142.6 (pyrazole 3-C^{min}), 136.0 (pyridoindole 8_a-C^{min}), 136.0 (pyridoindole 8_a-C^{maj}), 132.9 (pyridoindole 9_a-C^{maj+min}),

126.7 (pyridoindole 4_b-C^{maj}), 126.5 (pyridoindole 4_b-C^{min}), 122.3 (pyridoindole 7-C^{maj}), 122.1 (pyridoindole 7-C^{min}), 119.8 (pyridoindole 6-C^{maj}), 119.7 (pyridoindole 6-C^{min}), 118.3 (pyridoindole 5-C^{maj}), 118.1 (pyridoindole 5-C^{min}), 111.0 (pyridoindole 8-C^{maj}), 111.0 (pyridoindole 8-C^{min}), 108.1 (pyridoindole 4_a-C^{maj+min}), 55.7 (pyridoindole 1-C^{min}), 55.6 (pyridoindole 1-C^{maj}), 51.5 (2-H^{maj+min}), 42.8 (pyrazole 4-C^{maj}), 42.7 (pyrazole 4-C^{min}), 41.2 (pyridoindole 3-C^{maj}), 41.2 (pyridoindole 3-C^{min}), 33.3 (CH(Me)₂^{min}), 33.2 (CH(Me)₂^{maj}), 22.3 (pyridoindole 4-C^{maj}), 22.0 (pyridoindole 4-C^{min}), 20.2 (Me_a^{maj}), 20.1 (Me_a^{min}), 20.0 (Me_b^{min}), 19.9 (Me_b^{maj}); HRMS found MH⁺ 464.0941. C₁₉H₂₂IN₅O requires MH⁺ 464.0942. Regiochemistry could not be determined, compounds chosen based off HMBC evidence.

2-iodo-1-{1-isopropyl-1H,3H,4H,9H-pyrido[3,4-b]indol-2-yl}ethenone, **111**

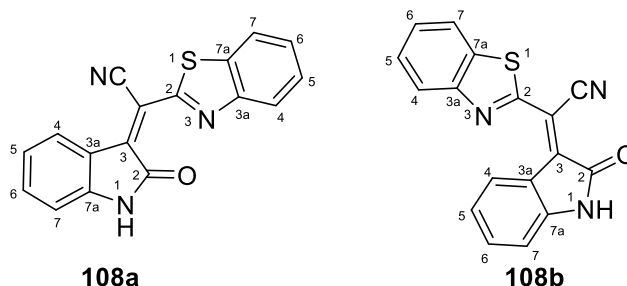


111

By general procedure D using, 2-diazo-1-{1-isopropyl-1H,3H,4H,9H-pyrido[3,4-b]indol-2-yl}ethenone, **S5** (0.11 g, 0.40 mmol), 3-amino-4-iodo-1H-pyrazole (0.17 g, 0.80 mmol) and Rh₂(pfb)₄ (4.23 mg, 0.004 mmol) followed by purification using preparative HPLC with gradient elution: 30:70 → 95:5 MeCN–water to yield *pyridoindole* **111** (0.01 g, 5%) as a yellow oil; *R_f* 0.71 (60:40 EtOAc–hexane); δ_H (501 MHz, CDCl₃); 7.88 (1H, s, NH), 7.47 (1H, d, *J* 7.7, pyridoindole 5-H), 7.34 (1H, d, *J* 8.0, pyridoindole 8-H), 7.18 (1H, t, *J* 7.4, pyridoindole 7-H), 7.11 (1H, t, *J* 7.5 Hz, pyridoindole 6-H), 5.42 (1H, d, *J* 8.6, pyridoindole 1-H), 4.03 (1H, dd, *J* 14.3, 5.7 Hz, pyridoindole 3-H_a), 3.88 – 3.81 (2H, m, 2-H), 3.69 – 3.60 (1H, m, pyridoindole 3-H_b), 3.05 – 2.96 (1H, m, pyridoindole 4-H_a), 2.85 (1H, dd, *J* 15.4, 4.1, pyridoindole 4-H_b), 2.16 (2H, dd, *J* 15.1, 8.1 Hz, CH(Me)₂), 1.18 (3H, d, *J* 6.7, isopropyl CH₃), 1.05 (3H, d, *J* 6.8, isopropyl CH₃); δ_c (126 MHz, CDCl₃); 167.5 (1-C), 136.0 (pyridoindole 8_a-C), 133.2 (pyridoindole 9_a-C), 126.5 (pyridoindole 4_b-C), 122.2 (pyridoindole 7-C), 119.8 (pyridoindole 6-C), 118.2 (pyridoindole 5-C), 111.1 (pyridoindole 8-C), 108.2 (pyridoindole 4_a-C), 55.1 (pyridoindole 1-C), 42.5 (pyridoindole 3-C), 33.7

(CH(Me)₂), 22.1 (pyridoindole 4-C), 20.2 (isopropyl CH₃), 19.7 (isopropyl CH₃), -3.6 (2-C); HRMS found MH⁺ 383.0615. C₁₆H₁₉N₂O requires MH⁺ 383.0615.

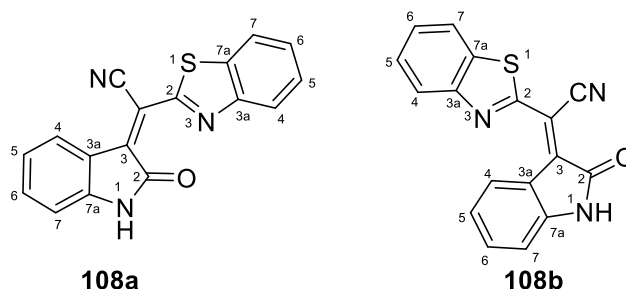
2-(1,3-benzothiazol-2-yl)-2-[(3E)-2-oxo-2,3-dihydro-1H-indol-3-ylidene], **108a**
and
2-(1,3-benzothiazol-2-yl)-2-[(3Z)-2-oxo-2,3-dihydro-1H-indol-3-ylidene]acetonitrile, **108b**



By general procedure D using, 3-(λ⁵-diazynylidene)-1H-indol-2-one **S2** (0.06 g, 0.40 mmol), 2-benzothiazole acetonitrile (0.14 g, 0.80 mmol) and Rh₂(pfb)₄ (4.23 mg, 0.004 mmol) followed by purification using preparative LC-MS with gradient elution: 30:70 → 95:5 MeCN–water to yield indolone⁶³ **108a** and **108b** (4.90 mg, 4%, *E/Z* or *Z/E* 23:77 by ¹H NMR) as an orange amorphous solid; *R_f* 0.44 (1:99 MeOH–CH₂Cl₂); ν_{max}/cm⁻¹ (film); 3216, 2920, 2187, 1714 and 1619; δ_H (501 MHz, CDCl₃); 8.85 (1H, d, *J* 8.0, oxindole 4-H^{maj}), 8.60 (1H, d, *J* 8.0, oxindole 4-H^{min}), 8.25 (1H, d, *J* 8.0, benzothiazole 4-H^{min}), 8.22 (1H, d, *J* 7.9, benzothiazole 4-H^{maj}), 8.05 – 8.02 (1H, m, benzothiazole 7-H^{maj}), 7.97 (1H, d, *J* 8.1, benzothiazole 7-H^{min}), 7.64 (1H, ddd, *J* 8.3, 7.2, 1.2, benzothiazole 5-H^{maj}), 7.60 – 7.55 (2H, m, benzothiazole 6-H^{maj} and benzothiazole 5-H^{min}), 7.54 – 7.51 (1H, m, benzothiazole 6-H^{min}), 7.46 – 7.41 (2H, m, oxindole 6-H^{maj} and oxindole 6-H^{min}), 7.19 (1H, td, *J* 7.8, 1.0 Hz, oxindole 5-H^{min}), 7.03 (1H, td, *J* 8.0, 1.0, oxindole 5-H^{maj}), 6.92 (1H, d, *J* 7.7, oxindole 7-H^{min}), 6.87 (1H, d, *J* 7.8, oxindole 7-H^{maj}); δ_c (126 MHz, CDCl₃); 166.3 (oxindole 2-C^{min}), 166.0 (oxindole 2-C^{maj}), 160.7 (benzothiazole 2-C^{maj}), 160.6 (benzothiazole 2-C^{min}), 153.9 (benzothiazole 3a-C^{maj}), 152.5 (benzothiazole 3a-C^{min}), 143.3 (oxindole 7a-C^{maj}), 139.1 (oxindole 7a-C^{min}), 137.4 (benzothiazole 7a-C^{min}), 137.1 (benzothiazole 7a-C^{maj}), 135.4 (oxindole 6-C^{maj}), 134.1 (oxindole 6-C^{min}), 129.3 (oxindole 4-C^{maj}), 127.5 (benzothiazole 5-C^{maj}), 127.5 (benzothiazole 5-C^{min}), 127.4 (benzothiazole 6-C^{maj}), 127.1 (oxindole 4-C^{min}), 126.6 (benzothiazole 6-C^{min}), 124.5 (benzothiazole 4-C^{maj} and benzothiazole 4-C^{min}), 123.6 (oxindole 5-C^{min}), 123.0 (oxindole 5-C^{maj}), 122.1

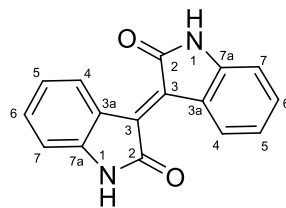
(benzothiazole 7- C^{maj}), 121.6 (benzothiazole 7- C^{min}), 120.7 (CN $^{\text{min}}$), 116.7 (CN $^{\text{maj}}$), 110.4 (oxindole 7- C^{min}), 110.4 (oxindole 7- C^{maj}), 108.9 (oxindole 3- C^{min}), 108.6 (oxindole 3- C^{maj}), 106.5 (2- C^{min}), 106.5 (2- C^{maj}); HRMS found MH^+ 304.0536. $C_{17}H_9N_3OS$ requires MH^+ 304.0539. E/Z isomers could not be structurally distinguished.

2-(1,3-benzothiazol-2-yl)-2-[(3E)-2-oxo-2,3-dihydro-1H-indol-3-ylidene], 108a
and **2-(1,3-benzothiazol-2-yl)-2-[(3Z)-2-oxo-2,3-dihydro-1H-indol-3-ylidene]acetonitrile, 108b**



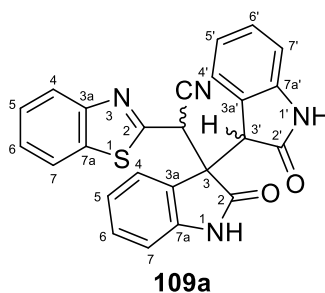
Isatin (0.74 g, 5.00 mmol) and 2-benzothiazoleacetonitrile (0.87 g, 5.00 mmol) were dissolved in EtOH (10 mL) and DBU (0.08 mL, 0.5 mmol) was added. The reaction was heated to 70 °C for 15 min. The resulting precipitate was filtered to yield indolone¹⁶³ **108a** and **108b** (1.22 g, 80%, E/Z or Z/E 7:93 by 1H NMR) as a purple amorphous solid; R_f 0.46 (1:99 MeOH- CH_2Cl_2); δ_H (501 MHz, $CDCl_3$); 8.83 (1H, d, J 7.8, oxindole 4-H), 8.22 (1H, d, J 7.9, benzothiazole 4-H), 8.03 (1H, d, J 8.2, benzothiazole 7-H), 7.65 – 7.62 (1H, m, benzothiazole 5-H), 7.59 – 7.54 (1H, m, benzothiazole 6-H), 7.44 – 7.40 (1H, m, oxindole 6-H), 7.02 (1H, t, J 7.6, oxindole 5-H), 6.88 (1H, d, J 7.9, oxindole 7-H); δ_C (126 MHz, $CDCl_3$); 166.0 (oxindole 2-C), 160.7 (benzothiazole 2-C), 153.9 (benzothiazole 3a-C), 143.3 (oxindole 7a-C), 137.1 (benzothiazole 7a-C), 135.4 (oxindole 6-C), 129.3 (oxindole 4-C), 127.5 (benzothiazole 5-C), 127.4 (benzothiazole 6-C), 124.5 (benzothiazole 4-C), 123.0 (oxindole 5-C), 122.1 (benzothiazole 7-C), 120.6 (oxindole 3a-C), 114.9 (CN), 110.5 (oxindole 7-C), 108.5 (oxindole 3-C), 106.7 (2-C); All data is consistent with known literature values.¹⁶³ E/Z isomers could not be structurally distinguished.

(E)-[3,3'-biindolinylidene]-2,2'-dione, 121

**121**

Isatin (1.50 g, 10.00 mmol) and indolin-2-one (1.35 g, 10.00 mmol) were suspended in glacial acetic acid (30 mL) and concentrated hydrogen chloride (0.5 mL) was added. The mixture was heated to reflux for 3 h. The resulting precipitate was collected, washed with MeOH, water, sodium bicarbonate and pentane to yield indolone^{156,202} **121** (2.33 g, 89%) as a purple amorphous solid; R_f 0.65 (60:40 EtOAc–hexane); δ_H (501 MHz, DMSO- d_6); 9.06 (2H, d, J 8.0, oxindole 4-H and oxindole 4'-H), 7.33 (2H, td, J 7.7, 1.0, oxindole 6-H and oxindole 6'-H), 6.99 – 6.92 (2H, m, oxindole 5-H and oxindole 5'-H), 6.84 (2H, d, J 7.7, oxindole 7-H and oxindole 7'-H), 3.34 (2H, s, NH); δ_C (126 MHz, DMSO- d_6); 169.0 (oxindole 2-C and oxindole 2'-C), 144.2 (oxindole 7_a-C and oxindole 7'_a-C), 133.4 (oxindole 3_a-C and oxindole 3'_a-C), 132.6 (oxindole 6-C and oxindole 6'-C), 129.3 (oxindole 4-C and oxindole 4'-C), 121.7 (oxindole 3-C and oxindole 3'-C), 121.1 (oxindole 5-C and oxindole 5'-C), 109.6 (oxindole 7-C and oxindole 7'-C); All data is consistent with known literature values.^{156,202}

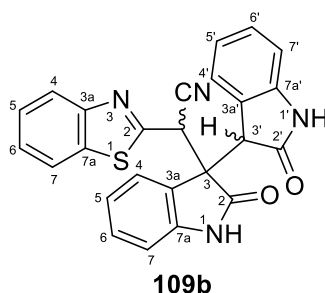
2-(1,3-benzothiazol-2-yl)-2-{2,2'-dioxo-1H,1'H,2H,2'H,3H,3'H-[3,3'-biindol]-3-yl}acetonitrile, 109a

**109a**

2-Benzothiazoleacetonitrile (0.01 g, 0.57 mmol) was dissolved in DMF (3.6 mL) and DBU (0.09 mL, 0.63 mmol) was added, and the resulting mixture was stirred at rt for 5 mins. (*E*)-[3,3'-biindolylidene]-2,2'-dione, **121** (0.15 g, 0.57 mmol) was added and the reaction was stirred at rt for 90 mins. The reaction mixture was dissolved in CH_2Cl_2 (10 mL), washed with water (4 × 20 mL), dried ($MgSO_4$) and concentrated at reduced

pressure. The crude mixture was purified using preparative LC-MS with gradient elution: 30:70 → 95:5 MeCN–water to yield *indolone 109a* (0.88 mg, 1%) as an orange amorphous solid; R_f 0.44 (60:40 EtOAc–hexane); $\nu_{\max}/\text{cm}^{-1}$ (film); 3255, 2924, 2107, 1712 and 1472; δ_{H} (501 MHz, MeOD); 7.92 – 7.89 (1H, m, benzothiazole 4-H), 7.82 – 7.79 (1H, m, benzothiazole 7-H), 7.47 – 7.43 (1H, m, benzothiazole 5-H), 7.37 (1H, ddd, J 8.3, 7.3, 1.1, benzothiazole 6-H), 7.34 – 7.31 (1H, m, oxindole 4'-H), 7.20 (1H, d, J 7.6, oxindole 4-H), 7.06 (1H, d, J 7.7, oxindole 6'-H), 6.99 (1H, td, J 7.7, 1.2, oxindole 6-H), 6.88 (1H, td, J 7.7, 0.9, oxindole 5'-H), 6.85 – 6.82 (1H, m, oxindole 5-H), 6.70 (1H, d, J 7.5, oxindole 7'-H), 6.44 (1H, d, J 7.8, oxindole 7-H), 6.28 (1H, s, CHCN), 4.42 (1H, s, oxindole 3'-H); δ_{C} (126 MHz, MeOD); 178.2 (oxindole 2'-C), 177.2 (oxindole 2-C), 161.1 (benzothiazole 2-C), 153.3 (benzothiazole 3a-C), 143.7 (oxindole 7a-C), 143.6 (oxindole 7'a-C), 136.8 (benzothiazole 7a-C), 133.7 (oxindole 3'a-C), 131.2 (oxindole 6-C), 130.1 (oxindole 6'-C), 127.6 (benzothiazole 5-C), 127.2 (benzothiazole 6-C), 125.6 (oxindole 4-C), 125.3 (oxindole 3a-C), 125.1 (oxindole 4'-C), 124.3 (benzothiazole 4-C), 123.6 (oxindole 5'-C), 123.2 (oxindole 5-C), 122.7 (benzothiazole 7-C), 116.7 (CN), 111.1 (oxindole 7-C), 110.9 (oxindole 7'-C), 56.4 (oxindole 3-C), 48.5 (oxindole 3'-C), 39.6 (CHCN); HRMS found MNa 459.0902. $C_{25}H_{16}N_4O_2S$ requires MNa 459.0892. Relative stereochemistry could not be confirmed using NOESY NMR.

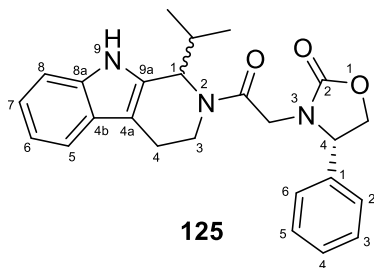
2-(1,3-benzothiazol-2-yl)-2-{2,2'-dioxo-1H,1'H,2H,2'H,3H,3'H-[3,3'-biindol]-3-yl}acetonitrile, 109b



2-Benzothiazoleacetonitrile (0.01 g, 0.57 mmol) was dissolved in DMF (3.6 mL) and DBU (0.09 mL, 0.63 mmol) was added, and the resulting mixture was stirred at rt for 5 mins. (*E*)-[3,3'-biindolylidene]-2,2'-dione, **121** (0.15 g, 0.57 mmol) was added and the reaction was stirred at rt for 90 mins. The reaction mixture was dissolved in CH_2Cl_2 (10 mL), washed with water (4 × 20 mL), dried (MgSO_4) and concentrated at reduced pressure. The crude mixture was purified using preparative LC-MS with gradient

elution: 30:70 → 95:5 MeCN–water to yield *indolone 109b* (3.24 mg, 1%) as a yellow amorphous solid; R_f 0.41 (60:40 EtOAc–hexane); $\nu_{\max}/\text{cm}^{-1}$ (film); 3265, 2961, 2107, 1711 and 1471; δ_{H} (501 MHz, MeOD); 7.98 (1H, d, J 7.0, oxindole 4-H), 7.85 (1H, d, J 8.2, benzothiazole 4-H), 7.83 (1H, d, J 8.0, benzothiazole 7-H), 7.47 – 7.41 (1H, m, benzothiazole 5-H), 7.38 (1H, m, benzothiazole 6-H), 7.35 (1H, dd, J 7.6, 1.3, oxindole 6-H), 7.29 (1H, t, J 7.8, oxindole 5-H), 7.13 (1H, t, J 7.7, oxindole 5'-H), 6.85 (1H, d, J 7.8, oxindole 4'-H), 6.66 (1H, d, J 7.7, oxindole 7-H), 6.58 (1H, t, J 7.6, oxindole 6'-H), 6.30 (1H, s, CHCN), 5.70 (1H, br s, oxindole 7'-H), 4.37 (1H, s, oxindole 3'-H); δ_{C} (126 MHz, MeOD); 177.3 (oxindole 2'-C), 176.1 (oxindole 2-C), 161.3 (benzothiazole 2-C), 153.4 (benzothiazole 3a-C), 144.5 (oxindole 7a-C), 144.4 (oxindole 7'a-C), 136.7 (benzothiazole 7a-C), 131.8 (oxindole 6-C), 130.2 (oxindole 5'-C), 128.1 (oxindole 3a-C), 127.6 (benzothiazole 5-C), 127.2 (benzothiazole 6-C), 125.9 (oxindole 4-C), 125.6 (oxindole 3'a-C), 125.4 (oxindole 7'-C), 124.2 (oxindole 5-C), 124.2 (benzothiazole 4-C), 122.7 (benzothiazole 7-C), 122.7 (oxindole 6'-C), 118.3 (CN), 111.6 (oxindole 7-C), 111.0 (oxindole 4'-C), 57.4 (oxindole 3-C), 48.9 (oxindole 3'-C), 40.6 (CHCN); HRMS found MNa 459.0893. $\text{C}_{25}\text{H}_{16}\text{N}_4\text{O}_2\text{S}$ requires MNa 459.0892. Relative stereochemistry could not be confirmed using NOESY NMR.

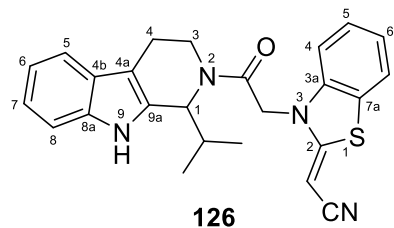
(4S)-3-{2-oxo-2-[1-(propan-2-yl)-1H,2H,3H,4H,9H-pyrido[3,4-b]indol-2-yl]ethyl}-4-phenyl-1,3-oxazolidin-2-one, 125



By general procedure E using 2-diazo-1-{1-isopropyl-1H,3H,4H,9H-pyrido[3,4-b]indol-2-yl}ethenone, **S5** (0.07 g, 0.26 mmol), (*S*)-(+)-4-phenyl-2-oxazolidinone (0.9 g, 0.52 mmol) and $\text{Rh}_2(\text{Piv})_4$ (1.59 mg, 0.003 mmol) followed by purification by preparative HPLC with gradient elution: 5:95 → 35:65 → 60:40 → 95:5 MeCN–water to yield *pyridoindole 125* (2.17 mg, 2%, *diastereomers* 58:42 by ^1H NMR) as a colourless amorphous solid; R_f 0.72 (70:30 EtOAc–hexane); $\nu_{\max}/\text{cm}^{-1}$ (film); 3320, 2963, 1749, 1650 and 1452; δ_{H} (501 MHz, CDCl_3); 8.21 (1H, s, pyridoindole N-H^{min}), 7.88 (1H, s,

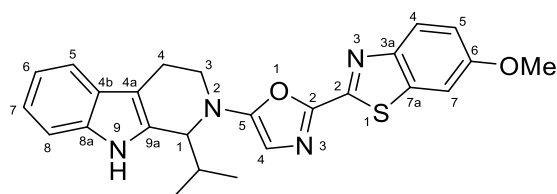
pyridoindole N-H^{maj}), 7.43 – 7.28 (10H, m, phenyl 3-H^{maj}, phenyl 3-H^{min}, phenyl 5-H^{maj}, phenyl 5-H^{min}, pyridoindole 5-H^{maj}, pyridoindole 5-H^{min}, pyridoindole 8-H^{maj}, pyridoindole 8-H^{min}, phenyl 4-H^{maj} and phenyl 4-H^{min}), 7.25 – 7.23 (4H, m, phenyl 2-H^{maj}, phenyl 2-H^{min}, phenyl 6-H^{maj} and phenyl 6-H^{min}), 7.20 – 7.14 (2H, m, pyridoindole 7-H^{maj} and pyridoindole 7-H^{min}), 7.12 – 7.07 (2H, m, pyridoindole 6-H^{maj} and pyridoindole 6-H^{min}), 5.43 (1H, d, *J* 8.2, pyridoindole 1-H^{min}), 5.39 (1H, d, *J* 8.3, pyridoindole 1-H^{maj}), 5.21 (1H, t, *J* 8.3, oxazolidinone 4-H^{min}), 5.13 – 5.09 (1H, m, oxazolidinone 4-H^{maj}), 4.74 (1H, d, *J* 8.9, oxazolidinone 5-H_a^{min}), 4.70 (1H, d, *J* 8.8, oxazolidinone 5-H_a^{maj}), 4.59 (1H, d, *J* 16.7, 1-H_a^{maj}), 4.47 (1H, d, *J* 16.4, 1-H_a^{min}), 4.19 (1H, d, *J* 8.9, oxazolidinone 5-H_b^{min}), 4.16 (1H, d, *J* 8.7, oxazolidinone 5-H_b^{maj}), 3.84 (1H, dd, *J* 14.4, 5.6, pyridoindole 3-H_a^{maj}), 3.70 (1H, dd, *J* 14.0, 5.4, pyridoindole 3-H_a^{min}), 3.58 – 3.50 (1H, m, pyridoindole 3-H_b^{min}), 3.50 (1H, d, *J* 16.6, 1-H_b^{min}), 3.44 – 3.37 (1H, m, pyridoindole 3-H_b^{maj}), 3.37 (1H, d, *J* 16.7, 1-H_b^{maj}), 2.69 (1H, dd, *J* 15.5, 3.9, pyridoindole 4-H_a^{maj}), 2.61 (1H, dd, *J* 15.4, 3.9, pyridoindole 4-H_a^{min}), 2.54 – 2.45 (2H, m, pyridoindole 4-H_b^{maj} and pyridoindole 4-H_b^{min}), 2.16 – 2.10 (1H, m, CH(Me)₂^{maj}), 2.09 – 2.02 (1H, m, CH(Me)₂^{min}), 1.17 (3H, d, *J* 6.7, Me_a^{maj}), 1.15 (3H, d, *J* 6.7, Me_a^{min}), 1.02 (3H, d, *J* 6.8 Hz, Me_b^{maj}), 0.92 (3H, d, *J* 6.8 Hz, Me_b^{min}); δ_c (126 MHz, CDCl₃); 166.3 (2-C^{maj}), 165.9 (2-C^{min}), 159.3 (oxazolidinone 2-C^{min}), 159.1 (oxazolidinone 2-C^{maj}), 137.4 (phenyl 1-C^{min}), 137.4 (phenyl 1-C^{maj}), 136.0 (pyridoindole 8_a-C^{min}), 135.9 (pyridoindole 8_a-C^{maj}), 133.4 (pyridoindole 9_a-C^{maj}), 133.0 (pyridoindole 9_a-C^{min}), 129.6 (phenyl 3-C^{min} and phenyl 5-C^{min}), 129.5 (phenyl 3-C^{maj} and phenyl 5-C^{maj}), 129.4 (phenyl 4-C^{min}), 129.3 (phenyl 4-C^{maj}), 127.6 (phenyl 2-C^{min} and phenyl 6-C^{min}), 127.5 (phenyl 2-C^{maj} and phenyl 6-C^{maj}), 126.5 (pyridoindole 4_b-C^{min}), 126.5 (pyridoindole 4_b-C^{maj}), 122.3 (pyridoindole 7-C^{maj}), 122.0 (pyridoindole 7-C^{min}), 119.8 (pyridoindole 6-C^{maj}), 119.6 (pyridoindole 6-C^{min}), 118.3 (pyridoindole 5-C^{min}), 118.1 (pyridoindole 5-C^{maj}), 111.0 (pyridoindole 8-C^{maj}), 110.9 (pyridoindole 8-C^{min}), 108.0 (pyridoindole 4_a-C^{maj}), 107.9 (pyridoindole 4_a-C^{min}), 70.4 (oxazolidinone 5-C^{min}), 70.3 (oxazolidinone 5-C^{maj}), 60.3 (oxazolidinone 4-C^{min}), 60.2 (oxazolidinone 4-C^{maj}), 55.6 (pyridoindole 1-C^{maj}), 55.0 (pyridoindole 1-C^{min}), 43.3 (1-C^{maj}), 43.1 (1-C^{min}), 40.3 (pyridoindole 3-C^{min}), 40.1 (pyridoindole 3-C^{maj}), 33.2 (CH(Me)₂^{min}), 33.2 (CH(Me)₂^{maj}), 22.0 (pyridoindole 4-C^{maj}), 21.9 (pyridoindole 4-C^{min}), 20.2 (Me_a^{min}), 20.2 (Me_a^{maj}), 20.1 (Me_b^{min}), 20.0 (Me_b^{maj}); HRMS found MH⁺ 418.2141. C₂₅H₁₆N₄O₂S requires MH⁺ 418.2125. Relative stereochemistry could not be confirmed using NOESY NMR.

2-[(2Z)-3-{2-oxo-2-[1-(propan-2-yl)-1H,2H,3H,4H,9H-pyrido[3,4-b]indol-2-yl]ethyl}-2,3-dihydro-1,3-benzothiazol-2-ylidene]acetonitrile, **126**



By general procedure E using 2-diazo-1-{1-isopropyl-1H,3H,4H,9H-pyrido[3,4-b]indol-2-yl}ethenone, **S5** (0.14 g, 0.50 mmol), 2-benzothiazoleacetonitrile (0.17 g, 1.00 mmol) and $\text{Rh}_2(\text{Piv})_4$ (3.05 mg, 0.005 mmol) followed by purification by preparative LC-MS with gradient elution: 30:70 \rightarrow 95:5 MeCN–water to yield *pyridoindole* **126** (7.14 mg, 3%) as a cream amorphous solid; R_f 0.61 (50:50 EtOAc–Hexane); $\nu_{\text{max}}/\text{cm}^{-1}$ (film); 3307, 3059, 2960, 2187, 1650, 1556 and 1470; δ_{H} (501 MHz, DMSO- d_6); 10.82 (1H, s, N-H), 7.65 (1H, dd, J 7.8, 0.8, benzothiazole 7-H), 7.44 (1H, d, J 7.8, pyridoindole 5-H), 7.32 (1H, d, J 8.0, pyridoindole 8-H), 7.25 (1H, td, J 8.1, 1.2 Hz, benzothiazole 5-H), 7.10 – 7.04 (3H, m, benzothiazole 4-H, benzothiazole 6-H and pyridoindole 7-H), 7.01 – 6.97 (1H, m, pyridoindole 6-H), 5.24 (1H, br s, pyridoindole 1-H), 5.21 (1H, d, J 10.0, 1- H_a), 5.02 (1H, d, J 17.6, 1- H_b), 4.69 (1H, s, CHCN), 4.20 (1H, dd, J 14.4, 5.6, pyridoindole 3- H_a), 3.60 (1H, ddd, J 14.4, 12.1, 4.4 Hz, pyridoindole 3- H_b), 3.12 – 3.04 (1H, m, pyridoindole 4- H_a), 2.79 (1H, dd, J 15.5, 4.0, pyridoindole 4- H_b), 2.18 (1H, tt, J 13.2, 6.6, CH(Me) $_2$), 1.08 (3H, d, J 6.7, Me), 0.91 (3H, d, J 6.8, Me); δ_{C} (126 MHz, DMSO- d_6); 163.8 (2-C), 162.8 (benzothiazole 2-C), 142.4 (benzothiazole 3a-C), 136.0 (pyridoindole 8a-C), 133.6 (pyridoindole 9a-C), 126.7 (benzothiazole 5-C), 126.2 (pyridoindole 4b-C), 122.6 (benzothiazole 6-C), 122.4 (benzothiazole 7-C), 122.2 (benzothiazole 7a-C), 121.0 (pyridoindole 7-C), 120.9 (CN), 118.5 (pyridoindole 6-C), 117.7 (pyridoindole 5-C), 111.1 (pyridoindole 8-C), 110.6 (benzothiazole 4-C), 106.9 (pyridoindole 4a-C), 55.1 (pyridoindole 1-C), 54.6 (CHCN), 45.7 (1- C_a and 1- C_b), 39.6 (pyridoindole 3-C), 32.6 (CH(Me) $_2$), 21.6 (pyridoindole 4-C), 20.0 (Me), 19.6 (Me); HRMS found MH^+ 429.1753. $\text{C}_{25}\text{H}_{25}\text{N}_4\text{OS}$ requires MH^+ 428.1744.

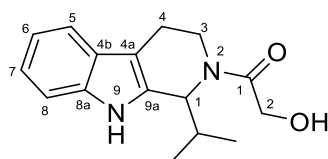
6-methoxy-2-{5-[1-(propan-2-yl)-1H,2H,3H,4H,9H-pyrido[3,4-b]indol-2-yl]-1,3-oxazol-2-yl}-1,3-benzothiazole, **127**



127

By general procedure E using 2-diazo-1-{1-isopropyl-1H,3H,4H,9H-pyrido[3,4-b]indol-2-yl}ethenone, **S5** (0.14 g, 0.50 mmol), 6-methoxy-1,3-benzothiazole-2-carbonitrile (0.19 g, 1.00 mmol) and $\text{Rh}_2(\text{Piv})_4$ (3.05 mg, 0.005 mmol) followed by purification by preparative HPLC with gradient elution: 5:95 \rightarrow 55:45 \rightarrow 75:25 \rightarrow 95:5 MeCN–water to yield *pyridoindole* **127** (0.91 mg, 1%) as a yellow oil; R_f 0.48 (90:10 EtOAc–Hexane); $\nu_{\text{max}}/\text{cm}^{-1}$ (film); 3311, 2960, 1595 and 1548; δ_{H} (501 MHz, DMSO- d_6); 10.92 (1H, s, NH), 7.95 (1H, d, J 8.9, benzothiazole 4-H), 7.68 (1H, d, J 2.7, benzothiazole 7-H), 7.41 (1H, d, J 7.9, pyridoindole 5-H), 7.34 (1H, d, J 8.1, pyridoindole 8-H), 7.13 (1H, dd, J 9.0, 2.6, benzothiazole 5-H), 7.06 (1H, td, J 6.8, 3.3, pyridoindole 7-H), 6.96 (1H, ddd, J 7.9, 7.1, 1.0, pyridoindole 6-H), 6.60 (1H, s, oxazole 4-H), 4.55 (1H, d, J 7.3, pyridoindole 1-H), 3.99 – 3.95 (1H, m, pyridoindole 3- H_a), 3.84 (3H, s, OMe), 3.66 – 3.62 (1H, m, pyridoindole 3- H_b), 3.00 – 2.91 (1H, m, pyridoindole 4- H_a), 2.74 – 2.70 (1H, m, pyridoindole 4- H_b), 2.34 – 2.24 (1H, m, $\text{CH}(\text{Me})_2$), 1.17 (3H, d, J 6.7, Me), 1.04 (3H, d, J 6.7, Me); δ_{C} (126 MHz, DMSO- d_6); 121.4 (pyridoindole 7-H), 119.0 (pyridoindole 6-H), 118.3 (oxindole 4-H), 118.1 (pyridoindole 5-H), 116.9 (benzothiazole 5-H), 111.5 (pyridoindole 8-H), 108.2 (benzothiazole 4-H), 104.9 (benzothiazole 7-H), 61.2 (pyridoindole 1-H), 55.8 (OMe), 39.6 (pyridoindole 3-H), 31.6 ($\text{CH}(\text{Me})_2$), 19.5 (Me), 18.9 (pyridoindole 4-H); HRMS found MH^+ 445.1708. $\text{C}_{25}\text{H}_{24}\text{N}_4\text{O}_2\text{S}$ requires MH^+ 445.1693. Carbon NMR determined by HSQC.

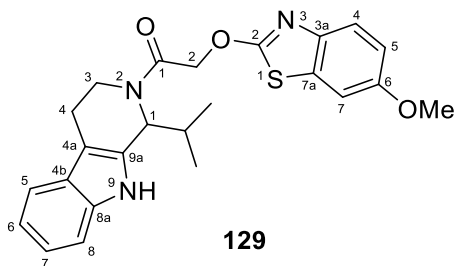
2-hydroxy-1-[1-(propan-2-yl)-1H,2H,3H,4H,9H-pyrido[3,4-b]indol-2-yl]ethan-1-one, 128



128

By general procedure E using 2-diazo-1-{1-isopropyl-1H,3H,4H,9H-pyrido[3,4-b]indol-2-yl}ethenone, **S5** (0.14 g, 0.50 mmol), 6-methoxy-1,3-benzothiazole-2-carbonitrile (0.19 g, 1.00 mmol) and $\text{Rh}_2(\text{Piv})_4$ (3.05 mg, 0.005 mmol) followed by purification by preparative HPLC with gradient elution: 5:95 \rightarrow 55:45 \rightarrow 75:25 \rightarrow 95:5 MeCN–water to yield *pyridoindole* **128** (1.72 mg, 1%) as a colourless oil; R_f 0.43 (90:10 EtOAc–Hexane); $\nu_{\text{max}}/\text{cm}^{-1}$ (film); 3466, 2901 and 1654; δ_{H} (501 MHz, CDCl_3); 7.86 (1H, s, N-H), 7.46 (1H, d, J 7.2, pyridoindole 5-H), 7.34 (1H, d, J 8.1, pyridoindole 8-H), 7.21 – 7.17 (1H, m, pyridoindole 7-H), 7.13 – 7.09 (1H, m, pyridoindole 6-H), 5.44 (1H, d, J 8.2, pyridoindole 1-H), 4.39 (1H, d, J 15.0, 2-H_a), 4.25 (1H, d, J 13.2, 2-H_b), 3.75 – 3.69 (1H, m, pyridoindole 3-H_a), 3.56 (1H, ddd, J 14.2, 10.2, 6.3, pyridoindole 3-H_b), 2.88 – 2.81 (2H, m, pyridoindole 4-H), 2.62 (1H, s, OH), 2.18 (1H, td, J 13.6, 6.8, $\text{CH}(\text{Me})_2$), 1.20 (3H, d, J 6.7, Me), 1.03 (3H, d, J 6.8, Me); δ_{C} (126 MHz, CDCl_3); 171.2 (1-C), 136.0 (pyridoindole 8_a-C), 133.1 (pyridoindole 9_a-C), 126.5 (pyridoindole 4_b-C), 122.4 (pyridoindole 7-C), 119.9 (pyridoindole 6-C), 118.2 (pyridoindole 5-C), 111.0 (pyridoindole 8-C), 108.1 (pyridoindole 4_a-C), 60.1 (2-C), 56.0 (pyridoindole 1-C), 39.1 (pyridoindole 3-C), 33.3 ($\text{CH}(\text{Me})_2$), 22.0 (pyridoindole 4-C), 20.1 (Me), 20.0 (Me); HRMS found MH^+ 273.1609. $\text{C}_{16}\text{H}_{20}\text{N}_2\text{O}_2$ requires MH^+ 273.1598.

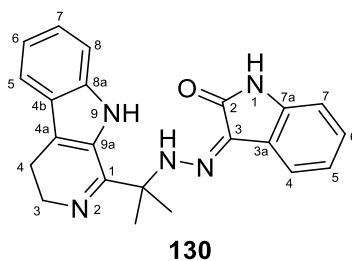
2-[(6-methoxy-1,3-benzothiazol-2-yl)oxy]-1-[1-(propan-2-yl)-1H,2H,3H,4H,9H-pyrido[3,4-b]indol-2-yl]ethan-1-one, 129



By general procedure E using 2-diazo-1-{1-isopropyl-1H,3H,4H,9H-pyrido[3,4-b]indol-2-yl}ethenone, **S5** (0.14 g, 0.50 mmol), 6-methoxy-1,3-benzothiazole-2-carbonitrile (0.19 g, 1.00 mmol) and $\text{Rh}_2(\text{Piv})_4$ (3.05 mg, 0.005 mmol) followed by purification by preparative HPLC with gradient elution: 5:95 \rightarrow 55:45 \rightarrow 75:25 \rightarrow 95:5 MeCN–water to yield *pyridoindole* **129** (2.16 mg, 1%) as a cream amorphous solid; R_f 0.17 (90:10 EtOAc–Hexane); $\nu_{\text{max}}/\text{cm}^{-1}$ (film); 3454, 2944, 2250 and 1657; δ_{H} (501 MHz, DMSO-d_6); 10.84 (1H, s, pyridoindole N-H), 7.43 (1H, d, J 7.8, pyridoindole 5-H), 7.34 –

7.30 (2H, m, benzothiazole 7-H and pyridoindole 8-H), 7.10 (1H, d, J 8.9, benzothiazole 4-H), 7.08 – 7.04 (1H, m, pyridoindole 7-H), 7.00 – 6.96 (1H, m, pyridoindole 6-H), 6.89 (1H, dd, J 8.9, 2.6, benzothiazole 5-H), 5.22 (1H, d, J 8.1, pyridoindole 1-H), 5.15 (1H, d, J 17.0, 2-H_a), 4.95 (1H, d, J 17.0, 2-H_a), 4.26 (1H, dd, J 14.4, 5.6, pyridoindole 3-H_a), 3.74 (3H, s, OMe), 3.60 (1H, ddd, J 14.5, 11.9, 4.5, pyridoindole 3-H_b), 3.02 – 2.94 (1H, m, pyridoindole 4-H_a), 2.80 (1H, dd, J 15.5, 4.2, pyridoindole 4-H_b), 2.21 – 2.15 (1H, m, CH(Me)₂), 1.08 (3H, d, J 6.7, Me), 0.90 (3H, d, J 6.8, Me); δ_c (126 MHz, DMSO-d₆); 168.9 (1-C), 164.8 (benzothiazole 2-C), 155.6 (benzothiazole 6-C), 135.9 (pyridoindole 8_a-C), 133.7 (pyridoindole 9_a-C), 131.3 (benzothiazole 3_a-C), 126.2 (pyridoindole 4_b-C), 122.1 (benzothiazole 7_a-C), 121.0 (pyridoindole 7-C), 118.5 (pyridoindole 6-C), 117.7 (pyridoindole 5-C), 113.1 (benzothiazole 5-C), 112.1 (benzothiazole 4-C), 111.1 (pyridoindole 8-C), 108.0 (benzothiazole 7-C), 106.7 (pyridoindole 4_a-C), 55.7 (OMe), 54.6 (pyridoindole 1-C), 43.8 (2-C), 40.1 (pyridoindole 3-C), 32.4 (CH(Me)₂), 21.6 (pyridoindole 4-C), 19.9 (Me), 19.7 (Me); HRMS found MH^+ 436.1707. C₂₄H₂₅N₃O₃S requires MH^+ 436.1689.

(3Z)-3-[2-(2-{3H,4H,9H-pyrido[3,4-b]indol-1-yl}propan-2-yl)hydrazin-1-ylidene]-2,3-dihydro-1H-indol-2-one, 130



By general procedure E using, 3-(λ⁵-diazynylidene)-1H-indol-2-one, **S2** (0.16 g, 0.98 mmol) and 1-isopropyl-2,3,4,9-tetrahydro-1H-β-carboline (0.47 g, 1.96 mmol) and Rh₂(Piv)₄ (5.98 mg, 0.01 mmol) followed purification by preparative LC-MS with gradient elution: 30:70 → 95:5 MeCN–water to yield *pyridoindole* **130** (7.18 mg, 2%) as a yellow oil; R_f 0.36 (50:50 EtOAc–hexane); ν_{max}/cm^{-1} (film); 3345, 2955, 2852, 1733, 1680, 1619 and 1491; δ_H (501 MHz, CDCl₃); 10.99 (1H, s, hydrazone N-H), 9.07 (1H, s, pyridoindole N-H), 7.86 (1H, s, oxindole N-H), 7.59 (1H, d, J 8.1, pyridoindole 5-H), 7.53 (1H, d, J 7.6, oxindole 4-H), 7.33 (1H, dt, J 8.3, 0.8, pyridoindole 8-H), 7.25 (1H, ddd, J 8.1, 6.9, 1.0, pyridoindole 7-H), 7.21 (1H, td, J 7.7, 1.2, oxindole 6-H), 7.14 – 7.10 (1H, m,

pyridoindole 6-H), 7.08 (1H, td, *J* 7.6, 0.9, oxindole 5-H), 6.88 (1H, d, *J* 7.8, oxindole 7-H), 3.98 (2H, t, *J* 8.3, indole 3-H), 2.91 (2H, t, *J* 8.5, indole 4-H), 1.74 (6H, s, (CH₃)₂); δ_c (126 MHz, CDCl₃); 163.3 (pyridoindole 1-C), 163.3 (oxindole 2-C), 138.0 (oxindole 7_a-C), 136.9 (pyridoindole 8_a-C), 128.3 (oxindole 6-C), 127.8 (oxindole 3-C), 126.8 (pyridoindole 9_a-C), 125.2 (pyridoindole 4_b-C), 125.0 (pyridoindole 7-C), 122.8 (oxindole 5-C), 122.0 (oxindole 3_a-C), 120.5 (pyridoindole 6-C), 120.1 (pyridoindole 5-C), 119.7 (pyridoindole 4_a-C), 118.9 (oxindole 4-C), 112.3 (pyridoindole 8-C), 110.4 (oxindole 7-C), 63.7 (C(CH₃)₂), 48.0 (indole 3-C), 26.2 ((CH₃)₂), 19.3 (indole 4-C); HRMS found *MH*⁺ 372.1830. C₂₂H₂₂N₅O₂ requires *MH*⁺ 372.1819.

5.2.4 X-Ray Structures

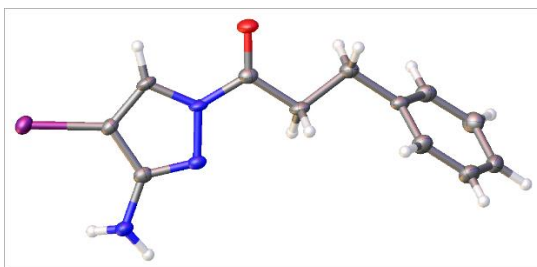


Figure S1: ORTEP diagram of S9 (Chapter 2), CCDC 1991665

Crystal data and structure refinement for S9	
Empirical formula	C ₁₂ H ₁₂ IN ₃ O
Formula Weight	341.15
Temperature/K	120.00(10)
Crystal system	triclinic
Space group	P-1
a/Å	4.1678(4)
b/Å	10.6544(9)
c/Å	14.6694(12)
α/°	73.012(7)
β/°	84.892(7)
γ/°	78.774(8)
Volume/Å ³	610.70(10)
Z	2
ρ _{calc} /cm ³	1.855
μ/mm ⁻¹	20.504
F(000)	332.0
Crystal size/mm ³	0.22 × 0.11 × 0.07
Radiation	CuKα (λ = 1.54184)
2θ range for data collection/°	8.818 to 146.602
Index ranges	-3 ≤ h ≤ 4, -11 ≤ k ≤ 13, -18 ≤ l ≤ 17
Reflections collected	3920
Independent reflections	2275 [R _{int} = 0.0278, R _{sigma} = 0.0360]
Data/restraints/parameters	2275/0/162
Goodness-of-fit on F ²	1.093
Final R indexes [I > 2σ (I)]	R ₁ = 0.0329, wR ₂ = 0.0868
Final R indexes [all data]	R ₁ = 0.0337, wR ₂ = 0.0880
Largest diff. peak/hole / e Å ⁻³	1.31/-1.17

5.3 Biology

5.3.1 Cell Lines and Media

Mueller-Hinton Agar II (MHA-II): A stock solution of MHA-II was prepared from MHA-II powder (19 g, BD™BBL™) and purified water (500 mL).

Iso-Sensitest Broth (ISB): A 1000 mL stock solution of ISB was prepared from ISB Powder (23 g, Oxoid) and purified water (1000 mL).

Cation-adjusted Mueller Hinton Broth (MHB-II): A 1000 mL stock solution of MHBII was prepared from MHB-II Powder (22 g, Sigma Aldrich) and purified water (1000 mL).

***S. aureus* strains in ISB:** A glycerol stock of either ATCC29213, SH1000 or USA300 JE2 was streaked onto MHA-II agar and incubated at 37 °C for 18 h. An individual colony (using a Sarstedt inoculation loop, 1 µL) was suspended in ISB (5 mL) and incubated at 37 °C for 24 h.

***S. aureus* strains in MHB-II:** A glycerol stock of either ATCC29213 or SH1000 was streaked onto MHA-II agar and incubated at 37 °C for 18 h. An individual colony (using a Sarstedt inoculation loop, 1 µL) was suspended in MHB-II (5 mL) and incubated at 37 °C for 18 h.

ESKAPE strains in MHB-II: A glycerol stock of either *S. aureus* strains SH1000¹⁰⁸ and ATCC29213;¹⁰⁷ *K. pneumoniae* strain ATCC700603;¹⁷⁷ *A. baumannii* strain ATCC19606;¹⁷⁸ *P. aeruginosa* strain PA01,¹⁷⁹ *E. cloacae* strain 051255 and *E. coli* strain BW25113 (*E. coli*)¹⁸⁰ was streaked onto MHA-II agar and incubated at 37 °C for 18 h. An individual colony (using a Sarstedt inoculation loop, 1 µL) was suspended in MHB-II (5 mL) and incubated at 37 °C for 18 h.

5.3.2 General Procedures

5.3.2.1 Evaluating the Antibacterial Activity of Quinazolinones

Minimum inhibitory concentration (MIC) values for selected compounds were determined by broth microdilution against *S. aureus* strains SH1000,¹⁰⁸ ATCC29213¹⁰⁷

and USA300 JE2,¹⁰⁹ according to CLSI guidelines for low solubility compounds except for using Iso-Sensitest Broth (ISB) in place of cation-adjusted Mueller-Hinton Broth (MHB-II).¹⁰⁶

A 2-fold dilution series of the isolated compounds in DMSO was prepared, ranging from 1600–1.6 $\mu\text{g mL}^{-1}$. Each dilution was transferred into a 96-well format at a final volume of 1 μL and 99 μL of the standardised culture was added to each well to give final antibiotic concentrations of 16–0.016 $\mu\text{g mL}^{-1}$ (1% DMSO in ISB). Plates were incubated for 16 h at 37 °C (Inkubator 1000, Heidolph) and the minimum inhibitory concentration (MIC) was determined visually as the lowest concentration at which growth was inhibited. Higher concentration ranges (128–0.128 $\mu\text{g mL}^{-1}$) were used for MIC determinations where no growth inhibition was observed at concentrations up to 16 $\mu\text{g mL}^{-1}$.

5.3.2.2 Screening of Crude Carbonylation Array Mixtures against ATCC29213

Reaction wells were diluted in ISB containing the standardised culture to ensure each screening well contained 1% DMSO and a final total product concentration of 50 μM . Plates were incubated for 10 h at 37 °C (Inkubator 1000, Heidolph) using a growth control (antibacterial free); the optical density was measured using a plate reader (FLUOstar Omega, BMG Labtech, $\lambda = 600 \text{ nm}$). The selection of the incubation time (10 h) was chosen because the control culture reached saturation at that point.

5.3.2.3 Screening of Crude α -Diazo Amide Array Mixtures against ATCC29213

Reaction wells were initially diluted 10-fold in water followed by a further 10-fold dilution in MHB-II containing the standardised culture to ensure each screening well contained 1% DMSO and a final total product concentration of 100 μM . Plates were incubated for 16 h at 37 °C (Inkubator 1000, Heidolph) using a growth control (antibacterial free); the optical density was measured using a plate reader (FLUOstar Omega, BMG Labtech, $\lambda = 600 \text{ nm}$).

5.3.2.4 Evaluating Antibacterial Activity of Isolated compounds from α -Diazo Amide Array

Minimum inhibitory concentration (MIC) values for selected compounds were determined by broth microdilution against *S. aureus* strains SH1000¹⁰⁸ and ATCC29213¹⁰⁷ according to CLSI guidelines.¹⁰⁶

A 2-fold dilution series of the isolated compounds in DMSO was prepared, ranging from 6400–6.25 $\mu\text{g mL}^{-1}$. Each dilution was transferred into a 96-well format at a final volume of 10 μL and 90 μL of water was added to each well to give stock concentrations of 640–0.625 $\mu\text{g mL}^{-1}$ (10% DMSO in water). Stock solutions were diluted to a final volume of 10 μL and 90 μL of the standardised culture was added to each well to give final product concentrations of 64–0.063 $\mu\text{g mL}^{-1}$ (1% DMSO in MHB-II). Plates were incubated for 16 h at 37 °C (Inkubator 1000, Heidolph) and the minimum inhibitory concentration (MIC) was determined visually as the lowest concentration at which growth was inhibited.

5.3.2.5 Assessing Eukaryotic Activity against HeLa cells

This screen was performed by Jack White. A 2-fold dilution series of the isolated compounds in DMSO was prepared, usually ranging from 6400–6.25 $\mu\text{g mL}^{-1}$. HeLa cells (2×10^4 cells mL^{-1}) were prepared and diluted with medium (Dulbecco's Modified Eagle Medium (DMEM) with 4.5 g L^{-1} glucose, 10% fetal bovine serum (FBS), 1% penicillin/streptomycin and without L-Glutamine) into a 96-well flat plate to obtain a concentration of 4000 cells per well. Plates were incubated (37 °C, 5% CO_2) for 24 hours. The medium was removed from the incubated cells and stock solutions of each compound (1 μL), dissolved in medium (99 μL) were added to give a dilution series with a final DMSO concentration of 1% and a total volume of 100 μL . All compounds were tested in triplicate. Plates were incubated (37 °C, 5% CO_2) for 48 h. To each well, MTT solution (20 μL , 5 mg mL^{-1} in PBS buffer) was added, and the plate was shaken (5 mins, 300 rpm). Plates were incubated for a further 4 h (37 °C, 5% CO_2) and the medium was removed. Each well was redissolved in DMSO (200 μL), shaken (5 mins, 300 rpm) and the optical density was measured at 570 nm to determine cell viability. Wells containing only 1% DMSO without compound were used as a 100% growth control and wells containing doxorubicin were used as a positive control.

5.3.2.6 Evaluating Antibacterial Activity against an ESKAPE Panel

Minimum inhibitory concentration (MIC) values for selected compounds were determined by broth microdilution against *S. aureus* strains SH1000¹⁰⁸ and ATCC29213;¹⁰⁷ *K. pneumoniae* strain ATCC700603;¹⁷⁷ *A. baumannii* stain ATCC19606;¹⁷⁸ *P. aeruginosa* strain PA01,¹⁷⁹ *E. cloacae* strain 051255 and *E. coli* strain BW25113 (*E. coli*)¹⁸⁰ according to CLSI guidelines.¹⁰⁶ Plates were prepared as described previously (Section 5.3.2.4) for all the strains listed within this section.

6 List of References

- 1 J. P. Hughes, S. S. Rees, S. B. Kalindjian and K. L. Philpott, *Br. J. Pharmacol.*, 2011, **162**, 1239–1249.
- 2 G. Karageorgis, M. Dow, A. Aimon, S. Warriner and A. Nelson, *Angew. Chemie - Int. Ed.*, 2015, **127**, 13742–13748.
- 3 S. M. Paul, D. S. Mytelka, C. T. Dunwiddie, C. C. Persinger, B. H. Munos, S. R. Lindborg and A. L. Schacht, *Nat. Rev. Drug Discov.*, 2010, **9**, 203–214.
- 4 S. Boyer, C. Brealey and A. M. Davis, in *Attrition in the Pharmaceutical Industry: Reasons, Implications, and Pathways Forward*, Wiley Blackwell, New Jersey, 2015.
- 5 R. W. Peck, D. W. Lendrem, I. Grant, B. C. Lendrem and J. D. Isaacs, *Nat. Rev. Drug Discov.*, 2015, **14**, 663–664.
- 6 I. Kola and J. Landis, *Nat. Rev. Drug Discov.*, 2004, **3**, 711–715.
- 7 S. Fox, S. Farr-Jones, L. Sopchak, A. Boggs, H. W. Nicely, R. Khoury and M. Biros, *J. Biomol. Screen.*, 2006, **11**, 864–869.
- 8 I. B. Campbell, S. J. F. Macdonald and P. A. Procopiou, *Drug Discov. Today*, 2018, **23**, 219–234.
- 9 A. Baxter, C. Bennion, J. Bent, K. Boden, S. Brough, A. Cooper, E. Kinchin, N. Kindon, T. McNally, M. Mortimore, B. Roberts and J. Unitt, *Bioorganic Med. Chem. Lett.*, 2003, **13**, 2625–2628.
- 10 H. Dowden and J. Munro, *Nat. Rev. Drug Discov.*, 2019, **18**, 495–496.
- 11 B. G. de la Torre and F. Albericio, *Molecules*, 2019, **24**, 809.
- 12 Novel Drug Approvals for 2020 | FDA, <https://www.fda.gov/drugs/new-drugs-fda-cders-new-molecular-entities-and-new-therapeutic-biological-products/novel-drug-approvals-2020>, (accessed 22 April 2020).
- 13 Novel Drug Approvals for 2019 | FDA, <https://www.fda.gov/drugs/new-drugs-fda-cders-new-molecular-entities-and-new-therapeutic-biological-products/novel-drug-approvals-2019>, (accessed 22 April 2020).
- 14 B. G. de la Torre and F. Albericio, *Molecules*, 2020, **25**, 1–13.
- 15 B. G. de la Torre and F. Albericio, *Molecules*, 2021, **26**, 1–14.
- 16 C. Lipinski and A. Hopkins, *Nature*, 2004, **432**, 855–861.
- 17 A. H. Lipkus, Q. Yuan, K. A. Lucas, S. A. Funk, W. F. Bartelt, R. J. Schenck, A. J. Trippe, W. F. B. Iii, R. J. Schenck and A. J. Trippe, *J. Org. Chem.*, 2008, **5**, 4443–4451.
- 18 S. D. Roughley and A. M. Jordan, *J. Med. Chem.*, 2011, **54**, 3451–3479.
- 19 T. W. J. Cooper, I. B. Campbell and S. J. F. MacDonald, *Angew. Chemie - Int. Ed.*, 2010, **49**, 8082–8091.
- 20 D. G. Brown and J. Boström, *J. Med. Chem.*, 2016, **59**, 4443–4458.

- 21 N. Schneider, D. M. Lowe, R. A. Sayle, M. A. Tarselli and G. A. Landrum, *J. Med. Chem.*, 2016, **59**, 4385–4402.
- 22 W. P. Walters, J. Green, J. R. Weiss and M. A. Murcko, *J. Med. Chem.*, 2011, **54**, 6405–6416.
- 23 A. L. Harvey, *Drug Discov. Today*, 2008, **13**, 894–901.
- 24 P. Ertl, S. Roggo and A. Schuffenhauer, *J. Chem. Inf. Model.*, 2008, **48**, 68–74.
- 25 K. V. Jayaseelan, P. Moreno, A. Truszkowski, P. Ertl and C. Steinbeck, *BMC Bioinformatics*, 2012, **13**, 1–6.
- 26 B. David, J. L. Wolfender and D. A. Dias, *Phytochem. Rev.*, 2015, **14**, 299–315.
- 27 P. M. Dewick, *Medicinal natural products : A Biosynthetic Approach 3rd Edition*, John Wiley & Sons, Ltd, Chichester, 2009.
- 28 B. B. Mishra and V. K. Tiwari, *Eur. J. Med. Chem.*, 2011, **46**, 4769–4807.
- 29 D. J. Newman and G. M. Cragg, *J. Nat. Prod.*, 2016, **79**, 629–661.
- 30 R. Verpoorte, Y. H. Choi and H. K. Kim, *J. Ethnopharmacol.*, 2005, **100**, 53–56.
- 31 M. S. Butler, A. A. B. Robertson and M. A. Cooper, *Nat. Prod. Rep.*, 2014, **31**, 1612–1661.
- 32 S. Wetzels, R. S. Bon, K. Kumar and H. Waldmann, *Angew. Chemie Int. Ed.*, 2011, **50**, 10800–10826.
- 33 S. L. Schreiber, *Nat. Chem. Biol.*, 2005, **1**, 64–66.
- 34 R. S. Bon and H. Waldmann, *Acc. Chem. Res.*, 2010, **43**, 1103–1114.
- 35 C. M. Dobson, *Nature*, 2004, **432**, 824–828.
- 36 H. Van Hattum and H. Waldmann, *J. Am. Chem. Soc.*, 2014, **136**, 11853–11859.
- 37 M. A. Koch, A. Schuffenhauer, M. Scheck, S. Wetzels, M. Casaulta, A. Odermatt, P. Ertl and H. Waldmann, *Proc. Natl. Acad. Sci. U. S. A.*, 2005, **102**, 17272–17277.
- 38 M. A. Koch, L. O. Wittenberg, S. Basu, D. A. Jeyaraj, E. Gourzoulidou, K. Reinecke, A. Odermatt and H. Waldmann, *Proc. Natl. Acad. Sci. U. S. A.*, 2004, **101**, 16721–16726.
- 39 A. Nören-Müller, I. Reis-Corrêa, H. Prinz, C. Rosenbaum, K. Saxena, H. J. Schwalbe, D. Vestweber, G. Cagna, S. Schunk, O. Schwarz, H. Schiewe and H. Waldmann, *Proc. Natl. Acad. Sci. U. S. A.*, 2006, **103**, 10606–10611.
- 40 R. Breinbauer, I. R. Vetter and H. Waldmann, *Angew. Chemie Int. Ed.*, 2002, **41**, 2878–2890.
- 41 I. R. Correa, A. Nören-Müller, H.-D. Ambrosi, S. Jakupovic, K. Saxena, H. Schwalbe, M. Kaiser and H. Waldmann, *Chem. - An Asian J.*, 2007, **2**, 1109–1126.
- 42 K. Kumar and H. Waldmann, *Angew. Chemie - Int. Ed.*, 2009, **48**, 3224–3242.
- 43 T. Leßmann, M. G. Leuenberger, S. Menninger, M. Lopez-Canet, O. Müller, S. Hümmer, J. Bormann, K. Korn, E. Fava, M. Zerial, T. U. U. Mayer and H. Waldmann, *Chem. Biol.*, 2007, **14**, 443–451.

- 44 F. J. Dekker, O. Rocks, N. Vartak, S. Menninger, C. Hedberg, R. Balamurugan, S. Wetzel, S. Renner, M. Gerauer, B. Schölermann, M. Rusch, J. W. Kramer, D. Rauh, G. W. Coates, L. Brunsveld, P. I. H Bastiaens and H. Waldmann, *Nat. Chem. Biol.*, 2010, **6**, 449–456.
- 45 T. Knoth, K. Warburg, C. Katzka, A. Rai, A. Wolf, A. Brockmeyer, P. Janning, T. F. Reubold, S. Eschenburg, D. J. Manstein, K. Hübel, M. Kaiser, H. Waldmann, T. Knoth, D.-B. K. Warburg, C. Katzka, A. Wolf, D.-I. A. Brockmeyer, P. Janning, K. Hübel, H. Waldmann, T. F. Reubold, S. Eschenburg, A. Rai, D. J. Manstein and M. Kaiser, *Angew. Chemie*, 2009, **121**, 7376–7381.
- 46 G. Karageorgis, S. Warriner and A. Nelson, *Nat. Chem.*, 2014, **6**, 872–876.
- 47 A. Green, F. Hobor, C. Tinworth, S. Warriner, A. Wilson and A. Nelson, *Chem. – A Eur. J.*, 2020, **26**, 10682–10689.
- 48 F. Von Nussbaum, M. Brands, B. Hinzen, S. Weigand and D. Häbich, *Angew. Chemie - Int. Ed.*, 2006, **45**, 5072–5129.
- 49 S. Rachakonda and L. Cartee, *Curr. Med. Chem.*, 2004, **11**, 775–793.
- 50 J. N. Steenbergen, J. Alder, G. M. Thorne and F. P. Tally, *J. Antimicrob. Chemother.*, 2005, **55**, 283–288.
- 51 T. J. Louie, M. A. Miller, K. M. Mullane, K. Weiss, A. Lentnek, Y. Golan, S. Gorbach, P. Sears, Y. Shue and OPT-80-003 Clinical Study Group, *N. Engl. J. Med.*, 2011, **364**, 422–431.
- 52 A. Koul, N. Dendouga, K. Vergauwen, B. Molenberghs, L. Vranckx, R. Willebrords, Z. Ristic, H. Lill, I. Dorange, J. Guillemont, D. Bald and K. Andries, *Nat. Chem. Biol.*, 2007, **3**, 323–324.
- 53 W. Balemans, L. Vranckx, N. Lounis, O. Pop, J. Guillemont, K. Vergauwen, S. Mol, R. Gilissen, M. Motte, D. Lançois, M. De Bolle, K. Bonroy, H. Lill, K. Andries, D. Bald and A. Koul, *Antimicrob. Agents Chemother.*, 2012, **56**, 4131–4139.
- 54 S. Schwarz, A. Loeffler and K. Kadlec, *Vet. Dermatol.*, 2016, **28**, 82.
- 55 R. J. Fair and Y. Tor, *Perspect. Medicin. Chem.*, 2014, **28**, 25–64.
- 56 F. M. Walsh and S. G. B. Amyes, *Curr. Opin. Microbiol.*, 2004, **7**, 439–444.
- 57 F. Cohn, *Studies on bacteria*, ASM Press, Washington, DC, 1999.
- 58 C. R. H. Raetz and C. Whitfield, *Annu. Rev. Biochem.*, 2002, **71**, 635–700.
- 59 S. G. Wilkinson, *Prog. Lipid Res.*, 1996, **35**, 283–343.
- 60 M. F. Richter and P. J. Hergenrother, *Ann. N. Y. Acad. Sci.*, 2019, **1435**, 18–38.
- 61 H. Nikaido, *Microbiol. Mol. Biol. Rev.*, 2003, **67**, 593–656.
- 62 M. Vaara and T. Vaara, *Antimicrob. Agents Chemother.*, 1983, **24**, 114–122.
- 63 R. E. W. Hancock, T. Falla and M. Brown, *Adv. Microb. Physiol.*, 1995, **37**, 135–175.
- 64 J. S. Chapman and N. H. Georgopapdakou, *Antimicrob. Agents Chemother.*, 1988, **32**, 438–442.
- 65 J. Sun, Z. Deng and A. Yan, *Biochem. Biophys. Res. Commun.*, 2014, **453**, 254–267.

- 66 T. J. Silhavy, D. Kahne and S. Walker, *Cold Spring Harb. Perspect. Biol.*, 2010, 2, 1–16.
- 67 K. Lewis, *Nat. Rev. Drug Discov.*, 2013, 12, 371–387.
- 68 H. D. Marston, D. M. Dixon, J. M. Knisely, T. N. Palmore and A. S. Fauci, *J. Am. Med. Assoc.*, 2016, **316**, 1193–1204.
- 69 L. Pray, *Nat. Educ.*, 2008, **1**, 30.
- 70 W. Zheng, N. Thorne and J. C. McKew, *Drug Discov. Today*, 2013, 18, 1067–1073.
- 71 M. A. Farha and E. D. Brown, *Nat. Prod. Rep.*, 2016, 33, 668–680.
- 72 A. M. Slee, M. A. Wuonola, R. J. McRipley, I. Zajac, M. J. Zawada, P. T. Bartholomew, W. A. Gregory and M. Forbes, *Antimicrob. Agents Chemother.*, 1987, **31**, 1791–1797.
- 73 K. L. Leach, S. J. Brickner, M. C. Noe and P. F. Miller, *Ann. N. Y. Acad. Sci.*, 2011, **1222**, 49–54.
- 74 S. J. Brickner, D. K. Hutchinson, M. R. Barbachyn, P. R. Manninen, D. A. Ulanowicz, S. A. Garmon, K. C. Grega, S. K. Hendges, D. S. Toops, C. W. Ford and G. E. Zurenko, *J. Med. Chem.*, 1996, **39**, 673–679.
- 75 C. Edlund, H. Oh and C. E. Nord, *Clin. Microbiol. Infect.*, 1999, **5**, 51–53.
- 76 M. J. Rybak, D. M. Cappelletty, T. Moldovan, J. R. Aeschlimann and G. W. Kaatz, *Antimicrob. Agents Chemother.*, 1998, **42**, 721–724.
- 77 Y. Qian, G. Allegretta, J. Janardhanan, Z. Peng, K. V. Mahasenan, E. Lastochkin, M. M. N. Gozun, S. Tejera, V. A. Schroeder, W. R. Wolter, R. Feltzer, S. Mobashery and M. Chang, *J. Med. Chem.*, 2020, **63**, 5287–5296.
- 78 R. Bouley, D. Ding, Z. Peng, M. Bastian, E. Lastochkin, W. Song, M. A. Suckow, V. A. Schroeder, W. R. Wolter, S. Mobashery and M. Chang, *J. Med. Chem.*, 2016, **59**, 5011–5021.
- 79 S. Gatadi, J. Gour, M. Shukla, G. Kaul, S. das, A. Dasgupta, Y. V. Madhavi, S. Chopra and S. Nanduri, *Bioorg. Chem.*, 2019, **83**, 569–579.
- 80 S. Gatadi, J. Gour, G. Kaul, M. Shukla, A. Dasgupta, R. Akunuri, R. Tripathi, Y. V. Madhavi, S. Chopra and S. Nanduri, *Bioorg. Chem.*, 2018, **81**, 175–183.
- 81 M. A. Al-Omar, S. G. Abdel-Hamide, H. A. Al-Khamees and H. I. El-Subbagh, *Saudi Pharm. J.*, 2004, **12**, 63–71.
- 82 S. El-Meligie, A. K. El-Ansary, M. M. Said and M. M. M. Hussein, *Indian J. Chem. - Sect. B Org. Med. Chem.*, 2001, **40**, 62–69.
- 83 D. J. Payne, M. N. Gwynn, D. J. Holmes and D. L. Pompliano, *Nat. Rev. Drug Discov.*, 2007, 6, 29–40.
- 84 C. Lazennec and T. Meinnel, *Anal. Biochem.*, 1997, **244**, 180–182.
- 85 R. J. Heath and C. O. Rock, *J. Biol. Chem.*, 1995, **270**, 26538–26542.
- 86 R. J. Heath and C. O. Rock, *J. Biol. Chem.*, 1996, **271**, 10996–11000.
- 87 C. V. Dang, D. C. H. Yang and T. D. Pollard, *J. Cell Biol.*, 1983, **96**, 1138–1147.

- 88 M. Yarus, *Proc. Natl. Acad. Sci. U. S. A.*, 1972, **69**, 1915–1919.
- 89 B. C. Stark, R. Kole, E. J. Bowman and S. Altman, *Proc. Natl. Acad. Sci. U. S. A.*, 1978, **75**, 3717–3721.
- 90 M. F. Richter, B. S. Drown, A. P. Riley, A. Garcia, T. Shirai, R. L. Svec and P. J. Hergenrother, *Nature*, 2017, **545**, 299–304.
- 91 V. J. Savage, C. Dric Charrier, A.-M. Salisbury, E. Moyo, H. Forward, N. Chaffer-Malam, R. Metzger, A. Huxley, R. Kirk, M. Uosis-Martin, G. Noonan, S. Mohmed, S. A. Best, A. J. Ratcliffe and N. R. Stokes, *J. Antimicrob. Chemother.*, 2016, **71**, 1905–1913.
- 92 K. Takrouri, H. D. Cooper, A. Spaulding, P. Zucchi, B. Koleva, D. C. Cleary, W. Tear, P. J. Beuning, E. B. Hirsch and J. B. Aggen, *ACS Infect. Dis.*, 2016, **2**, 405–426.
- 93 S. E. Motika, R. J. Ulrich, E. J. Geddes, H. Y. Lee, G. W. Lau and P. J. Hergenrother, *J. Am. Chem. Soc.*, 2020, **142**, 10856–10862.
- 94 E. N. Parker, B. S. Drown, E. J. Geddes, H. Y. Lee, N. Ismail, G. W. Lau and P. J. Hergenrother, *Nat. Microbiol.*, 2020, **5**, 67–75.
- 95 Penicillins - Infectious Disease and Antimicrobial Agents, <http://antimicrobe.org/d24.asp>, (accessed 1 May 2020).
- 96 M. Lobanovska and G. Pilla, *Yale J. Biol. Med.*, 2017, **90**, 135–145.
- 97 A. Leggott, J. E. Clarke, S. Chow, S. L. Warriner, A. J. O'Neill and A. Nelson, *Chem. Commun.*, 2020, **56**, 8047–8050.
- 98 A. Biffis, P. Centomo, A. Del Zotto and M. Zecca, *Chem. Rev.*, 2018, **118**, 2249–2295.
- 99 J. B. Peng, H. Q. Geng, W. Wang, X. Qi, J. Ying and X. F. Wu, *J. Catal.*, 2018, **365**, 10–13.
- 100 J. Schranck, A. Tlili, P. G. Alsabeh, H. Neumann, M. Stradiotto and M. Beller, *Chem. - A Eur. J.*, 2013, **19**, 12624–12628.
- 101 L. He, M. Sharif, H. Neumann, M. Beller and X. F. Wu, *Green Chem.*, 2014, **16**, 3763–3767.
- 102 C. Larksarp and H. Alper, *J. Org. Chem.*, 2000, **65**, 2773–2777.
- 103 C. F. J. Barnard, *Organometallics*, 2008, **27**, 5402–5422.
- 104 I. P. Beletskaya and A. V. Cheprakov, *Chem. Rev.*, 2000, **100**, 3009–3066.
- 105 M. M. Heravi, Z. Kheilkordi, V. Zadsirjan, M. Heydari and M. Malmir, *J. Organomet. Chem.*, 2018, **861**, 17–104.
- 106 CLSI, *Methods for Dilution Antimicrobial Susceptibility Tests for Bacteria That Grow Aerobically. Ninth Edition*, Clinical and Laboratory Standards Institute, Wayne, PA, 2012.
- 107 I. Soni, H. Chakrapani and S. Chopra, *Genome Announc.*, 2015, **3**, 1.
- 108 A. J. O'Neill, *Lett. Appl. Microbiol.*, 2010, **51**, 358–361.

- 109 B. A. Diep, S. R. Gill, R. F. Chang, T. H. Van Phan, J. H. Chen, M. G. Davidson, F. Lin, J. Lin, H. A. Carleton, E. F. Mongodin, G. F. Sensabaugh and F. Perdreau-Remington, *Lancet*, 2006, **367**, 731–739.
- 110 W. A. Warr, *J. Comput. Aided. Mol. Des.*, 2012, **26**, 801–804.
- 111 C. Gimbert and A. Vallribera, *Org. Lett.*, 2009, **11**, 269–271.
- 112 D. H. O' Donovan, P. Aillard, M. Berger, A. de la Torre, D. Petkova, C. Knittl-Frank, D. Geerdink, M. Kaiser and N. Maulide, *Angew. Chemie Int. Ed.*, 2018, **57**, 10737–10741.
- 113 X. Zhang and Z. Sui, *Tetrahedron Lett.*, 2006, **47**, 5953–5955.
- 114 P. Livant, Y. Jie and X. Wang, *Tetrahedron Lett.*, 2005, **46**, 2113–2116.
- 115 A. Ford, H. Miel, A. Ring, C. N. Slattery, A. R. Maguire and M. A. McKervey, *Chem. Rev.*, 2015, **115**, 9981–10080.
- 116 K. Wang, Z. Liu, G. Xu, Y. Shao, S. Tang, P. Chen, X. Zhang and J. Sun, *Angew. Chemie Int. Ed.*, 2021, **60**, 16942–16946.
- 117 X. He, Y. Wu, T. Zhou, Y. Zuo, M. Xie, R. Li, J. Duan and Y. Shang, *Synth. Commun.*, 2020, **50**, 2685–2697.
- 118 J. Gong, G. Lin, W. Sun, C.-C. Li and Z. Yang, *J. Am. Chem. Soc.*, 2010, **132**, 16745–16746.
- 119 Y. Wang, Y. Zhu, Z. Chen, A. Mi, W. Hu and M. Doyle, *Org. Lett.*, 2003, **5**, 3923–3926.
- 120 B. Alcaide, P. Almendros, C. Aragoncillo, R. Callejo, M. Ruiz and M. Torres, *J. Org. Chem.*, 2009, **74**, 8421–8424.
- 121 H. M. L. Davies, J. Qihui, P. Ren and A. Y. Kovalevsky, *J. Org. Chem.*, 2002, **67**, 4165–4169.
- 122 H. M. L. Davies and C. Venkataramani, *Angew. Chem. Int. Ed.*, 2002, **41**, 2197–2199.
- 123 H. M. L. Davies and T. Hansen, *J. Am. Chem. Soc.*, 1997, **119**, 9075–9076.
- 124 S. Sengupta and D. Sen Sarma, *Tetrahedron Lett.*, 2001, **42**, 485–487.
- 125 M. Anthony McKervey and P. Ratananukul, *Tetrahedron Lett.*, 1982, **23**, 2509–2512.
- 126 G. K. Tranmer and A. Capretta, *Tetrahedron*, 1998, **54**, 15499–15508.
- 127 P. Manitto, D. Monti, S. Zanzola and G. Speranza, *Chem. Commun.*, 1999, 543–544.
- 128 C. A. Merlic, A. L. Zechman and M. M. Miller, *J. Am. Chem. Soc.*, 2001, **123**, 11101–11102.
- 129 R. R. Nani and S. E. Reisman, *J. Am. Chem. Soc.*, 2013, **135**, 7304–7311.
- 130 E. M. D. Allouche and A. B. Charette, *Synthesis (Stuttg.)*, 2019, **51**, 3947–3963.
- 131 T. O. Zanakhov, E. E. Galenko, M. A. Kryukova, M. S. Novikov and A. A.

- Khlebnikov, *Molecules*, 2021, **26**, 1881.
- 132 P. A. A. Sakharov, M. S. Novikov and A. F. Khlebnikov, *J. Org. Chem.*, 2018, **83**, 8304–8314.
- 133 D. V. Kumar, R. Rai, K. A. Brameld, J. Riggs, J. R. Somoza, R. Rajagopalan, J. W. Janc, Y. M. Xia, T. L. Ton, H. Hu, I. Lehoux, J. D. Ho, W. B. Young, B. Hart and M. J. Green, *Bioorg. Med. Chem. Lett.*, 2012, **22**, 300–304.
- 134 G. Karageorgis, S. Liver and A. Nelson, *ChemMedChem*, 2020, **15**, 1776–1782.
- 135 S. Chow, A. I. Green, C. Arter, S. Liver, A. Leggott, L. Trask, G. Karageorgis, S. Warriner and A. Nelson, *Synth.*, 2020, **52**, 1695–1706.
- 136 L. Marek, L. Kolman, J. Váňa, J. Svoboda and J. Hanusek, *Beilstein J. Org. Chem.*, 2021, **17**, 527–539.
- 137 C. Hepples and G. K. Murphy, *Tetrahedron Lett.*, 2015, **56**, 4971–4974.
- 138 A. Padwa and D. J. Austin, *Angew. Chemie Int. Ed. English*, 1994, **33**, 1797–1815.
- 139 A. I. Green, C. P. Tinworth, S. Warriner, A. Nelson and N. Fey, *Chem. - A Eur. J.*, 2021, **27**, 2402–2409.
- 140 D. J. Miller and C. J. Moody, *Tetrahedron*, 1995, **51**, 10811–10843.
- 141 H. Wang, D. M. Guptill, A. Varela-Alvarez, D. G. Musaev and H. M. L. Davies, *Chem. Sci.*, 2013, **4**, 2844.
- 142 H. M. L. Davies, T. Hansen and M. R. Churchill, *J. Am. Chem. Soc.*, 2000, **122**, 3063–3070.
- 143 CLSI, *Performance Standards for Antimicrobial Susceptibility Testing*, Clinical and Laboratory Standards Institute, Wayne, PA, 2007.
- 144 D. Meyer and P. Renaud, *Angew. Chemie - Int. Ed.*, 2017, **56**, 10858–10861.
- 145 P. Dennis and J. Tamine, *J. Org. Chem.*, 1991, **56**, 2746–2750.
- 146 J. Velcicky, A. Soicke, R. Steiner and H.-G. Unther Schmalz, *J. Am. Chem. Soc.*, 2011, **133**, 6948–6951.
- 147 K. S. Levchenko, I. S. Semenova, V. N. Yarovenko, P. S. Shmelin and M. M. Krayushkin, *Tetrahedron Lett.*, 2012, **53**, 3630–3632.
- 148 T. V Hughes, S. L. Emanuel, A. K. Beck, S. K. Wetter, P. J. Connolly, P. Karnachi, M. Reuman, J. Seraj, A. R. Fuentes-Pesquera, R. H. Gruninger, S. A. Middleton, R. Lin, J. M. Davis and D. F. C. Moffat, *Bioorg. Med. Chem. Lett.*, 2007, **17**, 3266–3270.
- 149 N. Hauser and P. Kraft, *Synthesis (Stuttg.)*, 2018, **50**, 4490–4500.
- 150 S. Wakamatsu, J. A. Barltrop and A. C. Day, *Chem. Lett.*, 1982, **11**, 667–670.
- 151 T. Chidley and G. K. Murphy, *Org. Biomol. Chem.*, 2018, **16**, 8486.
- 152 C. Zhu, A. Yoshimura, P. Solntsev, L. Ji, Y. Wei, V. N. Nemykin and V. V. Zhdankin, *Chem. Commun*, 2012, **48**, 10108–10110.
- 153 M. Ochiai, Y. Kitagawa and S. Yamamoto, *J. Chem. Soc., Chem. Commun*, 1997,

- 119**, 11598–11604.
- 154 R. Zhao and L. Shi, *Angew. Chemie - Int. Ed.*, 2020, 59, 12282–12292.
- 155 N. Lu, L. Huang, L. Xie and J. Cheng, *European J. Org. Chem.*, 2018, **2018**, 3437–3443.
- 156 C. Klöck, X. Jin, K. Choi, C. Khosla, P. B. Madrid, A. Spencer, B. C. Raimundo, P. Boardman, G. Lanza and J. H. Griffin, *Bioorganic Med. Chem. Lett.*, 2011, **21**, 2692–2696.
- 157 M. Singh, S. K. Singh, M. Gangwar, G. Nath and S. K. Singh, *RSC Adv.*, 2014, **4**, 19013–19023.
- 158 M. T. Gabr, N. S. El-Gohary, E. R. El-Bendary, M. M. El-Kerdawy, N. Ni and M. I. Shaaban, *Chinese Chem. Lett.*, 2015, **26**, 1522–1528.
- 159 F. Naaz, R. Srivastava, A. Singh, N. Singh, R. Verma, V. K. Singh and R. K. Singh, *Bioorg. Med. Chem.*, 2018, **26**, 3414–3428.
- 160 M. Palkar, M. Noolvi, R. Sankangoud, V. Maddi, A. Gadad and L. V. G. Nargund, *Arch. Pharm. (Weinheim)*, 2010, **343**, 353–359.
- 161 S. Maddila, S. Gorle, N. Seshadri, P. Lavanya and S. B. Jonnalagadda, *Arab. J. Chem.*, 2016, **9**, 681–687.
- 162 S. S. AlNeyadi, A. A. Salem, M. A. Ghattas, N. Atatreh and I. M. Abdou, *Eur. J. Med. Chem.*, 2017, **136**, 270–282.
- 163 I. A. Abdelhamid, M. H. Mohamed, A. M. Abdelmoniem and S. A. S. Ghazlan, *Tetrahedron*, 2009, **65**, 10069–10073.
- 164 C. M. Chan, Q. Xing, Y. C. Chow, S. F. Hung and W. Y. Yu, *Org. Lett.*, 2019, **21**, 8037–8043.
- 165 J. Chen, X. Shen and Z. Lu, *J. Am. Chem. Soc.*, 2020, **142**, 14455–14460.
- 166 Z. Chen, N. Ren, X. Ma, J. Nie, F.-G. G. Zhang and J.-A. A. Ma, *ACS Catal.*, 2019, **9**, 4600–4608.
- 167 N. Shankaraiah, W. A. Da Silva, C. Kleber, Z. Andrade and L. S. Santos, *Tetrahedron Lett.*, 2008, **49**, 4289–4291.
- 168 N. F. H. Mahmoud and G. A. Elsayed, *J. Heterocycl. Chem.*, 2020, **57**, 1845–1862.
- 169 S. N. Mangasuli, *Chem. Data Collect.*, 2020, **29**, 100515.
- 170 S. I. Elewa, A. O. Abdelhamid, A. A. Hamed and E. Mansour, *Synth. Commun.*, 2021, **51**, 151–161.
- 171 O. O. Ajani, K. T. Iyaye, O. Y. Audu, S. J. Olorunshola, A. O. Kuye and I. O. Olanrewaju, *J. Heterocycl. Chem.*, 2017, **55**, 302–312.
- 172 J. Zheng, J. Qi and S. Cui, *Org. Lett.*, 2015, **18**, 128–131.
- 173 T. Mosmann, *J. Immunol. Methods*, 1983, **65**, 55–63.
- 174 F. Denizot and R. Lang, *J. Immunol. Methods*, 1986, **89**, 271–277.
- 175 Y. Maehara, H. Anai, R. Tamada and K. Sugimachi, *Eur. J. Cancer Clin. Oncol.*,

- 1987, **23**, 273–276.
- 176 M. S. Mulani, E. E. Kamble, S. N. Kumkar, M. S. Tawre and K. R. Pardesi, *Front. Microbiol.*, 2019, **10**, 539.
- 177 A. G. Elliott, D. Ganesamoorthy, L. Coin, M. A. Cooper and M. D. Cao, *Genome Announc.*, 2016, **4**, 438–454.
- 178 Y. Zhu, J. Lu, J. Zhao, X. Zhang, H. H. Yu, T. Velkov and J. Li, *Int. J. Med. Microbiol.*, 2020, **310**, 151412.
- 179 J. LaBaer, Q. Q. Qiu, A. Anumanthan, W. Mar, D. Zuo, T. V. S. Murthy, H. Taycher, A. Halleck, E. Hainsworth, S. Lory and L. Brizuela, *Genome Res.*, 2004, **14**, 2190–2200.
- 180 F. Grenier, D. Matteau, V. Baby and S. Rodrigue, *Genome Announc.*, 2014, **2**, 1038–1052.
- 181 R. A. Maplestone, M. J. Stone and D. H. Williams, *Gene*, 1992, **115**, 151–157.
- 182 J. L. Shi, Q. Luo, W. Yu, B. Wang, Z. J. Shi and J. Wang, *Chem. Commun.*, 2019, **55**, 4047–4050.
- 183 M. Groarke, M. A. Mckervey, H. Miel and M. Nieuwenhuyzen, *Org. Lett.*, 2000, **2**, 2393–2395.
- 184 T. O. Zanakhov, E. E. Galenko, M. A. Kryukova, M. S. Novikov and A. A. Khlebnikov, *Molecules*, 2021, **26**, 1881.
- 185 I. Nicolas, P. Le Maux and G. Simonneaux, *Coord. Chem. Rev.*, 2008, **252**, 727–735.
- 186 A. G. Renfrew, C. L. Butler and L. H. Cretcher, *J. Am. Chem. Soc.*, 1943, **65**, 2038–2039.
- 187 D. Gillingham and N. Fei, *Chem. Soc. Rev.*, 2013, **42**, 4918–4931.
- 188 M. Jansen, A. Wahida, S. Latz, A. Krüttgen, H. Häfner, E. M. Buhl, K. Ritter and H.-P. Horz, *Sci. Rep.*, 2018, **8**, 1–12.
- 189 H. Muroi and I. Kubo, *J. Agric. FoodChem*, 1903, **41**, 1102–1105.
- 190 J. Wang, J. P. Kutter, H. Mu, A. Moodley and M. Yang, *Int. J. Pharm.*, 2020, **590**, 119877.
- 191 S. Foerster, M. Unemo, L. J. Hathaway, N. Low and C. L. Althaus, *BMC Microbiol.*, 2016, **16**, 1–11.
- 192 L. Thieme, A. Hartung, K. Tramm, M. Klinger-Strobel, K. D. Jandt, O. Makarewicz and M. W. Pletz, *Biol. Proced. Online*, 2019, **21**, 1–5.
- 193 N. Y. T. Man, D. R. Knight, S. G. Stewart, A. J. McKinley, T. V. Riley and K. A. Hammer, *Sci. Rep.*, 2018, **8**, 1–9.
- 194 J. L. Martinez and F. Baquero, *Antimicrob. Agents Chemother.*, 2000, **44**, 1771.
- 195 N. A. Romero and D. A. Nicewicz, *Chem. Rev.*, 2016, **116**, 10075–10166.
- 196 B. Miriyala and J. S. Williamson, *Tetrahedron Lett.*, 2003, **44**, 7957–7959.

- 197 R. Gu, X. Wang, Z. Yang and S. Han, *Tetrahedron Lett.*, 2018, **59**, 2835–2838.
- 198 W. Dong, Y. Liu, B. Hu, K. Ren, Y. Li, X. Xie, Y. Jiang and Z. Zhang, *Chem. Commun.*, 2015, **51**, 4587–4590.
- 199 K. C. Nicolaou, P. S. Baran, Y. L. Zhong, S. Barluenga, K. W. Hunt, R. Kranich and J. A. Vega, *J. Am. Chem. Soc.*, 2002, **124**, 2233–2244.
- 200 J. Shah and S. Kumar, *Synthesis (Stuttg.)*, 2012, **44**, 1417–1426.
- 201 B. Ma, P. Wu, X. Wang, Z. Wang, H. X. Lin and H. X. Dai, *Angew. Chemie - Int. Ed.*, 2019, **58**, 13335–13339.
- 202 B. M. Trost and M. Osipov, *Angew. Chemie - Int. Ed.*, 2013, **52**, 9176–9181.
- 203 J. W. Medley and M. Movassaghi, *Org. Lett.*, 2013, **15**, 3614–3617.
- 204 M. Espinoza-Moraga, T. Petta, M. Vasquez-Vasquez, V. F. Laurie, L. A. B. Moraes and L. S. Santos, *Tetrahedron Asymmetry*, 2010, **21**, 1988–1992.

Appendix A

Growth Inhibition Calculations

Growth inhibition values were calculated within MATLAB using the optical density (OD) data obtained from the plate reader. All wells containing positive controls were averaged per plate. All wells containing negative controls were averaged per plate. Both biology duplicates were treated individually.

Plate Reader Raw Data:

User: USER	Path: C:\Program Files (x86)\BMG\Omega\User\Data\										File Name: 4530.dbf	
Test Name: OD 600 ABBIE	Date: 11/10/2019										Time: 09:52:32	
ID1: Abbie - Carbonylation 1 - ATCC 29213 A												
Absorbance	Absorbance values are displayed as OD											
Raw Data (600)												
	1	2	3	4	5	6	7	8	9	10	11	12
A	0.052	0.753	0.623	0.535	0.649	0.618	0.483	0.503	0.503	0.683	0.677	0.934
B	0.781	0.596	0.754	0.765	0.809	0.707	0.61	0.634	0.584	0.553	0.633	0.843
C	0.613	0.661	0.69	0.794	0.801	0.82	0.812	0.617	0.697	0.771	0.884	0.926
D	0.689	0.723	0.858	0.973	0.906	0.858	0.85	0.854	0.841	0.84	0.952	0.986
E	0.628	0.755	0.139	0.93	0.943	0.869	0.856	0.798	0.883	0.894	1.078	0.984
F	0.684	0.778	0.746	0.787	0.835	0.839	0.848	0.846	0.856	0.838	0.978	1.029
G	0.925	0.712	0.227	0.836	0.813	0.596	0.853	0.633	0.966	0.83	0.155	0.899
H	1.177	1.066	0.888	0.826	0.755	0.666	0.751	0.735	0.786	0.869	0.892	0.922

Growth Inhibition Calculation:

$$\text{Growth Inhibition (\%)} = \frac{(OD_{\text{NegativeControl}} - OD_{\text{ReactionWell}})}{(OD_{\text{NegativeControl}} - OD_{\text{PositiveControl}})} \times 100$$

Scaling Data between 0 – 100%:

All growth inhibition values above 100 were minimised to this value. All growth inhibition values below 0 were maximised to this value. This is possible as OD at 100% cell growth is extremely variable in cells.

Code Used to Normalise OD data:

```

        table=app.t(:,:,:); %Convert Table into a cell array
        IndexPos = strcmp(table,'Pos' ); %Locate position of Positive control
        IndexNeg = find(strcmp('Neg',table)); %Locate position of Negative control
        PA1_control = app.PA1(IndexPos); %Give all values for Positive Control using layout
        PA1B_control = app.PA1B (IndexPos);
        PA1_control = mean(PA1_control); %Give mean value for Positive Control using layout
        PA1B_control = mean(PA1B_control);
        NA1 = app.PA1(IndexNeg); %Give all values for Negative Control using layout
        NA1B = app.PA1B (IndexNeg);
        NA1 = mean(NA1); %Give mean value for Negative Control using layout
        NA1B = mean(NA1B);

        %First Repeat Plate

    PGAl = ((NA1 - app.PA1)/(NA1-PA1_control)*100); %Convert OD into Percentage Growth
    PGAl(PGAl < 0) = 0; %Convert values < 0 to 0
    PGAl(PGAl > 100) = 100; %Convert values > 100 to 100

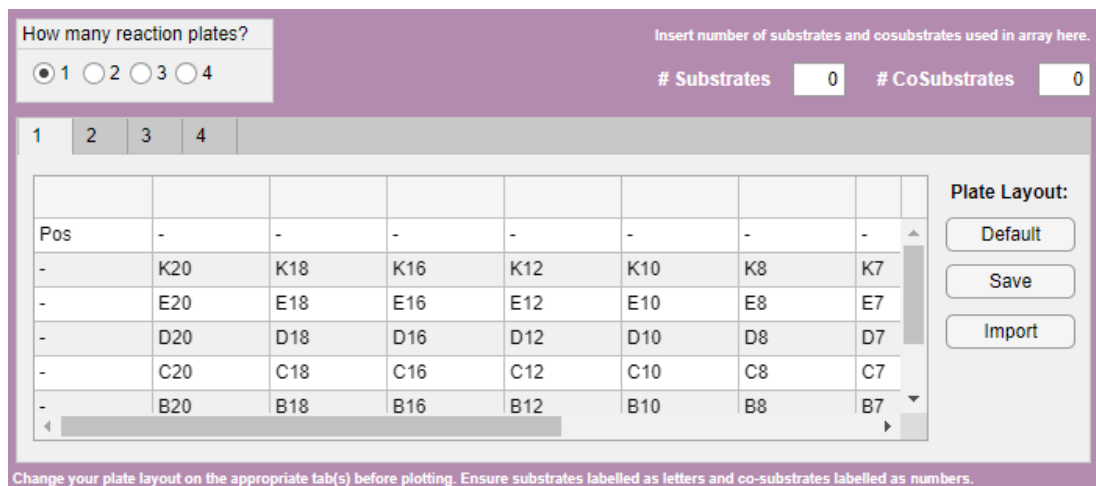
    %First plate sample B

    PGB1 = ((NA1B - app.PA1B)/(NA1B-PA1B_control)*100); %Convert OD into Percentage Growth
    PGB1(PGB1 < 0) = 0; %Convert values < 0 to 0
    PGB1(PGB1 > 100) = 100; %Convert values > 100 to 100

```

Interactive Plate Layout:

An app was created on MATLAB to allow automatic reorganisation of growth inhibition data for plotting. The app contained an interactive plate layout where substrates (letters) and co-substrates (numbers) were inputted in their respective locations within the reaction array. The number of 96-well plates used in the array could be altered in the top left, the layout on each plate could be changed by selecting the appropriate tab above the table and the number of substrates and co-substrates could be inputted in the top right.



Code to Reorganise Data to Plate Layout:

```

        % Find locations of Substrates and Co-substrates

Alphabet = 'ABCDEFGHJKLMNOPQRSTUVWXYZ'; %Creates a matrix containing alphabet letters
l = Alphabet(app.Substrate); %Provides a letter for the number inputted into substrates

output_location_y=1; %Creates a y co-ordinate

for i = 1:app.Substrate %Identifies number of loop times based on substrate number
    n = ['A':1]; %Provide letter identification for plate layout
    output_location_x=1; %Creates an x co-ordinate
    for num=1:app.CoSubstrate %Range of 1:number of CoSubstrates
        co_substrate_string=num2str(num); %Converts CoSubstrate Number to String
        find_location = strcat(n(i),co_substrate_string); %Labels locations A1...etc
        location_index = strcmp(table,find_location); %Finds the location of A1... etc
        location_index = num2cell(location_index); %Converts logical output into a cell array
        location_index(cellfun(@isempty, location_index)) = {nan}; %Converts empty cells to NAN
        location_index=cell2mat(location_index); %Converts location_index cell array to matrix
        output_matrix_A(output_location_x,output_location_y) = PGAl(location_index==1);
        %Creates an output matrix for the data at the specified index
        num = num +1; %Goes onto A2 then A3 etc
        output_location_x = output_location_x +1; %Makes sure next data is written in next co-ordinate
    end
    i = i + 1; %Goes onto B1 then C1 etc
    output_location_y = output_location_y + 1;
    %Makes sure next data is written in next co-ordinate
end
end

```

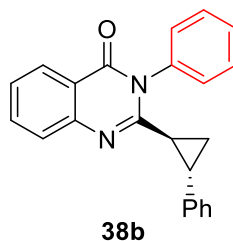
Data was output as an excel file containing a matrix with co-substrates as rows and substrates as columns (with biological duplicates positioned adjacent to one another). This was plotted in Origin as a heat map.

Data Output:

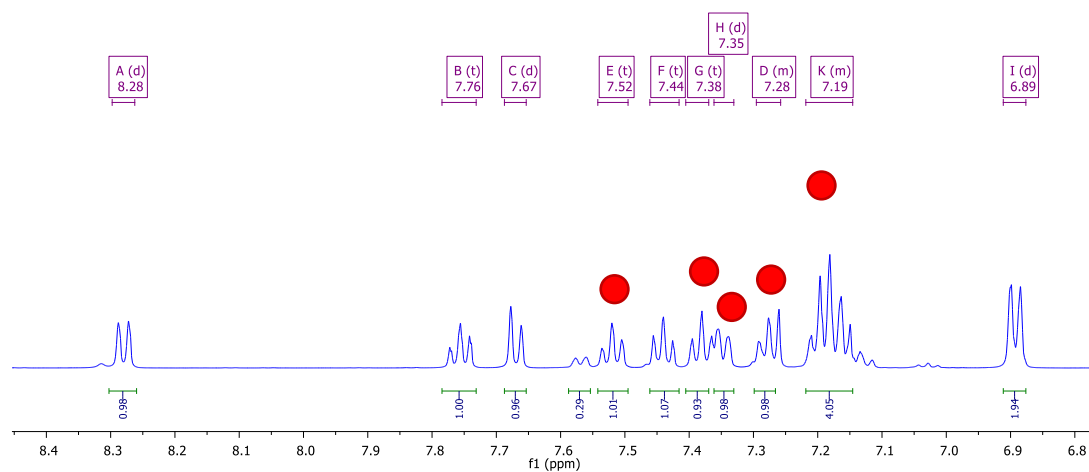
	A	B	C	D	E	F	G	H	I	J	K	L	M	N	O	P	Q	R	S	T	U	V
1	66.95085	77.11964	0	18.0195	0	19.84238	0	22.1304182	0	17.32554	0	0	2.87851325	36.54267	0	12.91028	23.96224	12.22615	100	97.0318	7.873646	23.90375
2	0	18.622032	0	9.317402	0	5.65654	0	12.8257277	0	4.665057	0	0	0	0	0	0	24.7816	11.90813	37.33803	27.06714	17.75938	25.10487
3	0	0	0	0	0	0	0	0	0	0	0	0	0	0	0	0	34.24431	31.83746	25.87307	23.93233	0	0
4	0	5.0864965	0	0	0	0	0	0	0	0	0	0	0	5.36105	0	0	28.51183	25.58304	52.35368	46.93647	0	0
5	0	20.784921	0	0	0	0	0	0	0	0	0	1.64138	0	0	0	0	33.60737	32.93753	48.53003	44.34623	0	0
6	0	0.6391223	0	6.114148	0	1.004195	0	4.4362527	0	0.24155	0	4.485777	0	96.06127	0	15.20788	30.87762	39.78799	100	95.01767	13.92788	11.83424
7	7.871646	0	0	2.224482	0	0	0	0	9.8491823	4.665057	0	16.19256	0.57892846	6.673361	0	25.60175	32.60646	44.5583	61.17789	58.86326	7.748043	14.04601
8	0	0	0	0	0	0	0	0.01271133	0	0	0	0	0	0.06790361	0	7.221007	23.87125	21.9788	26.601	46.14841	10.71437	14.42735
9	0	19.132455	0	8.391428	0	0	0	0	0	0	0	8.424508	17.8258144	97.70241	10.16053	10.39387	25.60009	24.20495	59.35805	54.73498	0	0
10	12.44472	0	0	0	0	0	0	4.58878861	0	9.01233	0	0	0	0	0	4.485777	18.77571	19.75265	21.77843	16.46643	0	5.351468
11	0	21.198038	0	10.14717	0	0	0	0	0	0	0	0	0	0	0	0	16.5395	19.22261	27.32894	30.45336	0	0
12	0	0	0	0	0	0	0	0	0	5.122664	0	5.579869	0	14.66083	0	0	32.63745	7.45583	26.51001	27.27915	0	7.258167
13	0	28.943971	0	4.776859	0	2.194681	0	9.63077718	0	7.585195	0	15.86433	0	7.221007	0	6.017505	30.05869	21.87279	35.15423	56.5371	0	0
14	0	36.896463	0	15.82752	0	5.912729	0	13.7619416	0	1.368448	0	8.643326	16.8037767	39.05908	0	93.65427	33.78935	24.20495	50.07689	53.67431	0	0
15	0	28.221017	0	22.74722	0	6.842241	0	0	0	8.907823	1.089947	1.750547	19.6143804	48.35886	0	97.48359	33.63836	28.97527	42.79754	64.0636	0	0
16	0	0	0	0	0	5.961612	0	4.4362527	0	0	0	0	2.11798439	0	0	0	28.14604	35.86572	27.98508	33.19399	0	4.83386
17	0	15.31128	0	0	0	0	0	0	0	0	0	76.72074	1.094092	0	23.52298	0	7.986871	26.18298	24.73498	38.15636	32.26148	0
18	58.05189	76.814542	0	0	68.9284	23.65578	0	4.35998475	0.8266359	4.13181	0	11.05033	73.1436043	94.74836	0	19.58425	16.13694	16.93647	100	98.09187	0	0.851659
19	0	0	0	0	0	0	0	0	0	0	0	0	22.8082482	96.06127	0	95.40481	25.41811	15.40636	61.63285	57.06714	0	0
20	0	1.2323986	0	0	0	0	0	5.04839634	4.4109392	6.648023	0	2.844639	0	4.923414	0	2.516411	27.14695	35.91713	40.52275	44.68431	12.44472	7.868311

Appendix B NMR Spectra

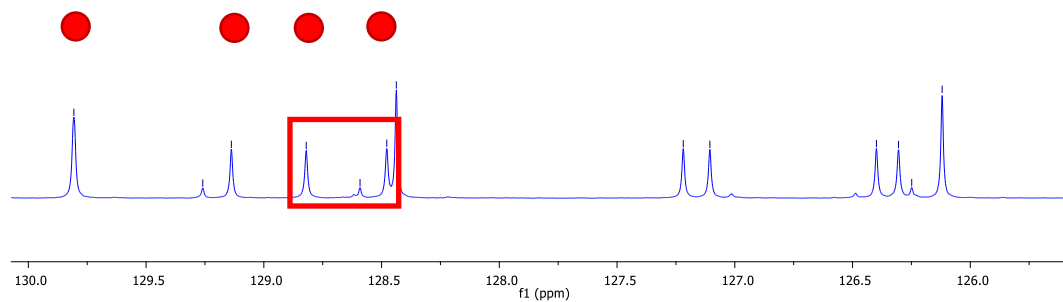
B.1 Identification of Rotamers within Quinazolinone 38b



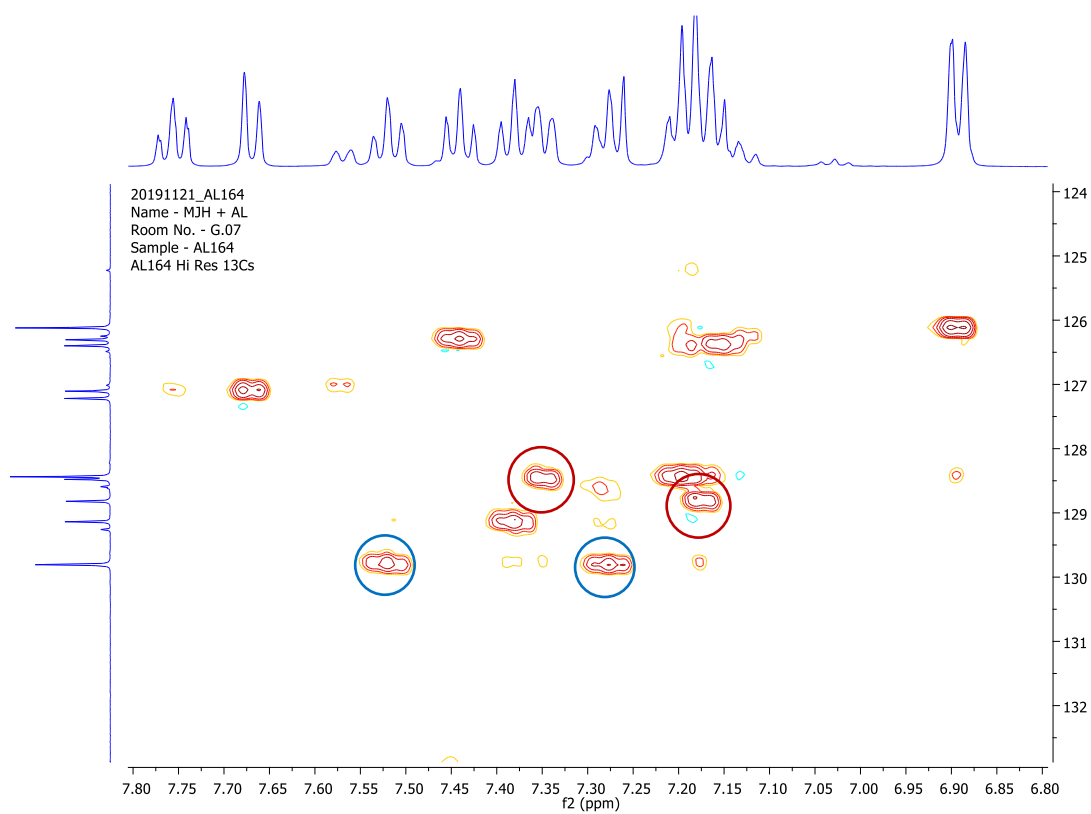
¹H NMR with 3-position phenyl protons indicated:



¹³C NMR with 3-position phenyl carbons indicated:

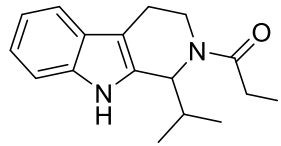


Protons 2-H and 6-H carbons have been indicated (red box).

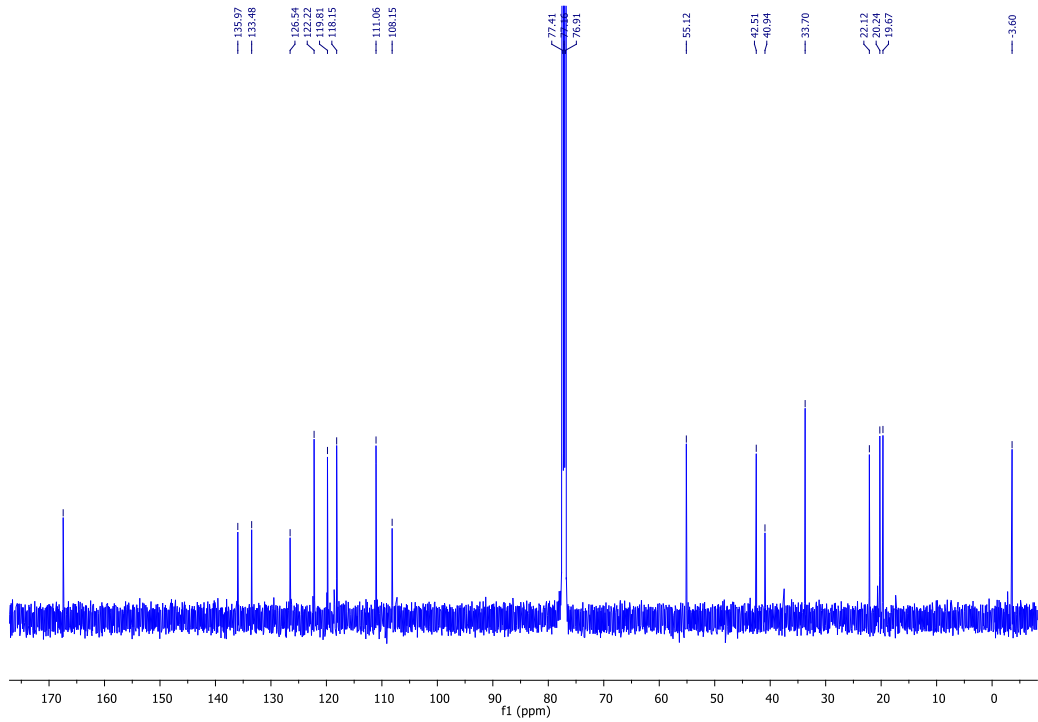
High resolution HSQC:

Peaks in position 2 and 6 on the phenyl ring have been indicated within the red circles and peaks position 3 and 5 have been indicated within the blue circles.

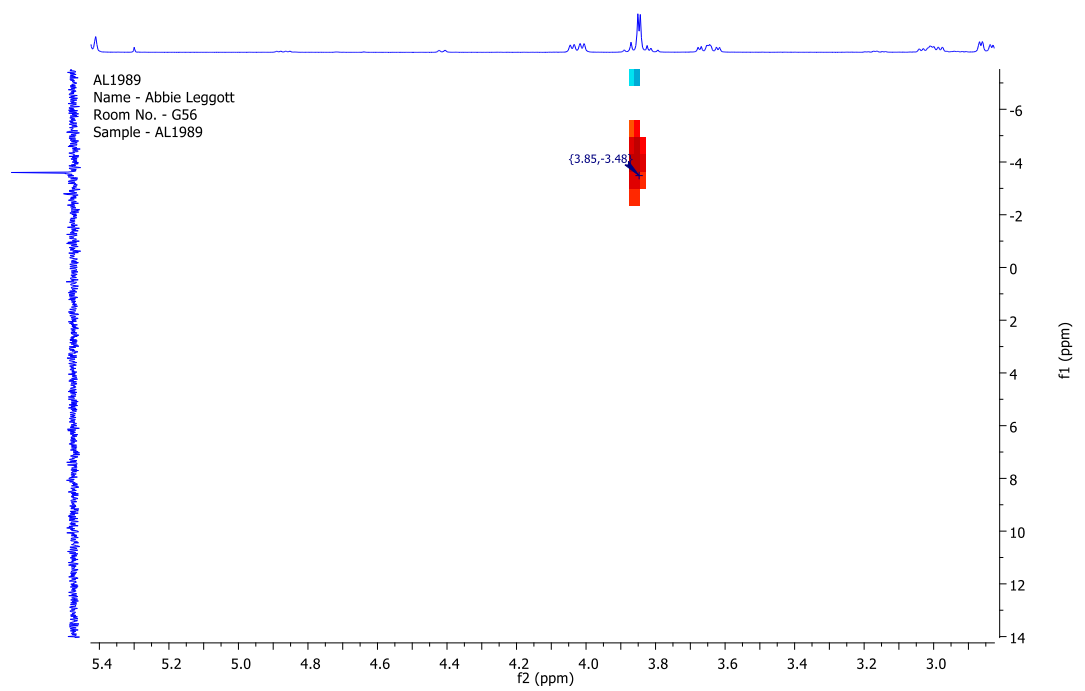
B.2 Confirmation of the Structure of 111

**111**

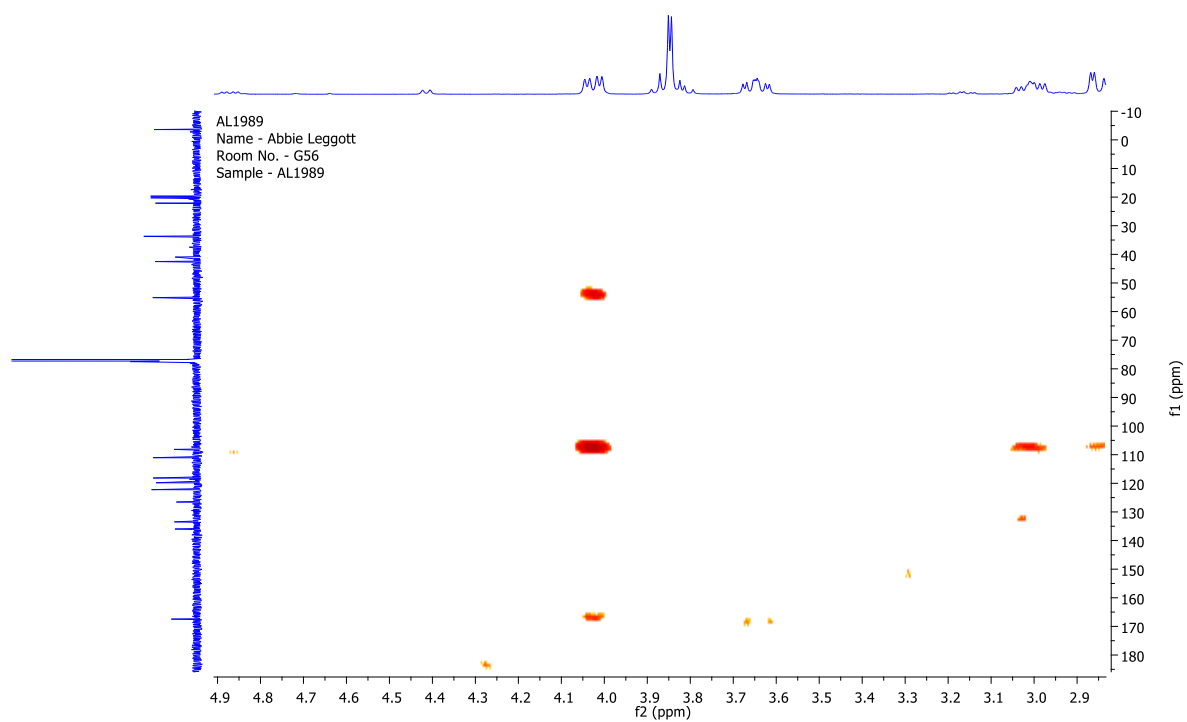
^{13}C NMR Spectra:



HSQC:



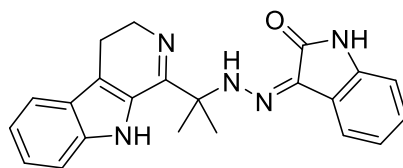
HMBC:



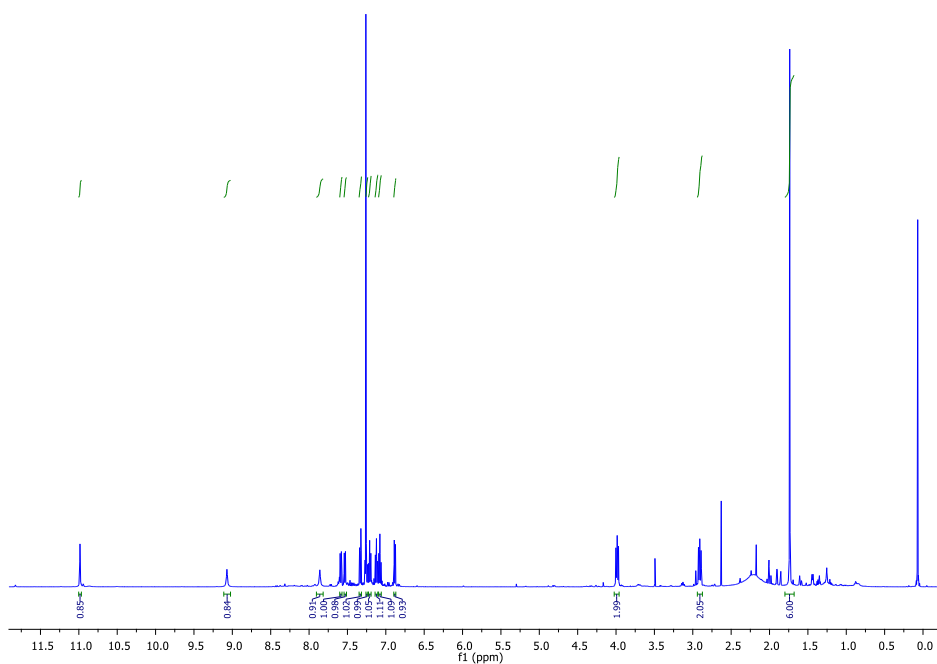
The proton on the carbon of interest does not lie three bonds away from another carbon.

B.3 Evidence to Support the Hypothesised Structure of 130

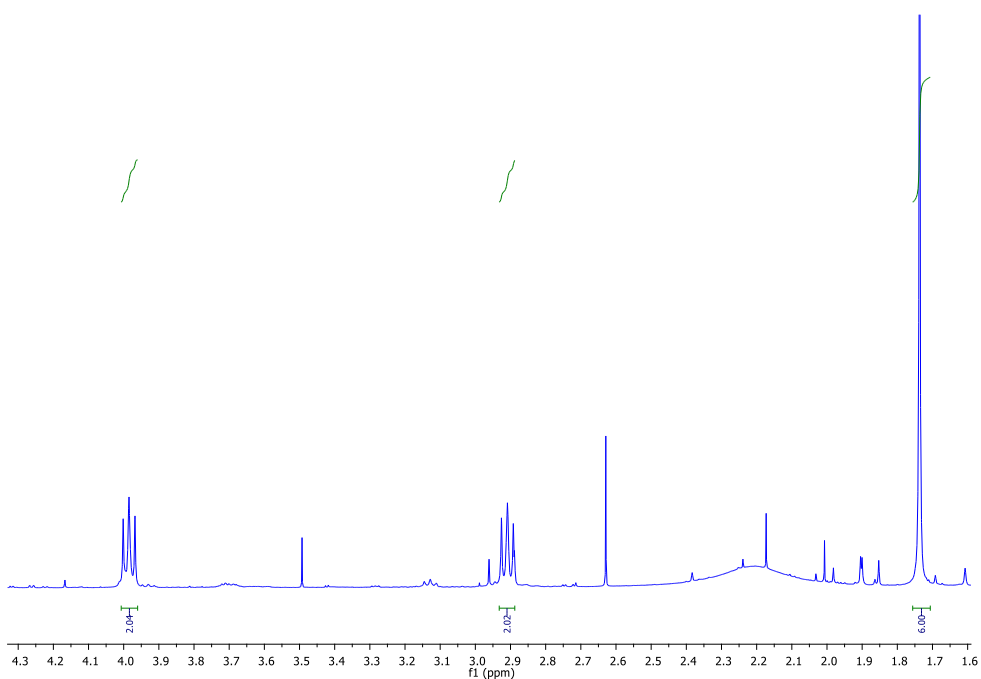
¹H NMR Spectra:



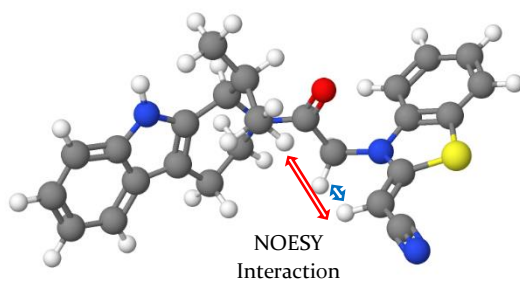
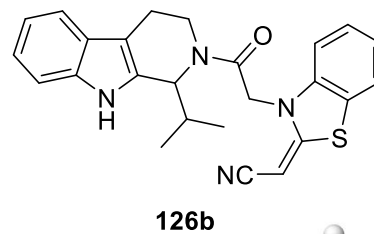
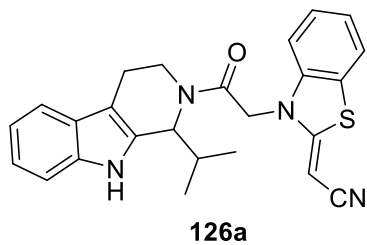
130



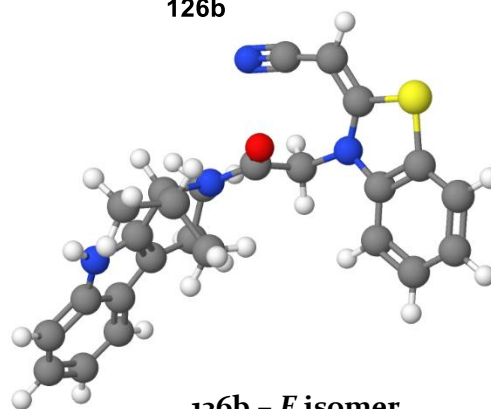
¹H NMR Spectra (Zoomed in to Key Peaks):



B.4 NOESY NMR Confirming Z Alkene in Compound 126

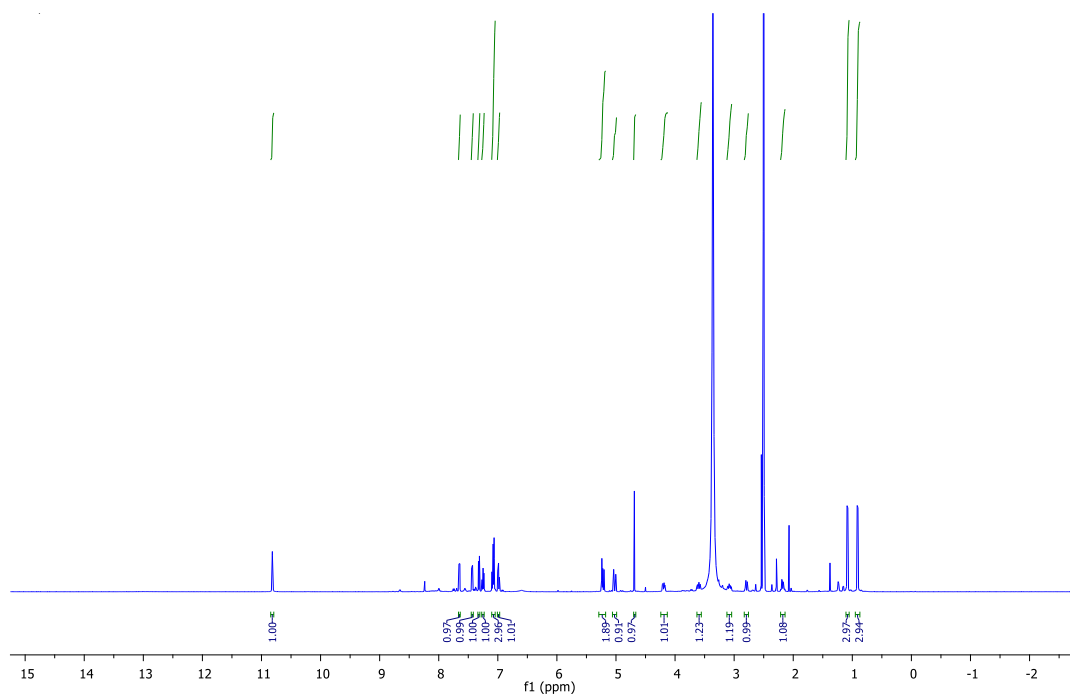


126a – Z isomer

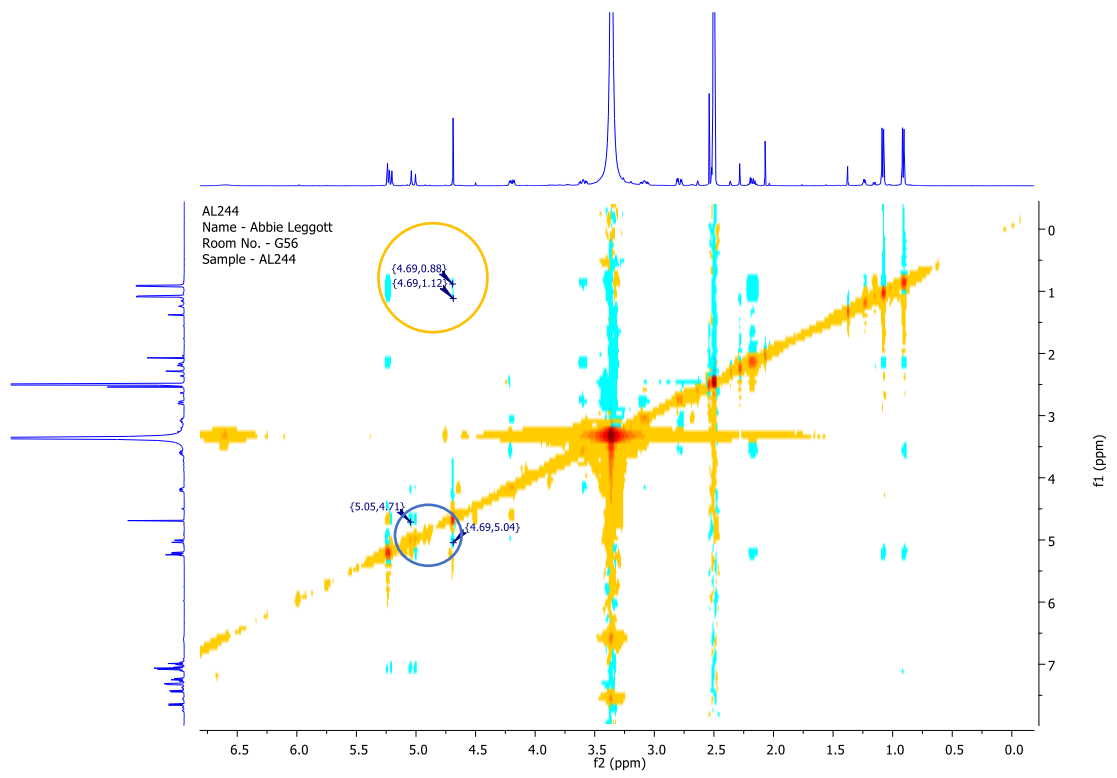


126b – E isomer

¹H NMR:



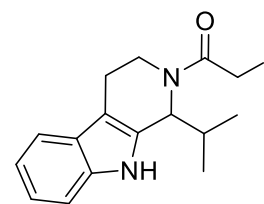
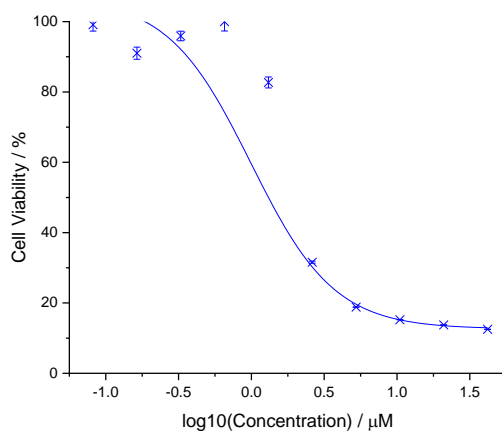
NOESY:



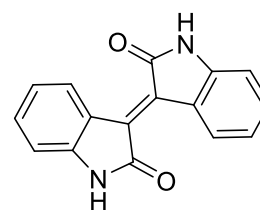
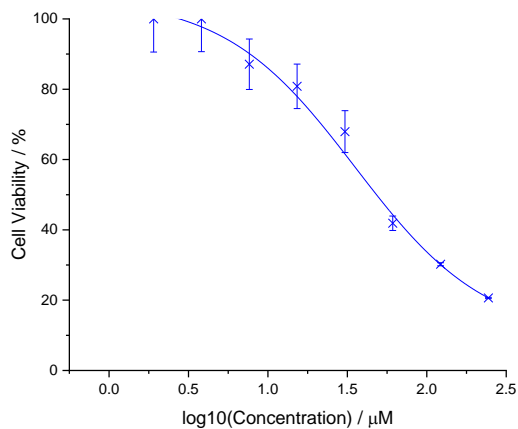
Appendix C

Dose Response Curves to Assess Eukaryotic Activity

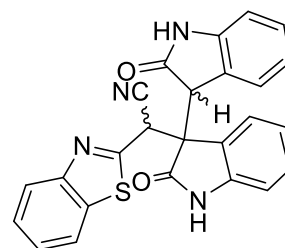
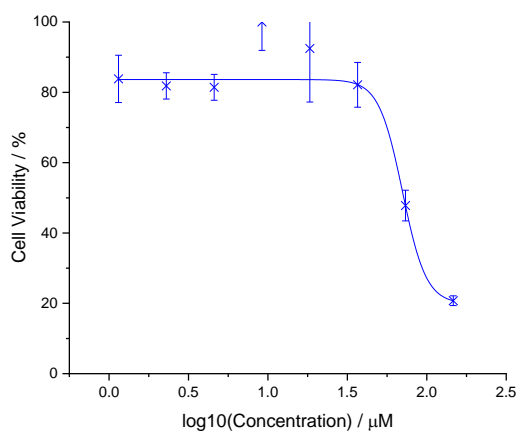
Product ^a	Product Mass	MIC / $\mu\text{g mL}^{-1}$	MIC / μM	IC ₅₀ / μM
		ATCC29213		HeLa Cells
111	382	16	42	1.0 \pm 0.4
121	262	2	7.6	35 \pm 7
109a	436	4-8	9.2 - 18.3	89 \pm 27
109b	436	2-4	4.6 - 9.2	66 \pm 4
127	444	4-8	9.0-18.0	38 \pm 6

Compound **111**:

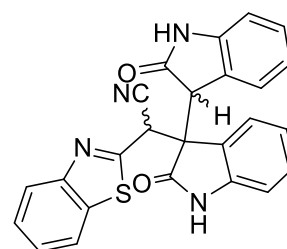
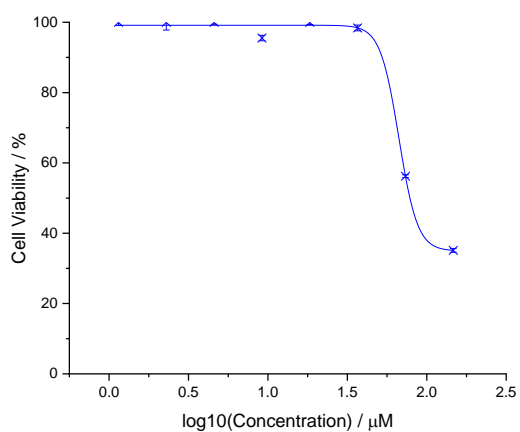
111, MIC = 16 $\mu\text{g mL}^{-1}$
IC₅₀ = 1 \pm 0.4 μM

Compound **121**:

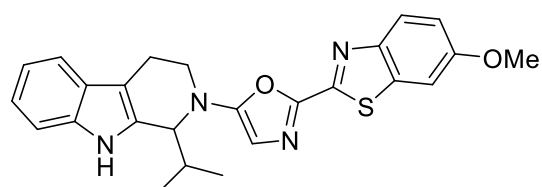
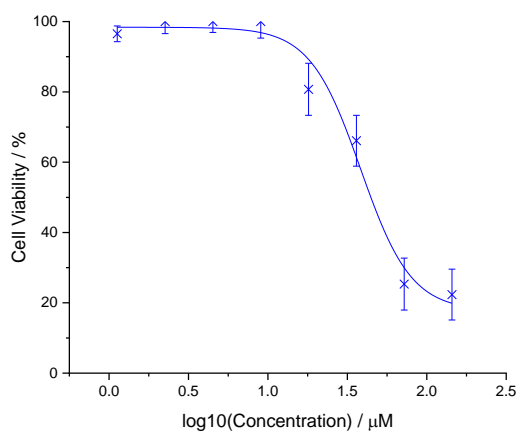
121, MIC = 2 $\mu\text{g mL}^{-1}$
IC₅₀ = 35 \pm 7 μM

Compound **109a**:

109a, MIC = 4-8 $\mu\text{g mL}^{-1}$
 $\text{IC}_{50} = 89 \pm 27 \mu\text{M}$

Compound **109b**:

109b, MIC = 2-4 $\mu\text{g mL}^{-1}$
 $\text{IC}_{50} = 66 \pm 4 \mu\text{M}$

Compound **127**:

127, MIC = 4-8 $\mu\text{g mL}^{-1}$
 $\text{IC}_{50} = 38 \pm 6 \mu\text{M}$